Precursor-Directed Biosynthesis of Azinomycin A and Related Metabolites by Streptomyces sahachiroi

Precursor-Directed Biosynthesis of Azinomycin A and Related Metabolites by *Streptomyces sahachiroi*

Abdel-Ilah Sebbar

Department of Biological Sciences
School of Science
Birkbeck College
University of London

A thesis submitted to the University of London for the degree of

Doctor of Philosophy

August 2014

Declaration

The work presented in this thesis in entirely on my own, except where I have either acknowledged help from a known person or given a published reference.

Signed: ……. Date:… 15/8/14 ……...

PhD student: Abdel-Ilah Sebbar

Department of Biological Sciences

School of Science

Birkbeck College

University of London

Signed: ..... Date: 15/8/14 ……...

Supervisor: Dr. Philip Lowden

Department of Biological Sciences

School of Science

Birkbeck College

University of London

Abstract

Azinomycins A and B are bioactive compounds produced by Streptomyces species. These naturally occurring antibiotics exhibit potent *in vitro* cytotoxic activity, promising *in vivo* antitumor activity and exert their effect by disruption of DNA replication by the formation of interstrand cross-links. The electrophilic C-10 and C-21 carbons contained within the aziridine and epoxide moieties are known to be responsible for the interstrand cross-links through alkylation of N-7 atoms of guanine bases. The naphthoate moiety (3-methoxy-5-methyl-naphthoate) is believed to play a role in the azinomycins' biological activity through hydrophobic interactions in the DNA major groove. In this study, precursor directed biosynthesis (PDB) has been investigated for the production of unnatural azinomycin analogues. A series of naphthoic acid analogues were fed to the azinomycin producing bacteria (*Streptomyces sahachiroi* ATCC 33158). LCMS analyses revealed that 1-naphthoic acid, 4-fluoro-1-naphthoic acid, 4-methyl-1-naphthoic acid and 3-methoxy-1-naphthoic acid were successfully incorporated into the azinomycin A biosynthesis pathway and resulted in the development of novel azinomycin A analogues. These novel products were isolated and purified using preparative HPLC and were characterised by diode array detection and electrospray tandem mass spectrometry. NMR characterisation and biological studies could not yet be conducted due to the low production levels (~100 µg in 500 mL fermentation broth) and the persistence of some impurities in these novel azinomycin A analogues.

In the course of this work, additional metabolites were found in the fermentations. LCMS analysis revealed that a range of naphthoic acids were biotransformed into primary amides. Column chromatography has been carried out towards purification of all the produced amides. As consequence, 1-naphthoic amide and 4-fluoro-1-naphthoic amide were successfully purified and characterised by NMR and LCMS. Further amides were so far only characterised by LCMS, as impurities hampered NMR analysis. Antibacterial and antifungal tests were carried out to investigate the biological activity of the purified amide. The results revealed that they were inactive against the tested microorganisms.

Dedication

I would like to dedicate this thesis to my dearest and respected parents, *Mrs. Soudia El Borji* and *Mr. Abdeslam Sebbar*, for their endless support and encouragement throughout my life.

To my brother Mohamed, my sisters Fatima, Anissa, Nadia and Asma for their constant emotional support.

Also to my adorable nieces Wisal, Huda, Sukayna, Hajar and Zainab and my lively nephews Youssef, Yasser and Youness.

Acknowledgments

I am grateful to my supervisor Dr. Philip Lowden for giving me the opportunity to work on this exciting project. His constant support, guidance and outstanding training were and still are invaluable to me.

I would proudly express my sincere acknowledgement to Dr. Jason Taylor, Dr. Katherine Thompson, Dr. Jane Nicklin and Dr. Salvador Tomas for their supports and advices.

Special thanks go to Dimitrios, Chandrakala, Davide, Tulika, Khadijo, Antima and Juan for their support as friends.

I want to express my special gratitude to all the technical staff of the Chemistry and Microbiology department for the help I have been given throughout my PhD life.

Abbreviations

ACP	Acyl carrier protein
AHBA	3-Amino-5-hydroxybenzoic acid
AMP	Adenosine monophosphate
AT	Acyl transferase
ATCC	American Type Culture Collection
ATP	Adenosine triphosphate
A.U	Arbitrary units
AVEDEV	Average of the absolute deviations
AviM	Avilamycin polyketide synthase
azi	Azinomycin
Azic	Azicemicin
BPC	Base peak chromatogram
CalO5	Calicheamicin polyketide synthase
C-A-PCP	Condensation-Adenylation-Peptidyl carrier protein domains
$CDCl_3$	Deuterated chloroform
CD_3OD	Deuterated methanol
CFU	colony forming unit
$CHCl_3$	Chloroform
^{13}C NMR	Nuclear magnetic resonance spectroscopy to carbon
CoA	Coenzyme A
COSY	Correlation spectroscopy
Cy domain	Cyclisation domain
DAD	Diode array detector
DAHP	3,4-Dideoxy-D-arabino-heptulosonic acid 7-phosphate
DDA	Disk diffusion assay
DEB	Deoxyerythronolide B
DEBS	Deoxyerythronolide B synthase
DH	Dehydratase
DHQ	Dehydroquinic acid
DHS	Dehydroshikimic acid

DMSO	Dimethyl sulfoxide
(1D) NMR	One-dimensional nuclear magnetic resonance
(2D) NMR	Two- dimensional nuclear magnetic resonance
E domain	Epimerase domain
EIC	Extracted ion chromatogram
EICs	Extracted ion chromatograms
E4P	Erythrose-4-phosphate
ER	Enoyl reductase
ESI	Electrospray ionisation
ESI-MS	Electrospray ionisation mass spectrometry
FAD	Flavin adenine dinucleotide
FAS	Fatty acid synthase
FAS/PKS	Fatty acid synthase/polyketide synthase
FC	Flash chromatography
^{19}F NMR	Fluorine-19 nuclear magnetic resonance
GYM	Clucose - Yeast - Malt medium
HMBC	Heteronuclear Multiple-Bond Correlation
HMQC	Heteronuclear Multiple Quantum Coherence
^{2}H-NMR	Deuterium (heavy hydrogen) Nuclear Magnetic Resonance
^{1}HNMR	Proton NMR
HPLC	High-Performance Liquid Chromatography
IC_{50}	Half maximal inhibitory concentration
ISC	Interstrand cross-link
ISCs	Interstrand cross-links
Jad	Jadomycin
ked	Kedarcidin
KR	Ketoreductase
KS	Ketosynthase
KS_{α}	Ketosynthase alpha
KS_{β}	Ketosynthase beta
LCMS	Liquid chromatography/mass spectrometry
malonyl-CoA	Malonyl-Coenzyme A
M domain	N-methylation domain

MDP	Maduropeptin
MdpB	Maduropeptin iterative type I polyketide synthase
MeOH	Methanol
MHz	Mega hertz
min	minute
mit	Mitomycin
mM	Millimolar
m.p.	Melting point
MS	Mass spectrometry
ms	Milliseconds
MSA	Methylsalicylic acid
MS/MS	Tandem mass spectrometry
MW	Molecular weight
m/z	Mass-to-charge ratio
NA	Nutrient Agar
NA2	N1999A2
NADPH	Reduced nicotinamide adenine dinucleotide
NCS	Neocarzinostatin
Ncs	Neocarzinostatin synthase
Nik	Nikkomycin
NMR	Nuclear magnetic resonance
NPA	Naphthoic acid
NRPs	Non ribosomal peptides
NRPS	Non ribosomal peptide synthetase
Ox domain	Oxidase domain
PCP	Peptidyl carrier protein
PDA	Potatoes Dextrose Agar
PDB	Precursor-directed biosynthesis
PEP	Phosphoenolpyruvate
PK	Polyketide
pKa	Logarithmic acid dissociation constant
PKS	Polyketide synthase
4′-PP	4′-phosphopantetheine

PPi	Pyrophosphate anion
ppm	Parts per million
prep HPLC	Preparative High-Performance Liquid Chromatography
PS5	Pharmamedia and Starch
psi	Pounds per square inch
Rap	Rapamycin
R domain	Reductase domain
R_f	Reference front
rpm	Revolution per minute
S.	*Streptomyces*
SAM	*S*-adenosylmethionine
SCGIA	Spot culture growth inhibition assay
SMA	Poly(styrene-*co*-maleic acid)
SMANCS	Poly(styrene-*co*-maleic acid)- neocarzinostatin
S_N2	Substitution nucleophilic
SRA	*Streptomyces refuineus* Agar
TE	Thioesterase
TIC	Total ion chromatogram
TLC	Thin-layer chromatography
TSA	Trypticase Soy Agar
UV/VIS	Ultra-violet/Visible

Table of Contents

List of Figures

Appendices Figures:

List of Tables

List of Schemes

CHAPTER 1: Introduction

1.1 Microbial secondary metabolites

1.1.1 Definition and history of secondary metabolites

Secondary metabolites, also known as natural products (Williams *et al*., 1989), are products of metabolism that are not essential for normal growth, development or reproduction of an organism. These substances are cited by many authors as molecules that are synthesized by living organisms but are not required for essential functions like cell division and metabolism (Carmichael, 1992; George *et al*., 1993). Alternatively, other opinions consider secondary metabolites either as playing a key role in fixing beneficial genetic characteristics within the producing organism or as having a strong connection with the primary metabolism at molecular and cellular levels (Roze *et al*., 2011).

In comparison to secondary metabolites, primary metabolites (such as nucleic acids, carbohydrates, lipids and proteins) are common for all biological organisms and vital for their growth and multiplication (Barrios-Gonzales *et al*., 2005).

It is well established that many types of living systems (both prokaryotes and eukaryotes) are producers of secondary metabolites. However, the major contributions are found within *Streptomyces* bacteria (Bérdy, 2005).

Since early times, secondary metabolites were mainly known as plant natural products. Microorganisms, and more specifically their secondary products, were used in food conservation and production of wine, bread, cheeses and other fermented milk products even before the discovery of the microorganisms. For example, as a method of preservation, yogurt was produced by the acidic fermentation of lactose sugar present in the milk (Zourari *et al*., 1992).

The first antibiotic secondary metabolite to be isolated and crystalized was a mycophenolic acid produced by *Penicillium glaucum* and published by Gosio in 1896 (Birkinshaw *et al*., 1948; Muth *et al*., 1975; Bérdy, 2005). The structure of the compound is shown in **Figure 1.1**.

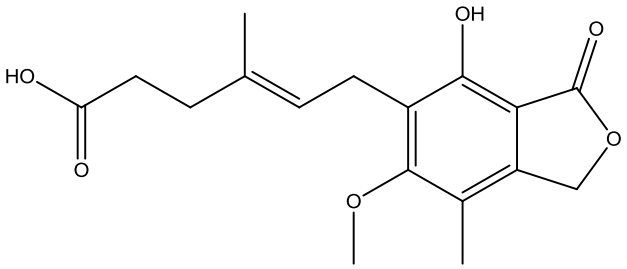

Figure 1.1: Structure of mycophenolic acid

The secondary metabolites produced by microbes that show signs of either antimicrobial (antibacterial, antifungal, antiprotozoal), antitumor and/or antiviral activities, used to be named antibiotics (Bérdy, 2005). Antibiotics were also defined as "…*chemical compounds produced by actinomycetes, fungi, or bacteria that interfere with some essential bacterial structure or process with no effects on the eukaryotic host having the infectious agents*" (Hiroshi and Ryoichi, 2006). These classical definitions of antibiotics were extended by Bérdy, to include all secondary metabolites controlling the growth routes, duplication processes, and affecting the life cycle of prokaryotic and eukaryotic cells at the biomolecular level, at low concentration.

1.1.2 Streptomycetes secondary metabolites

Streptomyces is a genus of filamentous Gram-positive bacteria occurring naturally in soil and also present in aquatic habitats (Moran *et al*., 1995). Members of the streptomyces genus are known to possess two growth phases during their developmental cycle: a vegetative and a reproductive phase (Manteca *et al*., 2005). During the first stage and once the growth conditions are favourable (availability of nutrients for example)**,** a streptomyces spore germinates into a germ tube that elongates into a branched vegetative mycelium. Then, and probably due to nutrient reduction, aerial branches emerge from the soil and start growing to form aerial hyphae. The second phase of the growth is marked by the formation of compartments in the branches of the aerial hyphae resulting in the development of the prespore segments that are transformed subsequently into mature spores **(Figure 1.2)** (Hopwood, 1999 review).

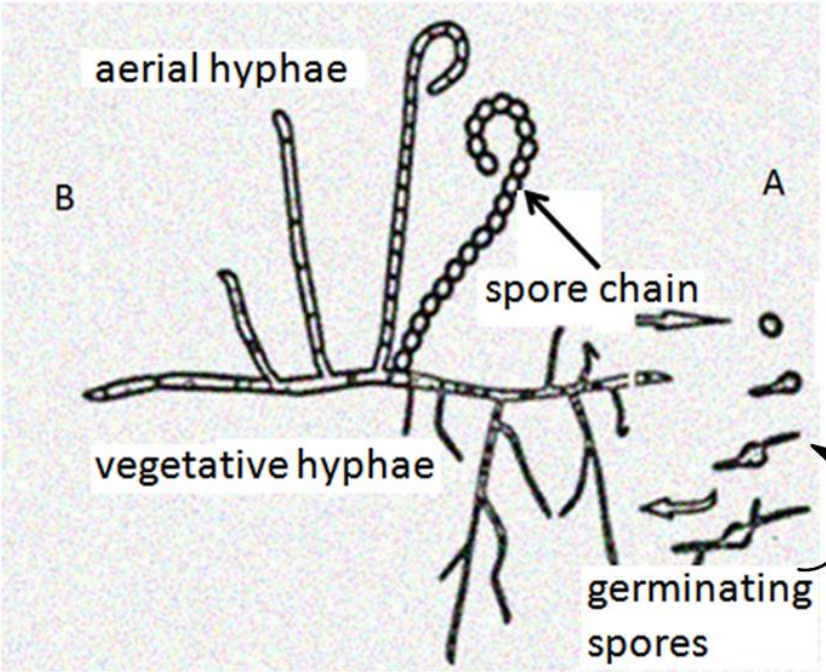

Figure 1.2: Schematic representation of the developmental life cycle of *Streptomyces coelicolor* (Edited from original source: Osmialowska *et al*., 2006). (**A)**: vegetative phase. A spore from aerial hyphae germinates into a germ tube that grows into vegetative hyphae. (**B)**: Reproductive phase. Development of aerial hyphae (from the vegetative one) and formation of a spore compartments which differentiate into mature spores.

Streptomyces species have been and continue to be an important source of bioactive natural products. Members of this group produce more than 7,600 known active metabolites. That represents about 33% of all known bioactive microbial natural products (Olano *et al*., 2009). These natural products have various biological activities such as antibiotics (tetracyclines, cephalosporins, aminoglycosides, macrolides for example) (Bérdy, 2005), anticancer drugs (such as anthracyclines: aclarubicin, daunomycin, adriamycin and doxorubicin for example) (Olano *et al*., 2009) or as immunosuppressive agents (rapamycin for example) (Gummert *et al*., 1999) (**Figure 1.3**).

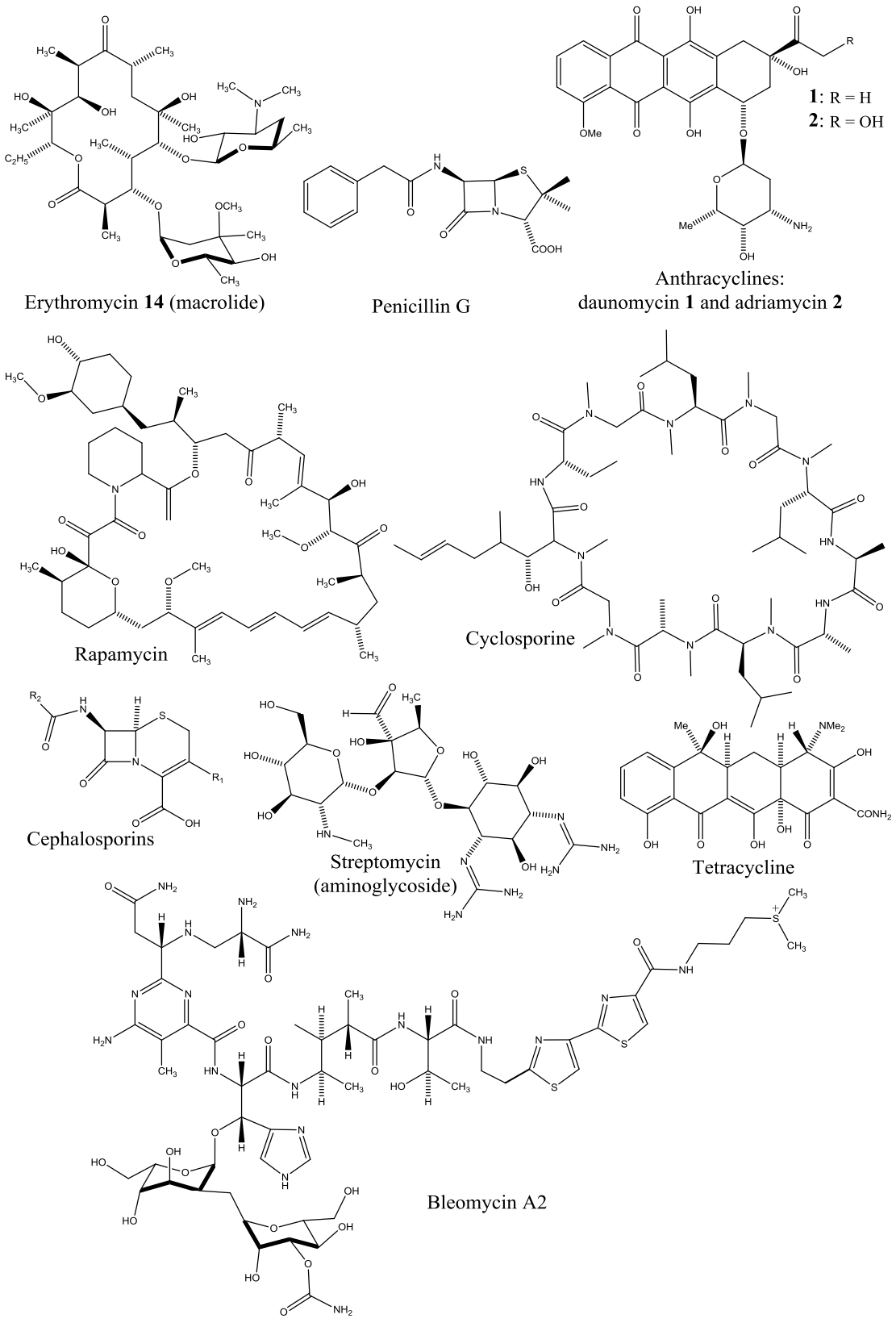

Figure 1.3: Examples of medicinally important natural products.

1.1.3 Streptomycetes secondary metabolites containing naphthoic acid moiety

The antitumor natural products azinomoycins A **3** and B **4** and some members of the enediyne natural products such as neocarzinostatin (NCS) **5**, kedarcidin **6**, and N1999A2 **7** are examples of secondary metabolites containing naphthoic acid (NA) moiety (**Figure 1.4A**).

A detailed discussion about the biological activity, mode of action and biosynthesis of azinomycins A **3** and B **4** is outlined in **section 1.6**. As to the role of the azinomycins' NA component in the inhibition of DNA synthesis, it was found (Zang and Gates, 2000; Coleman *et al*., 2002) that its intercalates into DNA and hence positioning the azinomycins into the major groove enabling the formation of interstrand cross-links (ISCs) which, are accompanied by alkylation of DNA (Terawaki and Greenberg, 1966a; Lown and Majumdar, 1977). As consequence, DNA synthesis is inhibited.

The enediyne natural products NCS **5**, kedarcidin **6**, and N1999A2 **7** belong to the nine-membered enediyne family of antitumor antibiotics, which are of great interest as potent anticancer agents. They possess a reactive enediyne core (in black in **Figure 1.4**) that is able to induce DNA damage and eventually cell death. Enediynes are capable of undergoing Bergman (or Myers-Saito) cyclization to form 1,4-benzenoid diradicals, which abstract hydrogen atoms from the sugar backbone of the DNA molecule resulting in single and double strand lesions (Shen *et al*., 2003). This high reactivity against DNA makes enediynes very toxic, limiting their use in clinical applications. However, their potent activity may be beneficial if used as modified enediynes to target the DNA of cancerous tumors specifically. For example, the conjugation of NCS with poly(styrene-*co*-maleic acid) (SMA) has significantly reduced the toxicity of NCS **5** and as result, the SMANCS derivative has been used to treat heptoma in Japan since 1994 (Galm *et al*., 2005). The enediynes compounds **5** and **6** are members of the 9-membered enediyne chromophore natural products also known as chromoproteins as they are non-covalently associated with an apo-protein (N1999A2 **7** lacks the apo-protein). The apo-protein is known to play a key role in protecting, carrying and delivering the biologically active enediyne chromophore to its DNA target (Shen *et al*., 2003; Galm *et al*., 2005; Luo *et al*., 2008; Lohman *et al*.,

2013). A brief discussion regarding the biosynthesis of NCS **5** and kedarcidin **6** is outlined in **section 1.3.2**.

The elucidation of NCS chromophore **5** was established in 1985 (Edo *et al*., 1985) and was initially isolated from the culture filtrate of *Streptomyces carzinostaticus* by Ishida and co-workers in 1965 (Ishida *et al*., 1965). Structurally, NCS chromophore **5** is characterised by a nine membered enediyne core (black), a deoxyaminosugare (green), a fucosamine fragment (red) and a NA moiety (blue). The latter plays a significant role in the action of NCS **5** bioactivity. Indeed, NA moiety is an important element in binding the NCS **5** chromophore to its apoprotein NcsA. Furthermore, it aids in positioning the chromophore **5** into the minor groove by intercalating into DNA (Luo *et al*., 2008).

The chromoprotein antitumor antibiotic kedarcidin **6** was isolated from broth filtrate of *Streptoalloteichus sp*. ATCC 5365 (formerly *actinomycete* L585-6) in 1992 by Leet and co-workers and its structure was elucidated on the basis of extensive spectroscopic analysis and chemical degradation (Leet *et al*., 1992). The original structural proposal was revised firstly in 1997 by Hirama and co-workers (Kawata *et al*., 1997) and secondly in 2007 by Myers and co-workers (Ren *et al*., 2007) with the final structure shown in **Figure 1.4**A (Lohman *et al*., 2013). In addition to the enediyne core (black), kedarcidin **6** possesses two peripheral moieties, a (*R*)-2-aza-3-chloro-β-tyrosine (red) and an iso-propoxy-bearing 2-naphthonate moiety (blue), as well as two deoxysugars (green). In a manner similar to NCS **5**, the NA moiety of kedarcidin **6** plays significant role in the biological activity by intercalating into DNA and therefore placing the chromophore **6** into the minor groove (Luo *et al*., 2008).

The nonprotein enediyne N1999A2 (NA2) **7**, isolated (in a stable form) from a culture supernatant of *Streptomyces sp*. AJ9493 (Ando *et al*., 1998), possesses a naphthoic acid moiety (blue) and an enediyne core (black) (**Figure 1.4A**). The chemical structure of NA2 **7** is analogous to the NCS chromophore **5** but differ in that compound **7** lacks the C10 amino-sugar residue and C13-C14 carbonate. In a manner similar to NCS **5**, the naphthoic acid moiety of NA2 **7** binds into DNA through

intercalative mechanism and therefore aids in placing the chromophore **7** in the minor groove (Luo *et al.*, 2008).

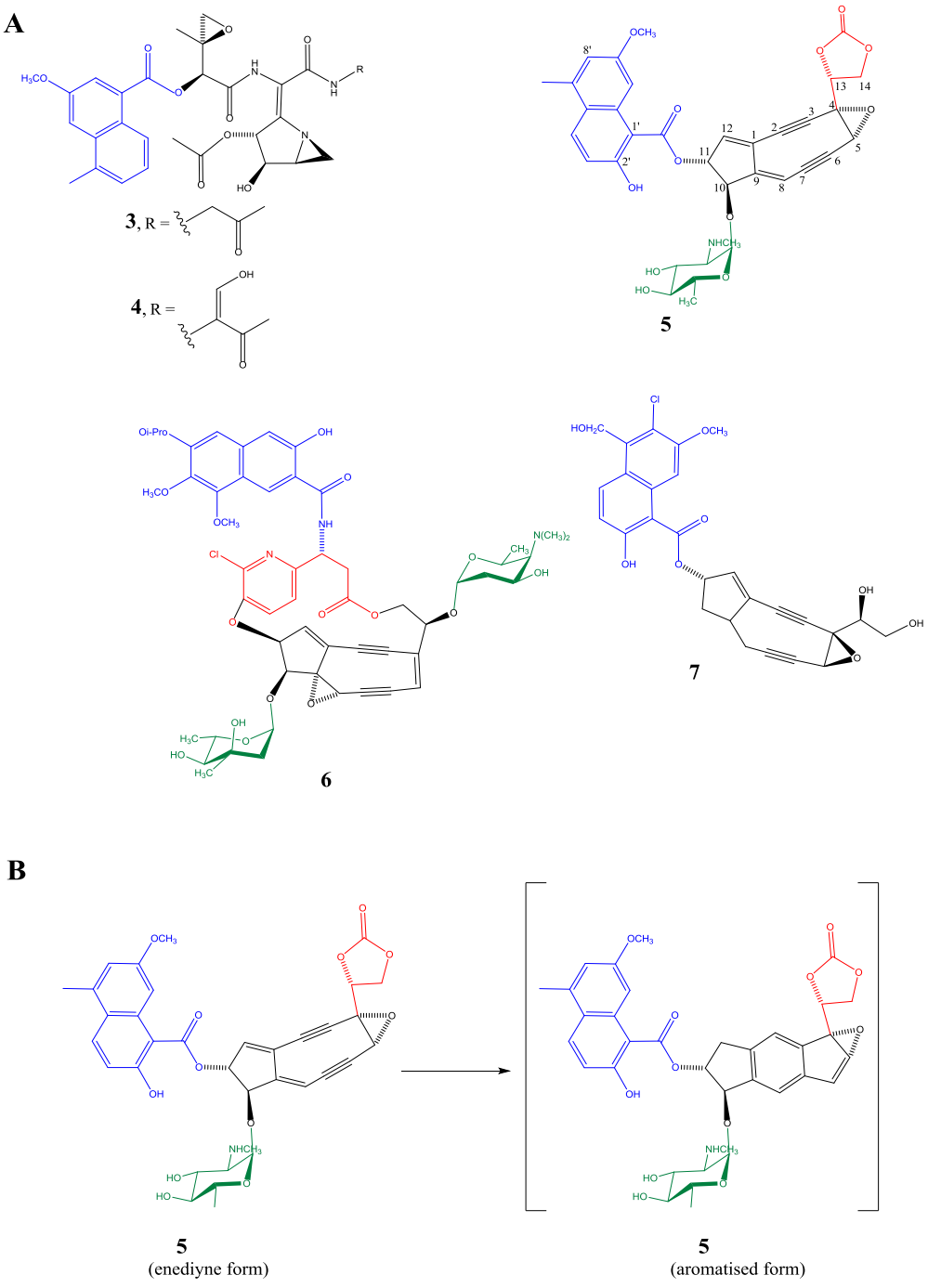

Figure 1.4: Examples of naphthoic acid moiety (highlighted in blue) containing natural products. (A): Azinomycin A **3**, azinomycin B **4**, neocarzinostatin **5**, N1999A2 **7** and kedarcidin **6**. (B): Structure of the NCS enediyne form and the proposed aromatised form (Galm *et al.*, 2005).

1.2 DNA and DNA binding secondary metabolites

As a genetic material of all cellular organisms, deoxyribonucleic acid (DNA) provides the chemical basis for storing and encoding genetic information (Kennard, 1993). The DNA double helix was identified by Watson and Crick in 1953 as the fundamental structure for DNA (Russel, 2002).

The bases in DNA are monocyclic or bicyclic structures and are referred to as pyrimidines (cytosine and thymine) or purines (guanine and adenine) respectively. DNA consists of two right handed helical chains running in opposite directions to form a double helix **(Figure 1.5A)**. Each strand is a series of nucleotides, and each nucleotide is composed of a sugar-phosphate compound attached to one of four nitrogen-containing bases. The sugar-phosphate compounds link together to form the backbone of the strand. The base pairs are responsible for holding two strands together and it is the sequence of bases in DNA that encodes the genetic information of the molecule.

There are three helical forms of DNA (A, B and Z) that vary with respect to a range of constraints that depict their three-dimensional structure. B-form DNA is the most biologically relevant as it persists under physiological conditions.

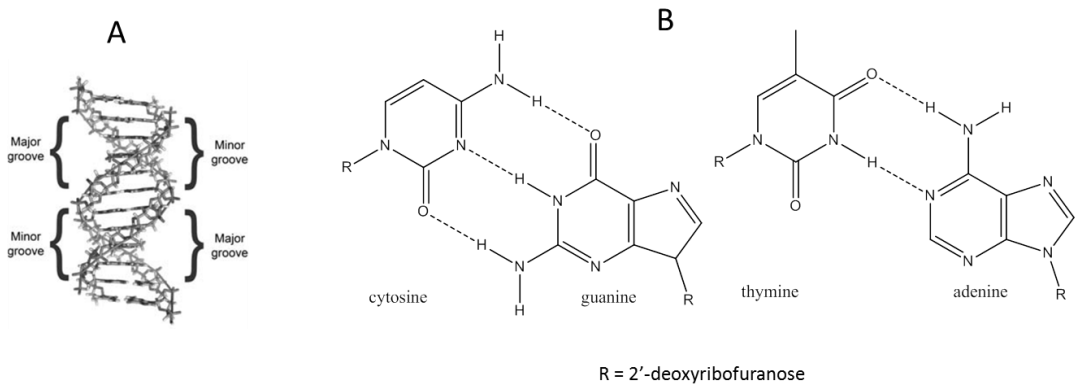

Figure 1.5: (A): Double strand DNA structure showing the presence of minor and major grooves (Picture taken from Brenno and Alexandre, 2009). (B): DNA base-paring: cytosine pairs with guanine and adenine pairs with thymine (original source: Wojciechowski and Leumann, 2011).

The space across the helix between each of the deoxyribose-base glycosidic bonds is about 10.8 Å and a purine-pyrimidine base pair fits perfectly within this space, whereas two pyrimidine bases would be too far away from each other to allow hydrogen bonding. The rotation angle made by the base pairs with respect to each adjacent pair is 36^{o} resulting in exact 10 base pairs per helical turn. Furthermore, the distance separating two base pair is precisely 3.4 Å (Reddy *et al*., 2001). As can also be seen from **Figure 1.5A**, two obvious grooves arise from this structure; the larger is known as the major groove, the narrower as the minor groove. Within the major groove, a large portion of the base is exposed and this is where most protein-DNA interactions occur whereas small molecules including many antibiotics, mostly bind in the minor groove, in many cases because they have complementary shape to it. Binding can be reversible, *e.g.* non-covalent minor groove binders netropsin and distamycin, or irreversible, *e.g.* covalent minor groove binders including anthramycin**.** Some ligands interact with specific bases, *e.g.* anthramycin interacts with guanine in the minor groove and azinomycin B reacts also with guanine bases but in the DNA major groove. This is important because they can be used in areas where there are known to be lots of guanine bases. As it is normally vacant, the minor groove represents a susceptible site of attack by anthramycin (Reddy *et al*., 2001) and the major groove an ideal alkylation site for azinomycins (Armstrong *et al*., 1992).

1.3 Polyketide natural products

1.3.1 Introduction to polyketides

Polyketides (PKs) represent a large class of structurally diverse and complex natural products, found in microbes and plants (Minow *et al*., 2007). Many clinically important drugs such as radicicol, rifamycin and lovastatin (**Figure 1.6**) are of polyketide origin.

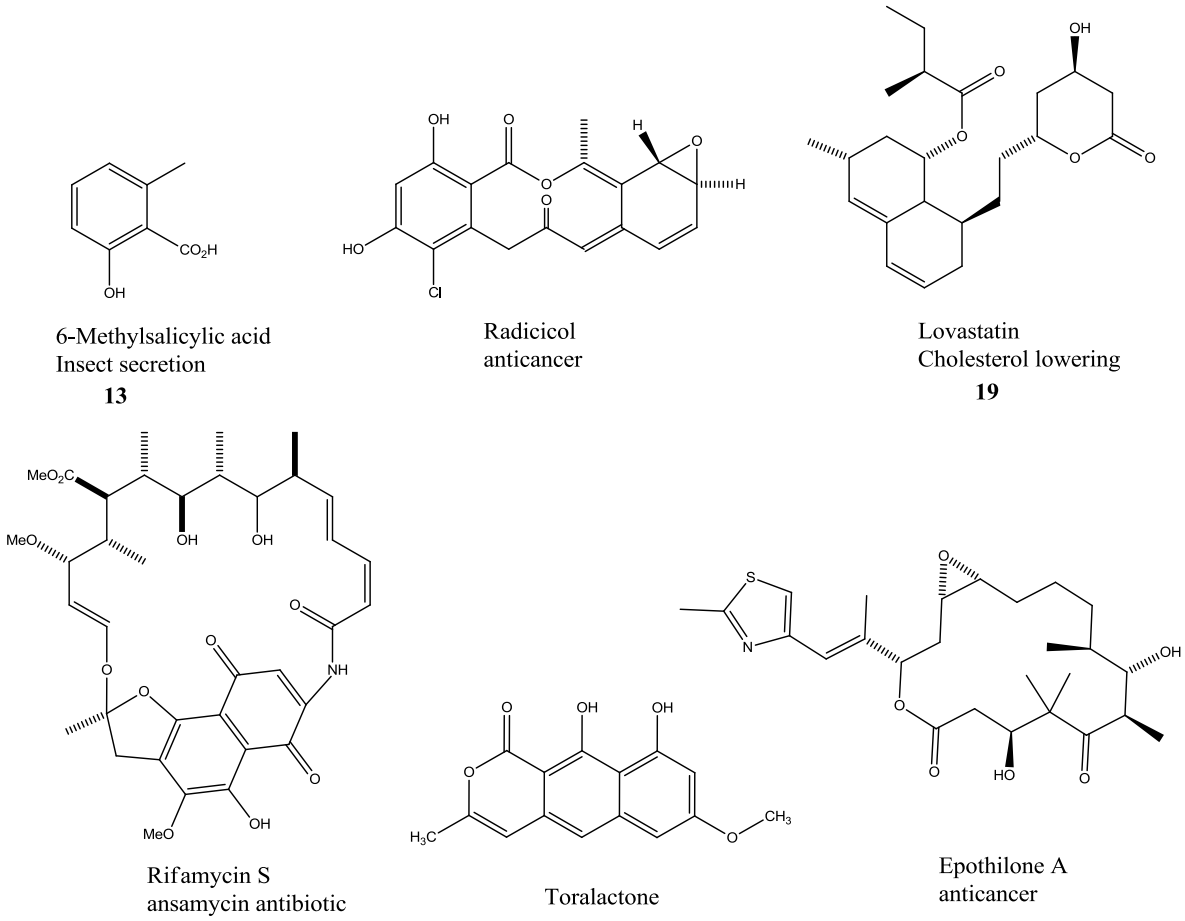

Figure 1.6: Polyketide structures.

It has been more than 100 years since J. N. Collie, an organic chemist, first introduced the term polyketide (PK) following the discovery of aromatic compounds produced while conducting organic synthesis studies on pyrones (Collie and Myers, 1893). In 1907, Collie rightly proposed that a triketone **8** was an intermediate molecule in the production of the aromatic compound, orcinol **9** following the treatment of pyrone **10** with water and strong alkali (**Figure 1.7**) (Collie, 1907). He also proposed that

polyketone compounds are intermediate metabolites formed by living cells during the production of many natural phenolic compounds. Collie also noted that the suggested polyketone intermediates could be hypothetically considered as polymers of ketenes **11**. Hence, he coined the terms ketides and polyketides. Sadly, his ideas and the polyketide field were not developed for more than half a century (Staunton and Weissman, 2001).

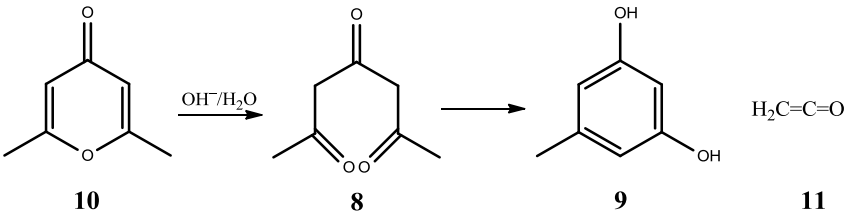

Figure 1.7: Synthesis of orcinol **9** from dehydroacetic acid **10.**

In the mid-1950s, Birch extended Collie's idea and suggested that the proposed polyketones might arise in living cells from acetate units by repeated condensation reactions (Birch *et al*., 1955). At that time the isotope tracer technique including carbon-14 was well established which enabled Birch to test his acetate hypothesis. Based on series of experiments involving the feeding of [1-^{14}C]-acetate **12** to the fungus *Penicillium patulum* that produces 6-methylsalicylic acid (6-MSA) **13**, he was able to confirm his biosynthetic proposal as described in **Figure 1.8**.

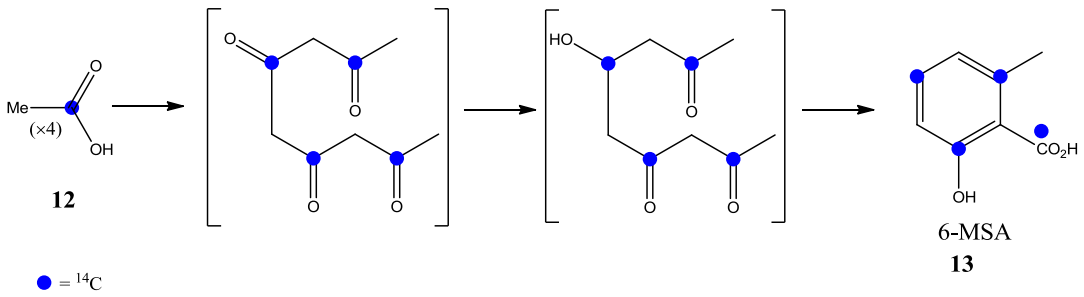

Figure 1.8: Feeding experiment showing that 6-MSA **13** is derived from four [1-^{14}C]-acetates.

The search in the field of natural products has thrived since the decade of the 1950s and as a consequence, there has been a sharp increase in the number and diversity of PK structures (Staunton and Weissman, 2001; Hertweck, 2009). Some highly renowned aromatic and aliphatic compounds are illustrated in **Figure 1.6**.

Birch had benefited from the advanced knowledge and carried out more acetate feeding studies to many organisms known to produce secondary metabolites. The results of these experiments established that both aromatic and non-aromatic compounds were biosynthetised from acetate units. Hence, Birch was able to produce a unified hypothesis known as "Collie-Birch polyketide hypothesis" (Staunton and Weissman, 2001). Birch's findings were based on mechanistic reasoning and on the fact that fatty acids were well known to be derived from acetates (Bentley and Bennett, 1999). The relationship between fatty acid biosynthesis and that of PKs continues to influence thinking in the PK field to this day. Therefore it is appropriate to give a brief illustration of the fundamental pathways employed in fatty acid biosynthesis. **Figure 1.9** elucidates detailed steps used in the fatty acid biosynthesis.

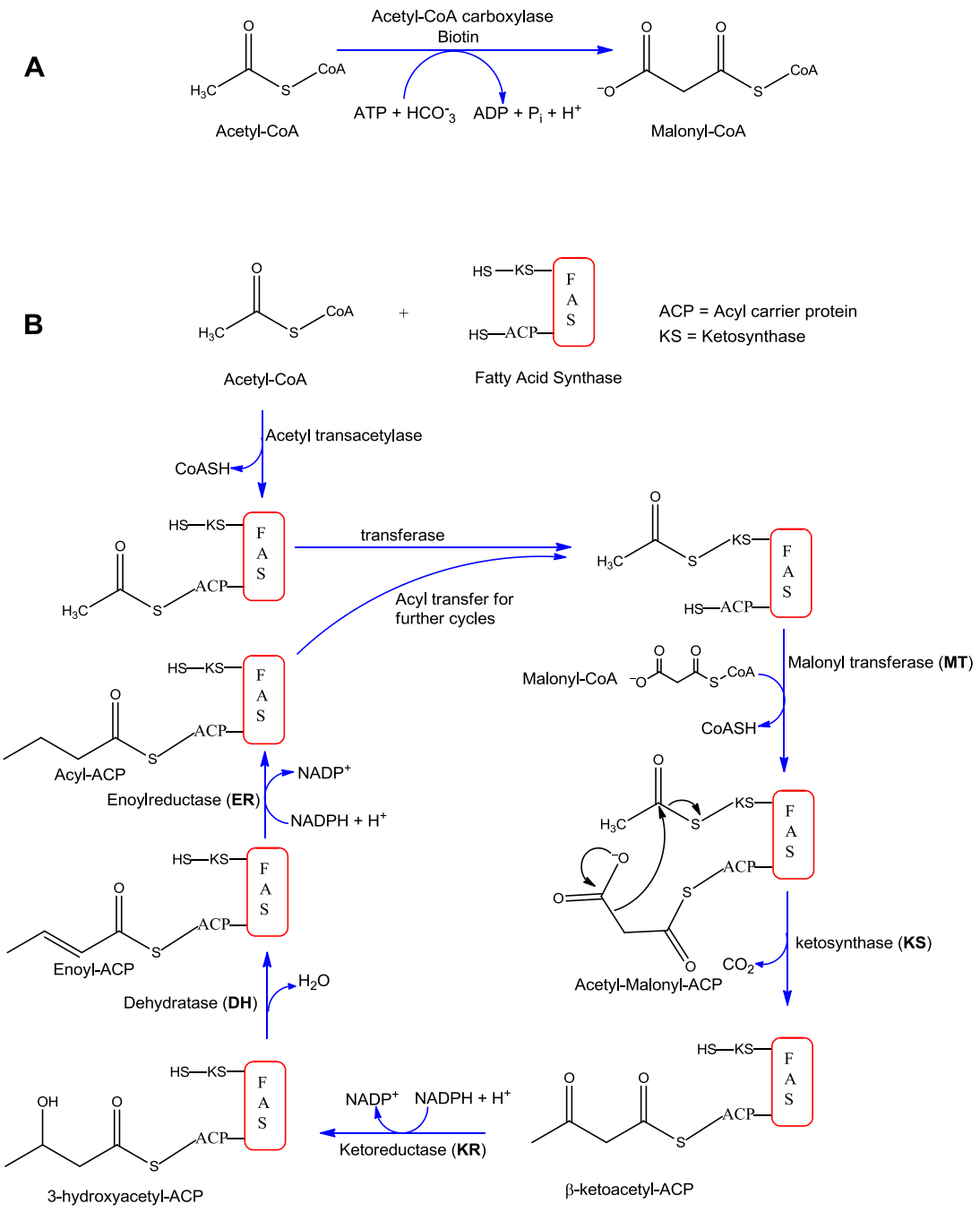

Figure 1.9: Fatty acid biosynthesis. (A): Synthesis of malonyl-CoA by the action of acetyl-CoA carboxylase. Biotin is a required as cofactor. (**B**): Detailed steps of fatty acid biosynthesis.

During the first step of fatty acid synthesis (**Figure 1.9B**), the acetyl group (starter unit) gets transferred from CoA to ACP by acetyl CoA-ACP transacylase (acetyl transacylase). The acetyl (acyl) group next gets transferred to the KS arm of FAS. Then the starter substrate bound to the KS active-site cysteine is condensed with the chain extender substrate (malonyl moiety), which has been transferred to the

phosphopantetheine thiol attached to the serine hydroxyl group on the ACP (the phosphopantetheinylation of ACP is illustrated in **Figure 1.10)**. The resulting β-ketoacyl moiety produced is fully processed by stepwise ketoreductase (KR)-, dehydratase (DH)-, and enoyl reductase (ER)-catalysed reactions prior to the next elongation step. Repeated cycles are carried out by the same enzymes until the correct length chain has been formed. At that stage, the fatty acid is cleaved from the ACP by a thioesterase (TE) enzyme.

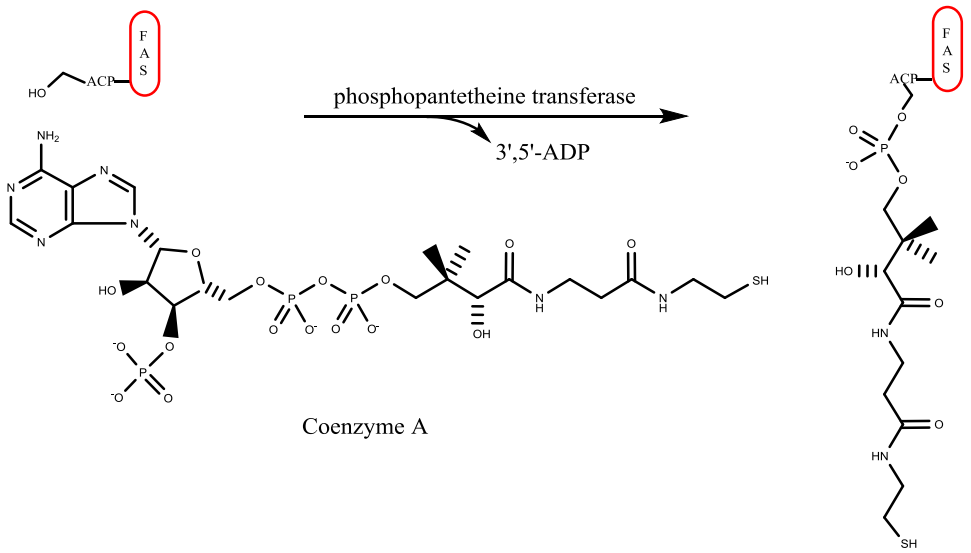

Figure 1.10: Phosphopantetheinylation of the acyl carrier protein (ACP).

The period from the 1950s through the 1980s saw few biochemical studies made in the area of polyketides since the main emphasis at that time was the development of new synthetic routes in organic chemistry (Smith and Tsai, 2007). The development of nuclear magnetic resonance (NMR) and mass spectrometry (MS) during the 1960s, as powerful new spectroscopic techniques, enabled the chemists and biochemists to accomplish several structural and elucidation studies of complex compounds within relatively short period of time (weeks or even days) rather than years as it used to be before (Staunton and Weissman, 2001). As consequence, several spectacular total syntheses of polyketides such as erythromycin **14** (**Figure 1.3**), toralactone and rifamycin (**Figure 1.6**) were completed. The period did see also the first successful isolation and characterization of the 6-methylsalicylic acid **13** synthase from *Penicillium patulum* (Smith and Tsai, 2007).

During the 1980s and with the advancement of genetic and molecular biology techniques, the way was opened towards the discovery of genes and their equivalent proteins involved in polyketide biosynthesis (Staunton and Weissman, 2001). The Hopwood group was a pioneer to study the genetics of *Streptomyces coelicolor*, a bacterium known to biosynthesise the aromatic PK actinorhodin **15** (**Figure 1.11**). Over a number of years of carefully designed experiments and thorough scientific research, the authors were able to sequence the genes coding for the enzymes of actinorhodin biosynthesis and established the primary sequence of the equivalent proteins. Further comparison studies between the discovered proteins and various known protein sequences, showed a strong homology with numerous enzymes of fatty acid synthases. The similarities were shown mainly at the active sites of enzymes such as KS, ACP and KR. The actinorhodin PKS was found to be type II dissociable system similar to FAS of bacteria. The scientific community was motivated by the important achievement in the genetic field and since then a wealth of new PKS systems were discovered **(**Malpartida and Hopwood, 1984; Hopwood and Sherman, 1990; Hopwood, 1997).

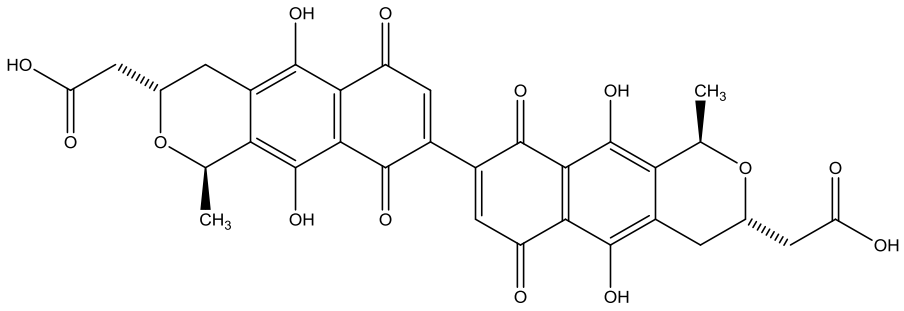

15

Figure 1.11: Structure of antibiotic actinorhodin produced by *S. coelicolor*.

1.3.2 Polyketide biosynthesis

Polyketides (PKs) are made by enzymes called polyketide synthases (PKSs). PKSs operate in a similar fashion to fatty acid synthases (FASs): they share common chemical mechanisms involved in chain extension and are alike in building a carbon backbone from simple acyl precursors, such as acetyl and malonyl units. Both PKSs and FASs assemble their products (PKs and fatty acids respectively) by successive rounds of decarboxylative Claisen condensation between an acyl thioester and an α-carboxythioester (**Figure 1.12**). However, PKSs diverge from FASs in that PKSs use

optional reductive steps to process the β-keto group, thus giving rise to a more complex pattern of functionalities and that FASs catalyse a full reductive cycle after each elongation cycle. Additional factors such as the broad spectrum of starting biosynthetic precursors (e.g. acetyl-, ethyl-, propionyl-, and butyryl-CoA) and the chain length control further expand the variability of the chemical structure of PK natural products compared to the relative simple structure of fatty acids. An additional aspect that set the PK chain apart from simple fatty acid chain is that the resulting polyketide, which is cleaved from the PKS system, can be subjected to tailoring modification reactions (Hertweck, 2009).

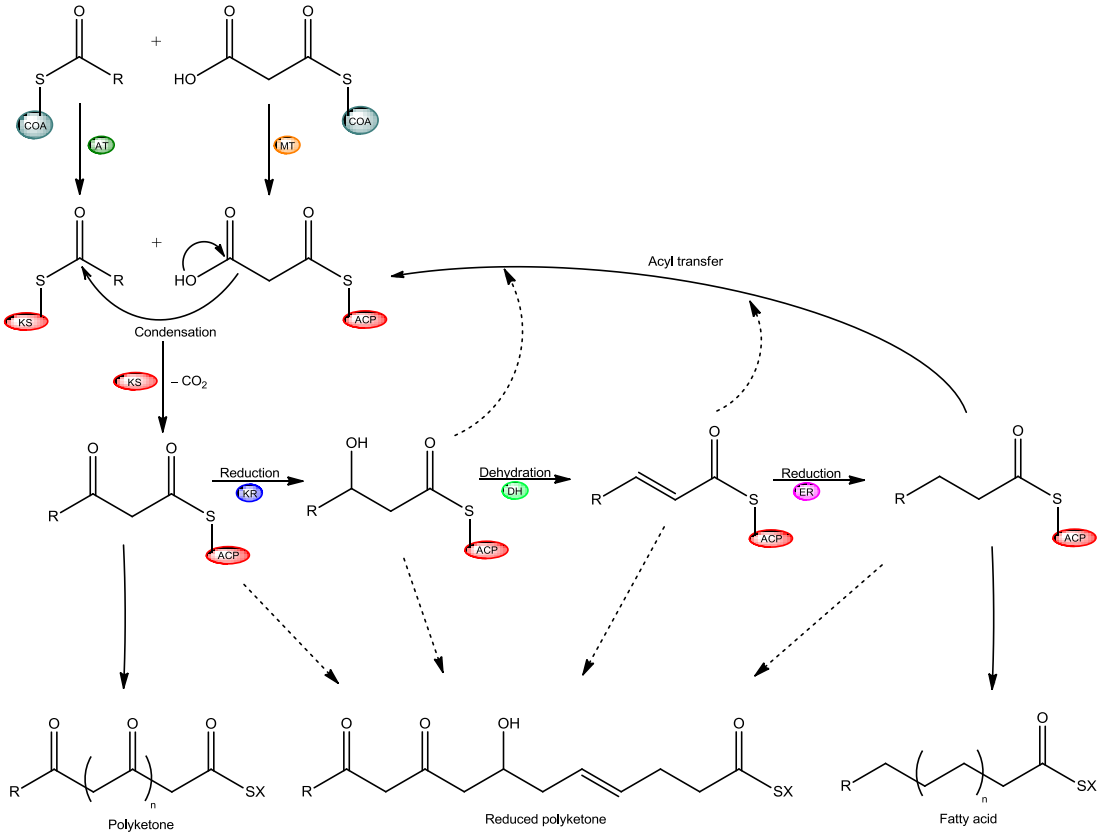

Figure 1.12: Generic reaction scheme for the biosynthesis of both fatty acids and polyketides (PKs). In fatty acid biosynthesis the β-ketoacyl unit produced after each chain elongation is completely reduced to a saturated carbon prior to the next condensation reaction. In PK biosynthesis, the reductive steps of the β-ketoacyl

moiety are optional: they can be partly or fully omitted before the next elongation cycle.

The biosynthesis of polyketides is initiated by decarboxylative Claisen condensation between an activated simple acyl starter unit attached to the ketosynthase (KS) active site with an extender unit, which is initially derivatised as thioester using active thiol group at the active site of acyl carrier protein (ACP). Before any condensation step, the ACP domain is first posttranslationally modified at the active site serine by attaching phosphopantetheine to the hydroxyl in fashion similar to fatty acids synthesis (**Figure 1.10)** (Fischbach and Walsh, 2006). Following each chain extension of the polyketide backbone, the β-ketoacyl thioester intermediate may retain its β-C=O group or can be selectively reduced by ketoreductase (KR), dehydratase (DH), and enoyl reductase (ER) tailoring domains. The elongation cycles are repeated until the defined PK chain lengths are obtained, and the thioester-bound products are cleaved from PKS systems. Further post-PKS modifications such as cyclisation, methylation and glycosidation are very common (Bentley and Bennett, 1999; Hertweck, 2009).

By analogy to FASs, PKSs can be classified into three different classes (type I, type II and type III) based on their architectures and catalytic mechanisms, (Hopwood, 1997; Staunton and Weissman, 2001; Hertweck, 2009): type I PKSs consist of one or more large multifunctional proteins containing covalently linked function domains which are organised into modules. Based on the number of elongation cycles catalysed by KS domain, type I PKSs can be further subdivided into two groups, modular (non-iterative) and iterative systems (these particular groups of PKSs will be detailed in the next paragraphs).

Type II PKS systems are composed of individual enzymes that carry a single set of iteratively acting activities. These protein systems are responsible for the biosynthesis of numerous bacterial aromatic polyketides such as actinorhodin **15** (**Figure 1.11**), tetracenomycin **16** and doxorubicin **17** (**Figure 1.13**). The minimal PKS needed for chain synthesis consists of two KS-like enzymes (KS_α and KS_β) and an ACP to anchor the growing PK chain. Additional proteins such as cyclases, aromatases and ketoreductases are required for a controlled cyclisation and aromatisation. Finally,

the polyphenols are tailored by oxygenases, glycosyl and methyl transferases (Flores-Sanchez and Verpoorte, 2009).

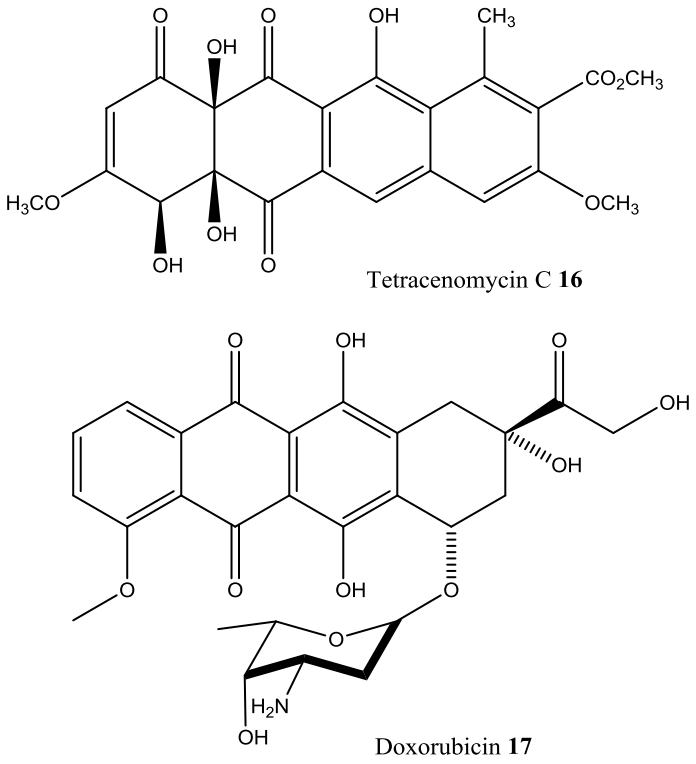

Figure 1.13: Structure of the aromatic polyketides tetracenomycin C **16** and doxorubicin **17**.

Type III PKSs are simple homodimers of ketosynthases (KSs) and act in an iterative manner. Their single active site in each monomer is used to carry out all decarboxylation, condensation, cyclisation and aromatisation reactions. Additional enzymes such as oxidoreductases, cyclases or glycosyl-transferases often modify the complete polyketide structure to generate the mature, biologically active polyketide natural product. In contrast to type I and type II PKSs that utilise substrates bound to an ACP, type III PKSs act on CoA thioesters directly. Despite their structural simplicity, type III PKSs produce a wide array of compounds such as chalcones, pyrones, stilbenes and resorcinolic lipids. Type III PKSs have been found in bacteria and fungi, as well as plants (Hertweck, 2009).

In modular type I PKS systems, which are found mainly in bacteria and recently in protozoans (Zhang *et al*., 2013), each catalytic domain catalyses a single chemical reaction and each module is responsible for the addition and modification of a single

building block to the growing polyketide chain that remains covalently attached to an acyl carrier protein domain. The modular system is best exemplified by 6-Deoxyerythronolide B synthase (6-DEBS) that catalyse the assembly of 6-deoxyerythronolide B **18** (6-DEB), the macrocyclic core of macrolide antibiotic erythromycin A **14** produced by *Saccharopolyspora erythraea* (Donadio and Katz, 1992) (**Figure 1.14).** 6-DEBS consists of three giant proteins designated DEBS 1, DEBS 2 and DEBS 3, organised into six catalytic modules. Each module harbours at least a set of 3 core domains (ketosynthase (KS), acyl transferase (AT), and acyl carrier protein (ACP)), satisfying the minimal requirement for each chain elongation (Khosla *et al*., 2007). All six modules harbour the ketoreductase domain for the subsequent reduction process of the newly generated β-ketone. Only module 4 carries dehydratase (DH) and enoyl-reductase domains that further modify the product of KR domain. At the front of DEBS 1 is an additional loading didomain (Load) that primes the KS of module 1 with propionyl-CoA. At the end of module 6, there is a thioesterase (TE) domain (denoted End in **Figure 1.14**) and responsible for the release and cyclisation of the completed PK chain.

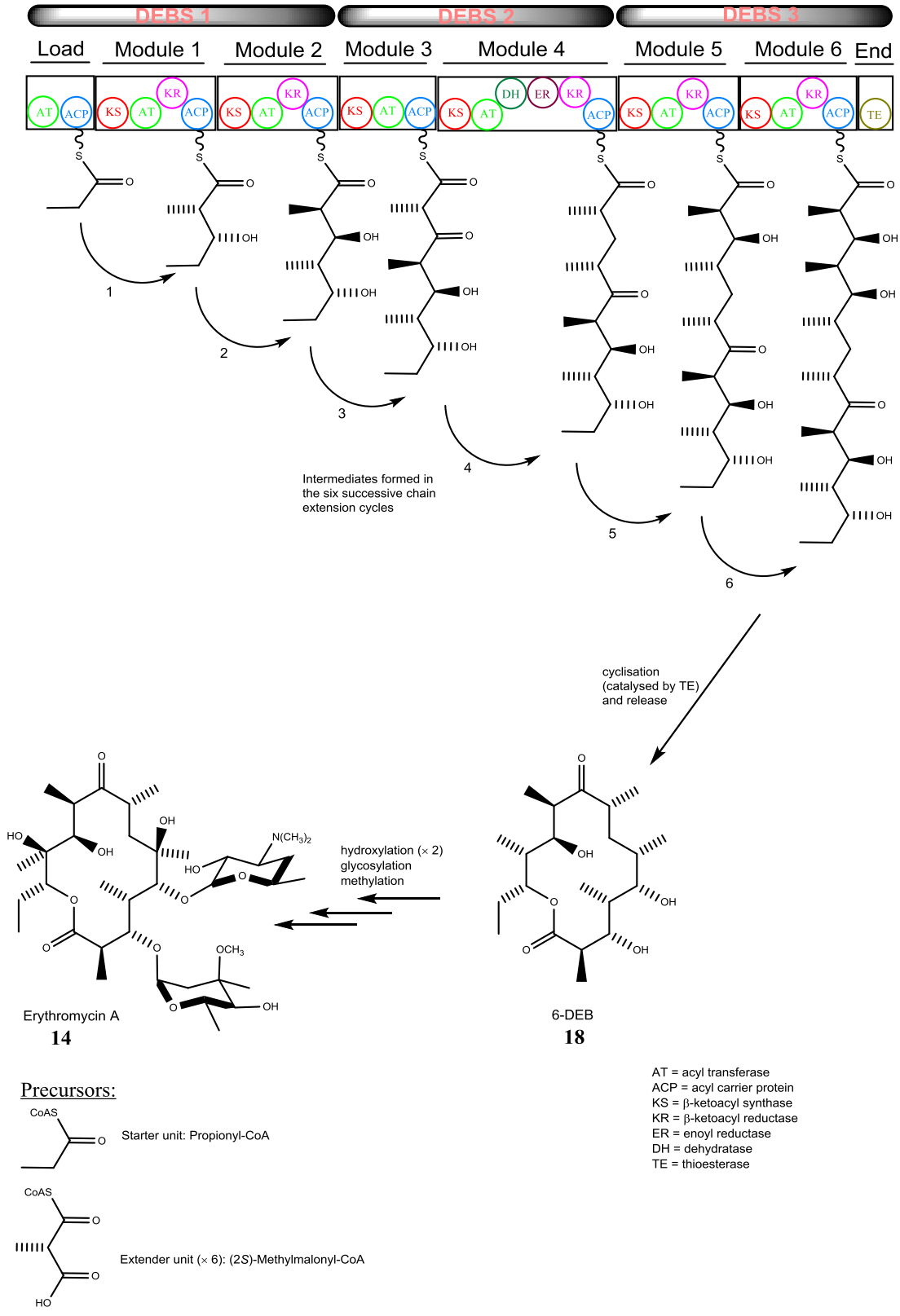

Figure 1.14: Modular organisation of the 6-deoxyerythronolide B synthase (DEBS) and putative intermediates.

In iterative type I PKSs, the same module repeatedly catalyses chain elongation and modification (Staunton and Weissman, 2001). Iterative type I PKSs such as 6-methylsalicylic acid **13** (6-MSA) synthase and lovastatin **19** (**Figure 1.6**) synthase were initially known to be found exclusively in fungi (Staunton and Weissman, 2001; Chan *et al*., 2009) until recent discovery of these enzymes in bacteria as well (Zhang *et al*., 2013). **Figure 1.15** illustrates the involvement of the iterative type I PKS in the biosynthesis of 6-MSA **13**. Indeed this PKS does not contain a distinct module for each round of chain extension; the single module of 6-methylsalicylic acid synthase is used iteratively.

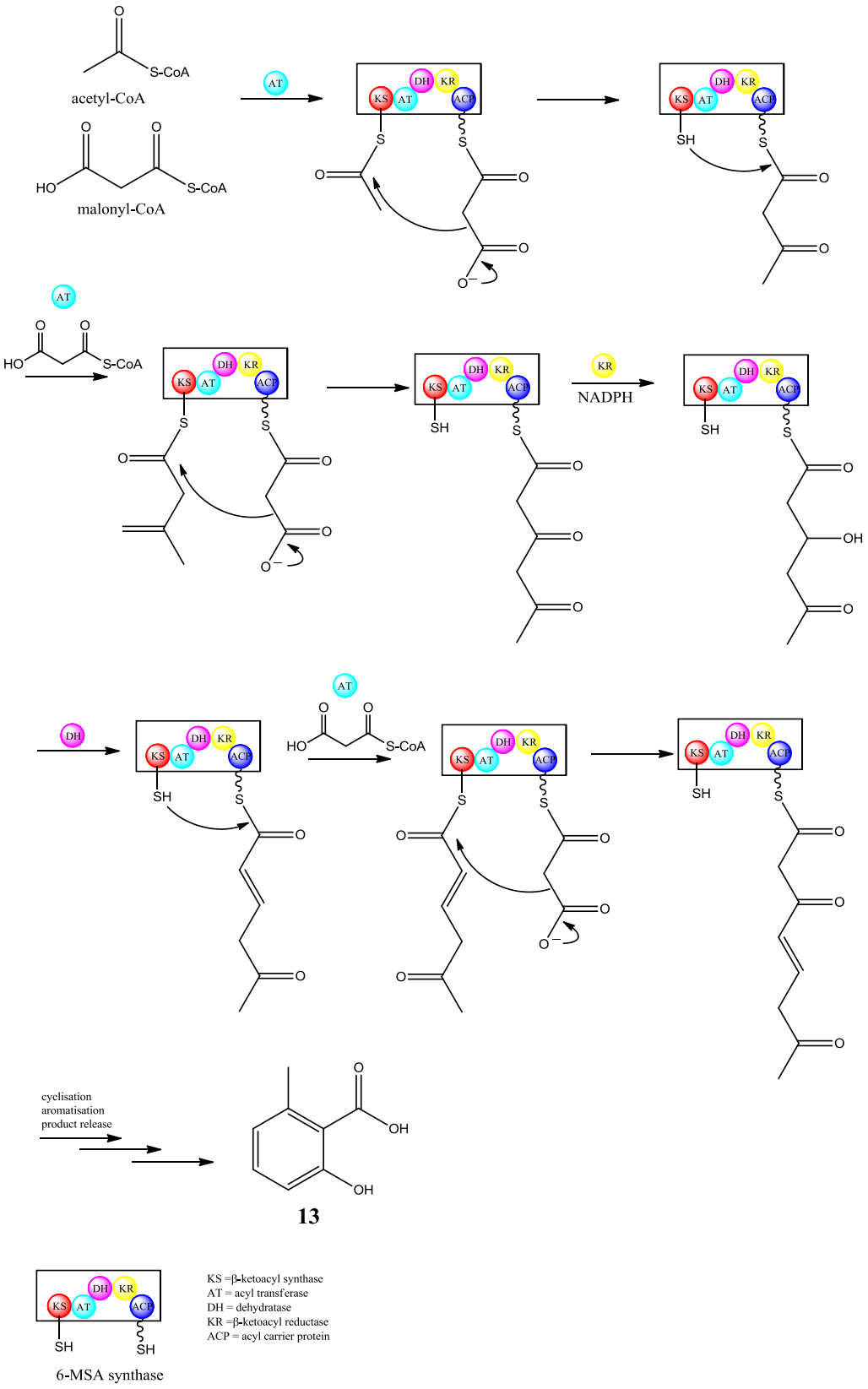

Figure 1.15: The biosynthetic pathway for 6-methylsalicylic acid **13** (6-MSA). The polyketide **13** is assembled from one acetyl-CoA entity and three units of malonyl-CoA catalysed by 6-MSA synthase.

Bacterial iterative type I PKSs catalyse relatively simple (mono- or bicyclic) aromatic polyketide products (**Figures 1.4A** and **1.16**) compared to the complex and multicyclic aromatic PKs produced by bacterial iterative type II PKSs (actinorhodin **15** and tetracenomycin **16** for example) (Zhang *et al.*, 2013). The first clone of an iterative type I PKS for bacterial PK biosynthesis was achieved by Bechthold and co-workers in 1997 (Gaisser *et al.*, 1997). The authors cloned successfully the avilamycin **20** PKS (AviM) that catalyses the biosynthesis of the orsellinic acid **21** moiety (**Figure 1.17**) produced by *Streptomyces viridochromogens* Tü57.

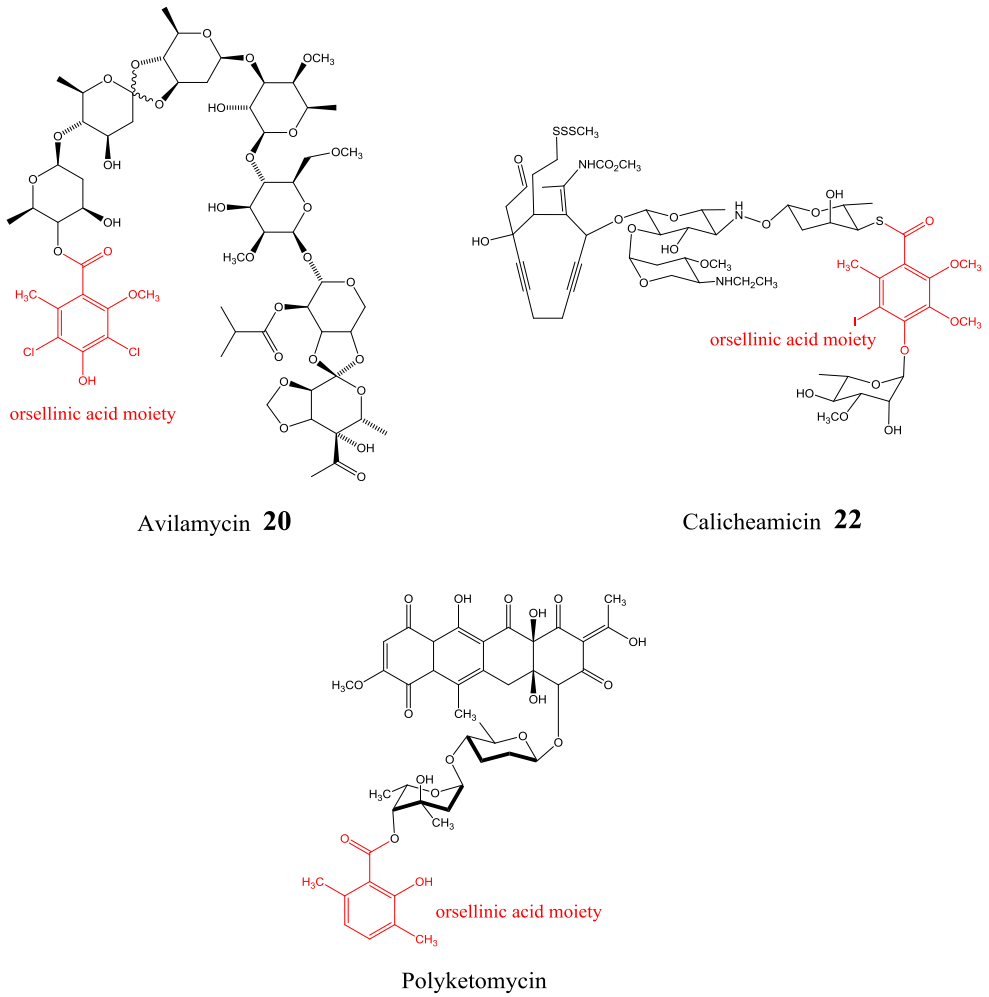

Figure 1.16: Example of bacterial natural products containing simple aromatic polyketide moieties (highlighted in red) catalysed by iterative type I PKSs.

Five years later, a second successful clone of a bacterial iterative type I PKS was achieved by Thorson and co-workers (Ahlert *et al.*, 2002). This PKS (CalO5) is responsible for the biosynthesis of the orsellinic acid **21** moiety of calicheamicin **22**

compound. Amazingly, CalO5 and AviM PKSs share high sequence homology and exhibit identical domain organisation (KS, AT, DH and ACP). It is worth to mention that both PKSs completely omit the KR function.

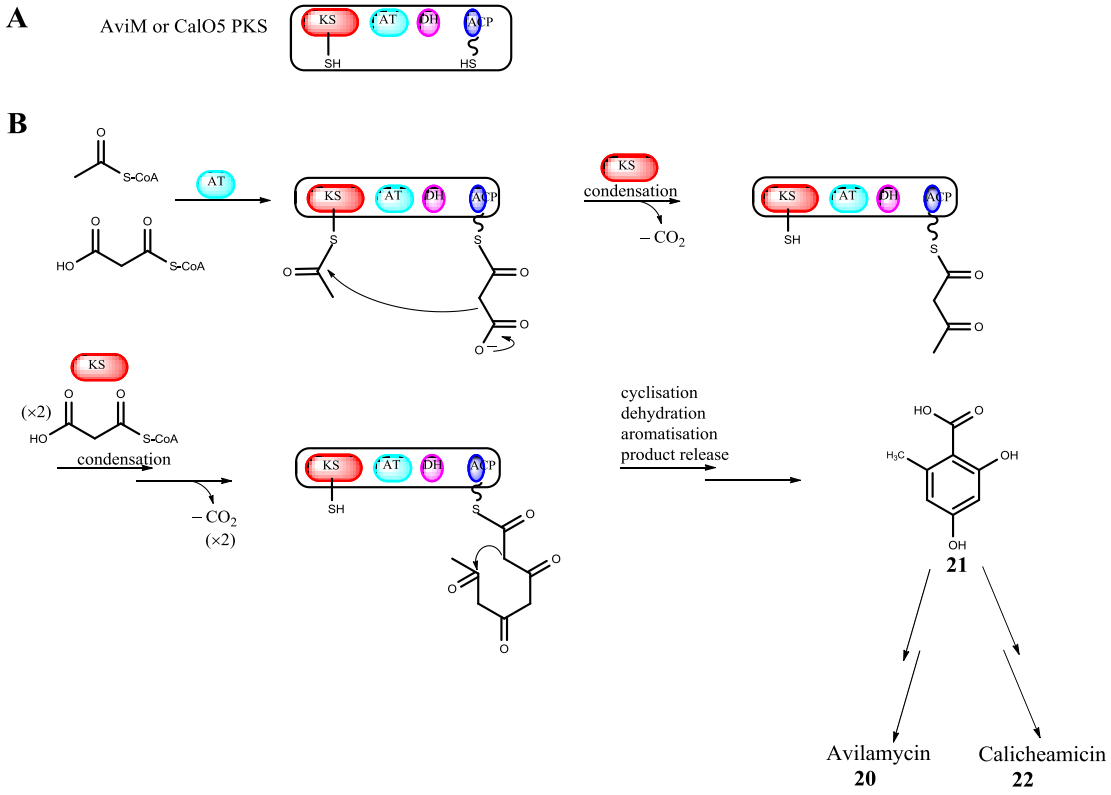

Figure 1.17: Biosynthesis of orsellinic acid **21**. (A): Identical domain organisation of bacterial aromatic iterative type I PKSs AviM and CalO5. KS, β-ketoacyl synthase; AT, acyl transferase; DH, dehydratase; ACP, acyl carrier protein. (B): Biosynthesis of **21** catalysed by AviM or CalO5.

In 2005, Shen and co-workers reported the cloning and sequencing of the NCS **5** biosynthetic gene cluster from *Streptomyces carzinostaticus* ATCC15944 (Liu *et al.*, 2005). The authors revealed the identification of two distinct type I PKSs, NcsE and NcsB (and other tailoring enzymes) catalysing the biosynthesis of the enediyne core and the naphthoic acid entity respectively. In addition, it was proposed that the deoxy aminosugar moiety is likely to be derived from D-mannose-1-phosphate. Based on mechanistic analogy and sequence homology with recently cloned and characterised enediyne PKSs, C-1027 (Liu *et al.*, 2002) and CalO5 (Ahlert *et al.*, 2002), Shen and co-workers proposed that NcsE catalyses the formation of the nascent linear PK

intermediate from one acetyl CoA and seven malonyl CoAs in an iterative process. Subsequently and upon other enzyme activities (NcsE1-E11 and epoxide hydrolases F1 and F2), the linear polyunsaturated chain is desaturated and cyclased to form the enediyne core (**Figure 1.18D**). On the basis of genetic analysis, It was also proposed that the biosynthesis and the incorporation of the naphthoic acid moiety into the enediyne core of **5** is catalysed by the iterative type I PKS NcsB and four other tailoring enzymes NcsB1, NcsB2, NcsB3 and NcsB4 (**Figure 1.18A-C)**. The biosynthetic steps towards the napthoic acid moiety were predicted (Cooke *et al*., 2007; Luo *et al*., 2008) as follow: First, NcsB catalyses the condensation of one acetyl-CoA with 5 malonyl-CoA units to form 2-hydroxy-5-methyl-1-naphthoic acid **23** as free intermediate, followed by the hydroxylation of the naphthoic acid **23** at position C7. The hydroxylation step is catalysed by the cytochrome P-450 hydroxylase NcsB3 generating the 2,7-dihydroxy-5-methyl-1-naphthoic acid **24** product. The generated acid **24** is subsequently methylated at C7 hydroxy group by *O*-methyltransferase NcsB1 to afford 2-hydroxy-7-methoxy-5-methyl-1-naphthoic acid **25**. Then the ATP-dependent CoA ligase (NcsB2) catalyses the activation of **25** into **26a** *via* the acyl-AMP **26b** as an intermediate. This later reaction was demonstrated *in vitro* by liu *et al*. (2005) and Cooke *et al*. (2007). As final step, the ester **26a** is incorporated into NCS **5** by the NcsB4 acyltransferase.

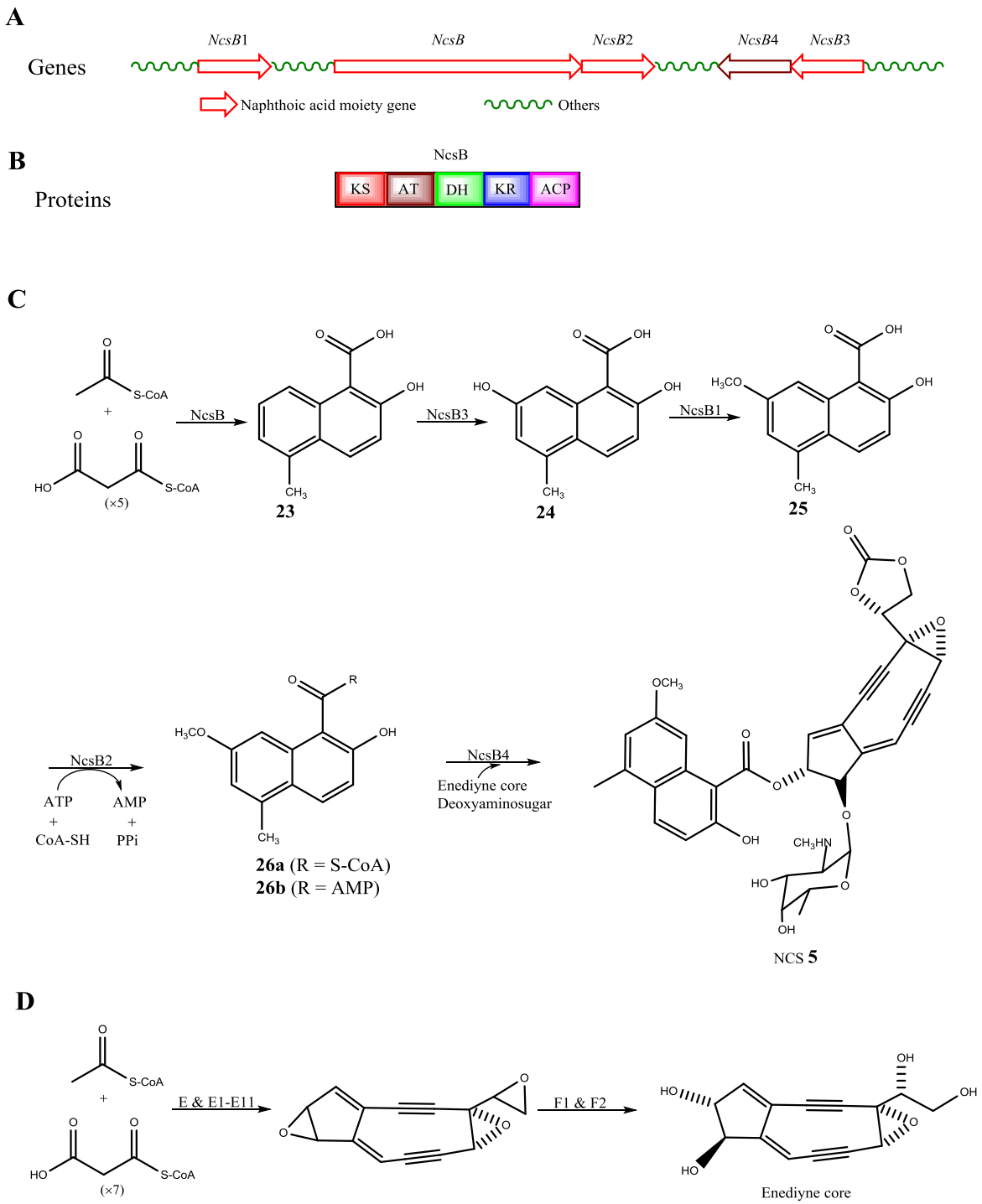

Figure 1.18: Proposed biosynthetic pathway for NCS chromophore **5** (Liu *et al.*, 2005; Luo *et al.*, 2008). (A): Genes encoding the enzymes NcsB, NcsB1, NcsB2, NcsB3 and NcsB4 for the biosynthesis and the incorporation of the naphthoic acid moiety **25** into **5**. (B): Domain organizations of NcsB. KS, ketoacylsynthase; AT, acyltransferase; DH, dehydratase; KR, ketoreductase; ACP, acyl carrier protein. (C): The biosynthesis of **26** and its incorporation into **5**. (D): Biosynthesis of the enediyne core.

In 2013, the biosynthetic gene cluster of kedarcidin **6** (*ked*) was cloned from *Streptoalloteichus sp*. ATCC 53650 and sequenced (Lohman *et al*., 2013). Based on bioinformatics analysis and comparative studies between *ked* gene cluster and the formerly cloned and characterised gene clusters of some of the 9- and 10-membered enediynes such as NCS **5** (Liu *et al*., 2005) and calicheamicin **22** (Ahlert *et al*., 2002), the authors revealed the identification of *kedE*, a gene in the cluster encoding for enediyne PKS and others (*kedE1-kedE11*, *kedM, kedS*, *kedL*, *kedJ, kedD2*, *kedF*) encoding accessory enzymes for enediyne core biosynthesis (**Figure 1.19C**). The identity of this cloned gene cluster was partly corroborated by the co-expression of *kedE–kedE10* in *E. coli* leading to the formation of a signature heptaene product previously implicated in enediyne core biosynthesis (Liu *et al*., 2002; Ahlert *et al*., 2002; Liu *et al*., 2005).

The disclosure of genes encoding for 2-aza-β-tyrosine moiety were sort of mystery for the authors as no biosynthetic work on 2-aza-β-tyrosine had been reported yet. Fortunately and upon comparative studies between the *ked* gene cluster with the biosynthetic clusters of enediynes C-1027 and maduropeptin (MDP), the authors revealed the presence of seven conserved genes (*kedY*, *kedY1* - *kedY5* and *kedE6*). Inspired by these findings, Shen and co-workers proposed a biosynthetic pathway for (*R*)-2-aza-3-chloro-β-tyrosine initiating from 2-aza-L-tyrosine in a manner similar to the biosynthesis pathway of L-tyrosine derived components in C-1027 and MDP (**Figure 1.19A**).

Insights into the biosynthesis of the iso-propoxy-bearing 2-naphthoic acid moiety were also based on comparative analysis between the *ked* cluster and the enediynes NCS **5** and MDP which naphthoate and benzoate moieties are biosynthesised by the iterative type I PKSs, NcsB (Liu *et al*., 2005) and MdpB (Van Lanen *et al*., 2007), respectively. A close examination of *ked* cluster revealed the presence of genes encoding for iterative type I PKS with a similar domain organisation as NcsB and MdpB. As consequence, Shen and co-workers proposed a role of type I PKS in the biosynthesis of the 2-naphthonate moiety. However, this proposal is awaiting validation as all experimental attempts carried by the authors to establish the exact biosynthetic origin of 2-naphthoic acid moiety failed.

The comparative analysis of *ked* cluster to NCS **5** and MDP also unveiled the identification of five genes, denoted KedN1-N5 and displaying high sequence homology with enzymes responsible for the biosynthesis of 1-naphthoic acid moiety in NCS **5**. These findings led the authors to propose the intermediacy of 3,6,8-trihydroxy-2-naphthoic **27** acid in kedarcidin biosynthesis (**Figure 1.19B**).
The biosynthetic steps towards the iso-propoxy-bearing 2-naphthoic acid moiety were proposed as illustrated in **Figure 1.19B**. The compound **27** is first hydroxylated at position C7 by the cytochrome P-450 monoxygenase KedN3 generating compound **28**. Catalysed by *O*-methyltransferase KedN1, the acid **28** is then triply *O*-methylated to produce compound **29**. In order to furnish the isopropoxy group, Shen and co-workers proposed double *C*-methylation of **29** by the radical *S*-Adenosyl methionine (SAM) methyltransferase KedN5 producing 3-hydroxy-7,8-dimethoxy-6-isopropoxy-2-naphthoic acid **30**. Lastly, the acid **30** is activated by KedN2 as a naphthonyl-CoA **31** and joined to the enediyne core via an amide linkage to the (*R*)-2-aza-3-chloro-β-tyrosine entity by the acyltransferase KedN4.

In regard to the biosynthesis of the two deoxysugars and their incorporation, Shen and co-workers proposed a D-glucose-1-phosphate as a common precursor and that both finally modified sugars are coupled to the enediyne core by two glycosyltransferases denoted KedS6 and KedS10.

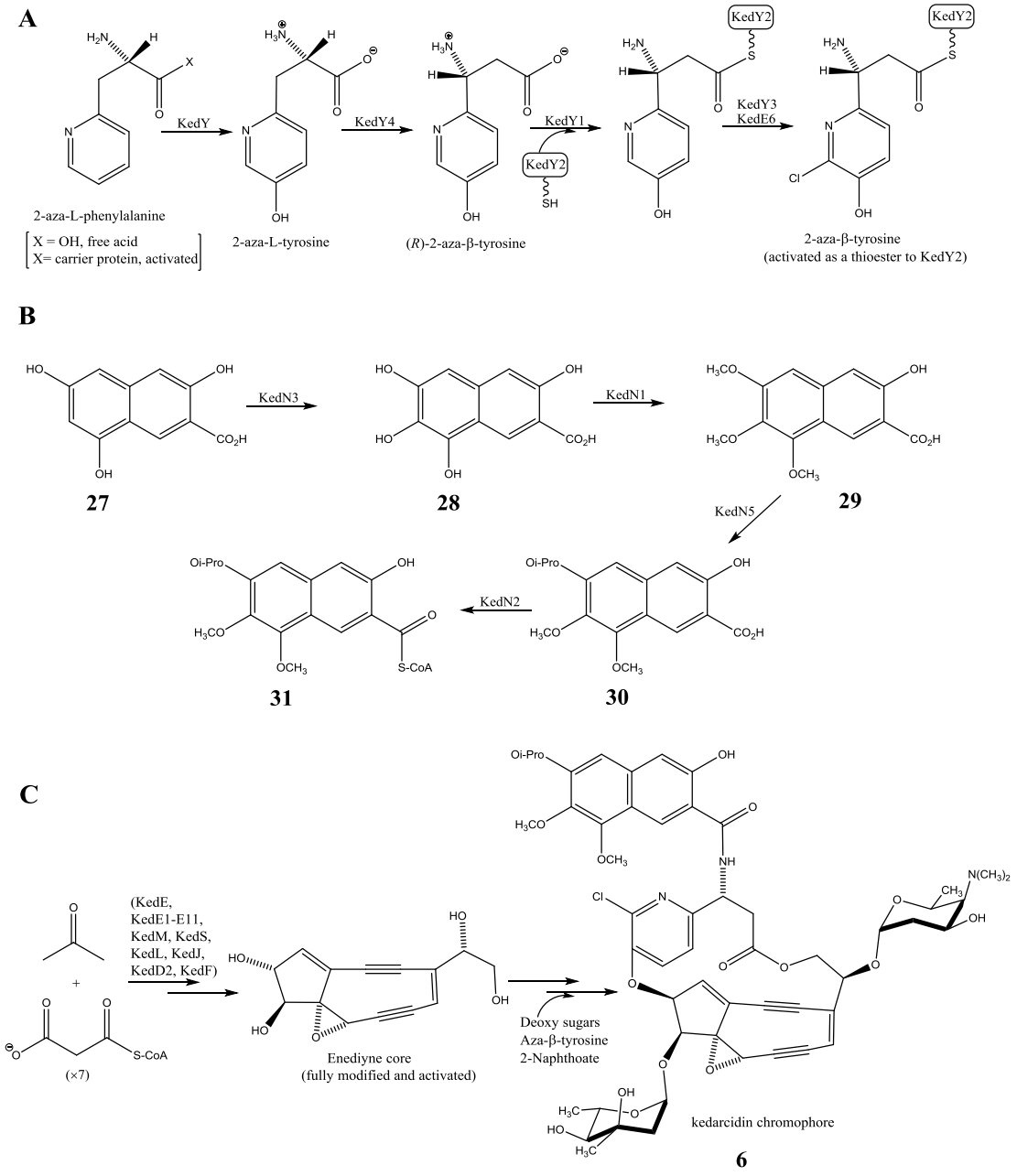

Figure 1.19: The kedarcidin chromophore **6** biosynthetic pathway (Lohman *et al*., 2013). (A): Biosynthetic pathway of (*R*)- 2-aza-β-tyrosine moiety from 2-aza-L-phenylalanine. (B): Biosynthetic pathway of naphthoic acid **30** from 3,6,8-trihydroxy-2-naphthoic **27** (C): Acetate origin of the enediyne core and its incorporation (in addition to the other moieties) into the chromophore **6**.

1.4 Nonribosomal peptide natural products

1.4.1 Introduction

Nonribosomal peptides (NRPs) represent a large family of structurally diverse natural products produced in the secondary metabolism of microorganisms such as bacteria and fungi (Fischbach and Walsh, 2006; Strieker *et al*., 2010). A vast majority of these

natural products exhibit important biological activities, such as antibiotics penicillin (Ozcengiz *et al*., 2013), immunosuppressive agent cyclosporine (Shu, 1998) and antitumor agent bleomycin (Glam *et al*., 2005) (**Figure 1.3)**.

1.4.2 Biosynthesis

NRPs are biosynthesised by large multidomain enzymes, the nonribosomal peptide synthetases (NRPSs), which link many simple amino acids (both proteinogenic and non-proteinogenic) building blocks by a cascade of condensation reactions (Fischbach and Walsh, 2006). NRPSs are organised into modules and each module catalyses one round of polypeptide chain elongation and associated functional group modifications. NRPSs could also function iteratively by using more than one module at a time during chain elongation (Fickers, 2012). A typical NRPS module consists of a least three core domains (C-A-PCP) catalysing a specific reaction for the incorporation of a monomer. The adenylation domain (A) selects the amino acid and activates it, by ATP-hydrolysis, as amino acyl adenylate. The activated amino acid is then transferred to the peptidyl carrier protein domain (PCP) (also known as a thiolation domain (T)) where it is covalently tethered to its 4′-phosphopantetheine (4′-PP) cofactor as thioester. The transfer of this cofactor to the conserved serine residue of PCP is catalysed by dedicated phosphopantetheinyl transferases (Fischbach and Walsh, 2006) (**Figure 1.20**).

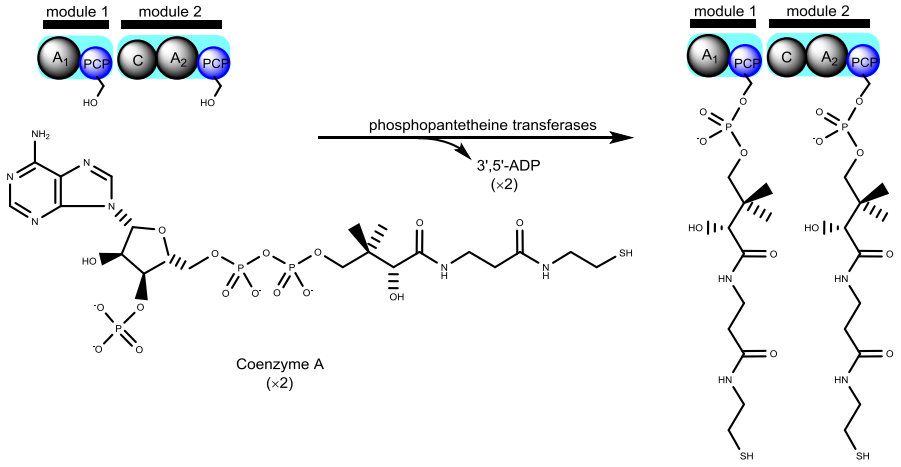

Figure 1.20: Postranslational modification of PCP domains by phosphopantetheinyl transferases.

The condensation domain (C) catalyses the formation of the peptide bond between the activated amino acids from two adjacent modules. A sketch of the fundamental activities of C-A-PCP core domains is illustrated in **Figure 1.21**.

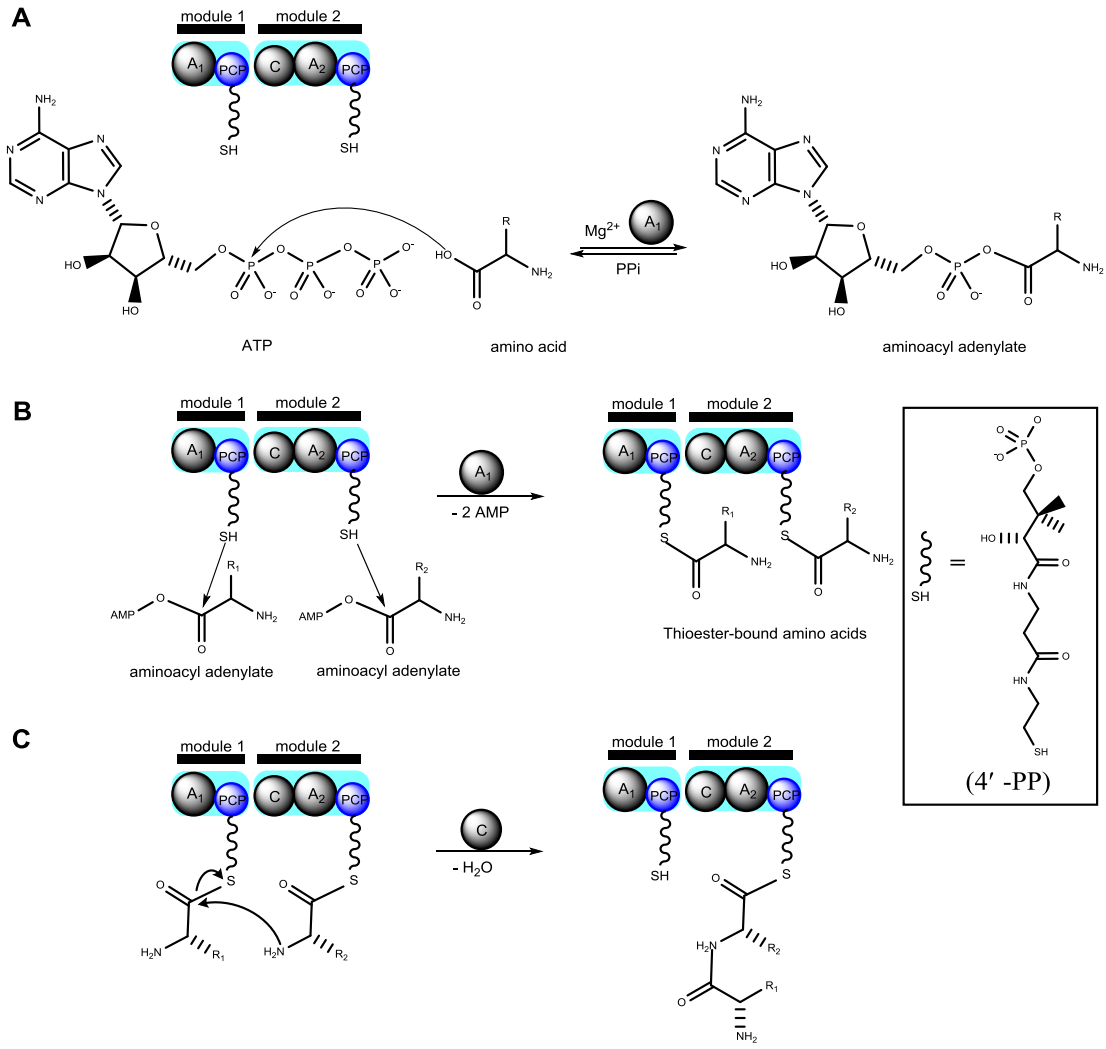

Figure 1.21: Core domains of NRPSs and their basic enzymatic reactions: (A): Recognition and activation of amino acid by the adenylation domain (A_1). (B): Transfer of the aminoacyl adenylate to the PCP domain where it is covalently tethered to its 4′-phosphopantetheine (4′-PP) cofactor as thioester. (C): An amide bond-forming condensation reaction between amino acyl substrates bound to PCPs of adjacent modules: the C domain catalyses the nucleophilic attack of the amine of the acceptor substrate onto the electrophilic thioester of the donor substrate.

Besides the core domains, each NRPS contains tailoring domains and two additional modules dedicated for chain-initiation and termination. The tailoring domains are supplementing the core domains and are involved in the diversification of the growing peptidyl chain by catalysing useful chemical modifications. For example, the

transformation of the thiazoline ring into thiazole during bleomycin biosynthesis is catalysed by an Oxidase (Ox) domain. Epimerase (E) domain alters the stereochemistry of α positions of aminoacyl groups. The initiation module is a two-domain A-C module involved in the activation and incorporation of the first amino-acid of the NRP. The most common termination domain in the last NRPS module is a thioesterase (TE) catalysing the release of the nascent aminoacyl chain (from the final PCP) by direct nucleophilic cleavage of the thioester. The product can then be released from the assembly line by two different mechanisms (Fischbach and Walsh, 2006): intermolecular hydrolysis as in vancomycin biosynthesis and intramolecular macrocyclisation affording macrolactones as in the biosynthesis of the core ring of rapamycin. In some PKS/NRPS hybrids, the TE domain of the final module is replaced by a reduction domain (R) as in azinomycin B biosynthesis (Zhao *et al*., 2008).

1.5 Similarities and differences between PKSs and NRPSs

Although NRPSs and PKSs catalyse two distinct classes of natural products (NRPs and PKs respectively), striking structural and catalytic similarities exist between NRPSs and type I PKSs. Both systems are multifunctional megasynthases organised into repeated functional units known as modules and assemble their products by sequential condensation of simple monomeric building blocks (amino acids and acyl-CoAs, respectively). Each module is responsible for catalysis of one cycle of PK (type I modular PKSs) or NRP chain elongation and associated functional group modifications. In both systems, carrier proteins (PCP for the NRPS and ACP for PKS) which bear a covalently attached 4′-phosphopantetheinyl prosthetic group are used to tether the monomers and the nascent polymers as thermodynamically activated thioesters. In addition to carrier protein domains PCP and ACP, each module consists of two more core catalytic domains denoted adenylation (A) and condensation (C) for NRPS and ketosynthase (KS) and acyltransferase (AT) for PKS. The three core domains are responsible for the central chain-building reactions of PK or NRP biosynthesis. Both PKSs and NRPSs share, in general, a dedicated thioesterase (TE) termination domain. In some NRPSs, the C-terminal TE domains are replaced by NADH-dependent reductase domains (saframycin for example) (Cane *et al*., 1998; Fischbach and Walsh, 2006; Walsh and Fischbach, 2010).

NRPSs and type I PKSs diverge in regard to monomer activation before being tethered into the modified carrier proteins. In PK biosynthesis, the monomers are activated as acyl-CoA thioesters and in NRP biosynthesis as aminoacyl-AMP. The two enzyme systems also diverge in respect to their fundamental building blocks: PKSs use a small number of simple acyl monomers however, NRPSs use more than 500 proteinogenic and nonproteogenic amino acids (Walsh and Fischbach, 2010). In regard to the mechanisms of biosynthesis, PKSs use KS domain to catalyse decarboxylative Claisen-like condensation to form C-C bond between the growing polyketide chain and the extender unit compared to NRPSs that use condensation domain (C) to catalyse the formation of amide linkage between two amino acids. The ultimate state of the modified intermediates is determined by combination of optional tailoring domains (KR, DH and ER) for PKSs and by different auxiliary domains (epimerisation (E), N-methylation (M) and cyclisation (Cy)) in the case of NRPSs.

1.6 The secondary metabolites Azinomycins (A and B)

1.6.1 Discovery and biological activities of azinomycins (A and B)

Azinomycins A **3** and B **4** (**Figures 1.4** and **1.22**) are naturally occurring bioactive compounds produced by Streptomyces species. Hata and co-workers were the first to isolate azinomycin B from *Streptomyces sahachiroi* and named it carzinophilin (Hata *et al*., 1954) however, its structure remained elusive until 1986, the time when Yokoi and co-workers determined the structures of azinomycins A **3** and B **4**. Based on spectroscopic and chemical properties, the authors were able to determine the molecular weights of metabolites **3** and **4** as 595 and 623 for molecular formulas of $C_{30}H_{33}N_3O_{10}$ and $C_{31}H_{33}N_3O_{11}$, respectively (Yokoi *et al*., 1986). In this work, natural products **3** and **4** were isolated from *Streptomyces griseofuscus* (Nagaoka *et al*., 1986; Yokoi *et al*., 1986) with three additional related metabolites **32**, **33** and **34** (**Figure 1.22**) that were found to be biologically inactive (Yokoi *et al*., 1986). About two decades later, it was found that the amide **32** exhibited cytotoxic activity against P388 murine leukemia cell line (Hashimoto *et al*., 2003). Early bioactivity tests have revealed that the azinomycins (**A** and **B**) possess *in vitro* cytotoxic activity when subjected to a cytotoxicity assay employing L5178Y tumor cells. It was found that the IC_{50} (the concentration for 50% inhibition of cell growth) for compound **3** was 0.07 μg mL^{-1} and 0.11 μg mL^{-1} for compound **4** showing that azinomycin A is more

potent than azinomycin B. Furthermore, antimicrobial activity studies have shown that **3** and **4** are active against Gram-positive and Gram-negative bacteria but inactive against yeast and fungi (Nagaoka *et al*., 1986). Additional *in vivo* studies on bioactivities of azinomycin A and B against various murine tumors showed that azinomycin B was more potent than azinomycin A (Ishizeki *et al*., 1987). Further *in vivo* studies reported by Kelly and co-workers showed the biological activity of azinomycin B against yeast cells. Experiments with fluorescence imaging and oligonucleotide microarrays demonstrated DNA damage as consequence of covalent bonding with azinomycin B (Kelly *et al*., 2006).

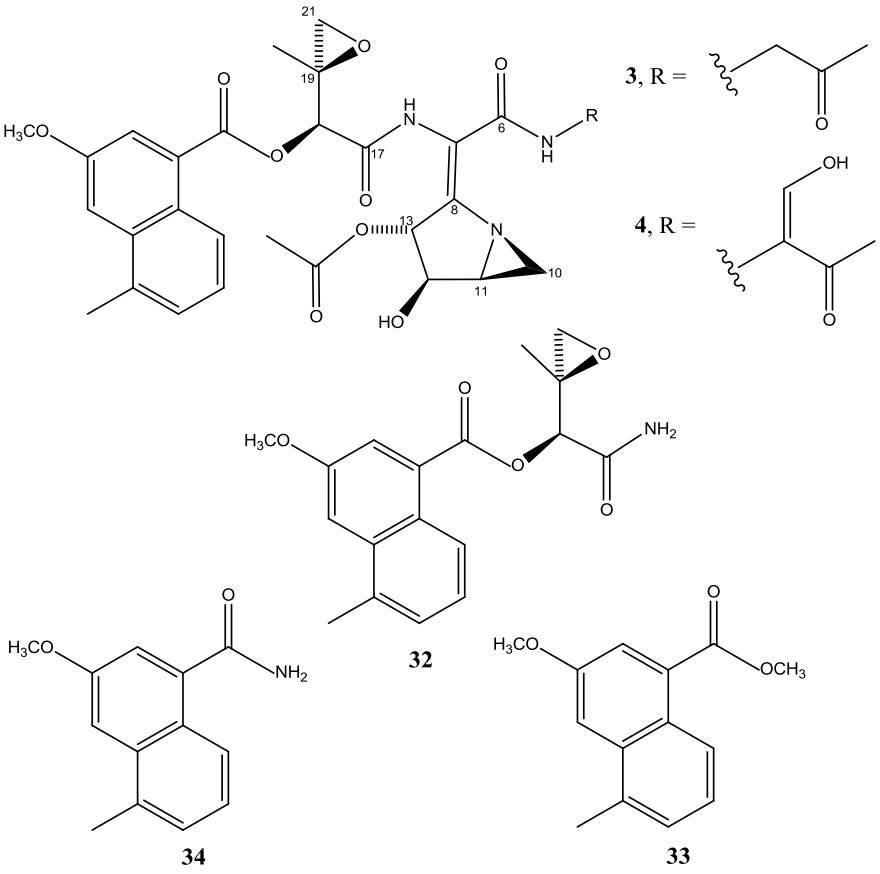

Figure 1.22: Structures of Azinomycin A **3** and B **4** and additional related metabolites (**32**, **33** and **34**) produced and isolated from *S. sahachiroi* and *S. griseofuscus*.

1.6.2 Mode of action of azinomycins (A and B)

The background surrounding the mode of action of azinomycins goes well back to the antibiotic activity studies done by Terawaki and Greenberg in 1966. They were first to indicate that azinomycin B inhibited DNA synthesis but had no inhibition effect over RNA or protein synthesis when tested against *Escherichia coli* strain B_0 and

Bacillus subtilis (Terawaki and Greenberg, 1966a). Moreover, the authors established the formation of the interstrand cross-links (ISCs) between azinomycin B and DNA of *E. coli* strain B_0 and *B. subtilis* and that this ISC was not irreversible (Terawaki and Greenberg, 1966b). Further studies based on ethidium fluorescence assays conducted by Lown and Majumdar showed that azinomycin B caused *in vitro* DNA damage as result of ISC formation accompanied by alkylation of DNA. These observations were detected experimentally by the reduction of ethidium fluorescence. Also the incubation of DNA with the intercalating dye prior to addition of azinomycin B inhibited the cross-linking (Lown and Majumdar, 1977). The authors also determined the basic nature of the reactive sites of azinomycin B requiring protonation to be active. In fact, both ISC and alkylation to DNA were shown to be pH-dependent and favoured lower pH. These findings shed more light on the tumor targeting of azinomycin B since the acidity in tumor cells is known to be lower than normal cells.

Further studies on the specific nature of the interstrand cross-links (ISCs) formed by azinomycin B were carried out by Armstrong and co-workers. It was found that azinomycin B alkylated guanine and either guanine or adenine two bases removed from one another on the opposite DNA strands. The authors reached this conclusion by incubating azinomycin B with ^{32}P-labelled synthetic DNA duplexes and following the cross-linking formation by denaturing polyacrylamide gel electrophoresis (Armstrong *et al*., 1992).

The first confirmation of the direct implication of the aziridine and epoxide moieties in the double alkylation of DNA was achieved by Saito et *al*. (Fujiwara and Saito, 1999). By following the incubation of both azinomycin B and its derivative 4-*O*-methyl-azinomycin with the DNA duplex $d(TAGCTA)_2$ and also through monitoring the reactions by HPLC analysis in association with mass spectrometry, the authors observed initial formation of a monoadduct corresponding to monoalkylation at the aziridine moiety, followed by interstrand cross-linked material indicating alkylation at the epoxide moiety. As consequence of these observations as well as the thermolysis of both alkylated adduct products (that resulted in depurination) the authors suggested that the second DNA alkylation (at guanine N-7) at the epoxide fragment was facilitated by the initial reaction between N-7 of adenine with the aziridine moiety (**Figure 1.23**). These findings seemed to contradict Armstrong's previous conclusions.

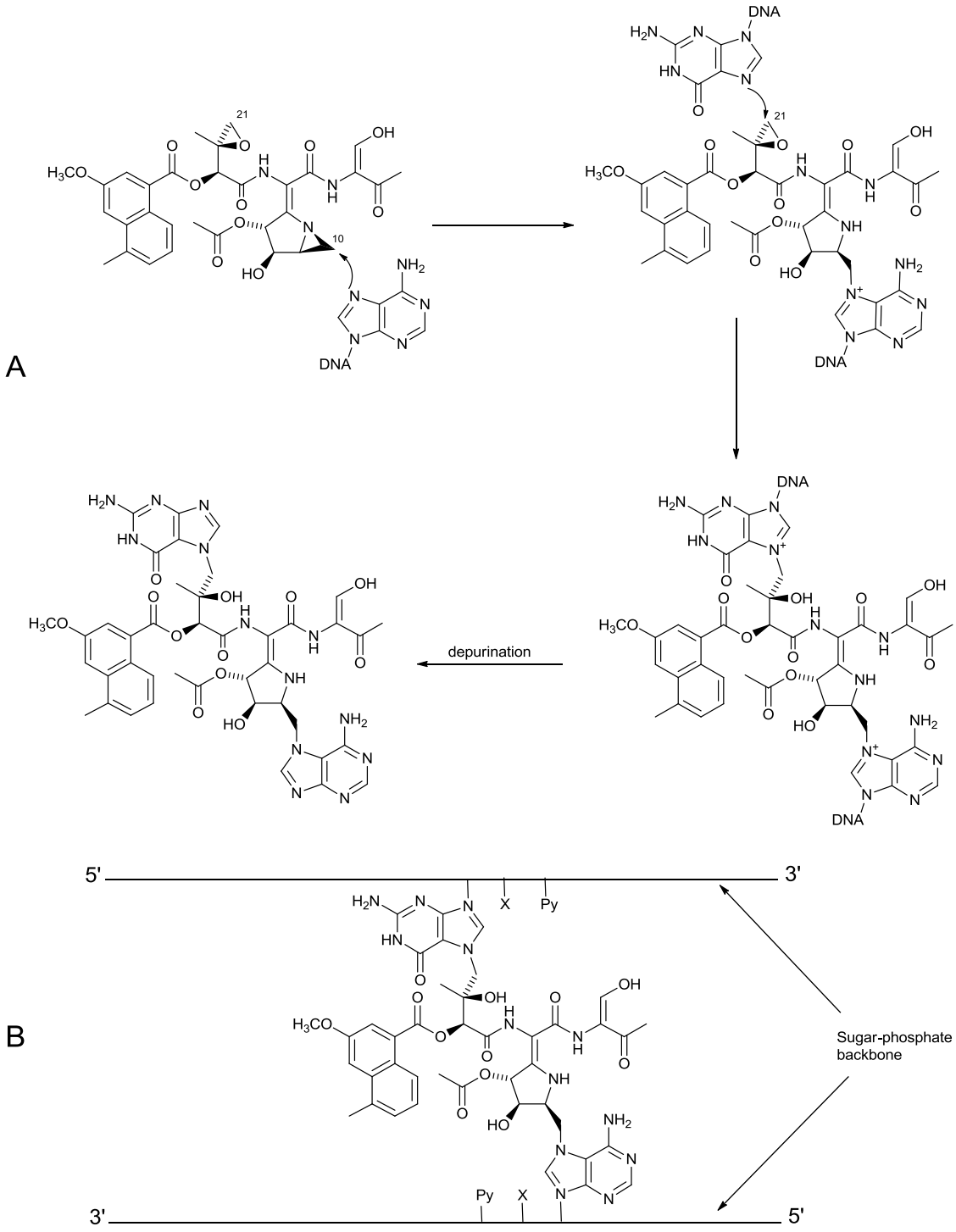

Figure 1.23: DNA alkylation by azinomycin B. (A): The interstrand cross-link is initiated by alkylation of adenosine (nitrogen N-7) by the aziridine C10 carbon, followed by a second alkylation of guanine (nitrogen N-7) by the epoxide carbon at C21. (B): Azinomycin B spanning over 3 base pairs and forms interstrand cross-links between purine bases on opposite strands two base pairs apart.

Further details in respect to the role of aziridine and epoxide moieties towards DNA cross-linking were revealed by Shipman and co-workers (Hartley *et al*., 2000). Using

plasmid DNA and synthetic epoxyaziridine analogues, they found that compound **35** (containing the epoxide and aziridine parts) shown in **Figure 1.24** triggered significant DNA cross-linking in contrast to compounds **36** and **37** (lacking the epoxide or aziridine moieties).

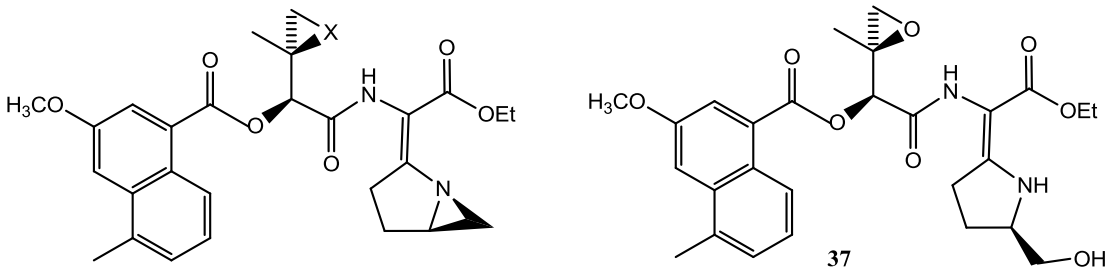

35, X = O
36, X = CH_2

37

Figure 1.24: Structures of epoxyaziridine analogues **35, 36** and **37**.

In vivo cross-linking and double alkylation of azinomycin B was further evaluated in a series of assays using yeasts as target organisms (Kelly *et al*., 2006). The results were consistent with the previous conclusions reached by the authors mentioned earlier in this section.

1.6.3 Biosynthesis of the azinomycins

A considerable amount of research has been carried out by a number of chemists and biochemists to understand the cytotoxicities, the antitumor activities and the mode of action of the azinomycins since the discovery of carzinophilin/azinomycin B in 1954. Despite all these decades of research efforts, no biosynthetic work on the azinomycins had been reported till the year 2004, when Lowden and co-workers reported the first biosynthetic studies on azinomycin B and established the polyketide origin of the naphthoate fragment (Corre and Lowden, 2004a). Isotope-labelled experiments based on feeding C1-, C2- and doubly labelled acetates to *S. sahachiroi* cultures and ^{13}C-NMR analyses, showed the incorporation of the labelled acetates into the azinomycin naphthoate fragment (**Figure 1.25A**). The results are consistent with the polyketide origin of the naphthoate fragment. Upon these findings, it was suggested that 5-methyl-1-naphthoic acid **41** (**Figure 1.26**) was the first enzyme-free intermediate in the azinomycin biosynthesis that has been formed on the basis of the condensation of

one molecule of acetyl-CoA with 5 of malonyl-CoA. The condensation reactions were mediated by a polyketide synthase (PKS) leading to the formation of a linear hexaketide chain that was subject to further modifications (reduction, cyclization, and dehydration/aromatization) by the PKS to form 5-methyl-1-naphthoic acid **41**. Moreover, it was suggested that metabolite **41** was then hydroxylated and methylated before incorporation into azinomycin B. By feeding methyl-^{13}C-labelled methionine to the azinomycin producer, a significant labelling (43%) was incorporated into only the methoxy carbon of the naphthoate fragment establishing the source of methyl group. Further isotopic labelling studies were conducted by Corre *et al*. to test the possibility that **41** is an intermediate metabolite and also to investigate the exact timing of the incorporation of the methoxy group (Corre *et al*., 2004b). Feeding synthetic deuterated naphthoate intermediates **38**-**40** (**Figure 1.25B**) to *S. sahachiroi* resulted in an efficient incorporation of deuterium from the feeding compounds into azinomycin B as revealed by ^{2}H-NMR analyses. The results demonstrated that 3-methoxy-5-methyl-NPA **43** was fully synthesised before elaboration into azinomycin B. Additional results of the acetate labelling experiments showed that ^{13}C-labelled acetates were incorporated in 5 carbons (C6-C7, C8 and C12-C13) of the aziridine moiety and 4 carbons (C1-C4) of the enol fragment. As consequence, it was proposed that the enol chain was of threonine origin with threonine in turn derived from oxaloacetate. Also it was proposed that α-ketoglutarate was the origin of the labelled carbons seen in the aziridine moiety after the subsequent metabolism of the labelled acetates through the Krebs cycle. In fact, any of the α-ketoglutarate derived amino acids (glutamate, glutamine, arginine and proline) would give the same results (Foulke-Abel *et al*., 2011a).

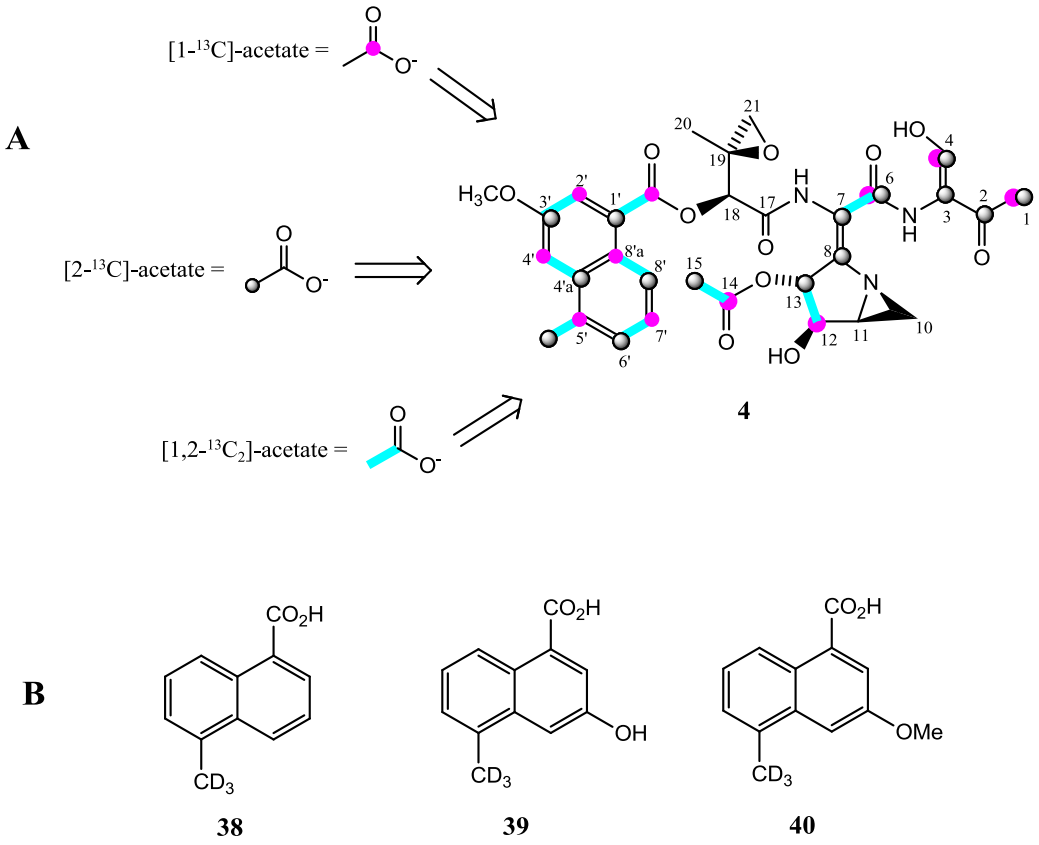

Figure 1.25: Studies on the azinomyicin naphthoate fragment based on feeding isotope labelled compounds to *S. sahachiroi*. (A): Schematic illustrations of the labelling patterns of azinomycin B subsequent to feeding labelled acetates to *S. sahachiroi*. (B): Structures of naphthoic acids in deuterium-labelled form.

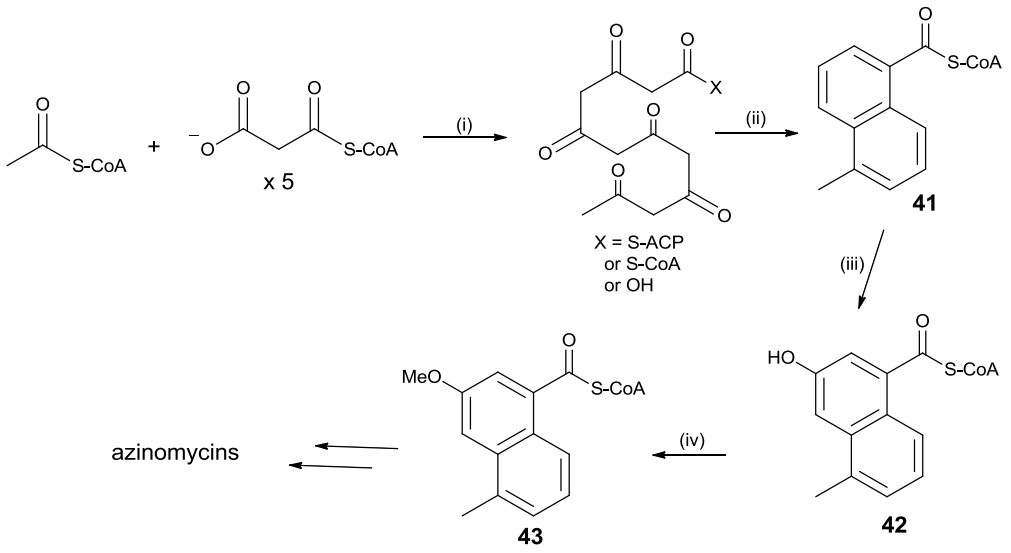

Figure 1.26: Pathway suggesting early stages to production of 3-methoxy-5-methyl-NPA **43** before incorporation into the azinomycin backbone. (i): Condensation reaction mediated by polyketide synthase (PKS). (ii): Reduction followed by cyclisation/aromatisation. (iii): Possible hydroxylation mediated by cytochrome P-450. (iv): Involvement of *S*-adenosylmethionine (SAM) in the methylation of **42**.

Further *in vitro* biosynthetic studies on azinomyicin B were conducted by Liu and co-workers using cell-free extracts of *S. sahachiroi*. The authors were able to reconstitute all the stages involved in the azinomycin biosynthetic pathway by identification of substrates and cofactors involved in the biosynthesis of azinomycin B (Liu *et al*., 2006). Results from enzyme assay using radiolabelled malonyl-CoA, acetyl-CoA and cofactors (NADPH, SAM and FAD) showed the significant importance of the NADPH and SAM in the azinomycin B biosynthesis. Other experiments using cerulenin (inhibitor of fatty acid synthase/polyketide synthase (FAS/PKS)) and miconazole (a cytochrome P-450 hydroxylase inhibitor) revealed the important role of PKS and cytochrome P-450 in azinomycin biosynthesis. Further enzyme assays using radiolabelled amino acid substrates (valine, threonine, glycine and ornithine) showed the positive incorporation of all the amino acids involved in the azinomycin B biosynthesis supporting the biosynthetic origin of azinomycin B. During these isotope-tracer experiments, ornithine was proposed as the precursor of the aziridine moiety. However, the details of the aziridine formation remain obscure.

Other biosynthetic studies were conducted by Kelly *et al.* in order to investigate the origin of the terminal enol fragment of azinomycin B (Kelly *et al*., 2008). The authors developed first a new optimised culture method allowing a reliable and

consistent supply of azinomycins A and B. The optimised method involved culturing *S. sahachiroi* on dehydrated plates, followed by multiple step seed culture and subsequent fermentation of the strain in nutrient limited medium. The development of the new culture method was a necessity for biosynthetic studies as the continuous production of azinomycins by *S. sahachiroi* was unreliable following the available literature protocols (Nagaoka *et al*., 1986; Yokoi *et al*., 1986; Corre *et al*., 2004a; Corre *et al*., 2004b). The authors started their investigations by feeding [U-^{13}C]-threonine followed by synthetic potential substrates **44-46** (**Figure 1.27**). It was found that threonine was incorporated into azinomycin B and gave labelling patterns at the carbons C1-C4 but no labelling was detected in azinomycin B after feeding [U-^{13}C]-compounds **44-46**. Hence, it was suggested that a nonribosomal peptide synthetase (NRPS) had incorporated the advanced precursor threonine with further chemical modification occurring after peptide assembly to construct the terminal (enol) fragment of azinomycin B.

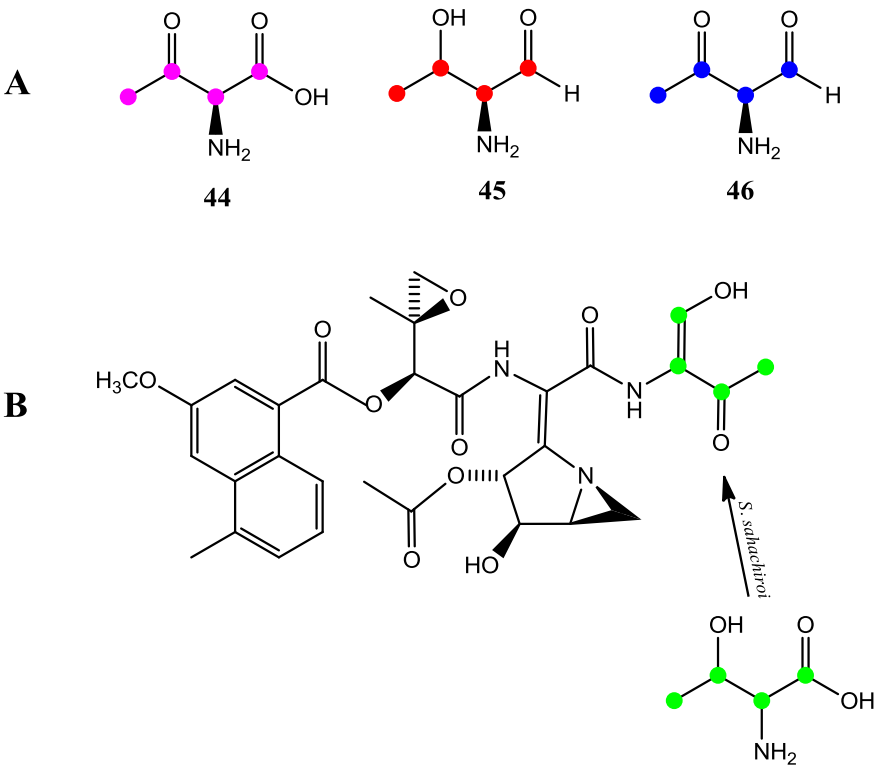

Figure 1.27: Investigation of the origin of the enol fragment of azinomyicin B. (A): Structure of the [U-^{13}C]-labelled synthetic compounds evaluated for incorporation into azinomycin B. (B): Schematic representation of [U-^{13}C]-threonine illustrating it incorporation into the terminal fragment of azinomycin B subsequent to feeding studies.

Azinomycin A, on the other hand, has a ketoamine as a terminal fragment and lacks the enol part within its structure. Based on a series of experiments involving the feeding of ^{15}N and ^{13}C labelled aminoacetone, threonine and glycine, it was proposed that the aminoacetone **50** was the last precursor of the first three carbons C1-C3 of azinomycin A and resulted from either glycine **47** or threonine **48** as described in **Figure 1.28**. The authors also proposed that the terminal aminoacetone moiety is fully constructed before being tethered to the NRPS (Sharma *et al*., 2009)**.**

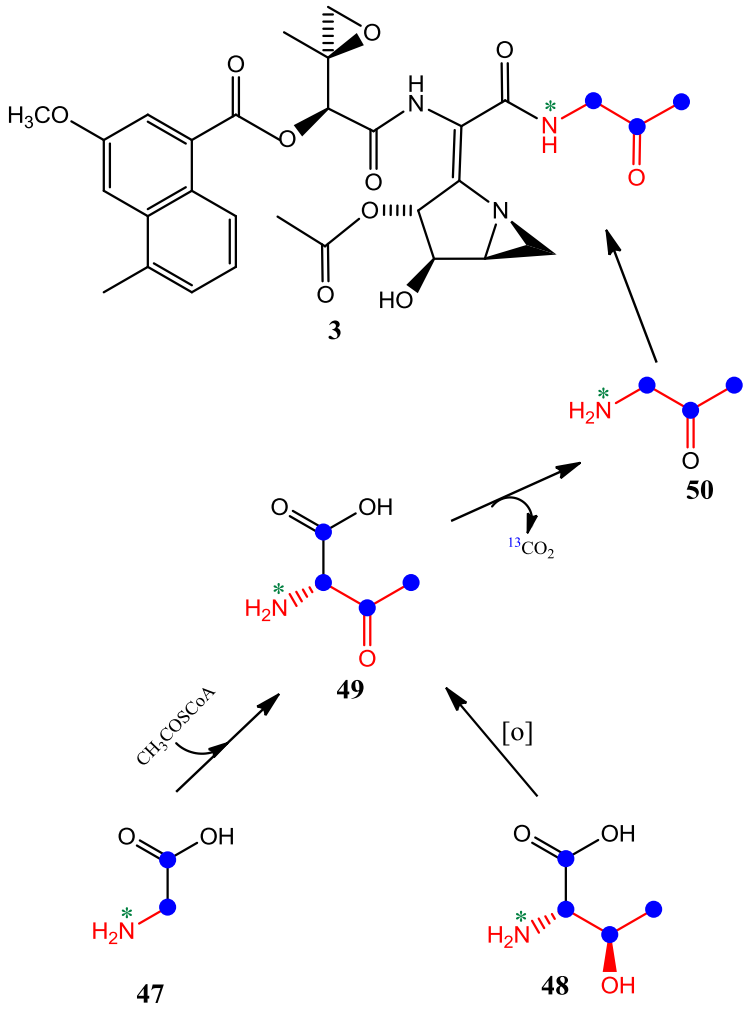

Figure 1.28: Proposed biosynthetic pathway of aminoacetone **50** and its incorporation into azinomycin A.

Sharma *et al*. (2009) suggest the action of threonine dehydrogenase or 2-amino-3-ketobutyrate coenzyme A ligase on threonine **48** and glycine **47**, respectively. In both

cases the amino acid **49** was the product and reacted by spontaneous decarboxylation to give precursor **50.**

Whole cell feeding studies, using ^{13}C-labelled potential substrates (such as valine and epoxyvaline) were carried out to investigate the biosynthetic origin of the epoxide moiety and the timing of its incorporation into the azinomycin backbone. These studies revealed that much of the valine tailoring occurs prior to being loaded onto the NRPS machinery. It was also revealed that neither of the epoxyvaline precursors showed incorporation into the natural product likely to their instability in aqueous medium. As consequence, the precise timing of the formation of the azinomycin epoxide moiety could not be revealed. Additionally, results from ^{13}C NMR analyses showed that amongst the nine [1-^{13}C]-valine derivatives utilised in this study, only precursors **51-54** were incorporated into the azinomycin epoxide leading the authors to suggest the biosynthetic route illustrated in **Figure 1.29** (Sharma *et al*., 2008).

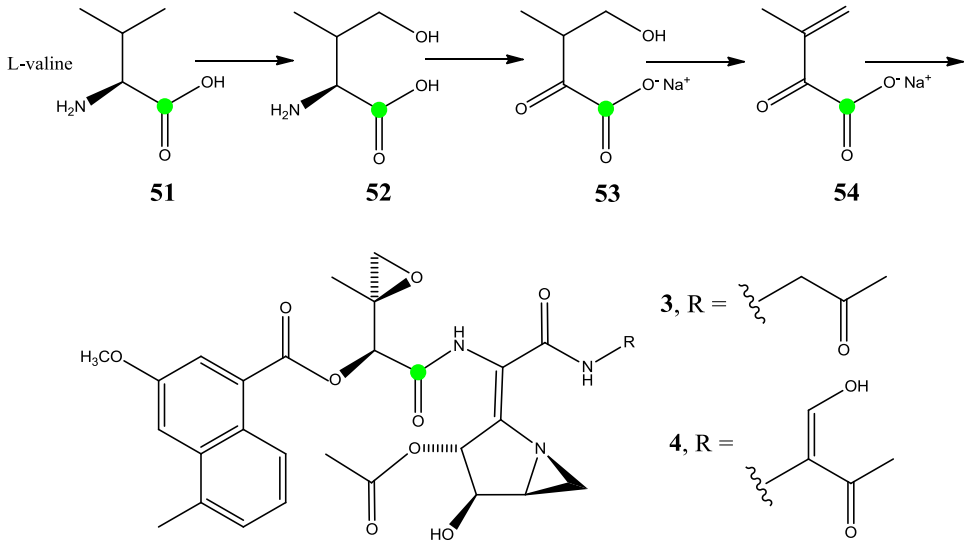

Figure 1.29: Evaluation of biosynthetic origin of the azinomycin epoxide moiety. Formation of γ-hydroxyvaline **52** by oxidation of L-valine **51**, followed by transamination to give α-keto acid **53** and dehydration to produce 3-methyl-2-oxobutenoic acid **54**.

The entire azinomycin B biosynthetic gene cluster *azi*, was cloned and sequenced by Zhao *et al.* (2008) facilitating the identification of numerous genes involved in the construction of individual fragments of azinomycin B. However, many other genes

are still of unidentified function and details of the biosynthetic formation of the aziridine moiety remain a mystery.

The sequencing of the azinomycin B gene cluster (*azi*) in conjunction with bioinformatic analysis helped to identify *aziB*, the gene encoding for the enzyme AziB, a type I iterative PKS responsible for the production of 5-methyl-NPA **41** by iterative decarboxylative condensation of one molecule of acetyl-CoA with 5 molecules of malonyl-CoA (**Figure 1.30**). In regard to the post modifications of 5-methyl-NPA to form 3-methoxy-5-methyl-NPA, Zhao *et al*. identified the genes *aziB1* and *aziB2* (within the *azi* gene cluster) encoding for AziB1 and AziB2 respectively, and proposed their involvement in the step wise addition of the methoxy group at carbon C3' of the naphthoate fragment. The authors suggested the role of cytochrome P-450 hydroxylase (AziB1) in the introduction of hydroxyl functional group at C3', followed by methylation catalysed by *S*-adenosylmethionine (SAM)-dependent *O*-methylransferase AziB2. Confirmation of their predictions was achieved by construction of an *S. albus* recombinant strain containing the genes *aziB*, *aziB1* and *aziB2*, followed by culturing the strain and detecting the metabolite 3-methoxy-5-methyl-NPA from the culture medium.

Further *in vitro* studies were conducted by Ding and co-workers (2010) to investigate the role of enzymes AziB1 and AziB2 in their respective hydroxylation and methylation of 5-methyl-NPA at carbon C3. Overexpression of the two enzymes in *E. coli* and their separate incubations with 5-methyl-NPA confirmed that AziB1 catalysed the C3 hydroxylation and AziB2 was responsible for 3-*O*-methylation of the free naphthoic acid. Additional investigations using an ATP-[^{32}P]-PPi exchange assay were carried out to determine the substrate specificity of AziA1. It was found that the substrates 3-methoxy-5-methyl-NPA, 5-methyl-NPA and 3-hydroxy-5-methyl-NPA were activated by AziA1 with a preference for the first naphthoic acid (Ding *et al*., 2010). Inspired by the apparent flexibility of the AziA1 active sites, the authors tested a range of commercially available naphthoic acid analogues in addition to 6-methylsalicyclic acid and orsellinic acid using ATP-[^{32}P]-PPi exchange assay. The results showed the activation of only compounds with a naphthalene ring. The findings suggested the requirement of a naphthalene ring for substrate recognition and activation by the adenylation domain of AziA1.

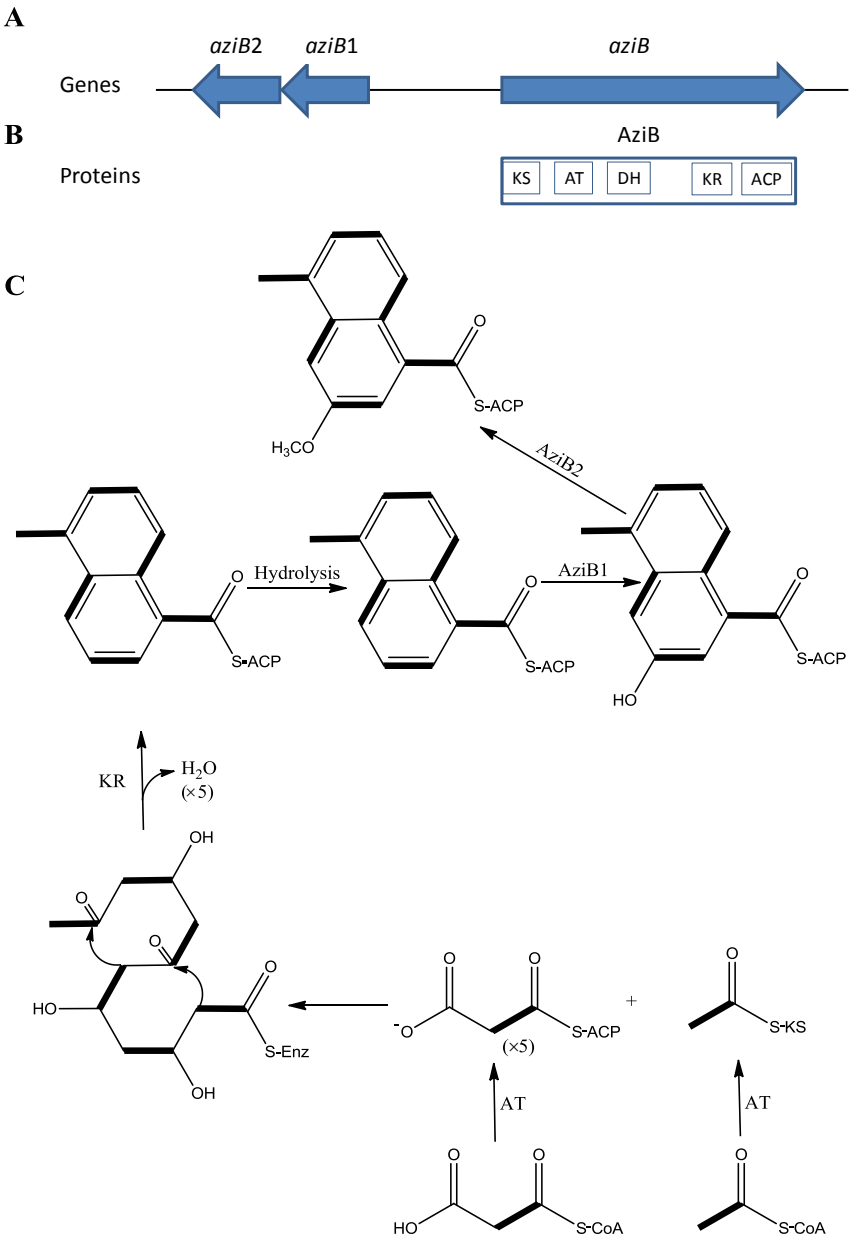

Figure 1.30: 3-methoxy-5-methyl-NPA biosynthesis. (A): Genes encoding the enzymes AziB, AziB1 and AziB2 for the biosynthesis of 3-methoxy-5-methyl-NPA. (B): Domain organizations of 3-methoxy-5-methyl-NPA. KS, ketoacylsynthase; AT, acyltransferase; DH, dehydratase; KR, ketoreductase; ACP, acyl carrier protein. (C): Pathway for 3-methoxy-5-methyl-NPA synthesised by AziB, AziB1 and AziB2.

The *azi* sequencing enabled likewise the identification of five modular nonribosomal peptide synthetase (NRPS) genes, *aziA1-aziA5* involved in the assembly of the azinomycin fragments as illustrated in **Figure 1.31**. Zhao *et al.* (2008) predicted a dual role of AziA1 that is composed of acyl-CoA ligase (A) and peptidyl carrier protein (PCP) domains. The (A) domain (also known as adenylation domain) is responsible for the recognition, incorporation and activation of the free 3-methoxy-5-

methyl-NPA before being transferred to the PCP domain and then to AziA2 for starting the assembly of azinomycin fragments. The condensation (C) domains allow the formation of amide bonds. The AziA3 module was proposed to activate the acid **55**, transfer it to its PCP domain and then reduce the ketone using the KR domain to form intermediate **56**. The adenylation domain (A) of AziA4 recognises and activates the aziridino[1,2a]pyrolidinyl compound **57** (or a partially processed intermediate amino acid) and then transfers it to the PCP domain. At the end of the four domain enzyme AziA5, there is a reductase (RE) domain responsible for the release of the final metabolite as an aldehyde for further functionalization.

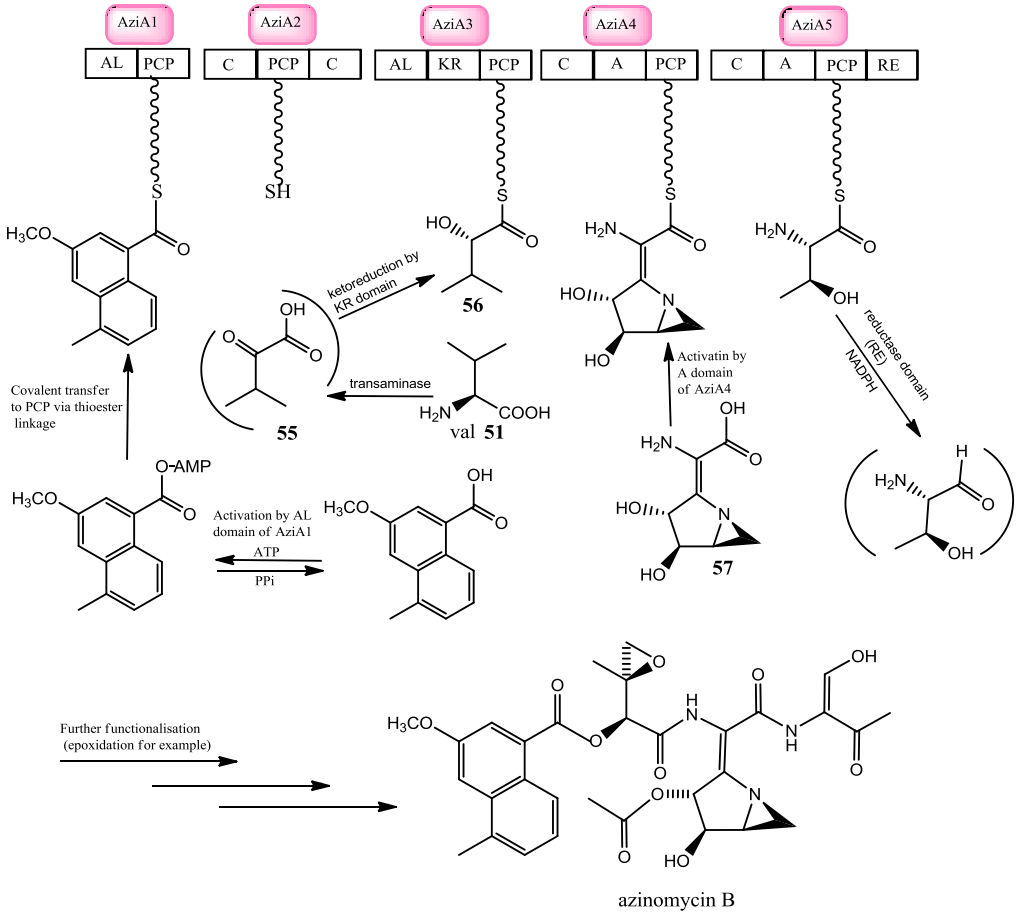

Figure 1.31: Proposed assembly of azinomycin B **4** building blocks by NRPS enzymes AziA1-AziA5. NRPS domains are: AL, acyl-CoA ligase; PCP, peptidyl carrier protein; C, condensation domain; KR, ketoreductase domain; A, adenylation domain; RE, reductive release domain.

Additional genes encoding for proteins required for tailoring reactions (such as acetylation, oxidations and methylation) were also identified by Zhao and co-workers (2008). Validation of the functional role of AziB in the azinomycin biosynthesis

pathway was accomplished by cloning and expressing the *aziB* gene into the expression host *S. albus* that was cultivated followed by characterisation of the metabolite 5-methyl-NPA formed in the fermentation culture.

Subsequent to genome sequencing of *S. sahachiroi*, an azinomycin B resistance protein was identified and characterised as AziR (Foulke-Abel *et al*., 2011b). The protein was overexpressed in the heterologous hosts *S. lividans* and *E. coli* and then its resistance effect was tested against azinomycin B. It was found that AziR exhibited protective effect against azinomycin B as the number of surviving cells was enhanced. *In vitro* protein assay revealed a reasonable binding between AziR and azinomycin B.

1.7 Other natural products containing aziridine moiety

There are only a small number of aziridine-containing natural products that have been identified compared to the tens of thousands (> 100,000) of natural products that have been characterized up to 2010 (Foulke-Abel *et al*., 2011a). Examples include mitomycins, ficellomycin, azicemicins, mirazidine and maduropeptin compounds (**Figure 1.32**). A discussion on the discovery, biological activity, mode of action and biosynthesis of mitomycins (mainly mitomycin C **58**), ficellomycin **59** and azicemicin A **60** and B **61** will be covered in this section.

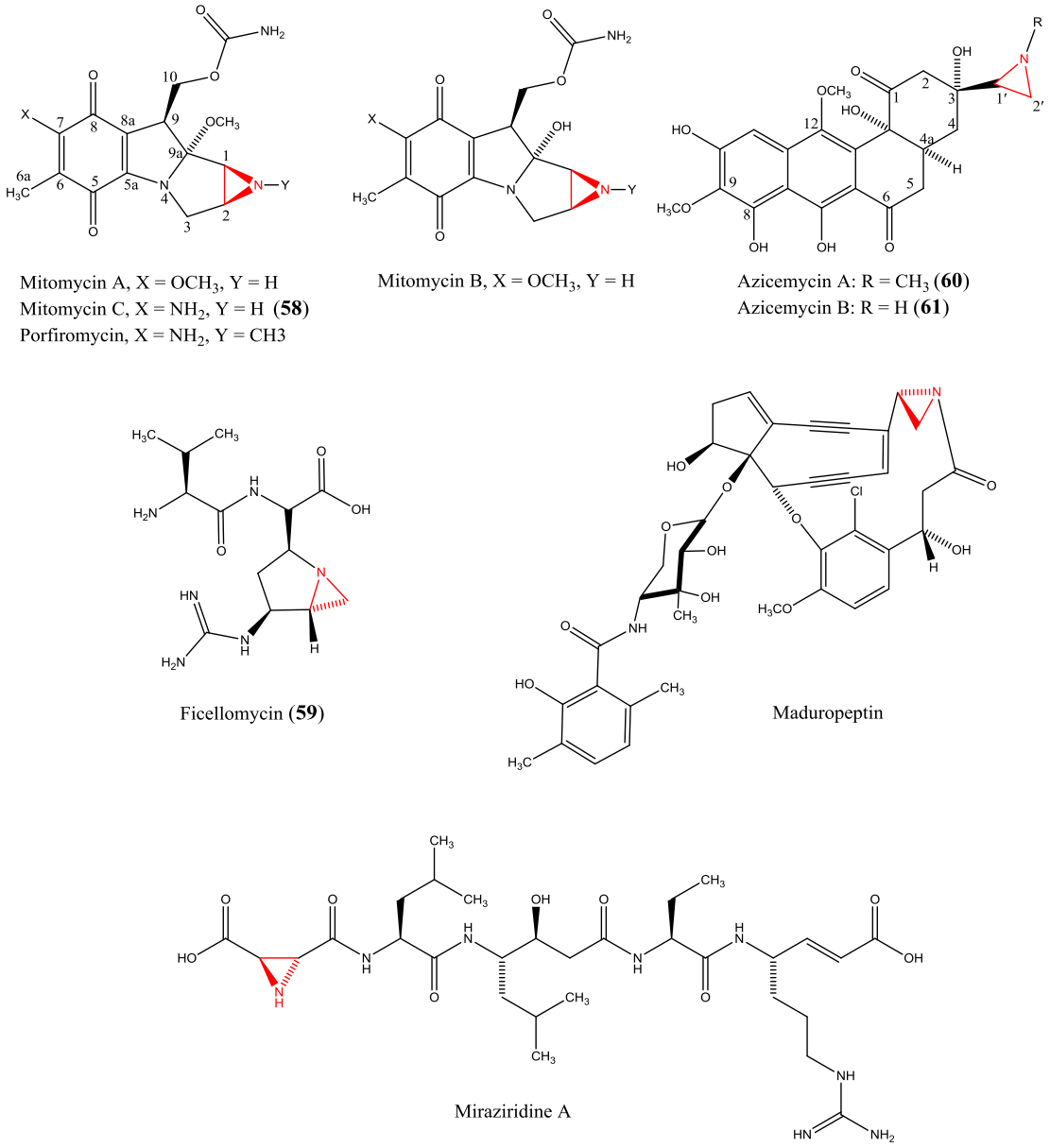

Figure 1.32: Structure of the aziridine-containing natural products mitomycins (A, B, C **58** and E), ficellomycin **59**, azicemycins (A **60** and B **61**), maduropeptin and miraziridine A.

The mitomycins are potent antibiotics that belong to the family of antitumor quinone. In 1956, Hata and co-workers isolated mitomycins A and B (**Figure 1.32**) from *Streptomyces caespitosus* (Hata *et al.*, 1956a; Hata *et al.*, 1956b) and shortly thereafter mitomycin C **58** was discovered from the same strain (Wakaki *et al.*, 1958). Few years after their discovery, Webb and co-workers established the absolute structure of the mitomycins (Webb *et al.*, 1962a; Webb *et al.*, 1962b). Further analysis by high-resolution X-ray crystallography (Shirahata and Hirayama, 1983)

and chemical studies (Hornemann and Heins, 1985) proved to be critical in resolving the final stereochemical structures of the mitomycins.

Mitomycin C **58**, which is widely used for the treatment of solid tumors (Begleiter, 2000), was found to cause diverse biological effects such as selective inhibition of DNA synthesis, mutagenesis, induction of DNA repair, sister-chromatid exchange, signal transduction and induction of apoptosis (Tomasz and Palom, 1997). Early investigations to understand and explain the mode of action of mitomycins revealed the ability of these natural products to form both inter- and intrastrand DNA cross links in the minor groove with a sequence specificity favouring 5′-CG-3′, and that these alkylation processes were the cause of the biological activities of these compounds (Iyer and Szybalski, 1963; Iyer and Szybalski, 1964). Also, it has been shown that the resulting alkylated mitomycin C-DNA complexes are not due to direct reaction between mitomycin C **58** and DNA, but require prior reductive activation of the quinone system by enzymatic (Suresh *et al*., 1997) or chemical means (Paz, 2009). Intensive work has been carried out by many researchers in order to establish the mechanisms of the reductive activation and the chemical steps leading to the formation of mitomycin C-DNA complexes and **Figure 1.33** illustrates the accepted mechanism of DNA cross-linking by reductive activation of mitomycin C **58** (Schiltz *et al*., 1993; Tomasz and Palom, 1997; Suresh *et al*., 1997).

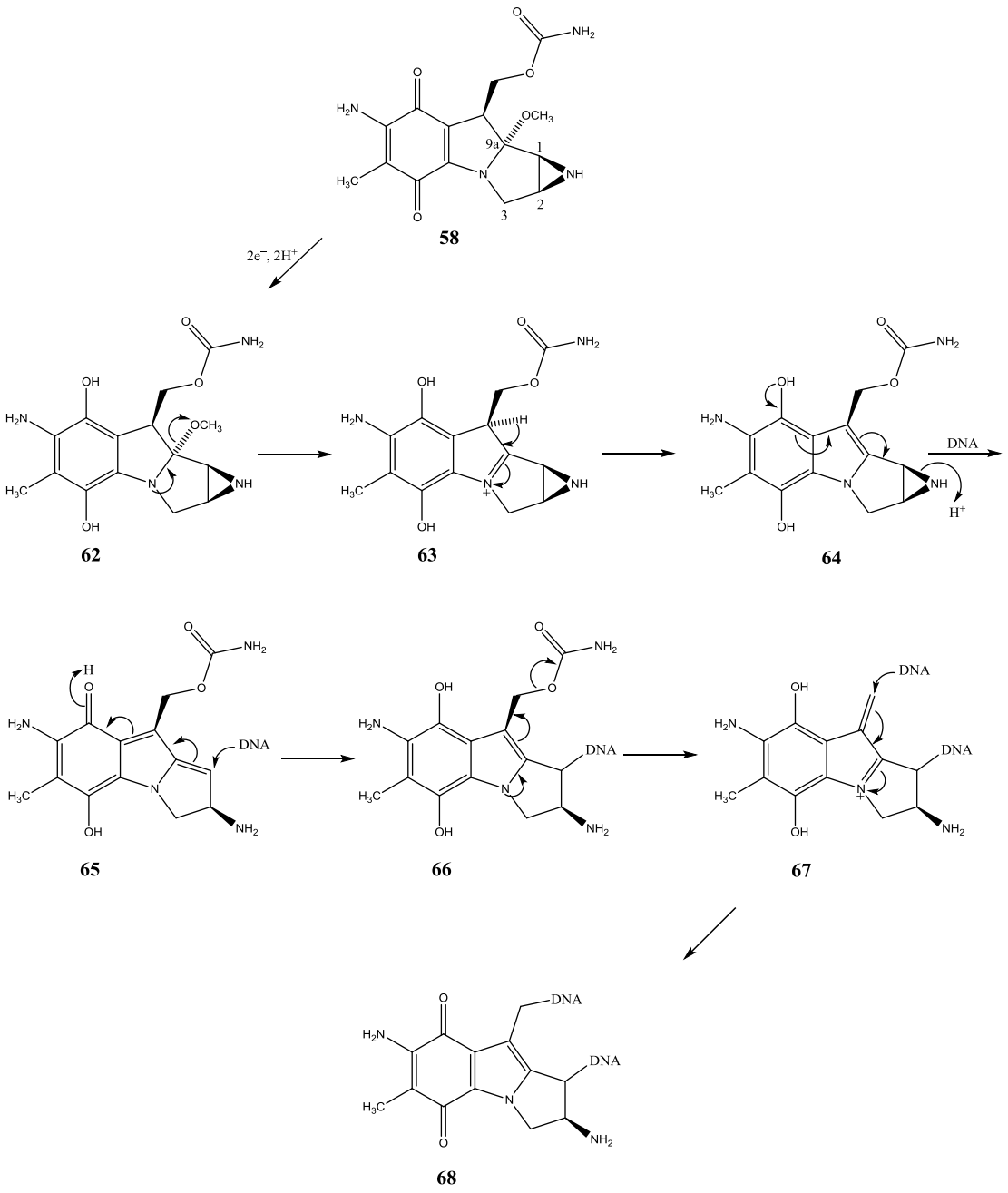

Figure 1.33: Proposed pathway of reductive activation of mitomycin C **58** and the mechanism of DNA cross-linking by the activated form of **58**.

The hydroquinone **62** is formed by two-electron reduction (or may be by two stepwise one-electron reduction) of the quinone moiety of **58**. Then the elimination of the methoxy group from the C9a position affords iminium ion **63**, which quenches itself *via* deprotonation/tautomerisation to afford net elimination of methanol from **62** and yielding intermediate leuco-aziridinomitosene **64**. The reactive intermediate methide **65** is formed next prior to aziridine-ring opening due to electron donation from the

hydroquinone indole core of **64**. The methide **65** can now alkylate DNA at the exocyclic nitrogen of guanine (N-2) at the C1 position to form species **66**, which can then produce the iminium intermediate **67** by elimination of the carbamate. Since a second alkylating site is been revealed now, a subsequent alkylation by a second guanine N-2 takes place leading to the formation of the final cross-linked adduct **68**.

Early biosynthetic studies on mitomycins (A, B and C) and porfiromycin were carried out in the laboratories of Kirsch (Kirsch and Korshalla, 1964), Vining (Bezanson and Vining, 1971) and Hornemann (Hornemann and Cloyd, 1971). Based on feeding [methyl-^{14}C]-L-methionine to *Streptomyces verticillatus*, it was established that the *O*- and *N*-methyl functionalities (but not the C6-methyl groups) of these mitomycins were derived from methionine. Additional incorporation experiments with radiolabelled precursors [guanidino-^{14}C]-L-arginine (Hornemann and Cloyd, 1971) and [ureido-^{14}C]-L-citrillune (Hornemann *et al*., 1974a) showed that the C10 carbamoyl groups originate from L-arginine or L-citrillune. These results are summarised for mitomycin C **58** in **Figure 1.34**.

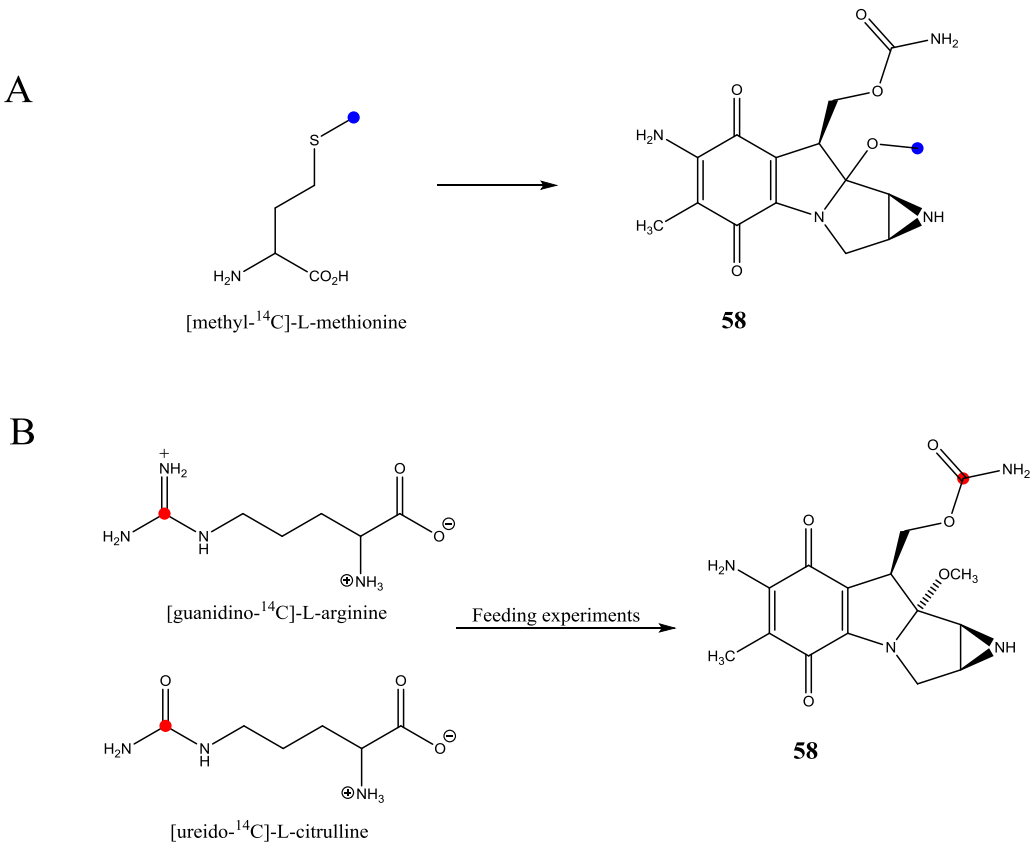

Figure 1.34: Biosynthetic origin of the *O*-methyl groups of mitomycin C **58**.

Further precursor incorporation experiments using [1-^{14}C]-, [1-^{14}C, ^{15}N]-, [1-^{13}C, ^{15}N]- and [6-^{14}C]-D-glucosamine followed by degradative studies and MS analyses (Hornemann and Cloyd, 1971; Hornemann and Aikman, 1973; Hornemann *et al*., 1974a) demonstrated that D-glucosamine can provide the nitrogen atome of the aziridine ring, the non-quinone C6 chain, the C10 of the carbamoyl group and can also fully incorporate into mitomycins as illustrated for mitomycin C **58** in **Figure 1.35**. Further feeding experiments using ^{14}C-labelled D-glucose and D-ribose showed an efficient incorporation into mitomycins, with ribose labelling the quinone ring (Hornemann and Cloyd, 1971). It was also demonstrated that C6a and C6 of mitomycin C **58** were originated from labelled pyruvate and D-glucose suggesting an early branch from shikimate pathway (Hornemann *et al*., 1974b). Since attempts to incorporate labelled shikimic acid and 3-dihydroquinic acid were unsuccessful, the authors proposed the intermediary of a "C_7N unit" *via* 4-amino-3,4-dideoxy-D-arabino-heptulosonic acid 7-phosphate subsequent to the condensation between pyruvic acid and erythrose-4-phosphate (E4P) . Additional studies showed that the

C7 unit of the mitomycins can be formed from [4-^{14}C]-D-erythrose and C5 from [3-^{14}C]-pyruvate subsequent to the incorporation of labelled erythrose and pyruvate into the mC_7N unit of mitomycin C (Hornemann *et al*., 1980). These results are summarised for mitomycin C **58** in **Figure 1.35**.

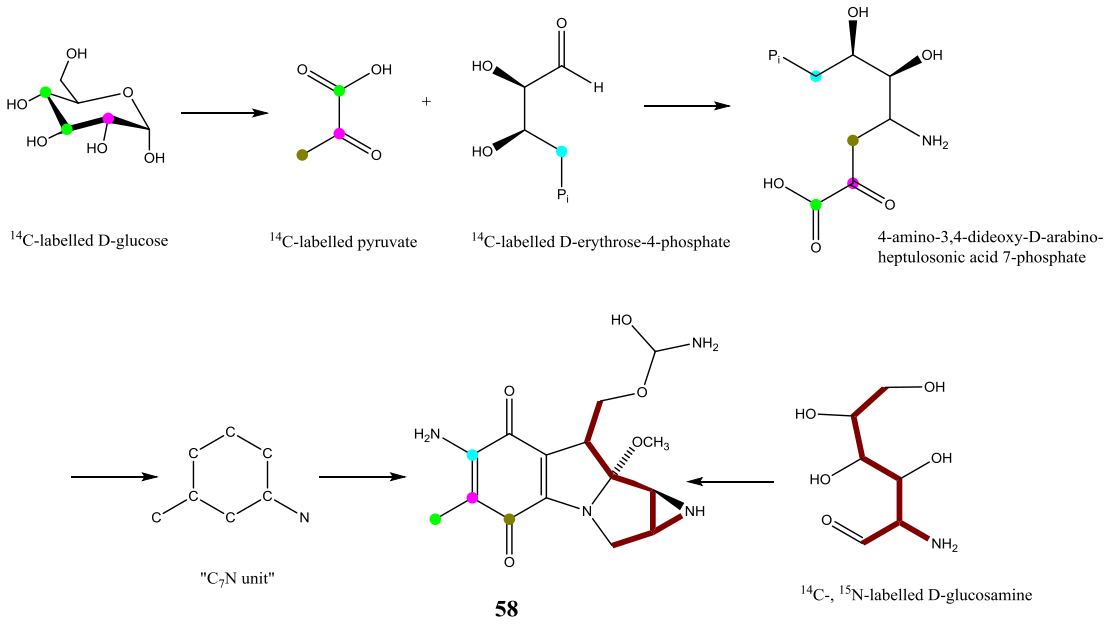

Figure 1.35: Radiolabelled precursors to the carbon skeleton of mitomycin C **58**.

Shortly afterwards, it was established that the quinone ring of the mitomycins is derived from 3-amino-5-hydroxybenzoic acid (AHBA) (Anderson *et al*., 1980), which is also a precursor of the mC_7N unit of ansamycin antibiotics (Kibby *et al*., 1980). Later work has repeatedly confirmed the intermediary role of AHBA in the biosynthesis of a range of natural products containing mC_7N structural fragment (Wu *et al*., 1987; Lee *et al*., 1994; Komoda *et al*., 2007). It was also established that the mitosane skeleton of mitomycins is originated from the coupling of AHBA and D-glucosamine (Hornemann *et al*., 1974a; Anderson *et al*., 1980).

More details regarding the biosynthesis of mitomycins have been revealed since the intensive work on genetics and enzymology of mitomycin C **58** carried by Sherman's group (Sherman *et al*., 1999) and extensive studies about AHBA biosynthesis (Kibby *et al*., 1980; Kim *et al*., 1996). The Sherman group have cloned and sequenced the gene cluster for biosynthesis of mitomycin C **58** in *Streptomyces lavendulae*. They

identified genes *mitA* and *mitB* related to AHBA synthases (MitA) and a group of glycosyltransferases (MitB). The group also identified homologues of seven genes (*rifG -H, -J, -K, -I, -M, -N*) which are necessary and sufficient for AHBA formaton in rifamycin producer *Amycolatopsis mediterranei* (Kim *et al*., 1998). Moreover, the Sherman's group identified a number of tailoring genes necessary for complete assembly of mitomycin C **58**. Examples include identification of three SAM-dependent methyltransferases that might be involved in the addition of *O*- and *N*-methyl groups and also identification of a putative carbamoyltransferase.

Based on what is known about AHBA biosynthesis (Kibby *et al*., 1980; Kim *et al*., 1996) and Sherman's findings, a representation of mitomycin C **58** biosynthesis is depicted in **Figure 1.36**.

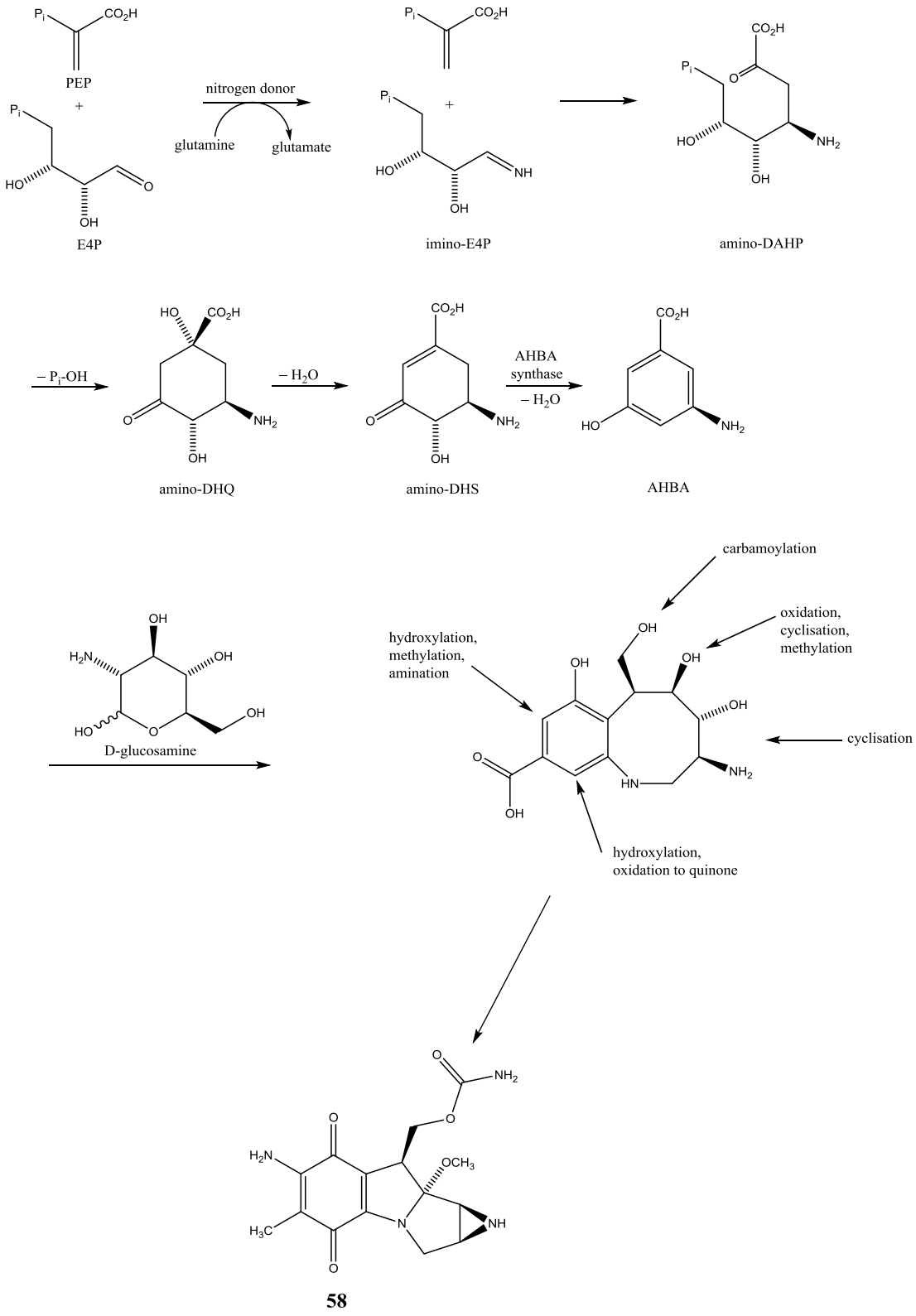

Figure 1.36: Summary of the biosynthetic pathway of mitomycin C **58**.

Beginning with the conversion of erythrose-4-phosphate (E4P) into imino-E4P, in which the ammonia is incorporated from the amide nitrogen of glutamine, the formation of 4-amino-3,4-dideoxy-D-arabino-heptulosonic acid 7-phosphate (amino-DAHP) is ensued *via* the coupling of imino-E4P and PEP (phosphoenolpyruvate). Then, amino-DAHP is processed through aminodehydroquinic acid (amino-DHQ) and aminodehydroshikimic acid (amino-DHS), which is then aromatised by the enzyme, AHBA synthase. The biosynthetic pathway proceeds then *via* the coupling of AHBA and D-glucosamine and also through a number of tailoring enzyme to furnish the final structure of mitomycin C **58** (**Figure 1.36**).

Because no biosynthetic genes were assigned an exact role in respect to the precise cyclisation and formation of aziridine ring, a hypothesis that cyclisation occurs through an S_N2 reaction might be a possibility. The carbons C2 and C3 from glucosamine might act as nucleophilic and electrophilic centres, respectively prior to the substitution of the glucosamine C3 hydroxy group with a good leaving functional group (such as halogen atoms).

Comparison between the mode of action of mitomycin C **58** and azinomycin B **4** shows that compound **58** requires bioreductive activation prior to DNA alkylation and cross-linking in contrast to compound **4** where the reactive sites (aziridine and epoxide rings) do not require such activation. Compounds **58** and **4 a**lso diverge in that the first one forms both inter- and intrastrand DNA cross-links in the minor groove whereas the latter forms interstrand DNA cross-links in the major groove. Regarding the biosynthetic origin of the aziridine moiety it was shown that D-glucosamine was the precursor of the aziridine ring of mitomycin C **58** while either ornithine or glutamate derivative is the precursor of the aziridine moiety in azinomyicin B **4**.

The second aziridine-containing natural product ficellomyicin **59** was isolated from a culture broth of *Streptomyces ficellus* in 1976 by Argoudelis and co-workers at Upjohn Research Laboratories (Argoudelis *et al*., 1976). It is the only natural product known to share the 1-azabicyclo[3.1.0]hexane ring system with the azinomycins (Foulke-Abel *et al*., 2011a). The compound **59** displays high *in vitro* activity against *Staphylovoccus aureus* infections in mice and inhibits the growth of Gram positive

bacteria *in vivo*. It is inactive against Gram negative bacteria, viruses and a variety of fungi. In 1989, Kuo and co-workers elucidated the structure of ficellomycin **59** based on NMR, MS and derivatisation studies (Kuo *et al*., 1989). However, the absolute stereochemistry of the compound remains undetermined.

Studies on the mode of action of ficellomycin **59** were carried by Reusser and co-workers (1977). It was found that compound **59** selectively impairs semiconservative DNA replication in *Eschirichia coli*, and this was found not to be due to direct inhibition of DNA polymerase. It was also found that **59** triggered the accumulation of DNA population of a mean size of 34S. In the light of these results, it was suggested that ficellomycin **59** may exert its biological activity by alkylation of DNA, possibly in similar manner to azinomycins. In 2011, Foulke-Abel research group revealed parts of an unpublished work on *S. ficellus* genome aiming at cross-comparing the biosynthetic pathways between azinomycins and ficellomycin (Foulke-Abel *et al*., 2011a). Despite the promising anti-cancer potential of ficellomycin **59**, no complete biosynthetic work had been published yet.

Azicemicins A **60** and B **61**, the third group of aziridine-containing natural products to be discussed in this section, were isolated in 1993 from *Amycolatopsis* sp. MJ126-NF4 (lately known as *Kibdelosporangium* sp. MJ126-NF4 (Ogasawara and Liu, 2009)) and shown to exhibit moderate activity against Gram positive bacteria and mycobacteria. Azicemicins **60** and **61** did not show any signs of toxicity when administrated to mice at a dose of 150 mg/Kg and 75.5 mg/Kg, respectively (Tsuchida *et al*., 1995a; Tsuchida *et al*., 1995b; Tsuchida *et al*., 1993). Structurally, antibiotics **60** and **61** contain an angucycline core (in black) and unprecedented aziridine moiety (in red) (**Figure 1.32**), though their mode of action has not been investigated yet. Meanwhile, biosynthetic studies on these compounds have been published by Ogasawara and Liu in 2009. Starting with feeding [1-^{13}C]- and [1, 2-$^{13}C_2$]acetates to the azicemicins producing organism, it was shown that the angucycline core of Azicemicin A **60** is of a decaketide origin and that its carbon skeleton is assembled by a type II polyketide synthase (PKS). Also it was suggested, based on results from labelling patterns seen on C1′, C2′ and C3 of compound **60** (**Figure 1.37**), that the acetate derived amino acid **77** might be the starter unit of azicemicin A **60** biosynthesis. The authors conducted further isotope tracing experiments in order to

investigate the azicemicins' biosynthetic pathway. The choice of amino-acids to be fed was based on the fact that the labelling of the acetate **69** and intermediates of TCA (tricarboxylic acid) cycle subsequently generate the labelling of the amino-acids originating from α-ketoglutarate and oxaloacetate **70** (Den Hollander *et al*., 1981; Glawischnig *et al*., 2001). Then deuterium-labelled amino-acids D-alanine, D,L-serine and D,L-aspartate were fed to the azicemicins producing strain and results showed that aspartic acid **71** is the precursor of the aziridine moiety since it was the sole amino-acid showing incorporation of deuterium into C1′ of azicemicin A **60** (**Figure 1.37**). The labelling patterns (from the same amino-acid) shown on the *O*- and *N*-methyl groups of **60** were justified by the conversion of amino-acid **71** to glycine **72** and subsequent transfer of deuterium through a series of steps, from **71** to **73** passing by **72**. Then finally deuterium was incorporated into the *O*- and *N*-methyl groups of **60** by means of the *S*-adenosyl-L-methionine (SAM)-dependent methyltransferase **74** (**Figure 1.37**). Results from deuterium-labelling experiments also showed the absence of deuterium in C2′ indicating that only one deuterium atom from aspartic acid **71** reached the finally constructed aziridine moiety and that the remaining two deuteria were washed away during the formation process. As consequence, it was suggested that the deuterium seen in C1′ in azicemicin A **60** could be derived either from α- or from β-deuterium and that the absence of deuterium in C2′ depended on the biosynthetic faith of **71** during the biosynthetic path a or b shown in **Figure 1.37**.

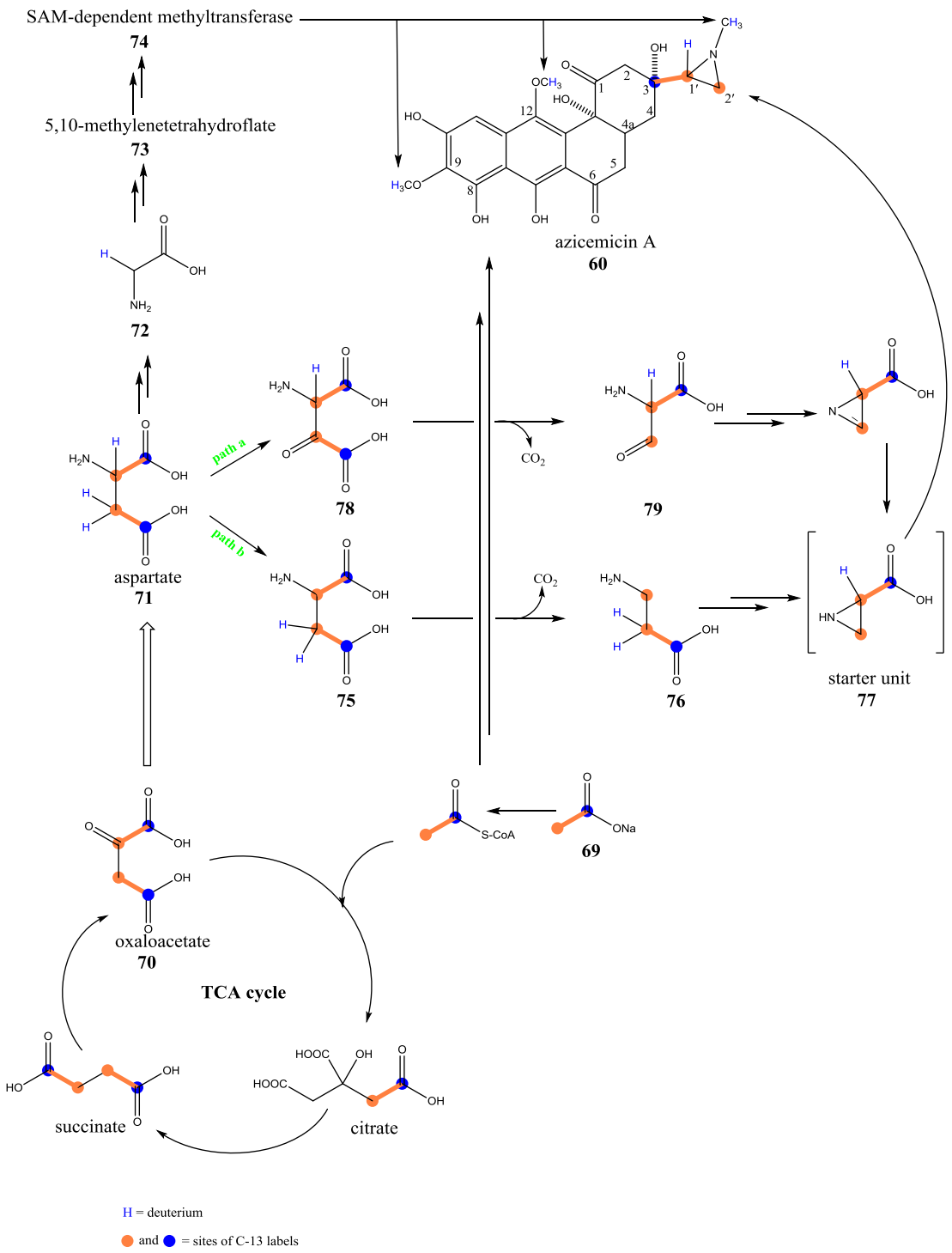

Figure 1.37: Incorporation of ^{13}C-labelled acetate and deuterium in aziridine starter unit **77** in azicemicin A **60**.

Ogasawara and Liu (2009) have made great advances in understanding of the genetics and enzymology of azicemicins' production. They have cloned and sequenced the azicemicin (*azic*) gene cluster and assigned functions to genes on the basis of

sequence comparison with known genes from the databank. In addition to genes encoding for type II PKS, the cluster harbours also two genes *azicM* and *azicV* encoding for two adenylyl transferases AzicM and AzicV, respectively. The authors investigated the substrate specificity of these enzymes based on gene expression experiments and enzyme activity assays and results showed that AzicM has preference for aspartate **71** (L and D forms). They concluded that AzicM catalyses the activation of L- or D-aspartate **71** by ATP-hydrolysis, as amino acyl adenylate. Additional genes contained in the cluster are a decarboxylase AzicN, that may play a role in the formation of the starter unit **77** by catalysing the decarboxylation of **80**, and an acyl carrier protein AzicP that tether the activated aspartate to it 4′-phosphopantetheine cofactor. The cluster also contains several oxygenase genes (*azicO*1, *azicO*2 and *azicO*6) encoding for enzymes involved in oxidation/hydroxylation reactions during the biosynthesis of the starter unit **81**. Additional oxygenase genes (*azicO*3, *azicO*4, *azicO*5 and *azicO*6) involved in the oxidation/hydroxylation of the angucycline core were also found contained in the cluster. The *azic* gene cluster reveals as well the presence of *azicT* gene encoding for AzicT enzyme that has sequence homology with numerous phosphopantetheinyl transferases and may play a role in the activation of AzicP during azicemicin biosynthesis. Unfortunately, all genetic manipulation efforts carried by the authors to verify the functions of these genes were unsuccessful and therefore they relied mainly on isotope labelling experiments and enzymatic studies, previously discussed, to propose the biosynthetic pathway for the formation of the aziridine carboxylate starter unit **83** in azicemicin A **60** (**Figure 1.38**).

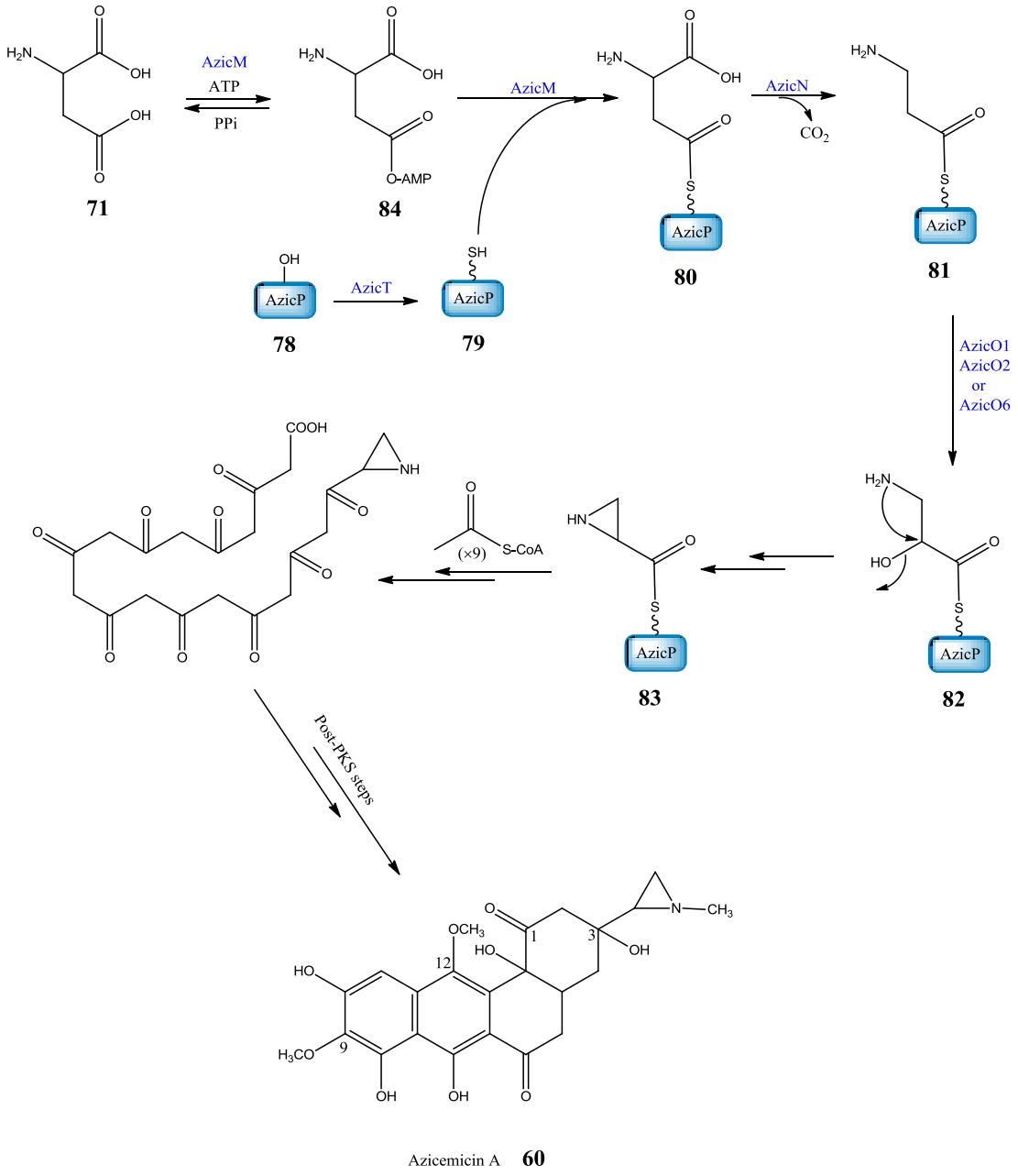

Figure 1.38: Aziridine carboxyl **83** formation in azicemicin A **60** biosynthesis.

During the first step of the formation of the aziridine carboxyl **83** (**Figure 1.38**), aspartate **71** (L or D) is activated by AzicM as amino acyl adenylate **84** before being transferred and tethered to the 4′-phosphopantetheine (4′-PP) cofactor of the carrier protein AzicP. The transfer of 4′-PP cofactor to the conserved serine residue of AzicP is catalysed by the phosphopantetheinyl transferase AzicT. Then, a decarboxylation reaction catalysed by AzicN led to the formation of AzicP-tethered β-alanine **81** from **80**. After a series of oxidation reactions catalysed by AzicO2, AzicO1 or O6 followed by cyclisation, compound **81** generated the AzicP-tethered isoserine **82** followed by the formation of the aziridine carboxyl starter unit **83**, respectively.

Although the mode of action of azicemicins A **60** and B **61** has not been studied yet, a reasonable hypothesis is that the antimicrobial activities of these compounds could be attributed to the aziridine moiety by analogy to the reactivity of the aziridine functional groups in azinomycins A **3** and B **4** and in several other aziridine-containing natural products (Ismail *et al*., 2009).

Comparison between the biosynthetic pathways of azinomycin B **4** and azicemicins A **60** and B **61** shows disparate strategies to generate the aziridine moieties. As matter of fact, feeding experiments and cloning and sequencing of gene clusters established that either ornithine or glutamate derivative is the precursor of the aziridine moiety in azinomyicin B **4** while aspartic acid **71** is found to be the precursor of the aziridine moiety in azicemicins' biosynthesis. Genetics efforts were unsuccessful in identifying the enzyme/enzymes catalysing the cyclisation of the aziridine moieties in both cases but succeeded to identify the origin of carbons C1′ and C2′ in azicemicins. Much remains to be discovered about the origin of carbons C10 and C11 of the aziridine ring in azinomycins.

1.8 Significance and definition of precursor-directed biosynthesis

Natural products from micro-organisms have traditionally played a significant role in clinical practice. These secondary metabolites with a broad spectrum of structural diversity cover a wide scope of biological activities ranging from antibiotics to immunosuppressants and from cytostatic to antitumor properties. Throughout thousands of years with continuous genetic mutations and environmental impacts, the devoted functions of these natural products were naturally enhanced and optimised. Furthermore, natural products present promising new scaffolds on which future drug development efforts can be focused (Grünewald and Mohamed, 2006).
However, natural products are not fully effective for the expected objective and generally do not exhibit optimum potency when tested against specific targets. In addition, they have the potential to cause unpleasant side-effects. The application of synthetic (or semi-synthetic) chemistry or combination of chemical and biological approaches (mutasynthesis and precursor-directed biosynthesis) to modify bioactive natural product leads are often seen as good solutions for problems such as increasing desired activity, or minimising toxic side effects.

Strategies and methods developed by organic chemists allowed the chemical synthesis of complicated natural product molecules such as vitamin B12 and chlorophyll a and also played a crucial role in the development of numerous medicinal drugs such as the antibiotic vancomycin and the anticancer agent epothilone (Nicolaou *et al*., 2000). However, organic synthesis has limitations in applicability for complex natural compounds that contain for example highly reactive groups such as azinomycin B **4**.

The semi-synthetic approach can be used as an alternative to develop new drugs with enhanced activity compared to the native natural compound. Some successful examples of drugs developed by this approach are the medically approved antibacterial drug tigecycline (analogue of tetracycline) and glycopeptide antibiotics that are in an advanced phase of clinical development. Furthermore, the combination of chemical and enzymatic tools proved to be a powerful technique to generate new lead drugs with improved activity such as analogues of epothilone and vancomycin (Lam, 2007).

Another important technique to generate novel drug leads from natural product producing organisms is through the mutasynthesis approach which developed from precursor-directed biosynthesis (see next paragraph). This technique is based on the cellular uptake of modified biosynthetic precursors that are fed to genetically engineered/mutant organisms which are blocked in various steps of the natural product biosynthesis pathway (Kennedy, 2008). One example of mutasynthesis was the production of the new bioactive compounds nikkomycins Lx and Lz (**Figure 1.39**) by the mutant of the wild type *Streptomyces tendae* Tü901. The mutant was obtained by inserting a kanamycin resistance gene in the nikkomycin biosynthesis gene *nikF* encoding a cytochrome P-450 monooxygenase. The new antibiotic compounds, which lack the oxygen atom of the pyridyl residues, are respective derivatives of the natural antibiotics nikkomycins X and Z (**Figure 1.39**) that are produced by *S. tendae* Tü901. Studies on the stability of nikkomycins Lx and Lz at various pH values using nikkomycins X and Z as references, showed that they were more stable under various condition than the reference compounds. Additional work on the biological activity of nikkomycins Lx and Lz showed a slightly lower or similar activity to nikkomycins X and Z when tested against a variety of fungi microorganisms (Bormann *et al*., 1999).

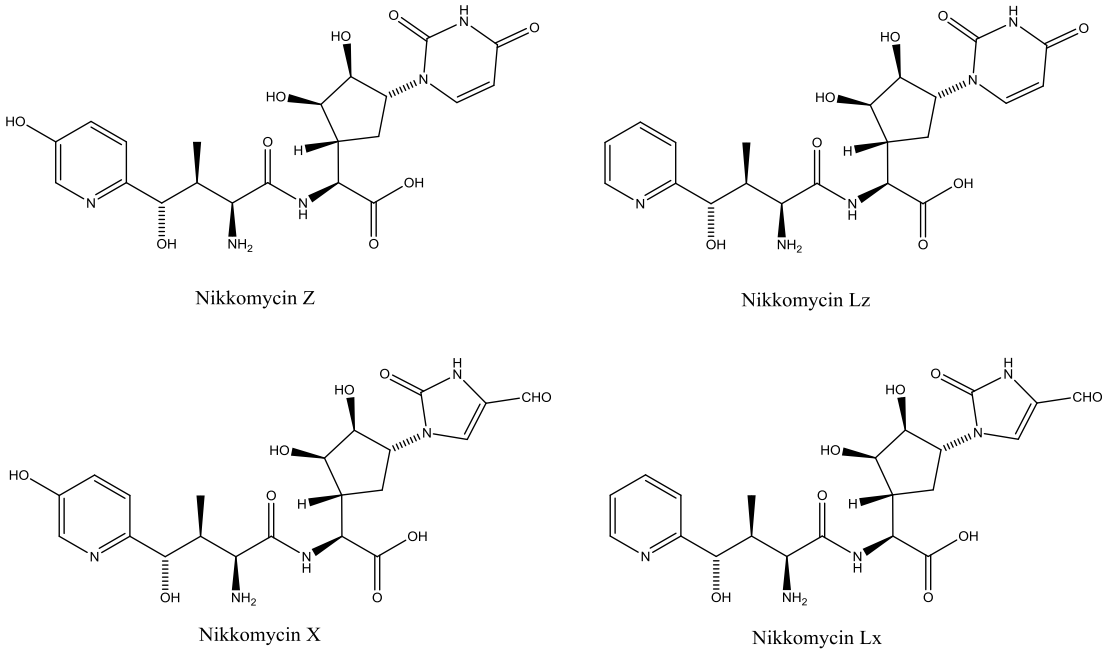

Figure 1.39: Structures of the natural antibiostics nikkomycins X and Z and the corresponding derivatives Lx and Lz.

PDB can also be used to generate natural product analogues by adding enzyme inhibitors (to the culture media), which are able to block a particular biosynthetic pathway biochemically. This approach has been used by Ritacco and co-workers (2005) to generate new rapamycin analogues by incorporating unusual analogues of the normal amino acid, L-pipecolate, into the rapamycin **85** compound. Rapamycin **85** is a polypeptide-polyketide natural product produced by *Streptomyces hygroscopicus* ATCC 29253 and exhibits potent immunosuppressive and anticancer activities which are useful properties to generate novel drug leads. Also compound **85** is known to involve several features in its biosynthesis and of particular note the enzyme lysine cyclodeaminase which is encoded by the gene *rapL* and known to catalyse the cyclisation and conversion of the amino acid L-lysine to L-pipecolate (Nancy *et al*., 1993; Khaw *et al*., 1998) (**Figure 1.40**).

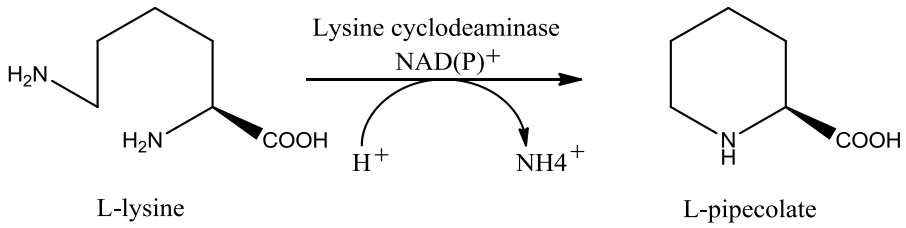

Figure 1.40: Lysine cyclodeaminase catalysing the cyclisation and conversion of L-lysine to L-pipecolate.

Another biosynthetic feature in rapamycin biosynthesis is the pipecolate-incorporating enzyme that is encoded by the *rapP* gene and recognised for its catalytic incorporation of L-pipecolate as well as the pre-rapamycin ring closure (Molnár *et al*., 1996). Based on the knowledge about the biosynthetic assembly of rapamycin **85** natural product, Ritacco and co-workers (2005) carried out feeding experiments using pipecolate analogues (1,4-thiazane-(3*S*)-carboxylic acid **86** and 1,3-thiazane-(4*S*)-carboxylic acid **87**) in the presence of racemic (±)-nipecotic acid **88** (inhibitor of L-pipecolate biosynthesis) **(Figure 1.41)**. Results showed incorporation of the two sulfur-containing analogues of L-pipecolate into the rapamycin **85** molecule yielding the new rapamycin analogues 20-thiarapamycin **89** and 15-deoxo-19-sulfoxylrapamycin **90**, respectively **(Figure 1.41)**. Structurally, the product **89** was identical to rapamycin **85** except for the presence of a sulfur atom on the pipecolate/thiazane ring while the second product **90** showed a new sulfoxide group which was derived from the oxidation of the thiazine sulfure and also revealed an absence of the C15 carbonyl indicating a possible disruption in the activity of the downstream cytochrome P-450 monooxygenase.

(A)

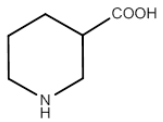

88

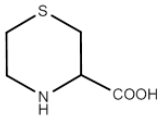

86

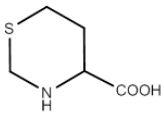

87

(B)

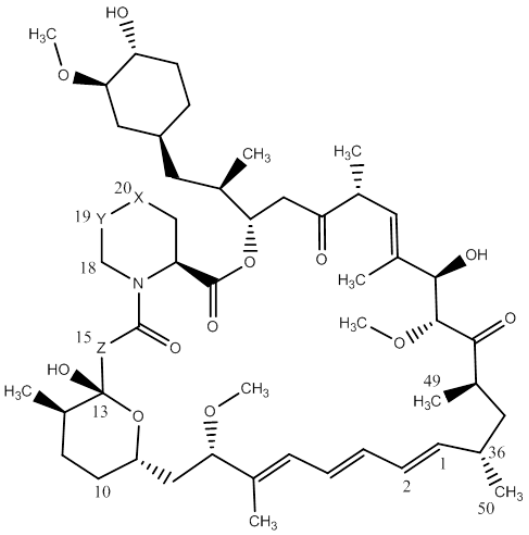

	X	Y	Z
rapamycin **85**	CH_2	CH_2	C=O
20-thiarapamycin **89**	S	CH_2	C=O
15-deoxo-19-sulfoxylrapamycin **90**	CH_2	S=O	CH_2

Figure 1.41: Structures of the fed precursors used in the study and their corresponding products. (A): Structures of (±)-nipecotic acid **88**, 1,4-thiazane-(3*S*)-carboxylic acid **86** and 1,3-thiazane-(4*S*)-carboxylic acid **87**. (B): Structures of rapamycin **85**, 20-thiarapamycin **89** and 15-deoxo-19-sulfoxylrapamycin **90**.

Bioactivity assays were carried by Ritacco *et al*. (2005) and results revealed that rapamycin analogues **89** and **90** were weaker binders to FKBP12 compared to the natural product rapamycin **85** and that **90** showed the least binding activity as consequence to the lack of the C15 carbonyl group.

One more powerful, attractive and easy approach toward trying to generate novel microbial natural product derivatives is precursor-directed biosynthesis (PDB). PDB involves the addition of biosynthetic precursor analogues to the culture broth of the producing organism. In order to become incorporated into the organism's metabolic

pathway and produce novel metabolites, the added precursor has to be channelled from the growth medium into the producing organism cells and accepted by the biosynthetic enzymes (Timothy *et al*., 2000). Thiericke has defined precursor-directed biosynthesis as "*the derivatisation of a secondary metabolite by feeding the biosynthetic precursor analogues to the fermentation broth of producing organisms*" (Thiericke and Rohr, 1993). The secondary metabolite biosynthetic enzymes often show a certain degree of flexibility as to what substrates they accept. Amide synthases and non-ribosomal peptide synthetases (NRPSs) are some examples of secondary metabolite biosynthetic enzymes exhibiting broad substrate specificity (Thiericke and Rohr, 1993; Kleinkauf and Von. Doeren, 1996). Over many years, a number of new lead compounds have been developed by the PDB approach (Goss *et al*., 2012). The lipopeptide antibiotic A54145 **(Figure 1.42)** is one example**.** This antibiotic which inhibits Gram positive bacteria is a complex of eight lipopeptide compounds [A, A1, B, B1, and C to F] produced by *Streptomyces fradiae* (Thiericke and Rohr., 1993). The similarities between the antibiotic A54145 components include four peptide cores that diverge by only few amino acids. Another feature of the A54145 complex is the diversity of the fatty acid side chains which form an amide bond with the N-terminus of the peptide nucleus. In an attempt to produce antibiotic analogues or to improve the biosynthesis of certain native metabolites, a range of fatty acid precursors (from acetate to oleate lipids) were fed to *Streptomyces fradiae* (strain NRRL 18158). New derivatives of the A54145 complex, containing previously undiscovered C6, C8 and C9 acyl units resulted from feeding hexanoate, caprylate and nonaoate, respectively. The produced compounds were detected and isolated from the culture media (Thiericke and Rohr, 1993).

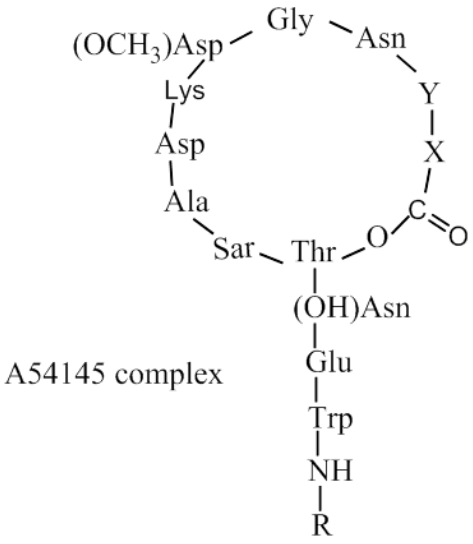

A54145 complex

Factor	MW	X	Y	R
(40) A	1643	Ile	Glu	8-Methylnonanoyl (iC_{10})
(41) A_1	1643	Ile	Glu	n-Decanoyl (nC_{10})
(42) B	1657	Ile	3-MethylGlu	n-Decanoyl (nC_{10})
(43) B_1	1657	Ile	3-MethylGlu	8-Methylnonanoyl (iC_{10})
(44) C	1657	Val	3-MethylGlu	8-Methyldecanoyl (aC_{11})
(45) D	1657	Ile	Glu	8-Methyldecanoyl (aC_{11})
(46) E	1671	Ile	3-MethylGlu	8-Methyldecanoyl (aC_{11})
(47) F	1629	Val	Glu	8-Methylnonanoyl (iC_{10})

Figure 1.42: Illustration of the A54145 complex (Adapted from Thiericke and Rohr, 1993).

Another example of the application of PDB is the generation of jadomycin analogues **91** (**Figure 1.43**) through amino acids feeding experiments. Jadomycin family of natural products are angucycline polyketides exhibiting potent antibacterial, anti-tumour, antiviral and Aurora-B kinase inhibitory activity. It is assumed that the addition of L-isoleucine and also amino acids **92** with the polyketide core **93** (**Figure 1.43**) is likely to be a non-enzymatic reaction (Rix *et al*., 2004). Cottreau and co-workers (2010) carried out their experiments by feeding a series of proteinogenic and non-proteinogenic amino acids to the producing bacteria *Streptomyces Venezuelae* ISP5230. Results revealed the production of jadomycin analogues which were then assessed for their DNA-cleaving profiles in the presence of metal catalysts.

Incorporation of alternative amino acids, in place of the natural L-isoleucine, into the metabolite resulted in modifications to the natural oxazolone ring. The unnatural amino acid starting units were processed with no racemisation at the α-carbon. These studies provided deeper insight into the flexible nature of the glycosyltransferase JadS, which acts upon the natural product following oxazolone formation. Cytotoxic assays reveal that the activity of these compounds increases in proportion to the polarity of the side chains (Syvitski *et al*., 2006; Borissow *et al*., 2007).

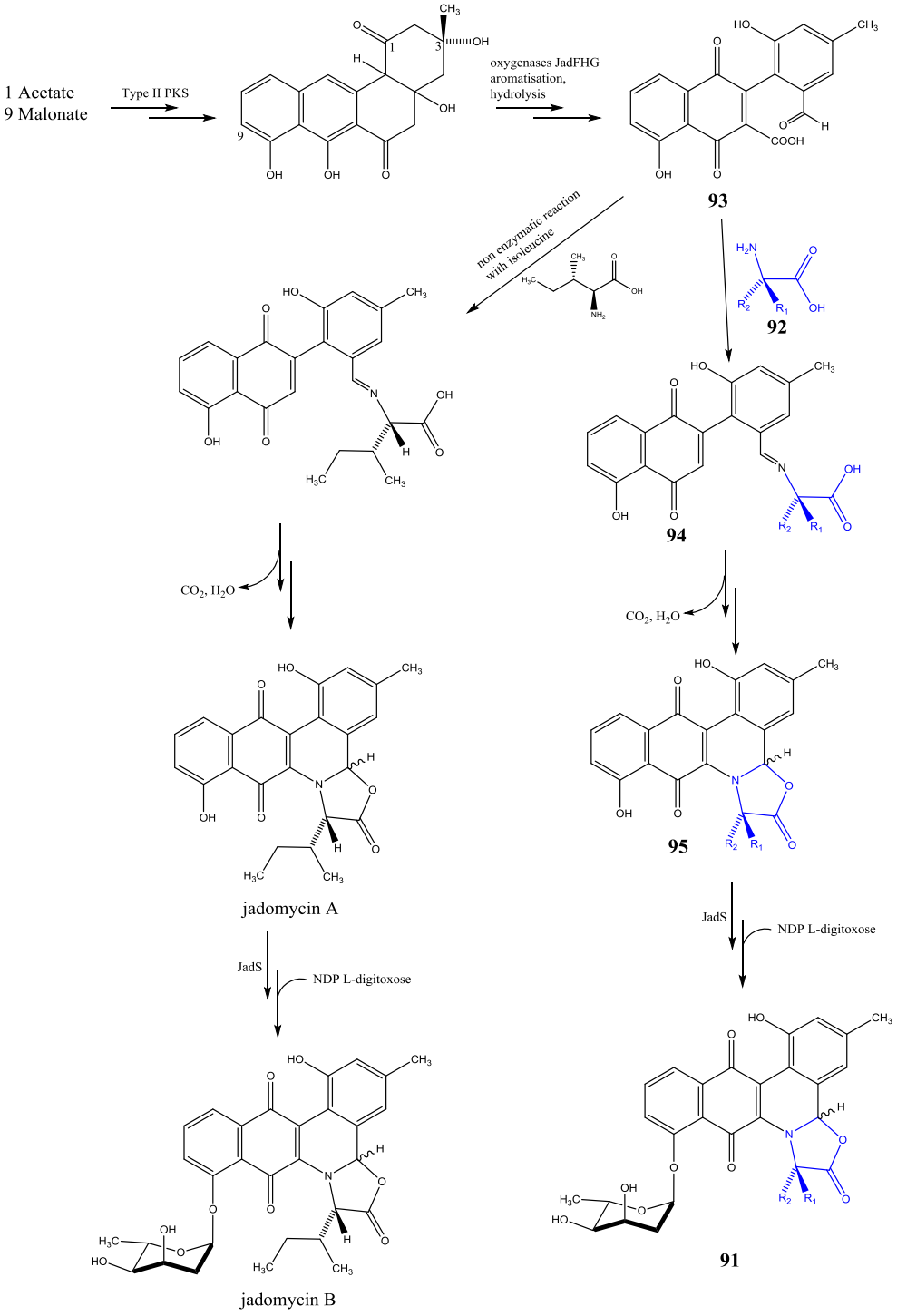

Figure 1.43: Biosynthesis of jadomycins A and B and related analogues **91**. Analogues were generated through feeding various natural and unnatural amino acids (in blue). A wide variety of natural and non-proteinogenic amino acids combine with the polyketide core **93** and it is postulated that this step is non-enzymatic (Rix *et al.*, 2004). The enzyme JadS is involved in installing the L-digitoxose sugar unit onto jadomycin B.

1.9 The use of fluorine compounds in PDB

During the last two decades fluorine-containing compounds have widely spread into medicinal chemistry and new highly effective drugs have emerged since then (Hans-Joachim *et al*., 2004; Iwao, 2004). The introduction of fluorine into molecules has been an important concept for many reasons. Firstly, fluorine atom(s) are introduced into the organic compounds to circumvent the low metabolic stability of the drug. Secondly, fluorine affects the physicochemical properties of the fluorinated molecule. Being a highly electronegative atom, fluorine vastly affects the acidity and basicity of the neighbouring functional groups by varying their dissociation constant (pKa). As a consequence, the binding affinity of the molecule is affected by this pKa change. Also, it has been shown that the binding affinity of the molecule increases by the effect of the fluorine on the lipophilicity of the molecule. Finally, a change towards a preferable molecular conformation can be triggered by the introduction of fluorine into the target molecule. For example, the substitution of the methoxy group of methoxybenzenes without ortho substituents with the trifluoromethoxy group (OCF_3) leads to a twist in the favoured planar conformation by many degrees (Hans-Joachim *et al*., 2004).

Natural products are considered as biologically validated lead structures, and a lot of research has been done to develop new fluorine compounds with novel or enhanced biological properties. Fluorinated natural compounds are considered rare compared to other halogenated compounds (Vaillancourt *et al*., 2006). However, precursor-directed biosynthesis (PDB) is one among many biotechnological approaches that can be used to generate novel fluorinated metabolite analogues. For example, Kawashima and co-workers prepared fluorinated derivatives of the antibiotic vulgamycin (**Figure 1.44**) that is produced by *Streptomyces hygroscopicus* (Kawashima *et al*., 1985). As the aromatic part of vulgamycin antibiotic is derived from benzoic acid, the authors used fluorobenzoic acids as precursors for directed biosynthesis. To the culture broth of *S. hygroscopicus*, they added fluorinated precursors such as *ortho*-, *meta*-, and *para*- fluorobenzoic acids at a concentration of 100 μg ml^{-1} and the cultivation was continued for 120 hrs. The identity of the fluorinated analogues, produced in the culture media, was elucidated by ^{19}F NMR spectroscopy. The results showed a very significant (70%) incorporation of the added compounds. ^{1}H and ^{13}C NMR analysis

were used to determine the structures of the isolated fluorovulgamycins. The antibacterial activities of the isolated fluoro-compounds were then tested and results indicated that they were not effective against the test organisms except for *Micrococcus luteus* ATCC 9341 and that para-fluorovulgamycin showed stronger activity than vulgamycin against this organism.

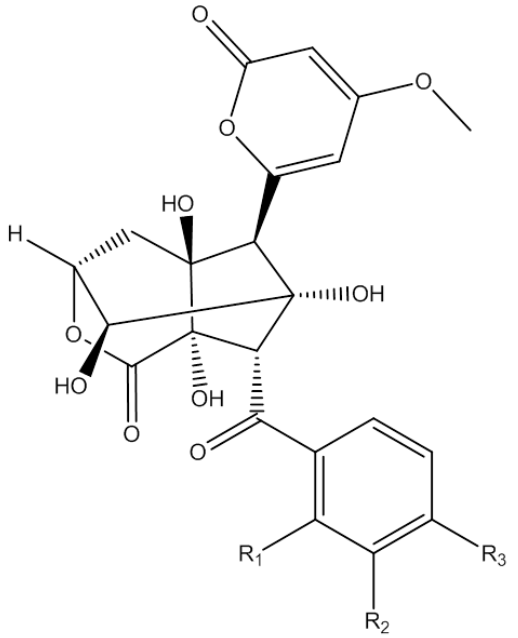

	R_1	R_2	R_3
Vulgamycin	H	H	H
Ortho-fluorovulgamycin	F	H	H
Meta-fluorovulgamycin	H	F	H
Para-fluorovulgamycin	H	H	F
3',4'- difluorovulgamycin	H	F	F

Figure 1.44: Structures of vulgamycins and fluorovulgamycins (**Figure** adapted from Kawashima *et al*., 1985).

The second example of the application of fluorinated compounds in PDB is the generation of soraphen A **96** analogues by Hill and Thompson (2003). Soraphen A **96** polyketide natural product was originally isolated from the culture broth of *Sorangium cellulosum,* a soil dwelling myxobacterium and exhibited inhibition activity against fungal growth (Gerth *et al*., 1994; Vahlensieck *et al*., 1994). The

complete biosynthetic gene cluster for the synthesis of soraphen A **96** was cloned and sequenced and results (**Figure 1.45**) revealed that **96** is biosynthesised by a type I PKS and that the first module in the soraphen PKS recognises and processes a rare benzoyl CoA as starter unit (Ligon *et al*., 2002). Hill and co-workers (2003) investigated the scope of the soraphen PKS-substrate flexibility by feeding various fluorinated forms of phenylalanine, cinnamate and benzoate to the wild type organism. Analysis of the crude broths by ^{19}F NMR and LC-MS showed the production of novel fluorine-containing soraphens (**Figure 1.45**) for the cultures fed *meta* and *para* substituted phenylalanine and cinnamate and that no production of soraphen analogues was seen in the other cultures. Also higher cell counts and soraphen titres were observed for cultures administered with *meta* and *para*-fluorocinnamates compared to phenylalanine. Additional feeding experiments were carried out by the authors to investigate whether chlorinated and brominated starter units (4-chloro and 4-bromocinnamate) could be recognised and loaded by the soraphen PKS starting domain. LC-MS analyses revealed the presence of chlorinated and brominated soraphen analogues in the crude extracts.

Biological activity tests were carried out against the fungus *Botrytis cinerea* using 3′-fluoro soraphen A and 4′-fluoro soraphen A and results showed that these novel compounds were less active than the natural soraphen A **96**.

These results showed that the soraphen starting domain can accept and process some non-natural starter units. However, production relative to soraphen A **96** itself was low, probably due to the preference of the PKS for the natural starter moiety, and none of the tested analogues exhibited a better bioprofile compared to **96**.

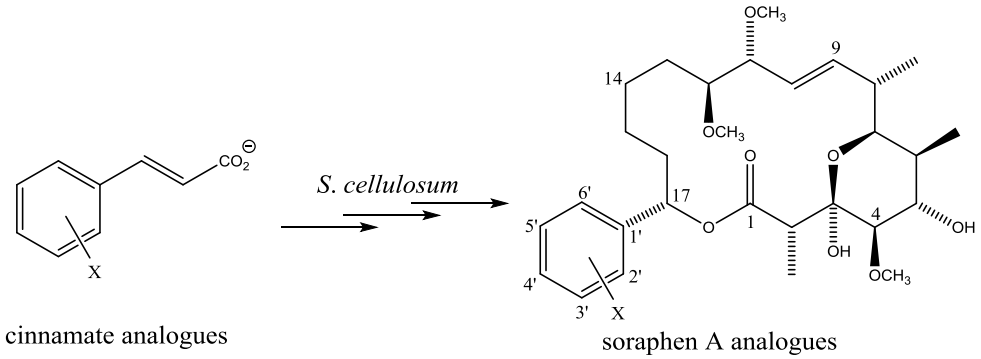

cinnamate analogues

soraphen A analogues

X = H soraphen A **96**
X = 3'-F, 3'-fluoro soraphen A
X = 4'-F, 4'-fluoro soraphen A
X = 3',4'-F_2, 3',4'-difluoro soraphen A
X = 3',5'-F_2, 3',5'-difluoro soraphen A
X = 4'-Cl, 4'-chloro soraphen A
X = 4'-Br, 4'-bromo soraphen A

Figure 1.45: Generation of soraphen A analogues by feeding cinnamate analogues to the producing bacteria *Sorangium cellulosum*.

1.10 General aims of the present study

The aim of this project was to investigate the scope of precursor-directed biosynthesis for the production of novel azinomycin metabolites by feeding commercially available and synthetic analogues of the naphthoate moiety. These new azinomycins might have improved anticancer activity, and results of this study will give insight into the substrate specificity of the azinomycin biosynthetic enzymes.

Chapter 2: Materials and Methods

2.1 Materials

2.1.1 Reagents

Reagents used for the feeding experiments were purchased from Sigma-Aldrich or Acros Organics unless otherwise stated and were used as received (purity: 97-99.5%). 3-Methoxy-1-naphthoic acid **97** (**Figure 2.1**) was a generous gift from Cyrille Landreau, a post doc in Exeter and 3-Fluoro-1-naphthoic acid **98** (**Figure 2.1**) was supplied by Mike Shipman who was Dr in Exeter, then was promoted to Prof at the University of Warwick, Coventry. Culture media were purchased from Oxoid or BDH. Commercial solvents were used as received from Sigma-Aldrich, Fisher Scientific, VWR or Acros Organics. Solvents used for LCMS (Liquid chromatography/mass spectrometry) experiments were of LCMS grade. Solvents used for all other experiments were of HPLC (High Performance Liquid Chromatography) grade unless otherwise stated. Flash column chromatography Silica 60A (40-63 micron) was purchased from Fisher Scientific. Thin-layer chromatography (TLC) aluminium sheets (20 × 20 cm) with 0.20 mm silica gel 60 was purchased from Alugram® or MERCK. Ultrafiltration filters (Millipore) were purchased from Fisher Scientific.

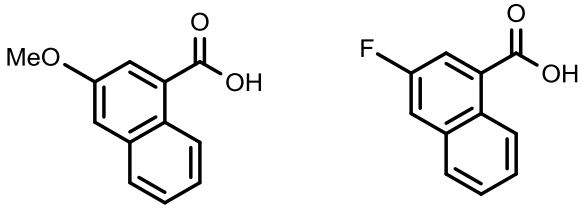

97 **98**

Figure 2.1: Structure of compounds **97** and **98.**

Feeding experiment reagents

All reagents used for fermentation feeding experiments are commercially available except reagents **97** and **98**.

2.1.2 Bacterial strains

Streptomyces sahachiroi (ATCC 33158) was used in this study and was obtained from the American Type Culture Collection (ATCC).

Escherichia coli K1 and K12 strains used in disk diffusion assay (DDA) and spot culture growth inhibition assay (SCGIA) (Evangelopoulos and Bhakta, 2010) were provided by Dr. Parissa Mortavazi. Other bacterial strains used in DDA, SCGIA and bioactivity tests are *Escherichia coli, Micrococcus luteus*, *Bacillus subtilis, Bacillus megaterium*, *Pseudomonas diminutus* and *Staphylococcus epidermis*. Fungi used in disk diffusion assay and bioactivity tests are *Trichoderma harzianum*, *Pyrenophora avenae*, *Rhizoctonia solani* and *Fusarium oxysporum*.

Both bacteria strains and fungi were obtained from the general stock in the Microbiology Research Laboratory at Birkbeck College.

2.1.3 Growth Media

All growth media were sterilised by autoclaving at 121 ^{o}C for 18 minutes and at 1.1 bar pressure in a Priorclave (Biocote Ltd) machine.

Glucose, Yeast extract and Maltose extract (GYM)

GYM agar medium contained the following components per litre of tap water: 5 g glucose monohydrate (BDH), 5 g yeast extract (Oxoid), 10 g malt extract (Oxoid), 2 g $CaCO_3$ (BDH) and 12 g agar (Oxoid). GYM liquid medium was made the same way except that $CaCO_3$ and agar were omitted. Both media were adjusted to pH 6.8 with 1 M NaOH and sterilised by autoclaving.

Pharmamedia and Starch (PS5)

PS5 liquid medium contained the following ingredients per litre of tap water: 5 g Pharmamedia (yellow cotton seed flour) (Traders Protein, Southern cotton oil company, USA) and 5 g soluble starch (BDH). The medium was adjusted to pH 7.0 with 1 M NaOH and sterilised by autoclaving.

Nutrient Agar (NA)

NA medium contained the following components per litre of distilled water (dH_2O):
1 g *'Lab-lemco'* powder (Oxoid), 2 g yeast extract (Oxoid), 5 g peptone (Oxoid), 5 g NaCl (Oxoid) and 5 g agar (Oxoid). The medium was adjusted to pH 6.8 with 1 M NaOH and sterilised by autoclaving.

Potatoes Dextrose Agar (PDA)

PDA medium contained the following components per litre of dH_2O:
4 g potato extract (Oxoid), 20 dextrose (Oxoid) and 15 g agar (Oxoid). The medium was adjusted to pH 5.6 ± 0.2 with 1 M NaOH and sterilised by autoclaving.

Trypticase Soy Agar (TSA)

TSA medium contained the following components per litre of dH_2O:
15 g tryptone (Oxoid), 5 g soytone (Oxoid), 5 g NaCl (Oxoid) and 15 g agar (Oxoid).

***Streptomyces refuineus* Agar (SRA)**

5 g NZ amine (casein hydrolysate) (Sigma), 2 g yeast extract (Oxoid), 2 g soytone (soya peptone) (Oxoid), 1 g soluble starch (BDH), 5 g D-mannitol (BDH), 15 mg $FeSO_4.7H_2O$ (BDH) and 20 g agar (Oxoid) were weighed and dissolved in 1 litre dH_2O. The medium was adjusted to pH 7.0 with 1 M NaOH and sterilised by autoclaving.

2.2 Methods

2.2.1 Chemistry

Extraction and evaporation

As cited on the literature (Hata *et al.*, 1954; Nagaoka *et al.*, 1986; Kelly *et al*., 2008), Liquid-liquid or solvent extraction technique was used in this study to separate the desired compounds (azinomycin A, azinomycin A analogues and other novel additional metabolites) from the bacterial supernatants subsequent to centrifugation.

In fact *S. sahachiroi*'s fermentation broths were centrifuged for 10 min at 6000 × g at 4 ^{o}C in a Beckman Avanti J-26XP centrifuge machine then supernatants were extracted with an equal volume of chloroform. The organic layers were dried over $MgSO_4$ and concentrated using a rotary evaporator.

Since the metabolites of interest were relatively small organic compounds (relative molecular weight (MW): 170-700 MW), they were expected to partition mainly into the organic layer. The expectation was not only based on literatures (Hata *et al.*, 1954; Nagaoka *et al.*, 1986) but was supported by the experimental work as well (**Chapter 4**).

Separation by High Performance Liquid Chromatography (HPLC or LC)

During HPLC separation methods, HPLC (Agilent 1100 LC system) was equipped with diode array detector (DAD) that recorded UV/VIS spectra up to six different wavelengths. Chromatograms were recorded at 350 nm. The system was also coupled to mass spectrometry (MS), a Bruker Esquire 3000 mass spectrometer with electrospray ionization (ESI) source operating on either positive (+) or negative (–) ionization mode. The instrument was operated with Agilent ChemStation and Bruker Esquire Control software, data was processed using Bruker Data Analysis software.

Preparative HPLC (prep HPLC)

Throughout chromatographic processes, separation was done with a pre-degassed mobile phase consisting of a mixture of water and methanol (45:55). Throughout the isolation process, C18 column (ACE5 250 × 21.2 mm) was used, the flow rate was of 5 mL min^{-1} and the injection volume of extract was 100 µl. The amount of sample injected was around 4-6 mg. Isolation and purification was processed by manual fraction collection based upon the online signal plot and mass-based identification. The signal plot was generated from DAD (using detection at 350 nm) and displayed by the instrument. The mass identification was based on the fact that the molecular mass of the compound of interest (azinomycin A or its analogues) was known and the detection mode was based on the ionization process used by the MS with the ESI source. The MS was operating on a positive ionization mode: ESI (+) with a nebulizer = 2 psi, a dry gas = 6 l min^{-1} and dry temperature = 330 ^{o}C.

Once the identified fraction was collected in a 50 mL Falcon tube, it was concentrated in a rotary evaporator, redisolved in methanol (0.5 mL) and LCMS analyses were done for confirmation of purity.

Analytical HPLC

Through chromatographic procedures, separation was done with a pre-degassed mobile phase consisting of a mixture of water and methanol (45:55). The separation was developed using either C8 microbore column (ACE3, 100 × 2.1mm) or C18 analytical column (ACE5, 250 × 4.6mm). The flow rate was 0.2 mL min^{-1} and the injection volume of extract was 5 µl when using C8 microbore column. The C18 analytical column was deployed when the flow rate and injection volume were increased (1 mL min^{-1} and 20 µl respectively). The amount of sample injected each time was very small (2-15 µg) in order not to exceed the column capacity. The target compounds were detected by DAD and mass-based identification.

Structure elucidation

MS and tandem mass spectrometry (MS/MS) were the main techniques used to elucidate and characterize the structures of purified azinomycin A **3** and its analogues (**Chapter 4**). NMR characterisation could not yet be conducted because of the low yields and the persistence of some impurities in the native azinomycin A **3** and its analogues. Attempt to characterise azinomycin A **3** by ^{1}H-NMR was unsuccessful as shown in **Figure 2.2** (**Appendix one**).

The MS, one and two dimensional NMR and infra-red (IR) spectrometry techniques were used to characterize the structures of purified 1-naphthoic amide **99a** and 4-fluoro-1-naphthoic amide **100a**. The remaining purified compounds (4-methyl-1-naphthoic amide **101a**, 2-methyl-1-naphthoic amide **102a**, 2-methoxy-1-naphthoic amide **103a**, 3-methoxy-1-naphthoic amide **97a** and 3-fluoro-1-naphthoic amide **98a**) were characterized by MS only as NMR analysis was hampered by impurities. Additionally, the apparent new compound resulting from feeding hydrazine dihydrochloride **111** was not identified yet and can be characterized by one and two dimensional NMR. Finally, melting points (m.p.) were determined for all purified compounds except azinomycin A analogues because of the low production levels.

All MS/MS were performed using a Bruker (Bruker Esquire 3000 mass spectrometer) with helium as collision gas. The first analyzer was used to isolate the precursor ion (parent ion) of chosen m/z ratio. By increasing the activation energy inside the spectrometer, collision between helium gas and the selected ion resulted in a fragmentation process generating product ions. Then a second mass spectrometer analyzed the product ions.

NMR spectra for naphthoic amides **99a** and **100a** were recorded on an AMX Bruker 300 MHz spectrometer while the apparent NMR spectrum for azinomycin A (**Figure 2.2, Appendix one**) was done on a Bruker AV600 spectrometer. One-dimensional (1D) NMR and two-dimensional (2D) NMR were performed at room temperature. Chemical shifts are given in ppm (δ) relative to $CDCl_3$ (7.26 ppm for ^1H NMR and 77.2 for ^{13}C NMR) and coupling constants (J) are reported in Hertz (Hz). Signals are designated as follows: s, singlet; d, doublet; t, triplet; q, quadruplet; m, multiplet; br s, broad singlet.

IR spectra were recorded using a Satellite FTIR Thermo Mattson spectrometer.

2.2.2 Microbiology

The following paragraphs describe the techniques and procedures used for the growth, conservation and maintenance, biological activity tests and feeding experiments of bacteria. This section also illustrates the antifungal activity tests used during this study.

Bacterial maintenance

Streptomyces sahachiroi K-534 (ATCC 33158) cultures were maintained by transfer onto GYM agar prepared plates. The plates were grown at 30 ^oC in a Scientific Isotemp. incubator for 5-7 days then kept at room temperature. New plates were spread every two weeks.

Spore suspensions Spore stocks:

5 mL of sterile distilled water were added to a fresh plate culture of *Streptomyces sahachiroi*. The surface of the culture was scraped with a sterile inoculating loop to suspend the spores. All the suspension was removed, pipetted into a 50 mL Falcon

tube and then centrifuged for 10 min at 4000 × g. The pellet (spores) was resuspended in 500 µL of 20% sterile glycerol, transferred to a 2 mL screw tap vial tube, flash frozen, and stored at – 80 ^{o}C.

Streptomyces sahachiroi batch cultures

First stage culture. One loopful of aging spores from a culture grown on a GYM agar plate at room temperature for 3-6 months was used to inoculate 50 mL of GYM liquid medium in a 250 mL Erlenmeyer flask containing a 30 cm spring to disperse spores. The culture was incubated in an orbital shaker at 30 ^{o}C for 24 h at 200 rpm.

Second stage culture. An aliquot (2 mL) from the first stage culture was used to inoculate 50 mL of PS5 medium in a 250 mL Erlenmeyer flask containing a 30 cm spring. The culture was incubated in an orbital shaker at 30 ^{o}C for 24 h at 200 rpm.

Fermentation cultures. 20 mL of the second stage culture were inoculated into 2 L Erlenmeyer baffled flasks containing 500 mL of PS5 medium. The culture was incubated at 30 ^{o}C for 64 h at 200 rpm.

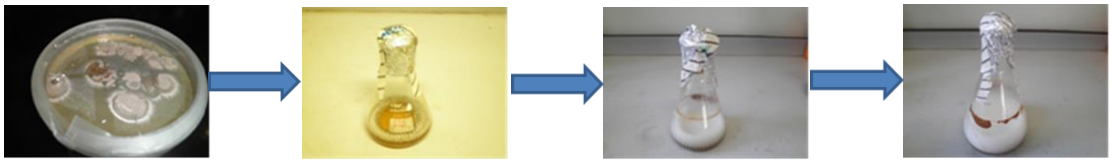

a b c d

Figure 2.2: Sequence of fermentation system: (a) GYM spores. (b) First stage culture. (c) Seed culture. (d) Fermentation broth.

Streptomyces sahachiroi growth curve

One loopful of aging spores from a culture grown on a GYM plate at room temperature for 3-6 months was used to inoculate 50 mL of GYM medium in a 250 mL Erlenmeyer flask containing a 30 cm spring. The culture was incubated in an orbital shaker at 30 ^{o}C for 24 h at 200 rpm. Samples (3 × 2 mL) were used to inoculate a triplicate 50 mL of PS5 medium in a 250 mL Erlenmeyer flask. The culture was incubated at 30 ^{o}C for 80 h at 200 rpm. Aliquots containing 0.1 mL were taken every 4 h (for 80 h), serially diluted in sterile saline solution (NaCl at 0.8 g %) and were subcultured in triplicate on GYM agar plates. The cultures were incubated at 30 ^{o}C for 48 h and the number of viable cells was determined by colony forming

units (CFU) using the formula: Number of colonies × dilution factor × 10 cells /mL). The number of viable bacteria cell per mL was measured over time and was plotted as a graph of average $\log_{10}$ viable cell number per mL against time.

Time course of the production of azinomycin A

One loopful of aging spores from a culture grown on a GYM solid plate at room temperature for 3-6 months was used to inoculate 50 mL of GYM liquid medium in a 250 mL Erlenmeyer flask containing a 30 cm spring. The culture was incubated in an orbital shaker at 30 ^{o}C for 24 h at 200 rpm. Samples (3 × 10 mL) were used to inoculate a triplicate 250 mL of PS5 medium in a 1 L Erlenmeyer flask. The culture was incubated at 30 ^{o}C for 80 h at 200 rpm. Aliquots containing 2 mL were taken every 4 h, transferred to a 15 mL Falcon tubes and stored in the freezer at –20 ^{o}C. Then cultures were centrifuged for 10 min at 6000 × g at 4 ^{o}C in a Beckman Avanti J-26XP centrifuge machine. The cell pellets were discarded and the supernatants extracted with the same volume of chloroform (1×). The organic layers were collected, concentrated in a HOWE Gyrovap centrifuge and redisolved in the minimum amount of chloroform. LCMS samples were prepared by mixing 50 µL from each sample with 950 µL of LCMS solvents system (water:methanol in the ratio of 65:35). The time course of azinomycin A production was followed by measuring the peak area for each HPLC chromatogram and then plotted as a graph of peak area against time.

Disk diffusion Assay (DDA)

Antibacterial test

A loopful of each bacterial culture (**section 2.1.2**) was used to inoculate nutrient agar plates. The cultures were incubated for 24-48 h at 37 ^{o}C. Using a sterile loop, a colony from each plate was emulsified in a sterile 15 mL Falcon tube containing 1 mL sterile saline solution (NaCl 0.8 g %), mixed thoroughly until no solid material from the colony was visible. The procedure was repeated until the solution became cloudy. The turbidity of the bacterial suspension was then adjusted to a prepared 0.5 McFarland turbidity standard. It was prepared by adding 0.5 mL of a 1.175% (*w*/*v*) barium chloride dihydrate ($BaCl_2.2H_2O$) solution to 99.5 mL of 1% (*v*/*v*) sulphuric acid. The turbidity standard aliquots (1 mL) were then transferred to a sterile 15 mL

Falcon tubes, sealed tightly with parafilm and stored in the dark at room temperature. Aliquots (100 µL) from bacterial suspension were then transferred to agar plates and spread evenly using a sterile glass spreader. Sterile Whatman antibiotic disks (Tong *et al*., 2011) were inoculated in triplicate with 10 µL of *S. sahachiroi* fermentation crude extracts or purified compounds (dissolved in methanol) at different concentrations (a range of concentrations from 120 to 5 mg mL^{-1} for crude extracts and 2 to 1 mg mL^{-1} for pure compounds). In some agar plates, two different compounds were used where each of them was inoculated in duplicate. In every plate, a control disk was used and was inoculated with 10 µL of methanol only. Using sterile forceps, the disks were applied to the plates at equal distances (4 or 5 disks per plate, of which one was used as control), gently pressed onto the surface of the agar, taking care not to press them into the agar and the plates were inverted and incubated for 24 hours at 37 ^{o}C.

Antifungal test

A disk of each precultured fungus colony (**section 2.1.2**) was cut with a cork-borer (5 mm diameter), and the trimmed colony disk was placed in the centre of the PDA media. The procedure of applying and inoculating the disks was the same as the one, described previously for antibacterial test except that the plates were not inverted and were incubated for 3-5 days at 25 ^{o}C.

Spot culture growth inhibition assay (SCGIA)

The assay was established for mycobacterial cultures (Evangelopoulos and Bhakta, 2010) and was used (with the following modifications: 2.5 mL was used in each well instead of 5 mL to increase the concentration of each tested compound) in this study towards determination of the minimum inhibitory concentration (MIC) of purified compounds against the tested $Gram^{+}$ and $Gram^{-}$ bacteria (**section 2.1.2**). Compounds were dissolved in methanol and two duplicated dilutions (2 mg mL^{-1} and 0.2 mg mL^{-1}) of each compound were made in 2 mL eppendorf tubes. After that, a small volume (2 × 5 µL) of each compound was transferred into a duplicated wells of a six well plate. Then 2.5 mL of nutrient agar medium (NA) which was kept at 50 ^{o}C (in order not to solidify) was poured into each well. The final dilutions of each compound were 4 and 0.4 µg mL^{-1} respectively (dilution factor = 1/500). The

remaining duplicate wells were used as positive control where 5 µl of methanol was poured in each one (no compound was added). Bacterial cultures were prepared as described in disk diffusion test section. A small bacterial inoculum (a drop of 5 µL) was transferred (spotted) in the middle of each well. The plates were carefully horizontally shacked and incubated at 37 ^{o}C up to 48 hours after being sealed with Parafilm. The minimum concentration of compound where there is no visual growth of bacteria was defined as MIC.

General feeding conditions for *Streptomyces sahachiroi*

One millimolar (1 mM) of each precursor compound (**Table 3.1, Chapter 3**) was solubilised in dimethyl sulfoxide (DMSO) solvent and was fed into the fermentation culture after 24 h growth of *Streptomyces sahachiroi*. Initially, a multiple small scale fermentation feeding experiments were carried out using each time 50 mL of GYM medium in a 250 mL Erlenmeyer flask containing a 30 cm spring. In fact, by repeating each feeding process at least 3 times, the consistence of the reproducibility of products of interest (azinomycin analogues or naphthoic amides for example) was checked. Afterward, a scale up feeding experiments were proceeded using for each compound a 2 L flask containing 500 mL fermentation broth as was described previously in **section 2.2.2** (***Streptomyces sahachiroi* batch culture**). The culture was harvested after 64 h incubation (at 30 ^{o}C at 200 rpm) and the fermentation products were extracted and isolated following the methods described in **section 2.2.1.**

The same process was followed for the commercial compounds shown in **Table 3.4**; **chapter 3** except that sterile distilled water was used instead of DMSO.

Separation and purification by chromatography

Once TLC plates were developed, the visualisation of different spots was done at 250 nm using a UV/VIS SPECTROLINE cabinet, MODEL ENF-260C/FE Lamp. Then flash chromatography (FC) separation technique was used to isolate the following produced amides: 1-naphthoic amide **99a**, 4-fluoro-1-naphthoic amide **100a**, 3-fluoro-1-naphthoic amide **98a**, 4-methyl-1-naphthoic amide **101a**, 2-methyl-1-naphthoic amide **102a**, 3-methoxy-1-naphthoic amide **97a** and 2-methoxy-1-naphthoic amide **103a**. FC was also used in an attempt to isolate the natural product azinomycin A **3** but the product had degraded due to the acidic nature of the stationary phase (silica

gel) of the column. A second attempt using fresh crude extract and base-washing silica with 1% triethylamine was also unsuccessful. However, azinoycin A was isolated by prep HPLC as mentioned in **section 2.2.1** (**Prep HPLC**). During each FC run, the mass of each bacterial crude extract used was in the range of 40 to 200 mg which was extracted from 500 mL fermentation broth. In addition, the adsorbent material (stationary phase) remained unchanged while the mobile phase consisted of ethyl acetate (40-60): petroleum ether at different ratios (**Table 2.1).**

Compound	**Ethyl acetate (40-60):petroleum ether ratios**
1-naphthoic amide	50:50
4-fluoro-1-naphthoic amide	60:40
3-fluoro-1-naphthoic amide	60:40
4-methyl-1-naphthoic amide	70:30
2-methyl-1-naphthoic amide	70:30
3-methoxy-1-naphthoic amide	70:30
2-methoxy-1-naphthoic amide	70:30

Table 2.1 Naphthoic amide compounds and the corresponding solvent system ratios used during FC isolation.

2.3 Data

Characterization of azinomycin A 3

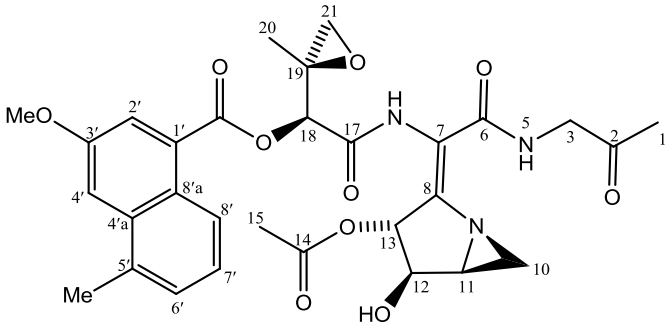

Whitish plates (45:55 water: methanol)

Molecular formula: $C_{30}H_{33}N_3O_{10}$

Molecular Weight: 595 $g.mol^{-1}$

m/z (ESI) 596.

m.p. 144-151 ^{o}C. (lit. 140 ^{o}C) (Nagaoka *et al*., 1986).

Characterization of azinomycin B 4

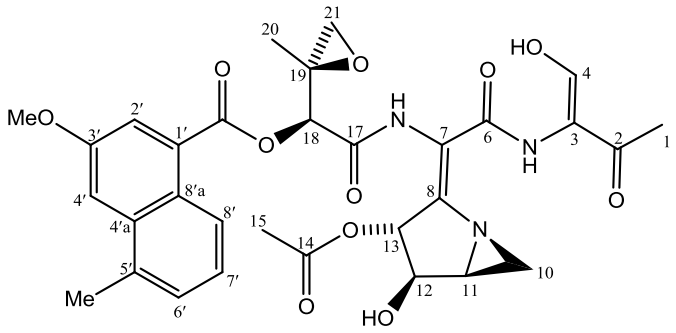

Molecular formula: $C_{31}H_{33}N_3O_{11}$

Molecular Weight: 623 g.mol^{-1}

m/z (ESI) 624.

m.p. 190 ^{o}C (from lit.) (Nagaoka *et al*., 1986).

Characterization of 3-methoxy-1-naphthoic amide 97a

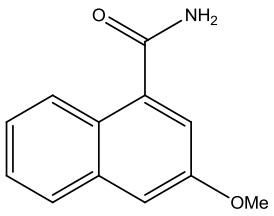

Light-grey amorphous residue (50:50 ethyl acetate/40-60: petroleum ether)

Molecular formula: $C_{12}H_{11}NO_2$

Molecular Weight: 201 g.mol^{-1}

m/z (ESI) 202.

m.p. 206-218 ^{o}C (lit. Not found).

Characterization of 3-fluoro-1-naphthoic amide 98a

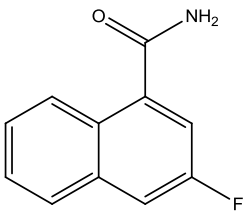

Beige needles (50:50 ethyl acetate/40-60: petroleum ether)

Molecular formula: $C_{11}H_8NFO$

Molecular Weight: 189 $g.mol^{-1}$

m/z (ESI) 190.

m.p. 225-233 ^oC (lit. Not found).

Characterization of 1-naphthoic amide 99a

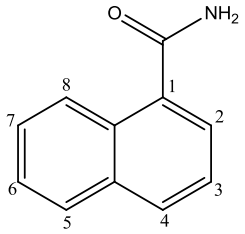

Beige amorphous needles (50:50 ethyl acetate/40-60: petroleum ether) δ_H (300 MHz, $CDCl_3$) 5.98 (2 H, br s, NH_2), 8.43 (1 H, d, $J_{7,8}$ 5.04, H-8), 7.95 (1 H, d, $J_{3,4}$ 5.01, H-4), 7.89 (1 H, d, $J_{5,6}$ 5.07, $J_{5,7}$ 0.70, H-5), 7.72 (1 H, d, $J_{2,3}$ 4.35, H-2), 7.59 (1 H, ddd, $J_{6,7}$ 5.43, $J_{7,8}$ 4.92, $J_{5,7}$ 0.75, H-7), 7.54 (1 H, ddd, $J_{5,6}$ 5.01, $J_{6,7}$ 4.14, $J_{6,8}$ 0.75, H-6), 7.48 (1 H, dd, $J_{2,3}$ 4.32, $J_{3,4}$ 4.95, H-3). ^{13}C NMR (300 MHz, $CDCl_3$) δ 171.67, 133.84, 133.08, 131.34, 130.11, 128.46, 127.40, 126.60, 125.50, 125.46, 124.69. IR (cm^{-1}) (KBr) 3150, 3080, 3030, 1680.

Molecular formula: $C_{11}H_9NO$

Molecular Weight: 171 $g.mol^{-1}$

m/z (ESI) 172.

m.p. 198-207 ^oC (lit. 200-202 ^oC) (http://www.matrixscientific.com/1-naphthamide-mfcd00014314-2243-81-4-c11h9no.html).

Characterization of 4-fluoro-1-naphthoic amide 100a

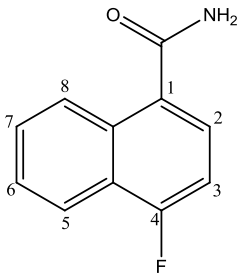

white-beige needles (60:40 ethyl acetate/40-60: petroleum ether) δ_H (300 MHz, $CDCl_3$) 5.97 (2 H, br s, NH_2), 8.48 (1 H, d, $J_{7,8}$ 4.86, H-8), 8.15 (1 H, d, $J_{5,6}$ 4.77, H-5), 7.69 (1 H, dd, $J_{2,3}$ 4.62, $J_{2,F}$ 3.21, H-2), 7.64 (1 H, ddd, $J_{5,6}$ 4.62, $J_{6,7}$ 4.17, $J_{6,8}$ 0.45, H-6), 7.60 (1 H, d, $J_{7,8}$ 4.86, H-7), 7.13 (1 H, dd, $J_{3,F}$ 6, $J_{2,3}$ 4.86, H-3). ^{13}C NMR (300 MHz, $CDCl_3$) δ 170.55, 159.50, 132.01, 128.40, 126.10, 121.40, 108.48. IR (cm^{-1}) (KBr) 3190, 3100, 3025, 1733.

Molecular formula: $C_{11}H_8NFO$

Molecular Weight: 189 $g.mol^{-1}$

m/z (ESI) 190.

m.p. 229-237 ^oC (lit. Not found).

Characterization of 4-methyl-1-naphthoic amide 101a

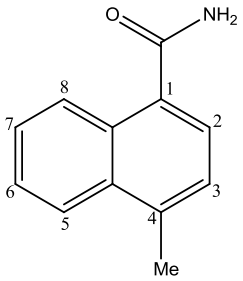

light-grey amorphous residue (70:30 ethyl acetate/40-60: petroleum ether)

Molecular formula: $C_{12}H_{11}NO$

Molecular Weight: 185 $g.mol^{-1}$

m/z (ESI) 186.

m.p. 187-192 ^oC (lit. 193 ^oC) (Frenzel *et al*., 1993).

Characterization of 2-methyl-1-naphthoic amide 102a

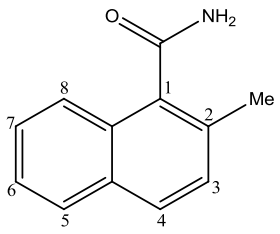

Brownish needles (50:50 ethyl acetate/40-60: petroleum ether)

Molecular formula: $C_{12}H_{11}NO$

Molecular Weight: 185 $g.mol^{-1}$

m/z (ESI) 186.

m.p. 102-111 ^{o}C (lit. 83.5-84.5 ^{o}C) (Dozen and Fujishima, 1972).

Characterization of 2-methoxy-1-naphthoic amide 103a

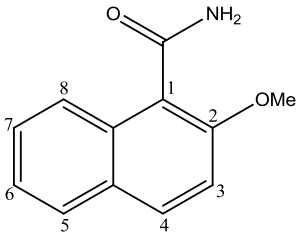

Brownish amorphous residu (50:50 ethyl acetate/40-60: petroleum ether)

Molecular formula: $C_{12}H_{11}NO_2$

Molecular Weight: 201 $g.mol^{-1}$

m/z (ESI) 202.

m.p. 185-194 ^{o}C (lit. 189 ^{o}C) (IG Farben Industrie AG, 1927).

Chapter 3: Novel Biotransformations of Naphthoic Acids by *Streptomyces sahachiroi*

3.1 Introduction

During the course of this study, we attempted to generate new azinomycin analogues through feeding analogues of the naphthoic acid intermediate (**Table 3.1**). A range of naphthoic acids were added to *S. sahachiroi* fermentations. As well as several unnatural azinomycin analogues (**Chapter 4**), additional metabolites were produced in the culture media. The fermentation crude extracts carrying the additional metabolites were further investigated in order to isolate and characterize these novel substances. Firstly, analytical samples were prepared, analysed by LCMS and then the additional metabolites were detected by ESI-MS. After that, scaled up fermentations were conducted, followed by LCMS separation and detection. Then flash chromatography (FC) was used for separation and purification purposes. The identity of the novel metabolites as naphthoic amide analogues was suggested by electrospray mass spectrometry. Further NMR characterisation was carried out for 1-naphthoic amide and 4-fluoro-1-naphthoic amide. Finally, antibacterial and antifungal activity studies were carried out in order to test the purified compounds for any potential biological activities.

These novel biotransformation reactions are of interest for the following reasons. On one hand, they may shed light on the flexibility of the azinomycin biosynthetic enzymes to unnatural substrates as well as on the mechanism of naphthoate activation and transfer to nucleophiles. On the other hand, the discovered biotransformation reactions could be extended to further carboxylic acid substrates to test if there is any useful chemo- and/or regioselectivity.

3.2 Results

3.2.1 Feeding experiment compounds

In order to assess the ability of *S. sahachiroi*'s enzymatic system to process unnatural substrates, a series of commercial and synthetic precursors (**97-114**) were fed to the bacterial fermentation culture after 24 h incubation at 30 ^{o}C and at 200 rpm (**Chapter 2**).

Feeding of naphthoic acid precursors

A variety of naphthoic acid compounds (**97-109**) were fed to *S. sahachiroi*. Some acids were biotransformed into primary amides. The results of the feeding experiments are shown in **Table 3.1**.

Compound	Expected amide	Result
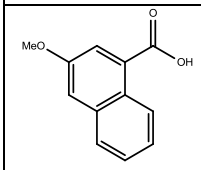 **97** 3-methoxy-1-naphthoic acid	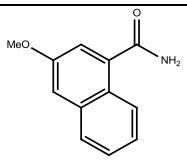 **97a**	~2 mg of light-grey amorphous residue of 3-methoxy-1- naphthoic amide (purification from 43 mg of crude extract).
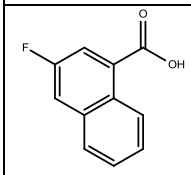 **98** 3-fluoro-1-naphthoic acid	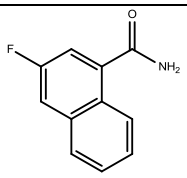 **98a**	~14 mg beige needles of 3-fluoro-1- naphthoic amide (purification from 97 mg of crude extract).
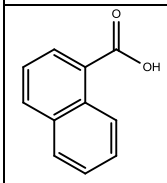 **99** 1- naphthoic acid	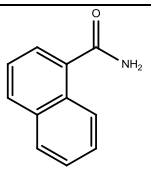 **99a**	~8 mg beige amorphous needles of 1-naphthoic amide (purification from 74 mg of crude extract).
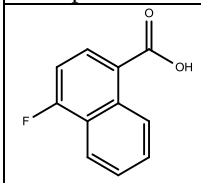 **100** 4-fluoro-1-naphthoic acid	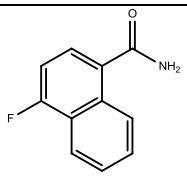 **100a**	~24 mg white-beige needles of 4-fluoro-1-naphthoic amide (purification from 150 mg of crude extract).
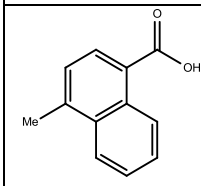 **101** 4-methyl-1-naphthoic acid	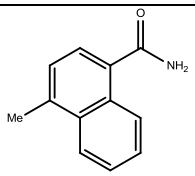 **101a**	~5 mg of light-grey amorphous residue of 4-methyl-1-naphthoic amide (purification from 180 mg of crude extract).
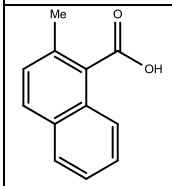 **102** 2-methyl-1-naphthoic acid	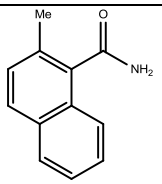 **102a**	~3 mg of brownish needles of 2-methyl-1- naphthoic amide (purification from 74 mg of crude extract).
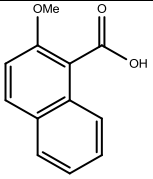 **103** 2-methoxy-1-naphthoic acid	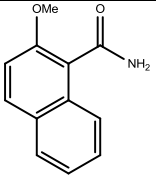 **103a**	~20 mg of grey- brownish amorphous residue of 2-methoxy-1-1naphthoic amide (purification from 80 mg of crude extract).

Table 3.1: Evaluation of naphthoic acid analogues for biotransformation into naphthoic amides after 64 h incubation of *S. sahachiroi* fermentation culture. 1 mM of each compound was added into a 500 mL culture broth after 24 h incubation.

Compound	Expected amide	Result
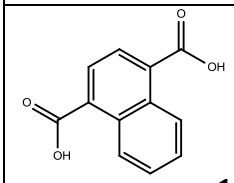 **104** 1,4-naphthalenedicarboxylic acid	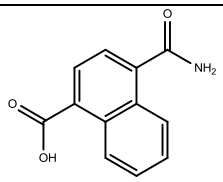 **104a**	No production.
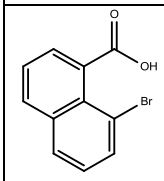 **105** 8-bromo-1-naphthoic acid	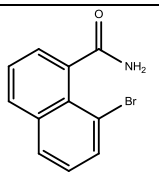 **105a**	No production.
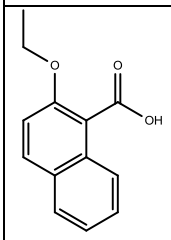 **106** 2-ethoxynaphthoic acid	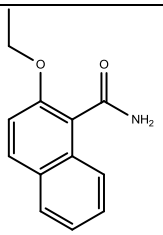 **106a**	No production.
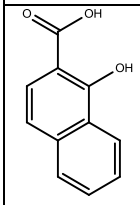 **107** 1-hydroxy-2-naphthoic acid	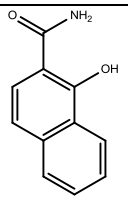 **107a**	No production.
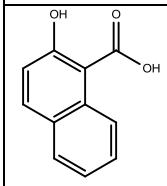 **108** 2-hydroxy-1-naphthoic acid	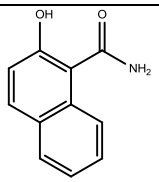 **108a**	No production.
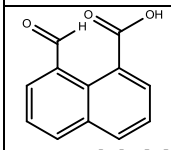 **109** 1,8-naphthalaldehydic acid	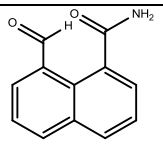 **109a**	No production.

Table 3.1: Evaluation of naphthoic acid analogues for biotransformation into naphthoic amides after 64 h incubation of *S. sahachiroi* fermentation culture. Each compound was added to a final concentration of 1 mM into a 500 mL culture broth after 24 h incubation.

The results from **Table 3.1,** LCMS figures and 1D and 2D NMR data (for amides **99a** and **100a**) show the production and purification of naphthoic amides subsequent to feeding naphthoic acids **97-103** to the fermentation cultures**.**

Isolation and purification of 1-naphthoic amide 99a

The isolation and purification steps are summarised in **chap**. **2** (**section**: **separation and purification by chromatography)** and are as follows**.** TLC analysis of the $CHCl_3$ extract of the culture using 50:50 ethyl acetate/40-60: petroleum ether showed a strong blue fluorescence spot with $R_f = 0.33$. Flash chromatography (FC) was used to isolate the target product using the same solvent system. The purified compound was identified as 1-naphthoic amide **99a** by LCMS (**Figure 3.1**), 1D and 2D NMR (**Figures 3.2** and **3.4-3.10**) and IR analyses (**Figure 3.11**). **Figures 3.2**, **3.6** and **3.11** are shown in the **Appendix one**.

8 mg of the amide was isolated from 74 mg of crude extract, a yield of 9% relative to the added acid.

LCMS data of 1-naphthoic amide 99a:

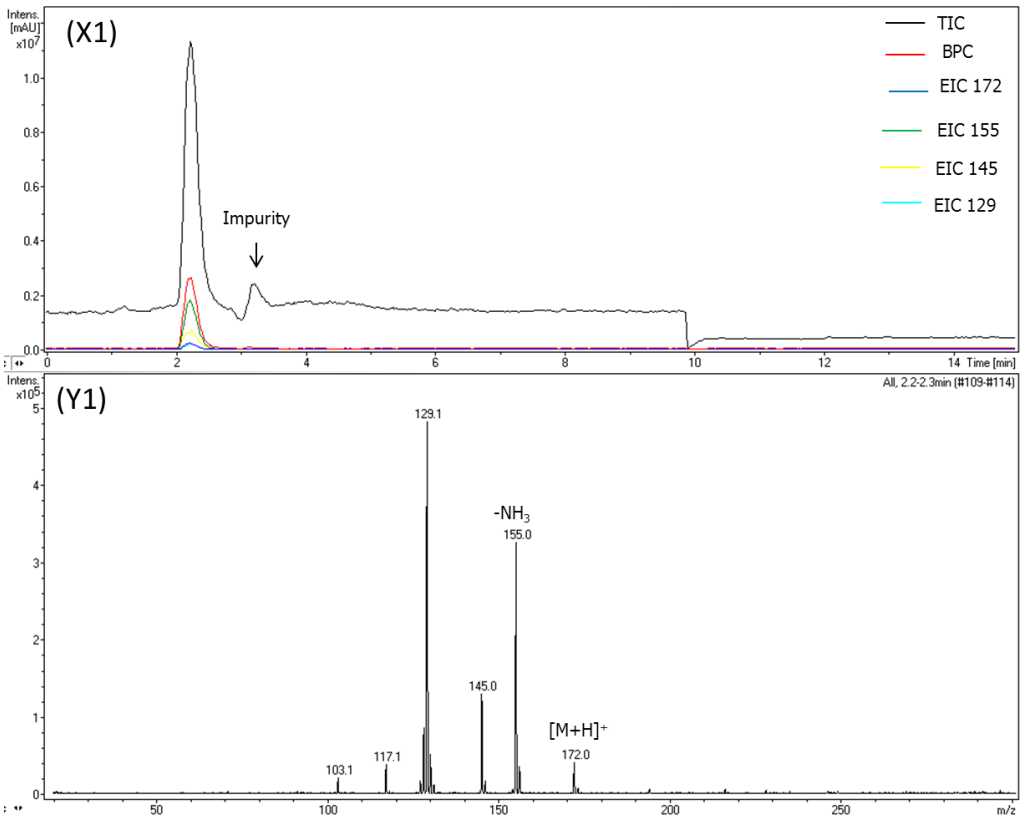

Figure 3.1: LCMS of purified 1-napthoic amide. (X1): LCMS chromatograms. (Y1): Positive ion electrospray mass spectrum for peak at R_t = 2.2-2.3 min.

Figure 3.1 shows a clear alignment between the HPLC total ion chromatogram (TIC), the base peak chromatogram (BPC) and extracted ion chromatogram (EIC) for naphthoic amide ion (m/z 172). EIC peaks for m/z of 155, 145 and 129 superimpose perfectly with EIC 172 indicating that these peaks are fragments of m/z 172.

A small impurity peak at 3.2 min could be seen in (X1) and some impurities also found in ^{1}H-NMR data (**Figure 3.2**). 1-naphthoic amide was identified by LCMS (**Figure 3.1**), 1D and 2D NMR (**Figures 3.2** and **3.4-3.10**) and IR analyses (**Figure 3.11**). The fragmentation patterns shown in **Figure. 3.1** can be explained by the fragmentation mechanisms described in **scheme 3.1**.

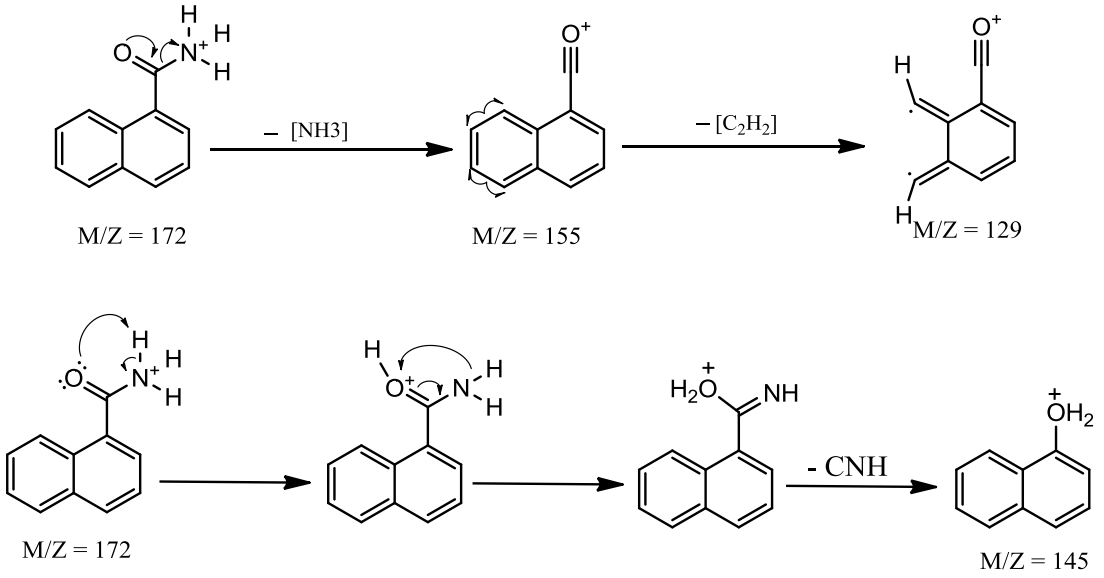

Scheme 3.1: Possible mechanisms of the fragmentation of 1-naphthoic amide.

The fragment with m/z 155 is produced after loss of ammonia from the protonated ion. The fragment with m/z 129 could be the result of a loss of acetylene (C_2H_2) from the naphthoyl fragment (m/z 155)**.** The fragment with m/z 145 could be the result of a loss of CNH from the molecular ion after an internal rearrangement of hydrogens between the amine and the carbonyl functional groups**.**

1D and 2D NMR data of 1-naphthoic amide 99a

An overview of the ^{1}H-NMR spectrum of **99a** in $CDCl_3$ is displayed in **Figure 3.2** (**Appendix one**). Expansions of different parts of the spectrum are represented in **Figures 3.4** and **3.5**.

Assignment of protons and carbons of 99a

In order to assign all naphthoic amide protons and carbons, 1D ^{1}H-NMR **(Figures 3.2, 3.4** and **3.5),** 1D ^{13}C-NMR **(Figures 3.6** (**Appendix one**) and **3.7),** and 2D NMR (COSY, HMQC and HMBC, **Figures 3.8-3.10**) were performed. It is possible to identify all 7 protons (H_2-H_8) of the naphthoic amide **99a** based on the COSY spectrum (**Figure 3.8**). The HMQC heteronuclear experiment was used to correlate directly bonded ^{1}H and ^{13}C peaks. The HMBC heteronuclear technique was used to connect ^{1}H and ^{13}C peaks separated by 2 or 3 bonds. It is clear from the ^{1}H-^{1}H COSY NMR spectrum of amide **99a** that protons δ 7.72 and δ 7.48 are interrelated but δ

7.72 and δ 7.95 are not correlated because the *meta* coupling was not resolved. Moreover, δ 7.95 and δ 7.48 are shown to be interrelated. From HMBC spectrum (**Figure 3.10**), δ 7.72 (1 H d) corresponds to 171.67 carbon ($CONH_2$) and is assigned to H2 that is also interrelated with 130.63 carbon (C1). Therefore, proton δ 7.48 is assigned to H3 and δ 7.95 to H4.

^1H-^1H COSY NMR also reveals that protons δ 8.43 and δ 7.59 are coupled to each other and that δ 8.43 is not coupled to δ 7.54. On the other hand δ 7.59 and δ 7.54 are coupled to each other. The *ortho* coupling between neighbouring protons is shown in ^1H-NMR spectrum but the *meta* coupling was not fully resolved (**Figure 3.4**). Furthermore δ 7.88 is correlated to δ 7.54 and not interrelated with δ 7.59. Therefore, proton δ 8.43 (1 H d) is assigned to H8, δ 7.59 (1 H ddd) is assigned to H7, δ 7.54 (1 H ddd) is assigned to H6 and proton δ 7.88 (1 H d) is assigned to H5.

HMQC spectrum of naphthoic amide **99a (Figure 3.9)** revealed all the 7 cross-peaks that correlate directly bonded ^1H and ^{13}C peaks. Consequently all the 7 carbons (C2-C8) were assigned as shown in the assignment table in **Figure 3.9**.

HMBC spectrum (**Figure 3.10**) shows (in addition to the interrelation between proton H2 and carbons C1 and $CONH_2$) that H8, giving the signal at δ 8.43 is coupled to C8a, giving the signal at δ 133.84. Also, this experiment shows the interrelation between δ 7.88 and δ 133.08 that is the coupling between H5 and carbons C4a over 2-bond length.

The summary of proton and carbon assignment of 1-naphthoic amide **99a** is illustrated in **Figure 3.3** and **Table 3.2**.

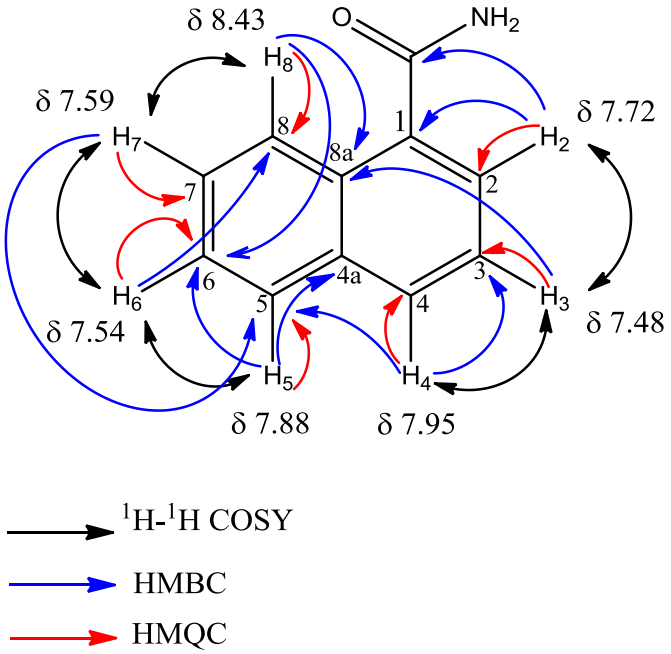

Figure 3.3: COSY, HMQC and HMBC correlations for **99a**. Black arrows highlight ^{1}H-^{1}H COSY correlations, blue arrows show ^{1}H-^{13}C HMBC correlations and red arrows represent ^{1}H-^{13}C HMQC correlations. ^{1}H-NMR chemical shifts (in ppm) are displayed next to each respective proton.

Position	1-naphthoic amide **99a**	
	^{1}H-NMR δ (in ppm)	^{13}C*-NMR δ (in ppm)
1	-	130.11
2	7.72	125.46
3	7.48	124.69
4	7.95	131.34
4a	-	133.08
5	7.88	128.46
6	7.54	126.60
7	7.59	127.40
8	8.43	125.50
8a	-	133.84
$CONH_2$	-	171.67

∗ ^{13}C-NMR data deduced from HMQC and HMBC spectra.

Table 3.2: ^{1}H-NMR and ^{13}C-NMR data of 1-naphthoic amide **99a**.

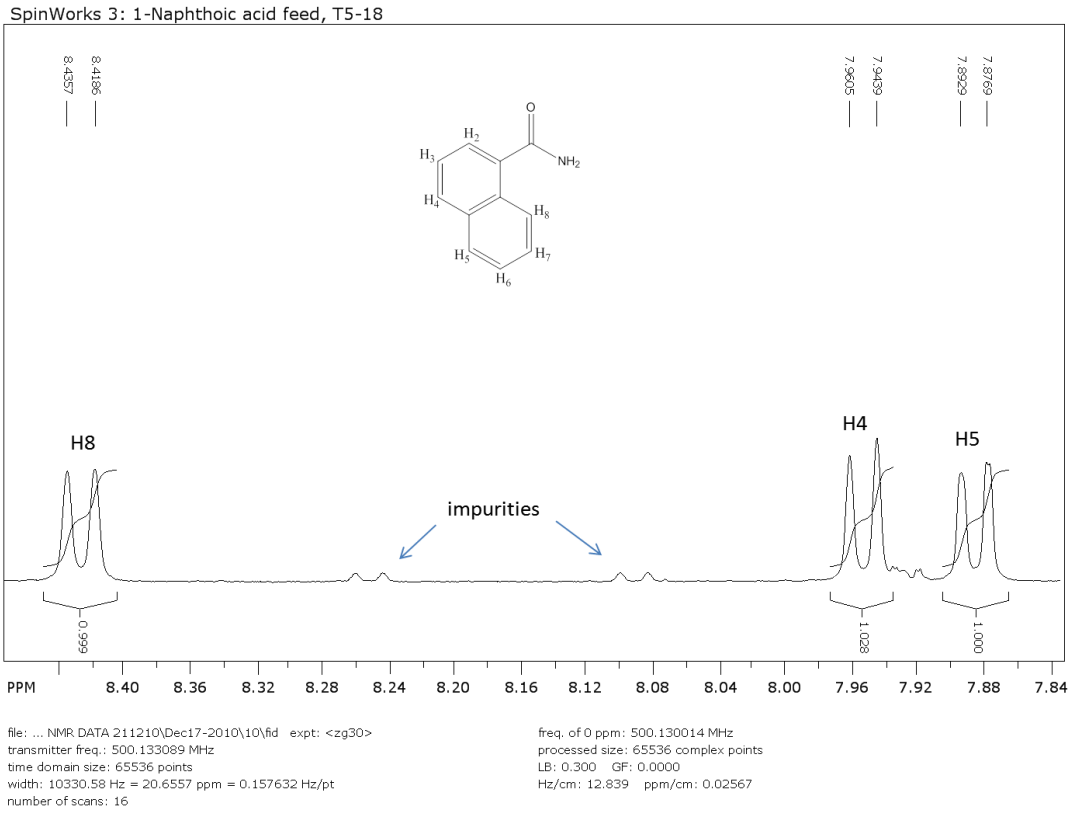

Figure 3.4: ^{1}H-NMR in $CDCl_3$ of 1-naphthoic amide **99a** (expanded view of **Figure 3.2**, region 7.84-8.48).

^{1}H-NMR spectrum in **Figure 3.4** exhibited only *ortho* couplings between H8 and H7, H4 and H3 and H5 and H6. The *meta* and the *para* couplings were not revealed by the experiment as the peaks were not fully resolved. The spectrum also shows the persistence of some impurities.

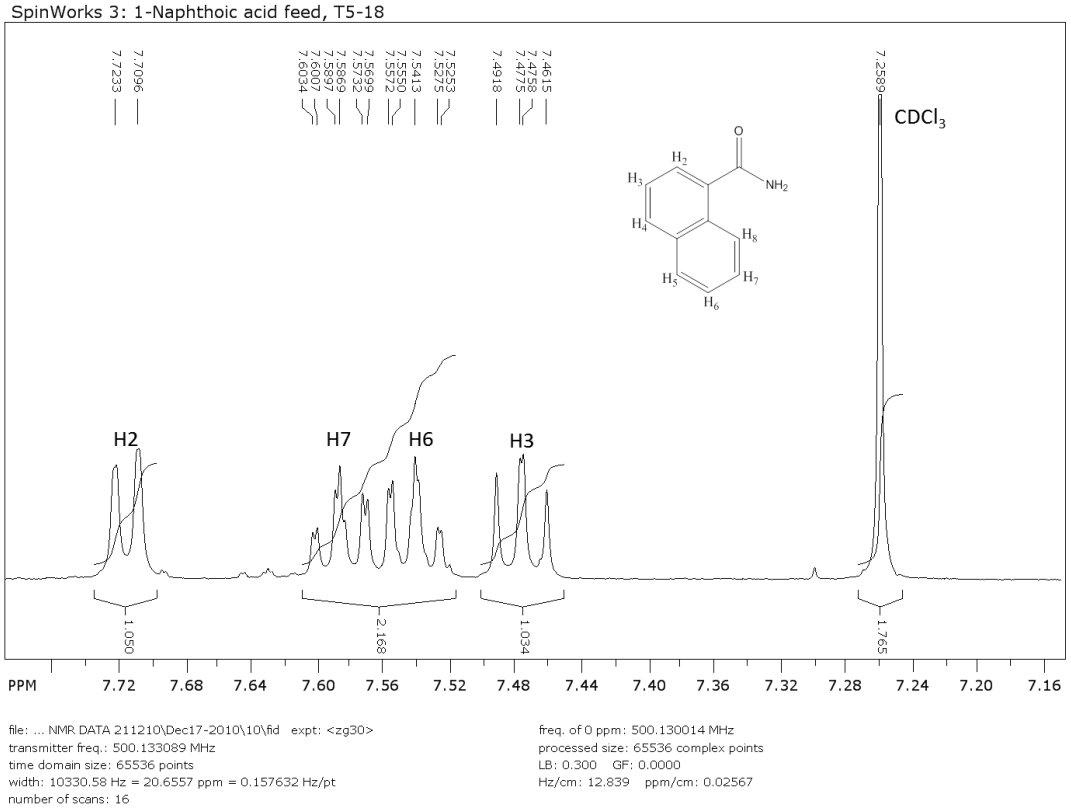

Figure 3.5: ^{1}H-NMR in $CDCl_3$ of 1-naphthoic amide **99a** (expanded view of **Figure 3.2**, region 7.16-7.78).

^{1}H-NMR spectrum in **Figure 3.5** shows the *ortho* couplings between H3 and both neighbouring protons H2 and H4. Furthermore, the proton H6 and H7 reveal *meta* couplings with H8 and H5 respectively, even if the peaks are not fully resolved.

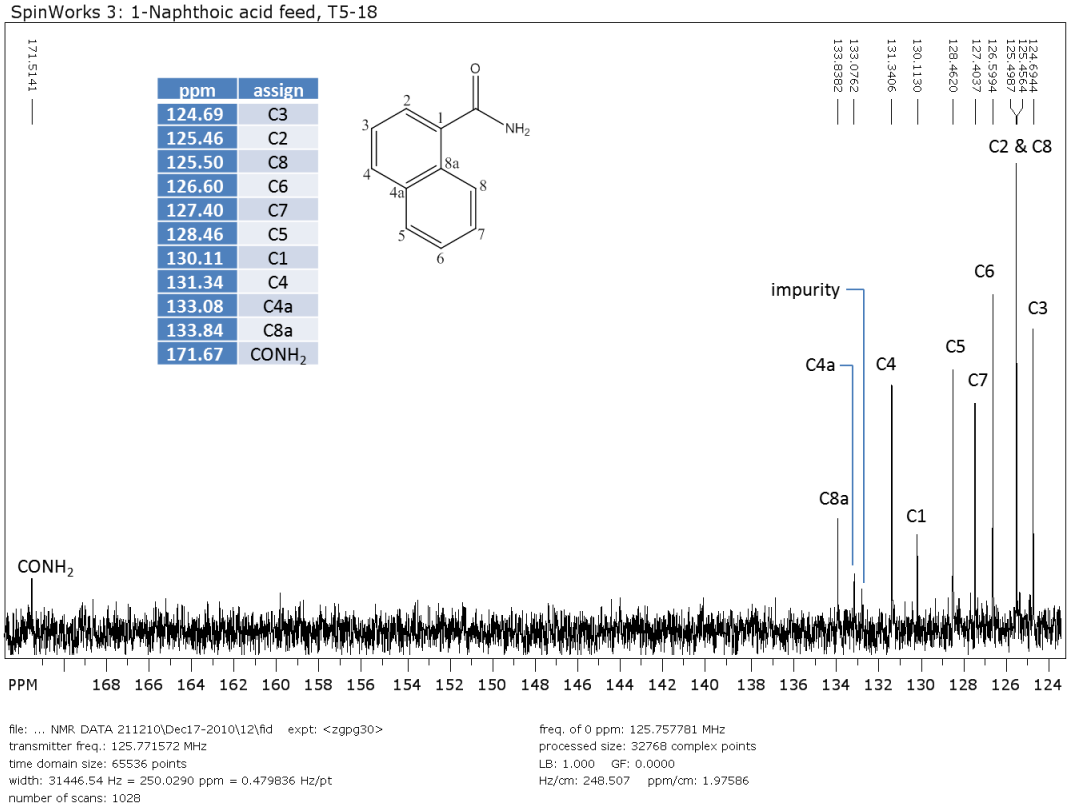

ppm	assign
124.69	C3
125.46	C2
125.50	C8
126.60	C6
127.40	C7
128.46	C5
130.11	C1
131.34	C4
133.08	C4a
133.84	C8a
171.67	$CONH_2$

Figure 3.7: ^{13}C-NMR in $CDCl_3$ of 1-naphthoic amide **99a** (expanded view of **Figure 3.6**, **Appendix one**) and assignment of the 11 carbon atoms.

^{13}C-NMR analysis of 1-naphthoic amide **99a** reveals clear signals for all the 11 carbon atoms constructing the skeleton of compound **99a**. The seven larger signals are assigned to the C2-C4 and C5-C8 carbons. The three smaller signals are assigned to C1, C4a and C8a because carbon atoms without attached hydrogen atoms relax very slowly when the delay time used is not very large. The amide carbon ($CONH_2$) appears downfield at δ 171.51.

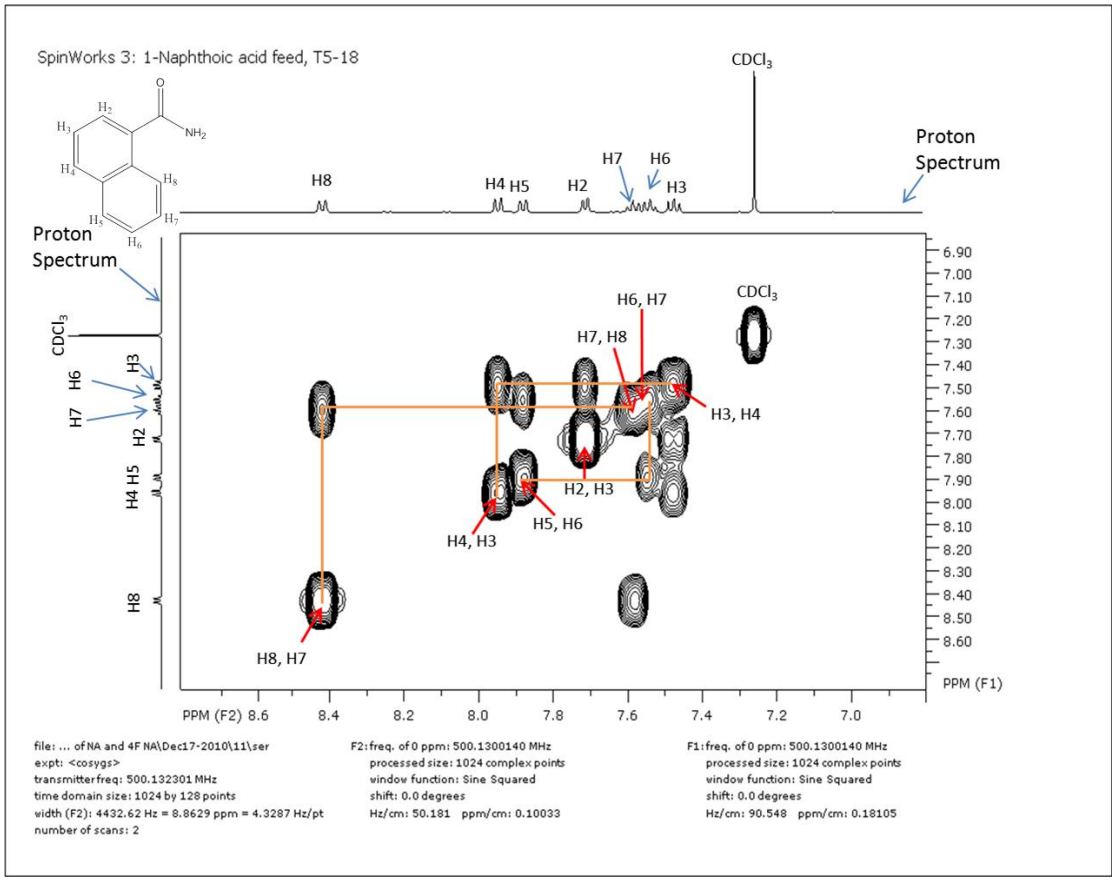

Figure 3.8: ^{1}H-^{1}H COSY NMR in $CDCl_3$ of 1-naphthoic amide **99a**.

The experiment presents a two-dimensional contour map, each dimension representing proton chemical shifts and the contours representing signal intensity. The diagonal (running bottom left (H8, H7) to top right ($CDCl_3$)) shows peaks that correspond to the 7 protons (H2-H8) of 1-napthoic amide **99a**. The off-diagonal peaks (cross-peaks) represent a coupling between the protons that are correlated by the cross-peak and are represented in **Figure 3.8** by solid perpendicular lines (in tangerine colour). The spectrum is symmetrical about the diagonal as a coupling from proton 8 to 7 will always be matched with one from 7 to 8. Based upon ^{1}H-^{1}H COSY experiment, we could identify coupling between protons H2 and H3, H3 and H4, H5 and H6, H6 and H7 and between H7 and H8.

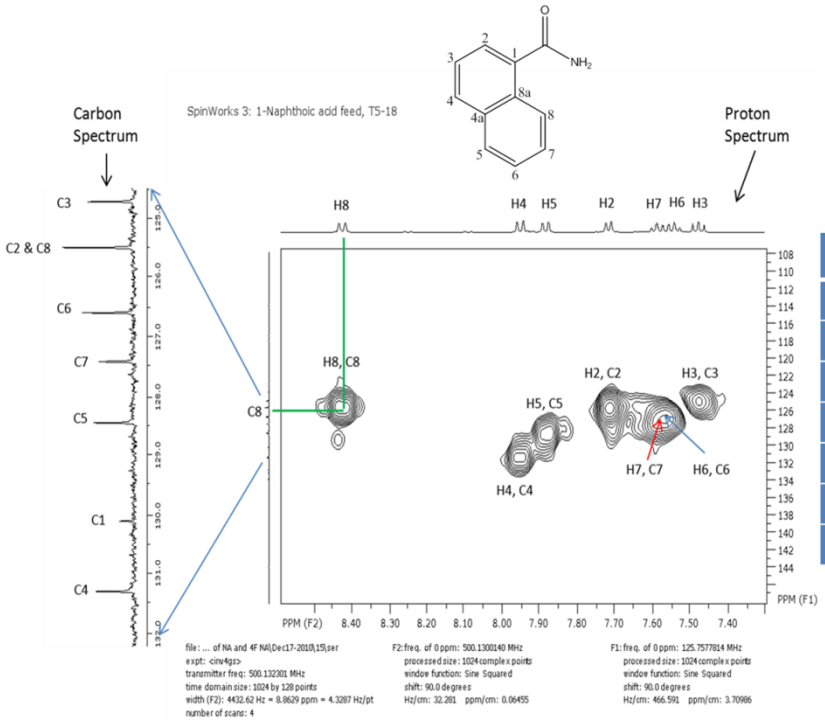

^{1}H	^{13}C	Assignment
8.43	125.65	8
7.95	131.45	4
7.89	128.69	5
7.72	125.61	2
7.59	127.42	7
7.54	126.60	6
7.48	124.77	3

Figure 3.9: HMQC-NMR in $CDCl_3$ of 1-naphthoic amide **99a**. The spectrum shows the correlation between directly bonded ^{1}H and ^{13}C peaks and provides carbon assignment (**Table** on the right).

As seen in the simulated spectrum above (**Figure 3.9**), assignment is made by drawing two lines (in green) at a right angle from the ^{1}H spectrum to the ^{13}C spectrum through the cross-peak. Thus, in the spectrum above, C8 is directly attached to H8. In a similar fashion, C2, C3, C4, C5, C6 and C7 are directly correlated and bonded to H2, H3, H4, H5, H6 and H7, respectively. This experiment provides assignment of carbons C2-C8 as illustrated in the joined **Table** in **Figure 3.9**.

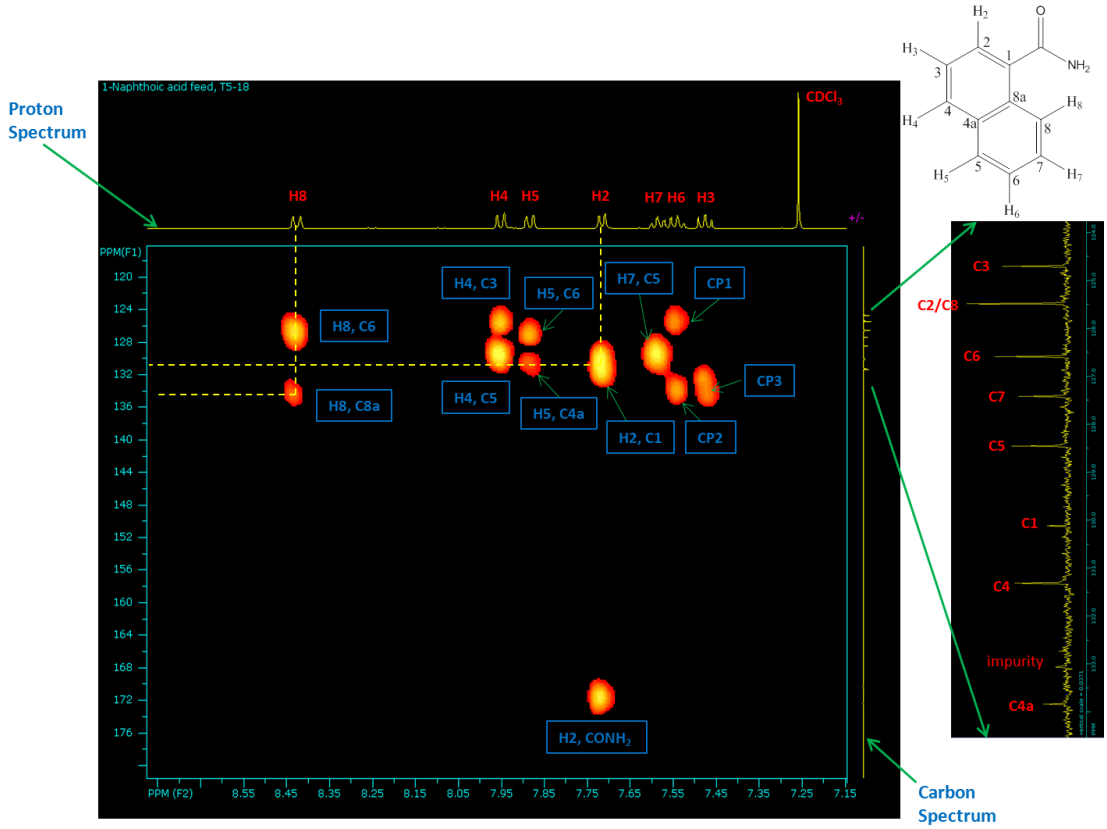

Figure 3.10: HMBC-NMR in $CDCl_3$ of 1-naphthoic amide **99a**. The spectrum shows the correlation between ^{1}H and ^{13}C peaks, mostly over 2-3 bond length.

Most of the peaks in **Figure 3.10** are consistent with the two- and three-bond couplings expected for molecule **99a**.

The cross-peak labelled CP2 shows coupling between carbon C8a and proton H6 over four-bond length which is possible in conjugated systems. Similarly, the cross-peak CP3 shows connectivity between C8a and proton H3 over four-bond length. Furthermore, cross-peaks CP1 and (H4, C3) are situated in the same horizontal line suggesting a possible coupling between H6 and the more distant C3. The cross-peak subtended by the horizontal and vertical dashed lines such as H8, C8a shows that H8, giving the signal at δ 8.43 is coupled to C8a, giving the signal at δ 133.84 over two-bond length. Similarly, proton H8 is connected to C6, giving the signal at δ 126.60 over three-bond length. Additionally, the cross-peak (H2, C1) reveals coupling between H2, at δ 7.72 and C1, at δ 130.11 over two-bond length. The remaining cross-peaks show couplings between respective protons and carbons over either two- or three-bond and could be explained in similar fashion as the cross-peaks (H8, C8a) and (H8, C6).

IR data of 1-naphthoic amide 99a

The IR spectrum of the amide **99a** is shown in **Figure 3.11** (Appendix one). The spectrum exhibits absorption band at about 1680 cm^{-1} which may be indicator of C=O stretching. The NH stretching of the NH_2 group of 1-naphthoic amide was not strong (may be because of the low concentration of the sample) and shows 2 distinct bands between 3080 and 3150 cm^{-1}. The spectrum also shows an absorption peak at approximately 3030 cm^{-1} and corresponds to CH stretching.

Isolation and purification of 4-fluoro-1-naphthoic amide 100a

Isolation and purification of 4-fluoro-1-naphthoic amide was achieved similarly to 1-naphthoic amide **99a** with the following changes:

The flash column chromatography was run with 60:40 ethyl acetate/40-60 petroleum ether and the product had an R_f of 0.23.

24 mg was purified from 150 mg of crude extract, a yield of 25% relative to the added acid.

LCMS data of 4-fluoro-1-naphthoic amide 100a:

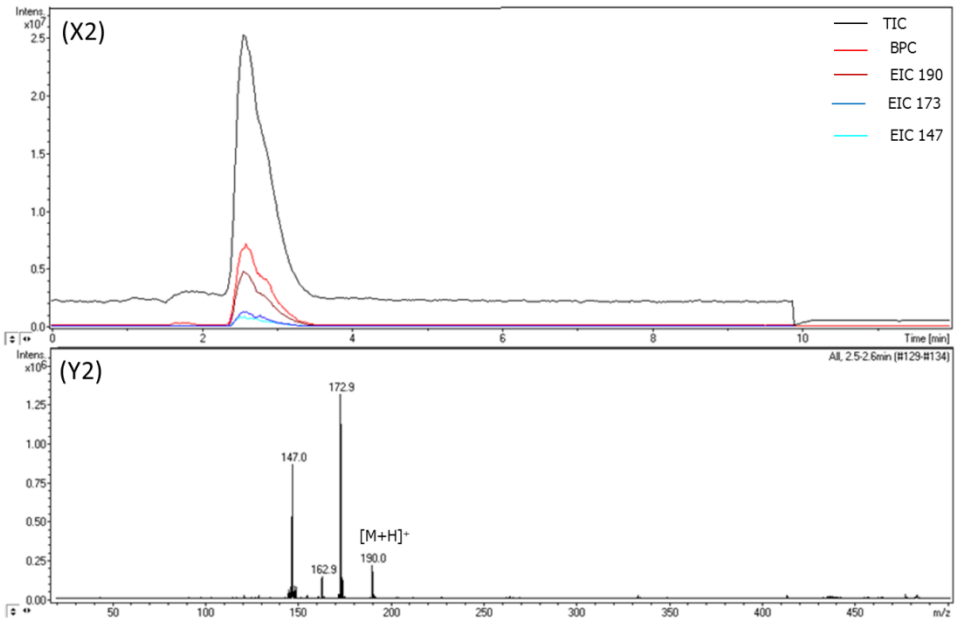

Figure 3.12: LCMS of purified 4-fluoro-1-naphthoic amide. (X2): LCMS chromatograms. (Y2): Positive ion electrospray mass spectrum for the new peak at R_t = 2.5-2.6 min.

Figure 3.12 shows a clear alignment between the HPLC total ion chromatogram (TIC), the base peak chromatogram (BPC) and extracted ion chromatogram (EIC) for the MH^+ ion for 4-fluoro-1-naphthoic amide ion (m/z 190). EIC peaks for m/z 173, 163 and 147 superimpose perfectly with EIC 190 indicating that these peaks are fragments of m/z 190.

4-fluoro-1-naphthoic amide was characterized by LCMS (**Figure 3.12**), 1D and 2D NMR methods (**Figures 3.13** and **Figures 3.15-3.21**) and IR analyses (**Figure 3.22**)**.** **Figures 3.13**, **3.17** and **3.22** are presented in the **Appendix one**. The fragmentation pattern is similar to that shown in **Figure 3.1** and the mechanisms could be explained in a similar fashion to that of 1-naphthoic amide in **scheme 3.1**.

1D and 2D NMR data of 4-Fluoro-1-naphthoic amide 100a:

An overview of the ^{1}H-NMR spectrum of **100a** in $CDCl_3$ is displayed in **Figure 3.13** (**Appendix one**). Expansions of different parts of the spectrum are represented in **Figures 3.15** and **3.16**.

Assignment of protons and carbons of 100a

^{1}H-^{1}H COSY NMR spectrum of amide **100a** (**Figure 3.19**) shows only 4 protons. Protons δ 7.60 and δ 8.48 do not appear within the data. Protons δ 8.15 and δ 7.64 are interrelated to each other and δ 7.13 and δ 7.69 are interrelated to each other as well. From HMBC spectrum **(Figure 3.21),** δ 7.69 (1 H dd) corresponds to 170.55 carbon ($CONH_2$) and is assigned to H2 that is also interrelated with 132.01 and 159.5 carbons. Therefore, proton δ 7.13 (1 H dd) is assigned to H3, δ 132.01 to C1 and δ 159.5 to C4. Carbons C1 and C4 were assigned by analogy to 1-naphthoic amide **99a**. HMBC spectrum did not show much data for further analysis. Furthermore, carbons giving signals at δ 126.10, δ 108.48, δ 121.40 and δ 128.40 were assigned as C2, C3, C5 and C6, respectively based on HMQC analysis. The assignment of the remaining protons (H5-H8) could be deduced from comparison to amide **99a**. Proton δ 8.48 (1 H d) is assigned to H8 and proton δ 8.15 (1 H d) is assigned to H5. From COSY experiment, δ 8.15 and δ 7.64 (1 H ddd) are interrelated to each other and therefore δ 7.64 is assigned to H6. Finally, the proton δ 7.60 (1 H d) is assingned to H7. The summary of proton and carbon assignment of amide **100a** is illustrated in **Figure 3.14** and **Table 3.3**.

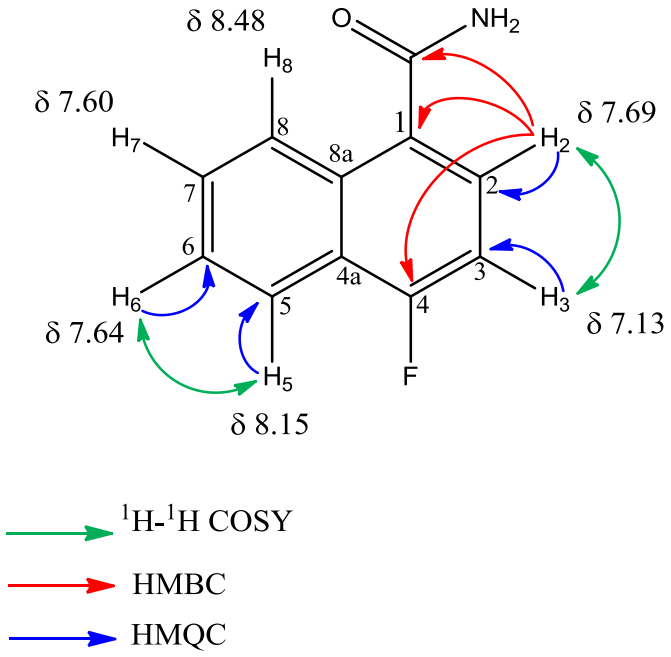

Figure 3.14: ^{1}H-^{1}H COSY, HMQC and HMBC correlations for **100a**. Green arrows show ^{1}H-^{1}H COSY correlations, red arrows represent HMBC correlations and blue arrows highlight HMQC coupling.

Position	4-fluoro-1-naphthoic amide **100a**	
	^{1}H-NMR δ (in ppm)	^{13}C*-NMR δ (in ppm)
1	-	132.01
2	7.69	126.10
3	7.13	108.48
4	-	159.50
4a	-	-
5	8.15	121.40
6	7.64	128.40
7	7.60	-
8	8.48	-
8a	-	-
$CONH_2$	-	170.55

* ^{13}C-NMR data deduced from HMQC and HMBC spectra.

Table 3.3: ^{1}H-NMR and ^{13}C-NMR data of 4-fluoro-1-naphthoic amide **100a**.

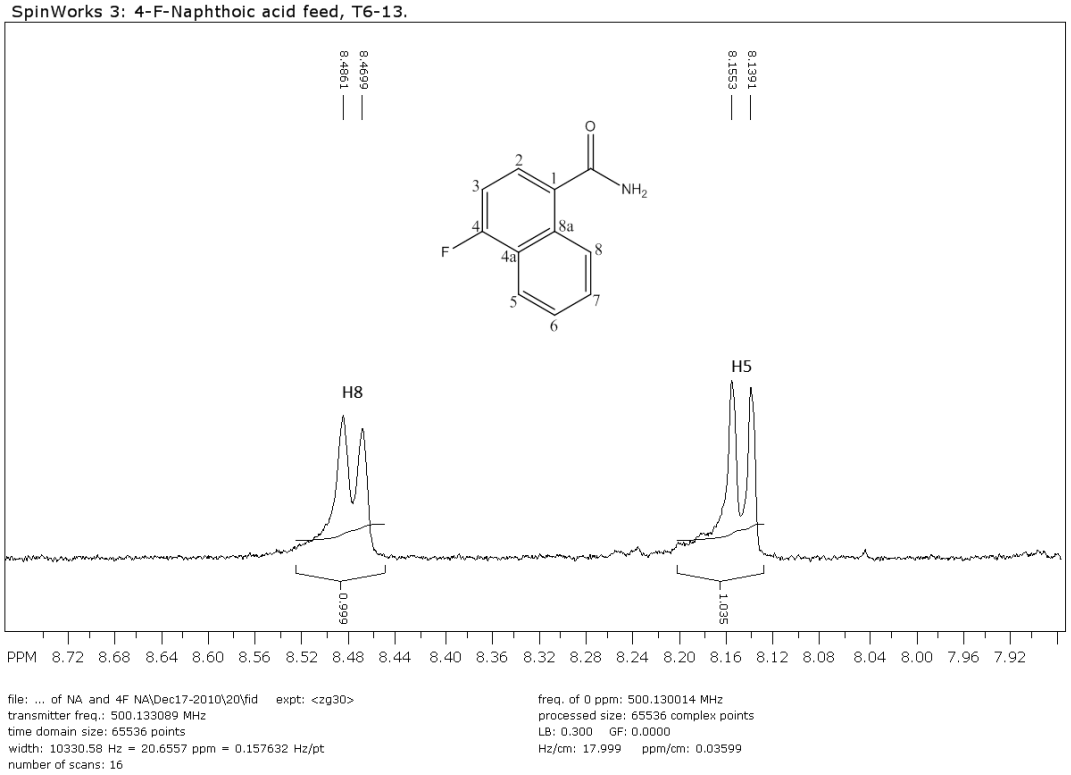

Figure 3.15: ^{1}H-NMR in $CDCl_3$ of 4-fluoro-1-naphthoic amide **100a** (expanded view of **Figure 3.13**, region 7.90-8.74).

The proton spectrum shown in **Figure 3.15** exhibits two peaks resolved as doublets and giving signals at δ 8.48 and δ 8.15. The peaks are assigned H8 and H5, respectively. The two signals appear as doublets because the *meta* and the *para* couplings were not revealed by the experiment as the peaks were not fully resolved.

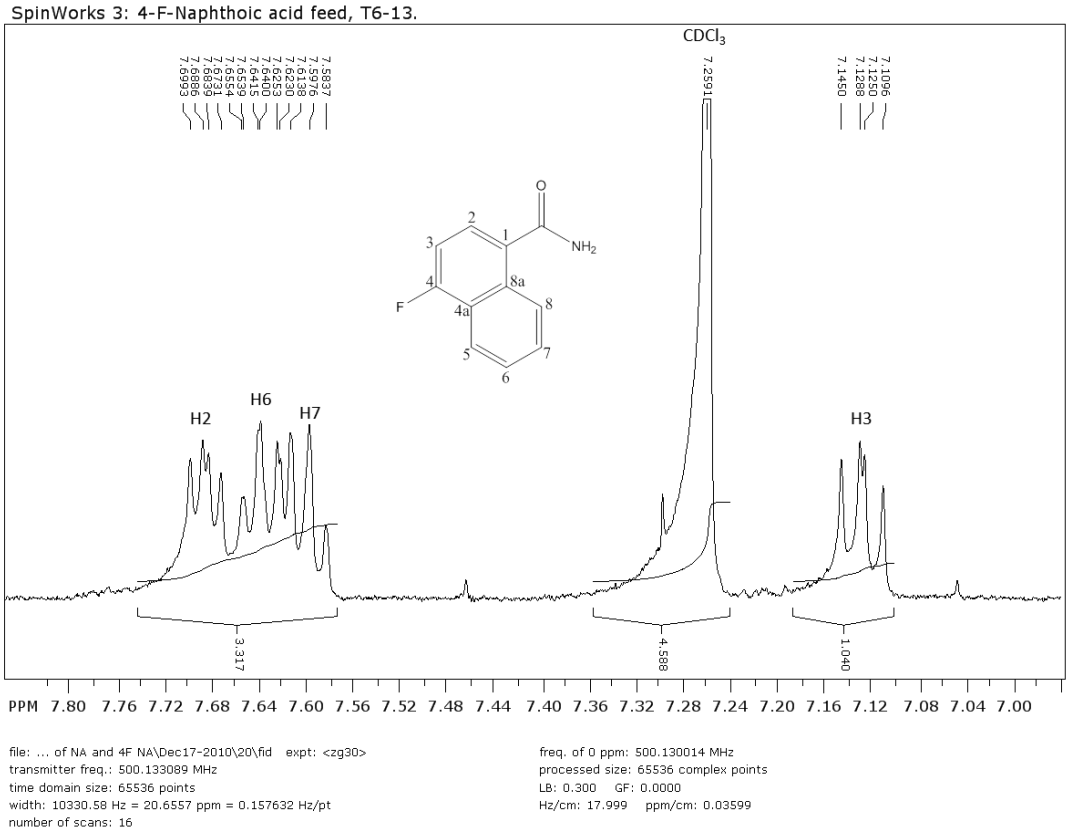

Figure 3.16: ^{1}H-NMR in $CDCl_3$ of 4-fluoro-1-naphthoic amide **100a** (expanded view of **Figure 3.13**, region 6.80-7.84).

Figure 3.16 shows 4 protons giving signals at δ 7.69, δ 7.64, δ 7.60 and δ 7.13 and assigned H2, H6, H7 and H3, respectively. The proton H3 is shown as double doublet revealing couplings with fluorine F4 and H2. As well as *ortho* couplings, protons H2 and H6 reveal also *meta* couplings with F4 and H8, respectively. Furthermore, the spectrum shows that H7 was just partially resolved.

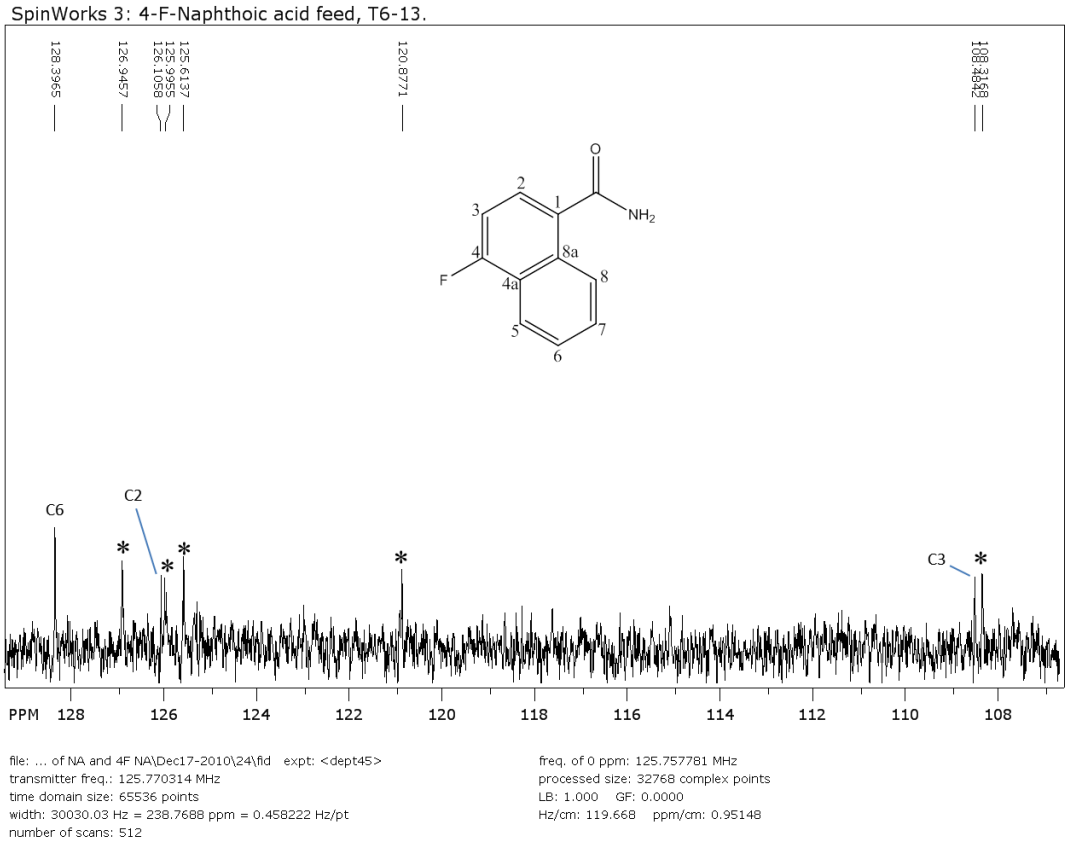

Figure 3.18: ^{13}C-NMR in $CDCl_3$ of 4-fluoro-1-naphthoic amide **100a** (expanded view of Figure 3.17, region 107-129 ppm). Peaks shown with ∗ could not be assigned yet.

The spectrum in **Figure 3.18** shows only 8 peaks among the 11 carbon atoms contained in compound **100a**. The absence of the remaining peaks might be due to the low concentration of the purified sample. Furthermore, only carbons C3, C2 and C6 giving signals at δ 108.48, δ 126.10 and δ 128.40 respectively, could be assigned due to the insufficient data collected from HMQC and HMBC experiments (**Figures 3.20** and **3.21** respectively). As consequence, peaks shown with ∗ in **Figure 3.18** remained unassigned.

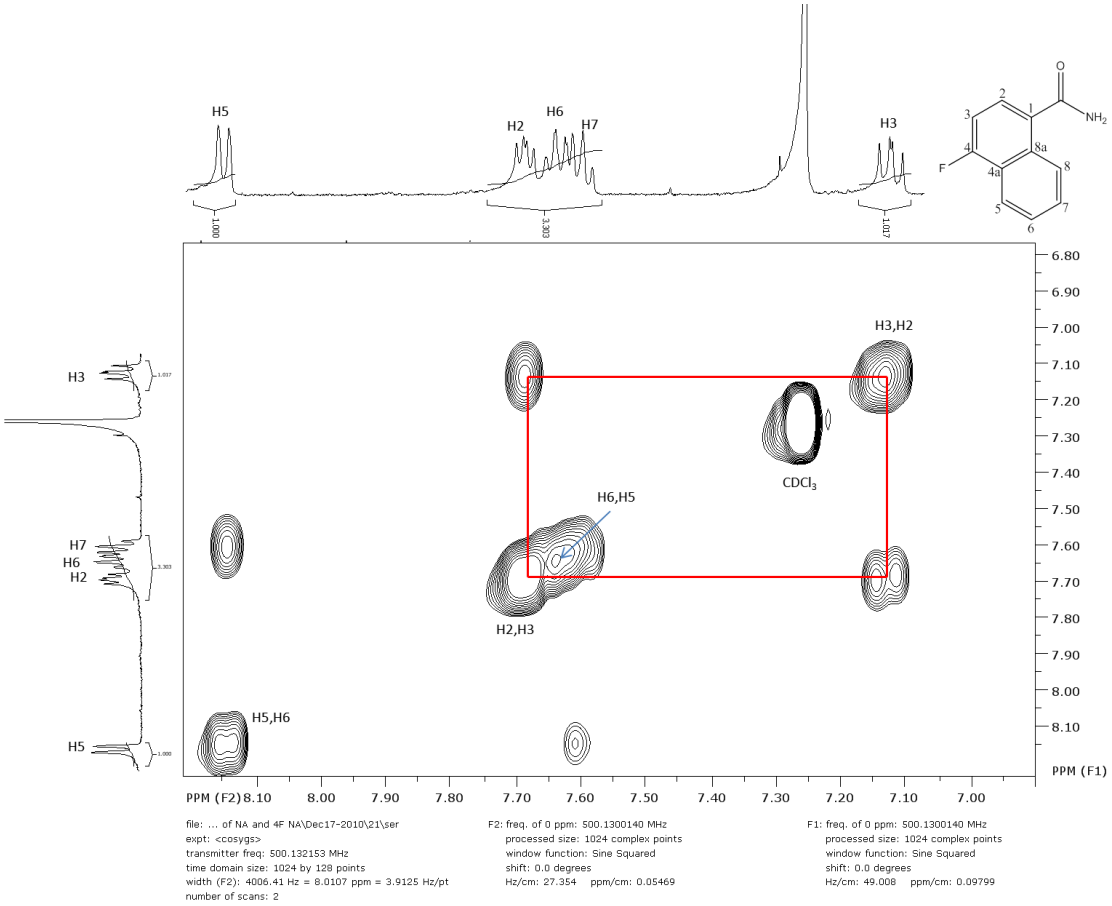

Figure 3.19: ^{1}H-^{1}H COSY NMR in $CDCl_3$ of 4-fluoro-1-naphthoic amide **100a**.

The COSY experiment was used to analyse the coupling protons in compound **100a**. The diagonal (running bottom left (H5, H6) to top right (H3, H2)) shows only 4 peaks that correspond to protons H5, H2, H6 and H3. The cross-peaks show coupling between protons H5 and H6 and also between H2 and H3. Solid perpendicular lines (in red, **Figure 3.19**) represent coupling between H2 and H3. Protons H7 and H8 could not be detected by this experiment.

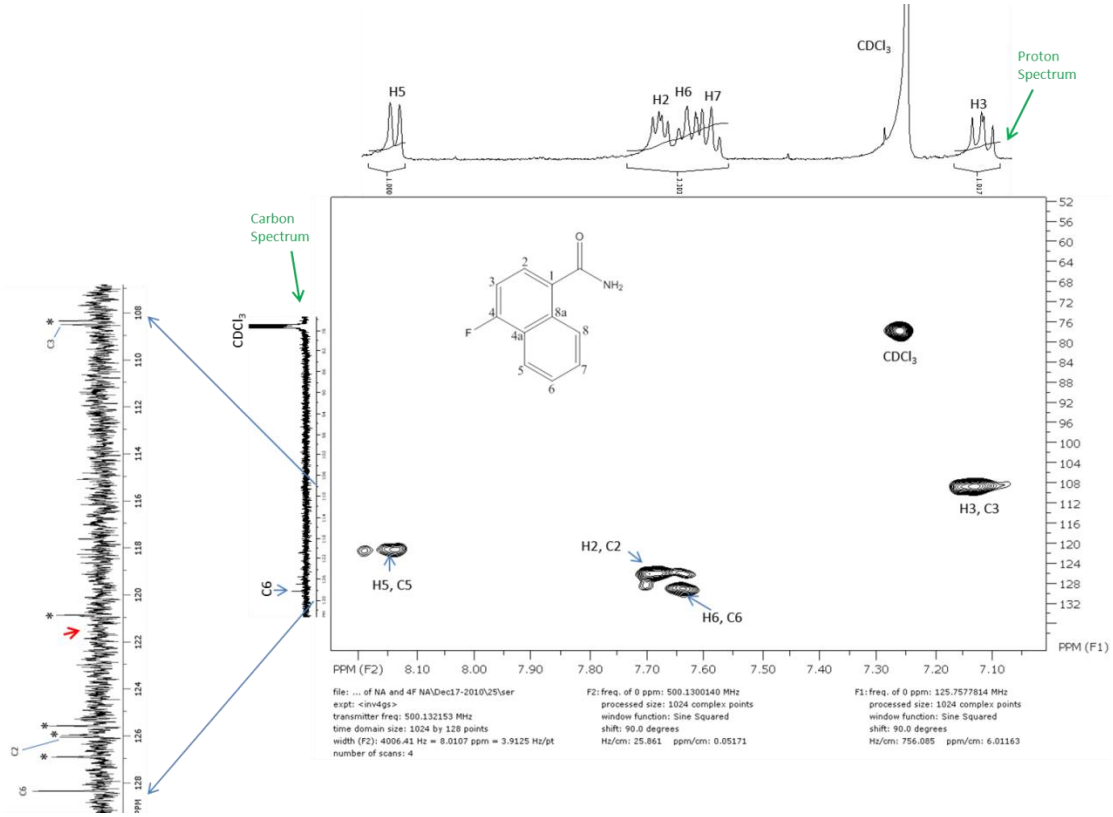

Figure 3.20: HMQC-NMR in $CDCl_3$ of 4-fluoro-1-naphthoic amide **100a**. The spectrum shows the correlation between directly bonded ^{1}H and ^{13}C peaks and provides assignment of C2, C3, C5 and C6 carbons.

The cross-peaks revealed in the spectrum above (**Figure 3.20**) show the correlation between directly bonded ^{1}H and ^{13}C peaks. The carbon assignment could be deduced from HMQC spectrum in a similar fashion to that of 1-naphthoic amide in **Figure 3.9**. Hence, carbon giving signal at δ 126.10 is assigned C2, δ 108.48 as C3, δ 121.40 as C5 and δ 128.40 as C6. It is noteworthy to mention that C5 giving the signal at δ 121.40 in HMQC spectrum was not shown in the carbon spectrum as shown by the red arrow. Also the peaks highlighted with ∗ in the carbon spectrum could not be assigned yet.

An outline of HMBC-NMR of **100a** in $CDCl_3$ is presented in **Figure 3. 21**.

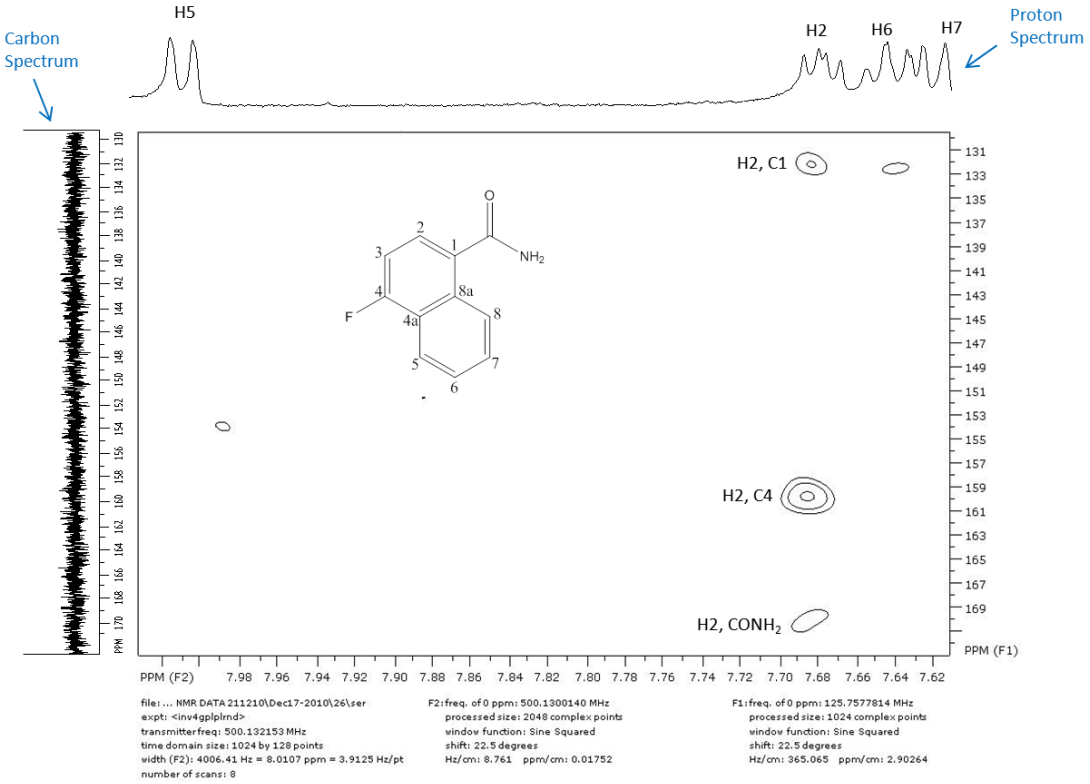

Figure 3.21: HMBC-NMR in $CDCl_3$ of amide **100a**.

Proton δ 7.69 (1 H dd) is correlated to 170.55 carbon that correspond to the amide group ($CONH_2$). Therefore δ 7.69 was assigned to H2. Also **Figure 3.21** shows the interrelation of proton δ 7.69 with 132.01 and 159.5 carbons. δ 132.01 could be assigned to C1 in analogy to amide **99a** and δ 159.5 could be assigned either C4 or C8a and not C3 as the latter gives signal at δ 108.48 (**Figure 3.21**). Comparison with carbon assignment of amide **99a** (**Table 3.2**) shows that δ 159.5 is further downfield compared to C8a (δ 133.84). Furthermore, the presence of a highly electronegative substituent (fluorine atom) at C4 could explain clearly the appearance of the peak further downfield. As consequence, δ 159.5 is assigned to C4. The region of the carbon spectrum projected in F1 dimension (**Figure 3.21**) did not reveal any of the carbon peaks (C1, C4 and $CONH_2$) highlighted by the HMBC-NMR experiment.

IR data of 4-fluoro-1-naphthoic amide 100a

The IR spectrum of the amide **100a** is shown in **Figure 3.22** (Appendix one). The spectrum shows absorption band at about 1733 cm^{-1} which may be indicator of C=O stretching. The NH stretching of the NH_2 group of **100a** was weak and reveals 2 distinct bands between 3100 and 3150 cm^{-1}. The peak appearing at about 3025 cm^{-1} corresponds to CH stretching.

Isolation and purification of 4-methyl-1-naphthoic amide 101a

Isolation and purification of 4-methyl-1-naphthoic amide was done in the same way as amide **99a** with the following exceptions. Flash column chromatography was performed with 70:30 ethyl acetate/40-60: petroleum ether, and the product had an R_f = 0.30.

5 mg was isolated from 180 mg of crude extract, a yield of 5% relative to the added acid.

LCMS data of 4-methyl-1-naphthoic amide 101a:

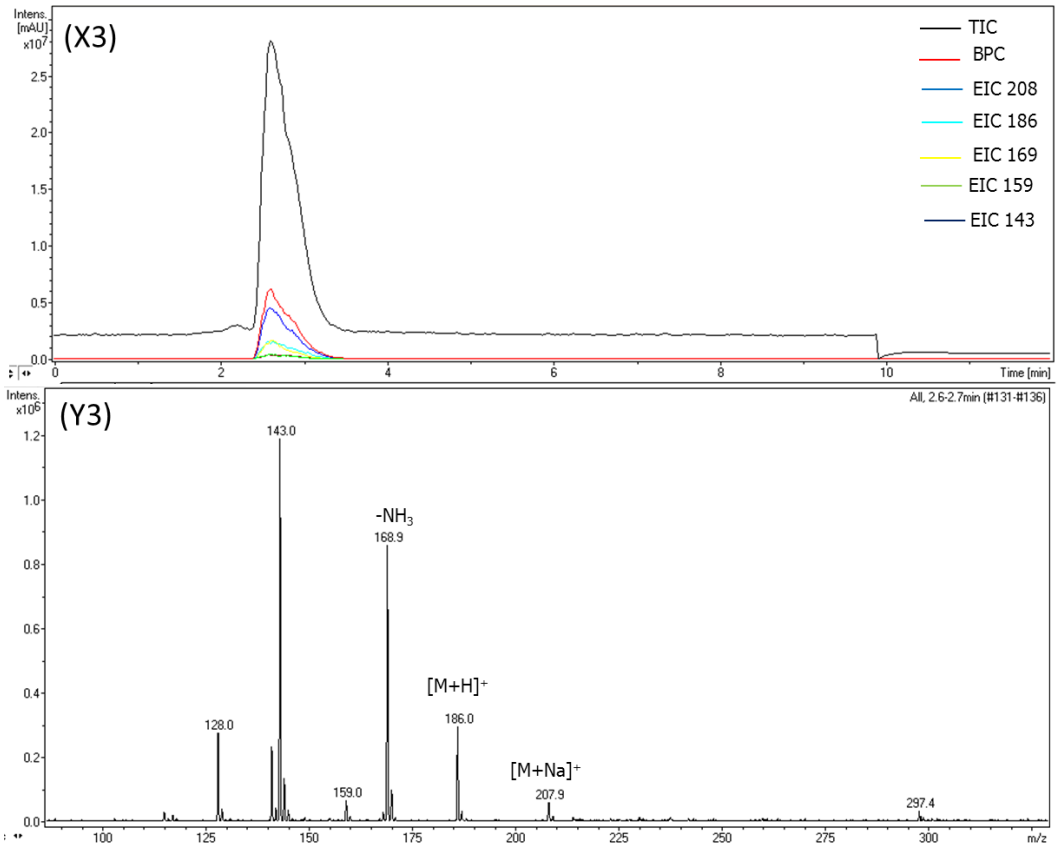

Figure 3.23: LCMS of purified 4-methyl-1-naphthoic amide. (X3): LCMS chromatograms. (Y3): Positive ion electrospray mass spectrum for the new peak at R_t = 2.6-2.7 min.

Figure 3.23 demonstrates a clear alignment between the HPLC total ion chromatogram (TIC), the base peak chromatogram (BPC) and extracted ion chromatogram (EIC) for 4-methyl-1-naphthoic amide ion (m/z 186). EIC peaks for m/z 169, 159 and 143 superimpose perfectly with EIC 186 indicating that these peaks are fragments of m/z 186. m/z 128 corresponds to background signal.

4-methyl-1-naphthoic amide **101a** was characterized only by LCMS (**Figure 3.23**), as impurities hampered NMR analysis. The fragmentation patterns that are shown in **Figure 3.23** display also strong correlations with those for 1-naphthoic amide in **Figure 3.1**. As consequence, the fragmentation mechanisms of amide **101a** could be explained in a similar fashion to that of 1-naphthoic amide **99a** in **scheme 3.1**.

Isolation and purification of 2-methyl-1-naphthoic amide 102a:

Isolation and purification of 2-methyl-1-naphthoic amide was done in identical way as amide **99a** except that TLC exibited an R_f of 0.48.

3 mg was purified from 74 mg of crude extract, a yield of 3% relative to the added acid.

LCMS data for 2-methyl-1-naphthoic amide 102a:

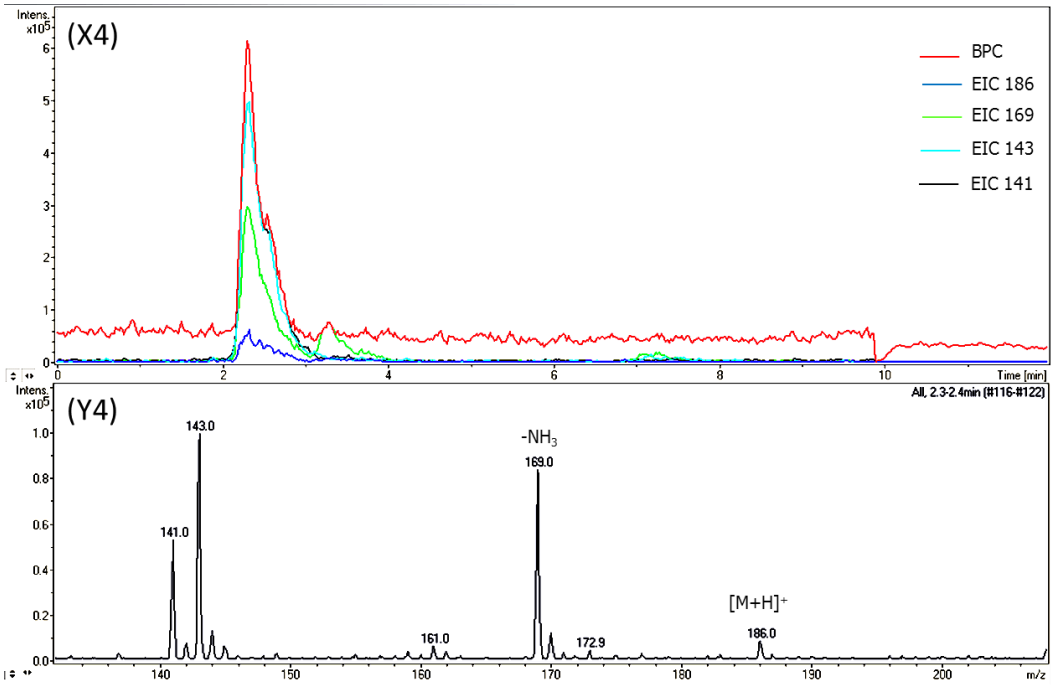

Figure 3.24: LCMS of purified 2-methyl-1-naphthoic amide. (X4): LCMS chromatograms. (Y4): Positive ion electrospray mass spectrum for the peak at R_t = 2.3-2.4 min.

Figure 3.24 demonstrates a clear alignment between the HPLC base peak chromatogram (BPC) and extracted ion chromatogram (EIC) for 2-methyl-1-naphthoic amide ion (m/z 186). EIC peaks for m/z of 169, 143 and 141 superimpose perfectly with EIC 186 indicating that these peaks are fragments of m/z 186.

The persistence of impurities was a major obstacle preventing NMR analysis. Therefore, amide **102a** was characterized only by LCMS (**Figure 3.24)**. The fragmentation patterns that are shown in **Figure 3.24** display also strong correlations with those seen for the other amides, formed by the same mechanisms (**Scheme 3.2**).

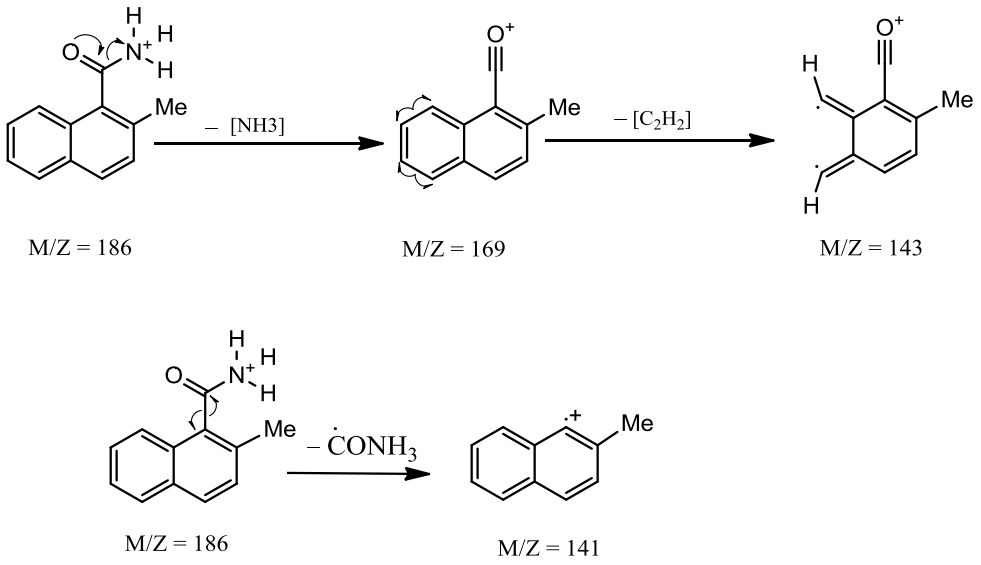

Scheme 3.2: Fragmentation mechanisms of 2-methyl-1-naphthoic amide.

Isolation and purification of 2-methoxy-1-naphthoic amide 103a:

Isolation and purification of 2-methoxy-1-naphthoic amide was achieved similarly to 1-naphthoic amide except that TLC exibited an R_f of 0.41.

20 mg was purified from 80 mg of crude extract, a yield of 20% relative to the added acid.

LCMS results after feeding 2-methoxy-1-naphthoic amide 103a:

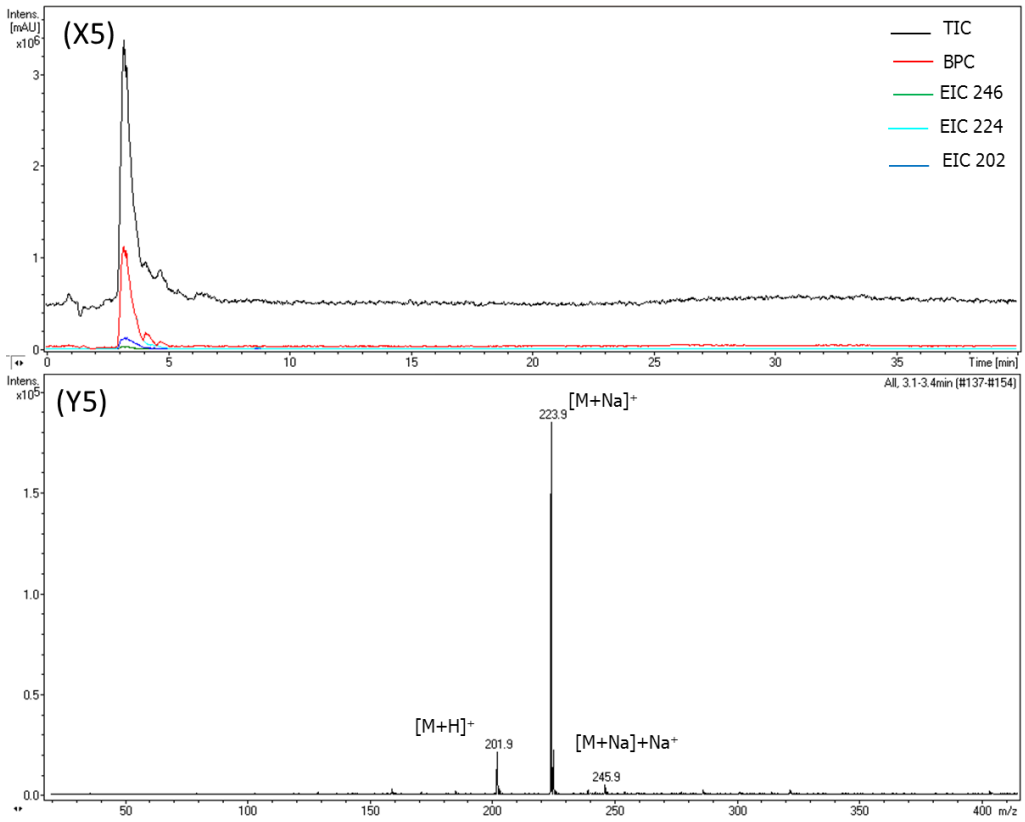

Figure 3.25: LCMS of purified 2-methoxy-1-naphthoic amide. (X5): LCMS chromatograms. (Y5): Positive ion electrospray mass spectrum of the peak at R_t = 3.1-3.4 min.

Figure 3.25 shows a clear alignment between the HPLC total ion chromatogram (TIC), base peak chromatogram (BPC) and extracted ion chromatogram (EIC) for 2-methoxy-1-naphthoic amide ion (m/z 202). EIC peak for m/z 224 is the sodium adduct of the main amide ion $[M+H]^+$ for m/z 202. The persistence of impurities was a major problem preventing NMR analysis. Hence, amide **103a** was characterized only by LCMS.

Isolation and purification of 3-fluoro-1-naphthoic amide 98a:

Isolation and purification of 3-fluoro-1-naphthoic amide was achieved similarly to 4-fluoro -1-naphthoic amide. The product had R_f = 0.21.

14 mg was purified from 97 mg of crude extract, a yield of 15% relative to the added acid.

LCMS data of 3-fluoro-1-naphthoic amide 98a:

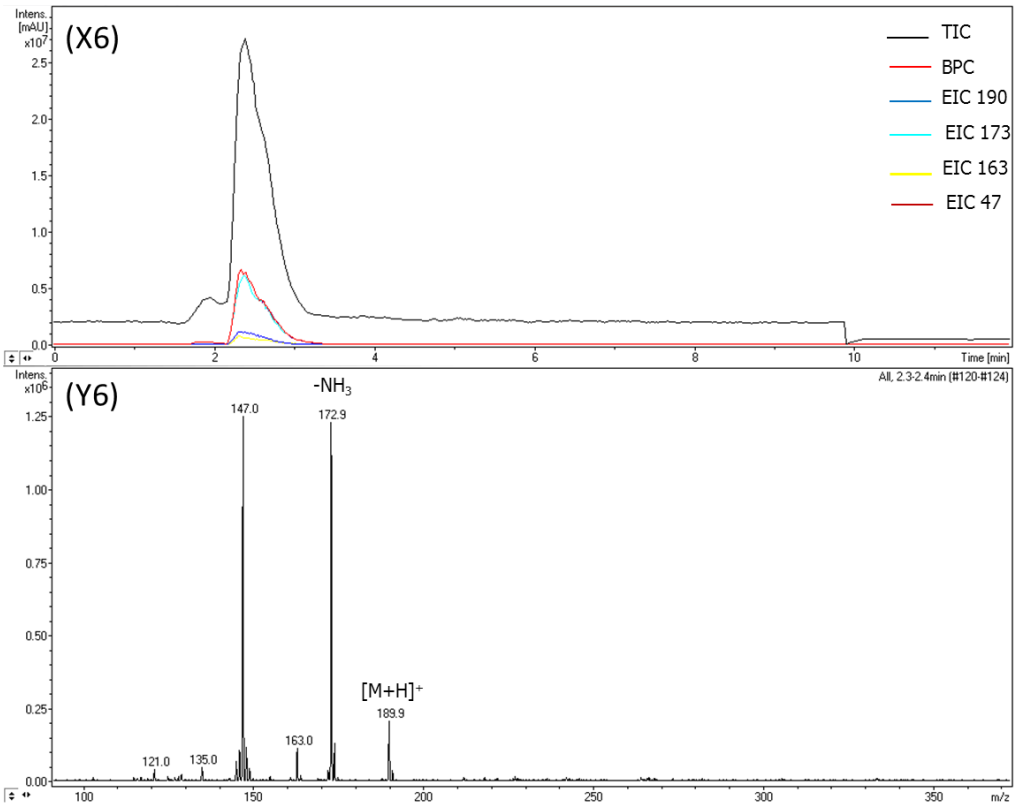

Figure 3.26: LCMS of purified 3-fluoro-1-naphthoic amide. (X6): LCMS chromatograms. (Y6): Positive ion electrospray mass spectrum of the peak at R_t = 2.3-2.4 min.

There is clear alignment between the HPLC total ion chromatogram (TIC), the base peak chromatogram (BPC) and extracted ion chromatogram (EIC) for 3-fluoro-1-naphthoic amide ion (m/z 190). EIC peaks for m/z of 173, 163 and 147 superimpose perfectly with EIC 190 indicating that these peaks are fragments of m/z 190.

3-fluoro-1-naphthoic amide was characterized only by LCMS since the existence of impurities hampered NMR analysis. The fragmentation patterns for amide **98a** (**Figure 3.26**) is similar to amides **99a** and **100a** (**Figures 3.1 and 3.12, respectively)**

and the mechanisms could be explained in a similar fashion to that of 1-naphthoic amide **99a** in **scheme 3.1**.

Isolation and purification of 3-methoxy-1-naphthoic amide 97a:

Isolation and purification of 3-methoxy-1-naphthoic amide was achieved similarly to naphthoic amide except that TLC R_f was 0.46.

2 mg was purified from 43 mg of crude extract, a yield of 2% relative to the added acid.

LCMS results after feeding 3-methoxy-1-naphthoic amide 97a:

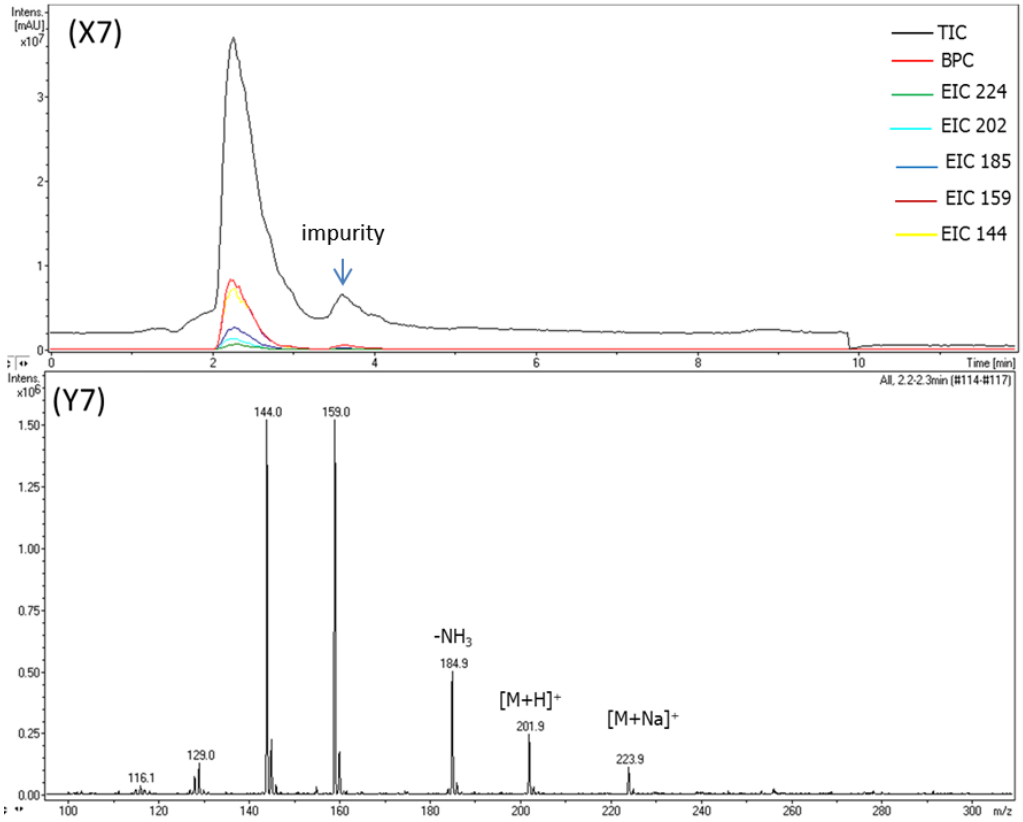

Figure 3.27: LCMS of purified 3-methoxy-1-naphthoic amide. (X7): LCMS chromatograms. (Y7): Positive ion electrospray mass spectrum of the peak at R_t = 2.2-2.3 min.

The peak at R_t = 2.2-2.3 min has MS data consistent with 3-methoxy-1-naphthoic amide ion with m/z 202 for the MH^+ ion. Also the EIC peaks for m/z of 185 and 159 superimpose perfectly with EIC 202 indicating the fragmentation origin of these ions according to the same mechanism as 1-naphthoic amide (**Scheme 3.1**). The EIC peak

for m/z of 144 could be explained by the loss of the methyl group from fragment m/z of 159. 3-methoxy-1-naphthoic amide was characterized only by LCMS (**Figure 3.27**), as impurities hampered NMR analysis.

Feeding amine derivatives in conjunction with naphthoic acid

In an attempt to test the ability of *S. sahachiroi* to biotransform naphthoic acid with different amines (other than ammonia), compounds, a series of amine salts (**110-114**, **Table 3.4)** were added in various concentrations along with 1 mM naphthoic acid, 24 h after inoculation. The results are shown on **table 3.4**.

Compound	Result
Methylamine hydrochloride CH_3NH_2 . HCl **110**	No production.
Hydrazine dihydrochloride H_2NNH_2 .2HCl **111**	No production. (apparent new metabolite of MW = 792 which, not identified yet, was produced instead).
Dimethylamine hydrochloride CH_3NHCH_3 . HCl **112**	No production.
Ethylamine hydrochloride $CH_3CH_2NH_2$. HCl **113**	No production.
Hydroxylamine hydrochloride NH_2OH . HCl **114**	No production.

Table 3.4: Evaluation of amine analogues for biotransformation into naphthoic amides after 64 h incubation of *S. sahachiroi* culture.

The chloroform extracts of feeding compounds **110-114** were analysed by LCMS method but no peaks consistent with the anticipated amide compounds were seen (**Table 3.4)**. However, new peaks were seen whilst analysing the hydrazine dihydrochloride **111** feeding extract suggesting the production of a new metabolite **(Figures 3.28-3.29)**. Several reasons might be behind the non-production of amide metabolites. Firstly, it is possible that the added amines were not incorporated into

the bacterial enzymatic machinery. Secondly, the bacterial membrane might have restricted the diffusion of the fed compounds. Finally, the fed compounds could be degraded by an unknown catabolic pathway.

Isolation and attempted purification of hydrazine feeding extract

Isolation and purification of hydrazine feeding extract was performed the same way as naphthoic amide with the following exceptions.

Flash column chromatography was performed with 75:25 ethyl acetate/40-60 petroleum ether, with the main product (MW = 792 $g.mol^{-1}$ and $[M+H]^+$ = 793) eluting with an R_f of 0.28.

LCMS results after feeding hydrazine dihydrochloride 111:

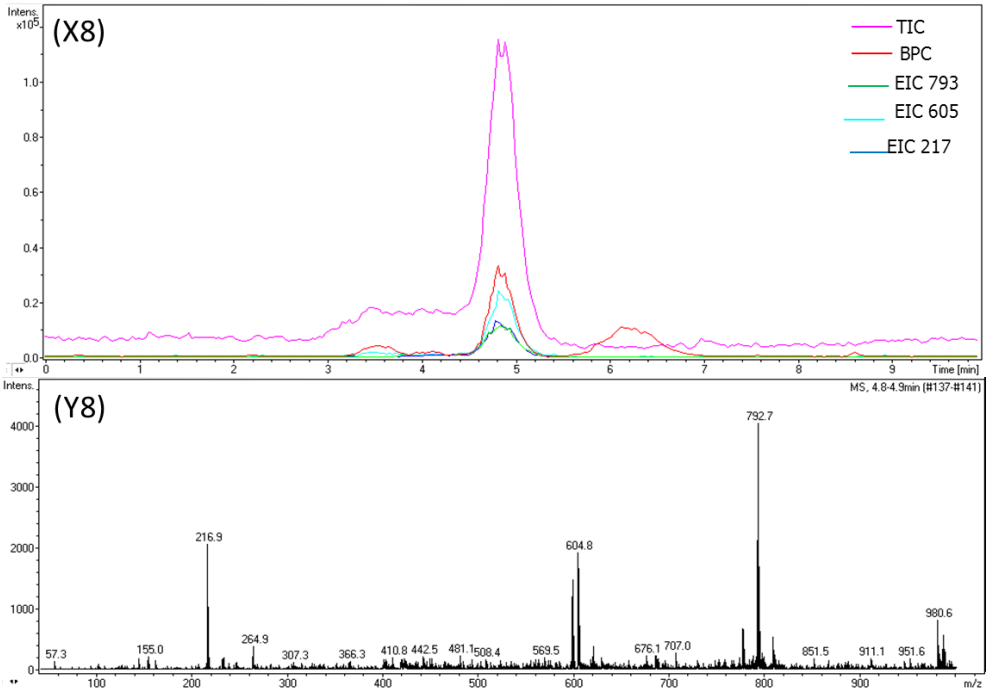

Figure 3.28: HPLC of crude extract from feeding 1-naphthoic acid and hydrazine dihydrochloride to *S. sahachiroi*. (X8): HPLC chromatograms. (Y8): Positive ion electrospray mass spectrum.

The new metabolite was isolated and purified by flash column chromatography and gave the LCMS data presented in **Figure 3.29**.

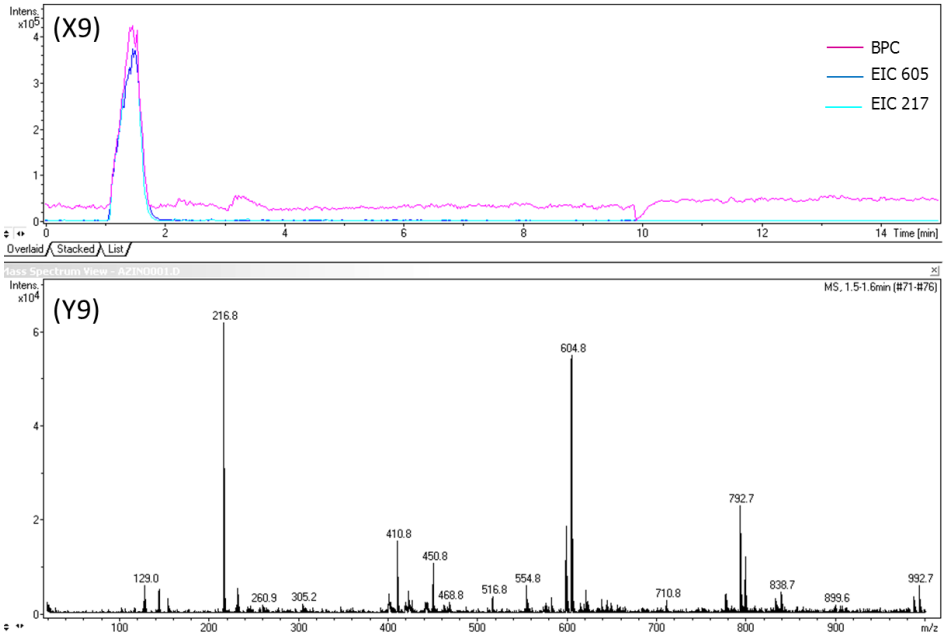

Figure 3.29: HPLC of purified compound from feeding hydrazine hydrochloride to *S. sahachiroi*. (X9): HPLC chromatograms. (Y9): Positive ion electrospray mass spectrum. The main ions observed in (Y9) come from the same compound.

The identity of the apparent new metabolite (MW = 792 g.mol^{-1} and m/z (ESI) = 793) subsequent to feeding hydrazine dihydrochloride to *S. sahachiroi* could not be confirmed yet as NMR analysis was hampered by impurities.

3.2.2 Antibacterial and antifungal activity tests

Target microorganisms

Disk diffusion (DDA) and spot culture growth inhibition (SCGIA) assays **(chap. 2, section 2.2.2 Microbiology**) were used to assess the antimicrobial activity of the methanol extract of *S. sahachiroi* and the methanol solution (by redisolving the dried chloroform extracts) of the purified compounds (**97a**-10**3a** as well as the purified one from feeding hydrazine **111**) against several target microorganisms as is shown in **table 3.5**. In total 8 bacteria (4 Gram-positive and 4 Gram-negative) and 4 fungi strains were target for antimicrobial activity.

Bacteria strains		Fungi
Gram^{+}	Gram^{-}	
Micrococcus luteus	*Escherichia coli K1*	*Trichoderma harzianum* T1
Bacillus subtilis	*Escherichia coli K12*	*Pyrenophora avenae*
Bacillus megaterium	*Escherichia coli*	*Rhizoctonia solani*
Staphylococcus epidermis	*Pseudomonas diminutus*	*Fusarium oxysporum*

Table 3.5: Microorganisms used as target to assess the antibacterial and antifungal activity of *S. sahachiroi*'s crude extracts and the purified compounds (**97a-**10**3a** and the purified one from feeding hydrazine **111**).

Disk diffusion assay (DDA) and spot culture growth inhibition (SCGIA) assay

During DDA, filter paper disks were firstly soaked either with the purified compound at two different concentrations (2 to 1 mg mL^{-1}) or impregnated with *S. sahachiroi*'s crude extracts at a range of concentrations (120 to 5 mg mL^{-1}). Then the disks were placed on the agar plate already inoculated with target bacteria (**Table 3.5**). The plates were then incubated for 24 hours at 37 ^{o}C.

With fungi, a trimmed colony disk of a precultured fungus was placed in the centre of the PDA media. Then the paper disks were impregnated with the test compounds, placed on the agar plates and incubated for 3-5 days at 25 ^{o}C.

During spot culture growth inhibition assay, the tested compounds were dissolved in methanol and two duplicated dilutions (2 mg mL^{-1} and 0.2 mg mL^{-1}) of each compound were made in 2 mL eppendorf tubes. Using a six well plate, a volume of 2 × 5 µL (of each compound) was transferred into a duplicated wells, followed by 2.5 mL of nutrient agar (NA) in each individual well. The final dilutions were 4 and 0.4 µg mL^{-1} respectively. The procedure was the same for the remaining two wells but no compound was added because the wells were used as positive control. After bacterial (5 µL) transfer and horizontal shaking, the plates were sealed and incubated at 37 ^{o}C for 48 hours.

Results from DDA and SCGIA

In general there were no sign of any inhibition zones around the disks (for DDA) or inhibition of growth of the tested microorganisms (for SCGIA) except for the purified compound from feeding hydrazine **111** (not identified yet) and against one sole isolate strain (*M. luteus*). An (average) inhibition zone of about 8 mm was seen at a concentration of 2 mg mL^{-1} (**Figure 3.30**). The same compound (from feeding hydrazine **111**) has also shown a growth inhibition at minimum inhibitory concentration (MIC) of 0.4 µg mL^{-1} during SCGIA (**Figure 3.31**). In the same plate (**Figure 3.31**), it was found that 1-naphthoic amide had no effect on *M. luteus* growth.

Since many data from DDA and SCGIA looked alike, only results from testing 1-naphthoic amide **99a** for DDA (**Figures 3.36-3.47**, **Appendices two and three**) and results from testing **99a** and 4-fluoro-1-naphthoic amide **100a** for SCGIA (**Figures 3.48-3.55**, **Appendix four**) are presented in this study.

Results from DDA

Figure 3.30: Antibacterial test result of purified compound from feeding hydrazine **111** against *M. luteus*. Inhibition zones (average ~ 8 mm) are seen around all disks except control disk (c). Methanol (MeOH) was used as control.

Results from SCGIA

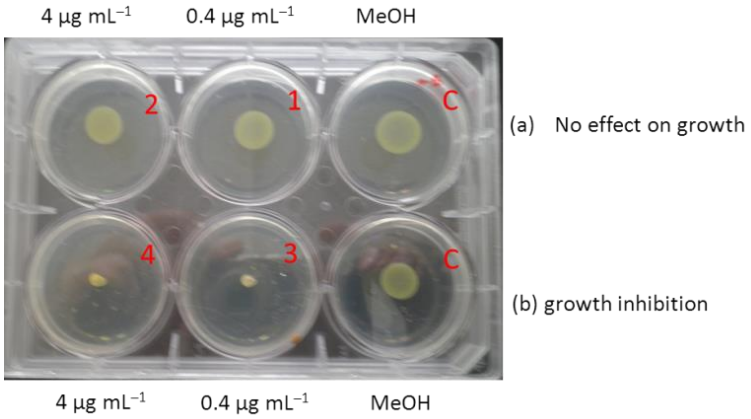

Figure 3.31: Spot culture growth inhibition assay (SCGIA) of **99a** and purified compound from feeding **111** against *M. luteus*: Result showing (a) no growth inhibition with increased concentration (wells 1 and 2) of 1-naphthoic amide **99a** and (b) growth inhibition with the increased concentration (wells 3 and 4) of purified compound from feeding **111**. (c) represents methanol (MeOH) control.

The purified compound from feeding hydrazine **111** shows a biological activity against *M. luteus* solely. There was no activity against the other bacteria or fungi when compounds **97a**-10**3a** were tested.

3.3 Discussion

3.3.1 Bacterial biotransformation

While attempting to discover, by precursor directed biosynthesis, novel azinomycin analogues **(Chapter 4)**, additional novel metabolites appeared in some of the fermentation broths. These metabolites were clearly the result of microbial modification of the fed chemicals, which were biotransformed into their analogous primary amides (**Table 3.1**). However, no secondary amide metabolites were seen in the fermentation broths following the co-feeding of naphthoic acid and amine precursors.

These results suggest that the biotransformed precursors diffused (passively or by active transport) through the first bacterial barriers (cell wall and cytoplasmic membrane). Secondly, the enzyme involved in the biotransformation of acids to amides shows some degree of flexibility towards a range of substrates (**97a-103a**). On the other hand, there was no production of naphthoic amides after feeding the remaining naphthoate compounds (**Table 3.1**). That result might be due to the lack of diffusion of these compounds through the bacterial cell wall and/or cytoplasmic membrane or could be due to their degradation in the fermentation media. Likewise there is a possibility of the non-compatibility of these compounds with the enzyme's active site.

It is likely that the enzymes involved in the biotransformation of naphthoic acids to amides belong to the amide synthases family using ammonia molecules from the culture medium or from internal catabolism pathways. It is difficult to be sure of the identity of the enzymes involved in the present biotransformation as no enzymes have yet been isolated from *S. sahachiroi* that are involved in the biotransformation of naphthoic acids into amides. It was reported that both amide synthases (Thiericke & Rohr., 1993) and nonribosomal peptide synthetases (Bushley and Turgeon, 2010) show low substrate specificity.

It has been experimentally determined that the AziA1 NRPS di-domain serves to load and activate 3-methoxy-5-methyl-1-naphthoic acid as expected for its role in initiating azinomycin biosynthesis (Zhao *et al*., 2008; Ding Zhao *et al*., 2010). It was also demonstrated that this enzyme could activate unnatural substrates. However, modified naphthoate derivatives were not isolated in these studies. It is therefore

possible that the AziA1 NRPS enzyme activates the naphthoic acids in the formation of amides but then fails to pass them on to the hydroxyl group on the epoxide fragment, with ammonia acting as an alternative nucleophile (**Figure 3.32**).

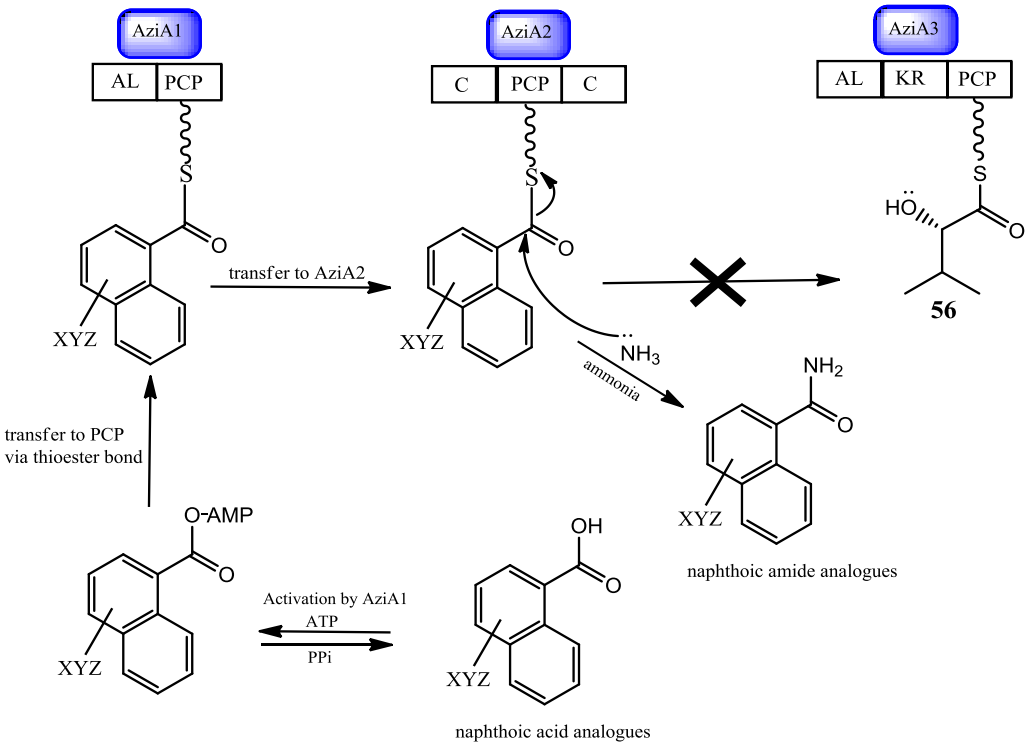

Figure 3.32: Proposed strategy for the bioconversion of naphthoic acid analogues into the corresponding amides by the azinomycin NRPS.

Figure 3.32 shows that naphthoic acid analogues are first activated by the adenylation domain of the enzymatic module AziA1 and then transferred to the peptidyl carrier protein (PCP) domain of the same enzyme module. The tethered thioester is then transferred to the PCP of the second module AziA2 in order to initiate the assembly of azinomycin A analogue fragments. However, the azinomycin NRPS might have failed to catalyse the latter step and instead alternate ammonia molecules, acting as nucleophiles, catalyse amidation reactions and consequently bioconvert naphthoic acid analogues into corresponding amide products.

It is worth emphasizing that *Streptomyces* bacteria are not only well known for their leading role as important source of bioactive natural compounds, they also offer a wide spectrum of enzymes that are useful for microbial biotransformation. Indeed, it is well cited in the literature that *Streptomyces'* enzymes cover a wide array of

reactions allowing the bioconversion of a broad spectrum of organic substrates into useful compounds (Sutherland, 1986; Brunati *et al*., 2003; Gurram *et al*., 2009). They are less substrate specific than enzymes of primary metabolism, but may reveal high chemo-, regio- and enantioselectivity (Mara *et al*., 2004). Examples of some of these microbial bioconversions include hydroxylation of aliphatic and cyclic compounds (Gurram *et al*., 2009), demethylation of vanillic acid (Sutherland, 1986), methylation of catechin by *Streptomyces griseus* (**Figure 3.33**) (Das and Rosazza., 2006) and amidation of cinnamic acid (Brunati *et al*., 2003). Biotransformation of aromatic carboxylic acids to amides is known to occur with many *streptomyces* strains. Examples of these biotransformations are the transformation of mycophenolic acid by *Streptomyces albidoflavus* (**Figure 3.34**) (Jekkel *et al*., 2002), and cinnamic acid to cinnamamide by *Streptomyces halstedii* (**Figure 3.35**) (Mara *et al*., 2004). Microbial enzymatic machinery can be used in many occasions as an alternative route to classical synthetic processes. Certainly, many difficulties encountered during organic synthesis such as protecting functional groups or isomerisation and racemisation problems are lessened by the use of biological systems (Gurram *et al*., 2009).

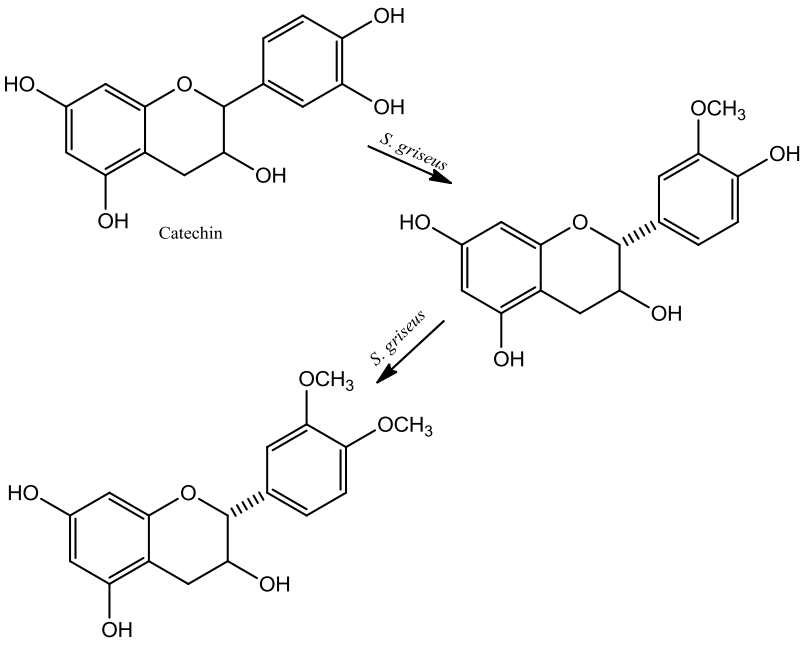

Figure 3.33: Methylations of (+)-catechin by *S. griseus*.

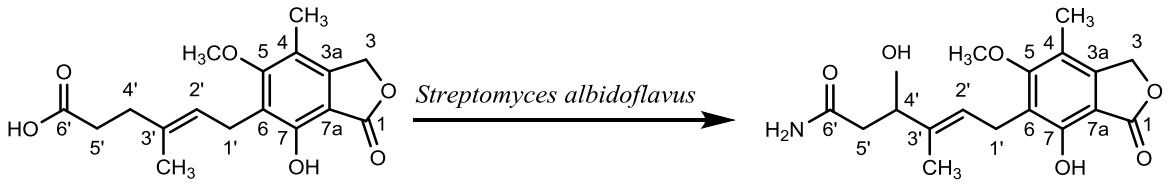

Figure 3.34: Bioconversion of mycophenolic acid by *Streptomyces albidoflavus*.

Figure 3.35: Amidation of cinnamic acid by *Streptomyces halstedii*.

3.3.2 Biological activity of the purified compounds

Comparison of DDA and SCGIA

Both DDA and SCGIA are reliable, easy, simple to perform and inexpensive compared to many other MIC determination methods **(**Jorgensen and Ferraro, 1998; Gaudreau *et al*., 2007; Evangelopoulos and Bhakta, 2010). However DDA shows many drawbacks. The results are in general qualitative; the test is unsuitable for hydrophobic compounds as their diffusibility through the agar is restricted (Brouwer *et al*., 2005). Additionally DDA is not generally automated test but could be automated sometimes (Hejblum *et al*., 1993).

In contract, SCGIA is a quantitative test, suitable for hydrophobic and large molecular weight compounds. Furthermore, the compounds do not interfere with the assay (Evangelopoulos and Bhakta, 2010).

Chapter 4: Precursor-Directed Biosynthesis of Azinomycin A Analogues

4.1 Introduction

The aim of this part of the project was the discovery of novel azinomycin analogues by precursor-directed biosynthesis (PDB).

On analysis of the chemical structure of the azinomycins**,** it is difficult to imagine how to modify by PDB the 1-azabicyclo[3.1.0]hexane ring system. The idea of feeding any alternative potential precursor analogues to *S. sahachiroi* culture was discarded, since the detailed biosynthetic origin of carbons C10 and C11 of the aziridine functional group as well as its biocyclisation remain unidentified. Also, the synthesis of any structural analogues would be very challenging.

The epoxide moiety is relatively small so there are limited options for structural analogues of this fragment. Another likely approach to PDB of azinomycin analogues could be modification of the metabolic precursor aminoacetone. However, the role of this metabolite in azinomycin biosynthesis was published (Sharma *et al*., 2009) well after the start of this project.

We decided that the most fruitful approach was to attempt to modify the substitution of the naphthoate fragment by feeding naphthoic acid analogues to the azinomycin producer culture. There is also the fact that Lowden and co-workers had already established that naphthoic acids are taken up by the cells during the feeding of native precursors **38-40** (**Figure 4.1)** (Lowden *et al*., 2004b).

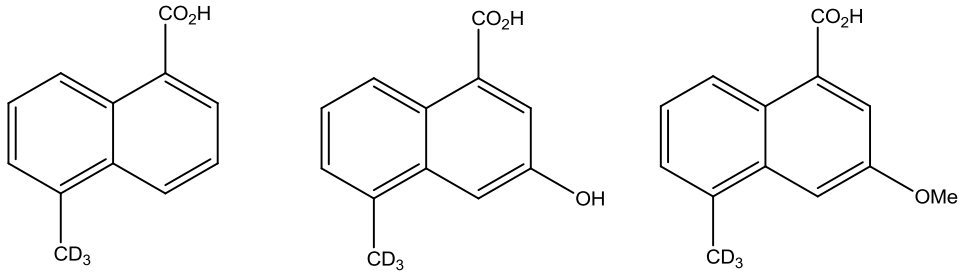

38 **39** **40**

Figure 4.1: Structures of compounds **38**, **39** and **40**.

3-Methoxy-5-methylnaphthoic acid (3-Methoxy-5-methyl-NPA) plays an important role in the biological activities of the azinomycins through a non-covalent interaction with the double stranded DNA. A study done by Zang and Gates has shown that azinomycin analogue **115 (Figure 4.2)** containing both an intact epoxide moiety and the naphthoate fragment (but lacking the aziridine residue) intercalates into the DNA duplex and retains significant biological activity. On the other hand non-epoxy analogues **116** and **117 (Figure 4.2)** that contain the naphthalene ring showed weak biological activity. (Zang and Gates, 2000).

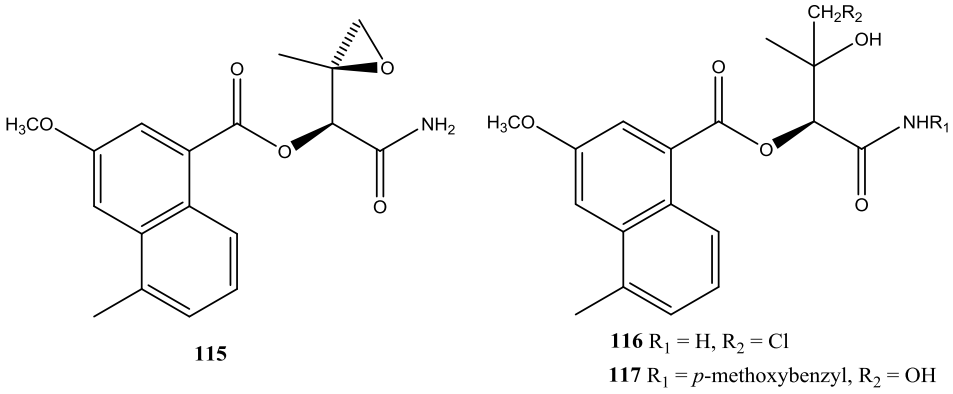

Figure 4.2: Structures of compounds **115**, **116** and **117**.

In a later study by Coleman and co-workers, it was shown that the viscosity of the calf thymus DNA solution did not rise with the increase of naphthoic acid compound **118 (Figure 4.3)** indicating a failure of an effective intercalation between acid **118** and calf thymus DNA (Coleman *et al*., 2002a). However, and in a support to the significant functional importance of the naphthoate moiety, it was revealed in another study done by Coleman and co-authors that compounds lacking the naphthoate fragment **119** and **120 (Figure 4.3)** react weakly with DNA and show no biological activity (Coleman *et al*., 2002b).

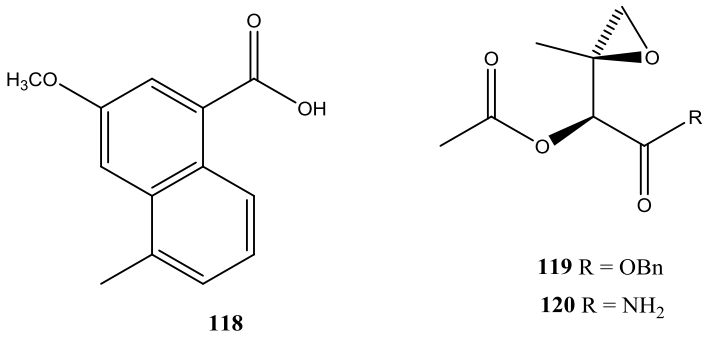

118

119 R = OBn

120 R = NH_2

Figure 4.3: Structures of compounds **118**, **119** and **120**.

Modification of the aromatic ring in synthetic azinomycin analogues resulted in a change in their biological activity. A study done by Landreau and co-workers showed that the effect of removing either 5'-methyl **121** or 3'-methoxy **122** (or both **123**) **(Figure 4.4)** substituent(s) from the naphthalene ring resulted in a significant decrease in the efficiency of DNA interstrand cross-linking (Landreau *et al*., 2004).

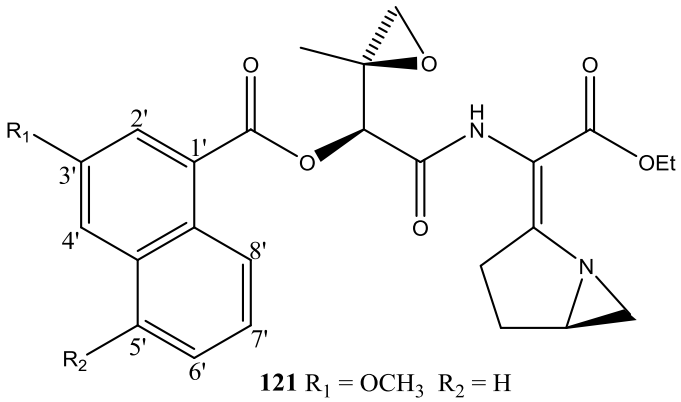

121 $R_1 = OCH_3$ $R_2 = H$

122 $R_1 = H$ $R_2 = CH_3$

123 $R_1 = H$ $R_2 = H$

Figure 4.4: Structures of compounds **121**, **122** and **123**.

The direct chemical modification of azinomycins is impeded by difficulties due to the chemical instability of the 1-azabicyclo[3.1.0]hexane ring system and the poor availability of the natural products. An alternative approach could be the development of novel azinomycin analogues by the PDB method. PDB has a significant advantage as it combines the power of synthetic chemistry and biosynthesis. During the deployment of the method, a range of naphthoic acid analogues **(Table 4.2, Results)** were added to the azinomycin producer fermentation

broth, and fermentations analysed for the presence of new metabolites incorporating these unnatural naphthoates.

First, we needed to achieve a consistent production of azinomycin A from *S. sahachiroi* batch cultures. For that purpose the culture method was optimised using a fresh *S. sahachiroi* strain (instead of the old strain) that was ordered from the American Type Culture Collection (ATCC). The strain was maintained and grown on batch cultures as described in **section 2.2.2.** The main difference between the optimised conditions and the unsuccessful ones lies on the age of the inoculating spores. During the unsuccessful conditions, fresh *S. sahachiroi* spores (from both, old and new strains) that were grown for 5-7 days at room temperature were used for initial seed cultures. However, during the optimised conditions aging spores (incubated for 3-6 months at room temperature) were the source for initial seed cultures. Hence a reliable production of azinomycin A was achieved.

4.2 Results

4.2.1 Bacterial growth and azinomycin production

The growth of the azinomycin producing organism has been checked in GYM, TSA, PDA, SRA and NA solid media. It was found that *S. sahachiroi* grows and sporulates best in GYM solid medium **(Table 4.1)**. Therefore this solid medium was used for growth and maintenance of *S. sahachiroi* during the course of this study.

Plate	Growth	Formation of spores	
GYM	Robust, with mature and grey spores of *S. sahachiroi* after two weeks incubation at room temperature.	**Yes**	
PDA	Rapid growth of *S. sahachiroi* after 48 h incubation at 30 ^{o}C. Grey spore formation after two weeks incubation at room temperature.	**Yes**	
TSA	Rapid growth of *S. sahachiroi* after 48 h incubation at 30 ^{o}C. Then the culture was left at room temperature for 2 weeks.	**No**	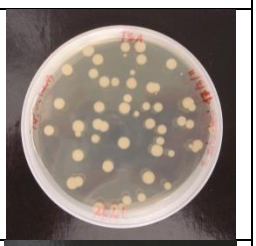
SRA	Rapid growth of *S. sahachiroi* after 48 h incubation at 30 ^{o}C.	**No**	
NA	Rapid growth of *S. sahachiroi* after 48 h incubation at 30 ^{o}C. Then the culture was left at room temperature for 2 weeks. (*M. luteus* and *S. epidermis* bacteria streaked in perpendicular line with *S. sahachiroi)*	**No**	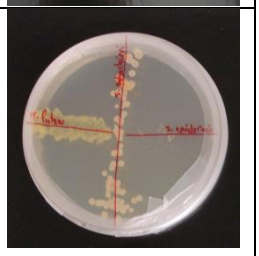

Table 4.1: Evaluation of solid media for growth and formation of spores of *S. sahachiroi*

Different conditions were attempted for optimisation of production of azinomycins A and B as follows: Starting always with fresh spores for initial seed culture, the volume of culture broth was decreased from 50 mL to 40 mL (in the 250 mL Erlenmeyer flask) in order to rise the volume of oxygen in the flasks available for the culture. Also the volume of spores' inoculum was increased gradually from 4 to 8% (culture broth was kept constant at 50 mL) so that the competition for nutrients would intensify leading to a bacterial stress and possibly to a reliable production of azinomycins. Additionally 1-5% dimethyl sulfoxide (DMSO) was added to the fermentation broth 24 h after incubation with the intention of inducing stress among *S. sahachiroi* bacteria and consequent production of secondary metabolites in response to this stress. Finally, commercially available chemicals such as naphthoic acid and naphthoic acid analogues (at 1 mM) were fed to the fermentation culture 24 h after incubation for the same purpose as for the feeding of DMSO. However, a consistent production of azinomycins was difficult to achieve. The production of azinomycins A and B was seen in some of the fermentation culture extracts for a few weeks then disappeared for a few months. It then appeared again for a short period of time and vanished for a lengthy period of time. During some of these attempts, both azinomycins (A and B) were seen in some samples during LCMS analysis (**Figures 4.5** and **4.6**). The final optimised conditions involved three phases, two seed and one fermentation cultures. During the first phase, *S. sahachiroi*'s spores grown on GYM solid plates for 3 to 6 months were used to initiate the first seed culture in Erlenmeyer flasks containing GYM liquid medium and then incubated as described in **chap. 2**, **section 2.2.2**. Afterward, 4% inoculum from previous seed culture was used to inoculate similar flasks but containing PS5 liquid medium and then incubated as described in **chap. 2**, **section 2.2.2**. The final fermentation batch culture was composed of 4% inoculum from the second stage culture and half litre of PS5 medium and then incubated as described also in **chap. 2**, **section 2.2.2**.

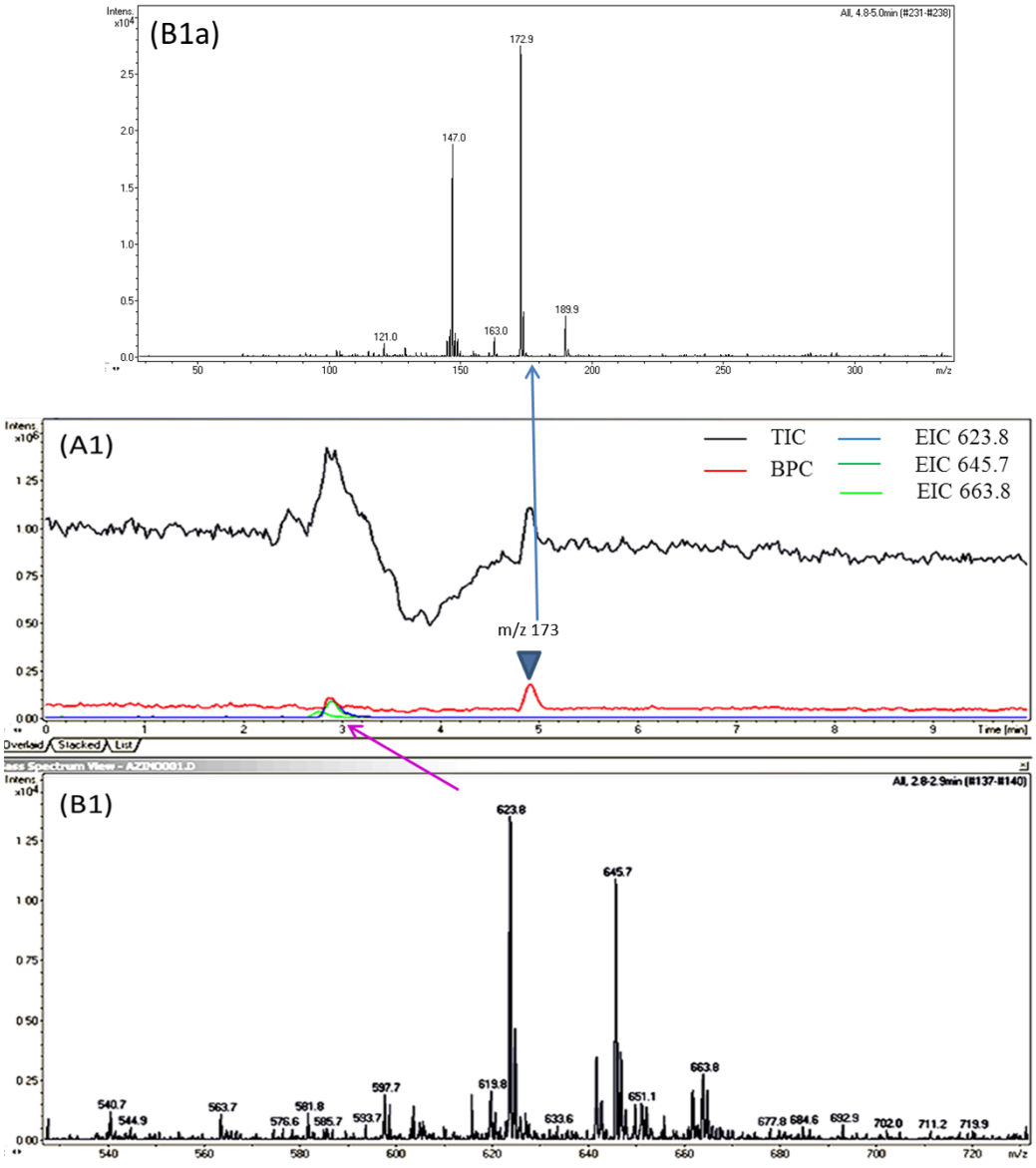

Figure 4.5: LCMS of *S. sahachiroi* chloroform crude extract from feeding 4-fluoro-1-naphthoic acid. (A1): HPLC chromatograms of *S. sahachiroi* chloroform extract showing new peaks at 2.8-2.9 min. (B1) and (B1a): Positive ion electrospray mass spectra. (B1) is displaying peaks for ions consistent with $[M+H]^+$ for m/z = 624, $[M+Na]^+$ for m/z = 646 and the hydrolysed form $[M+Na]^+ + H_2O$ at m/z = 663.8 consistent with azinomycin B production. (B1a) shows peaks for ions consistent with naphthoate fragment (m/z = 173) and related ions (m/z = 190, m/z = 163 and m/z = 147) as previously discussed (**Figure 3.12, Chapter 3**).

A total ion chromatogram (TIC) represents a measure of the overall intensity of ion production as function of time. An extracted ion chromatogram (EIC) designates the signal intensity at selected m/z range plotted against retention time. A base peak chromatogram (BPC) represents the plot of the base peak ion signal obtained from a series of mass spectra as a function of retention time (Murray, 2010).

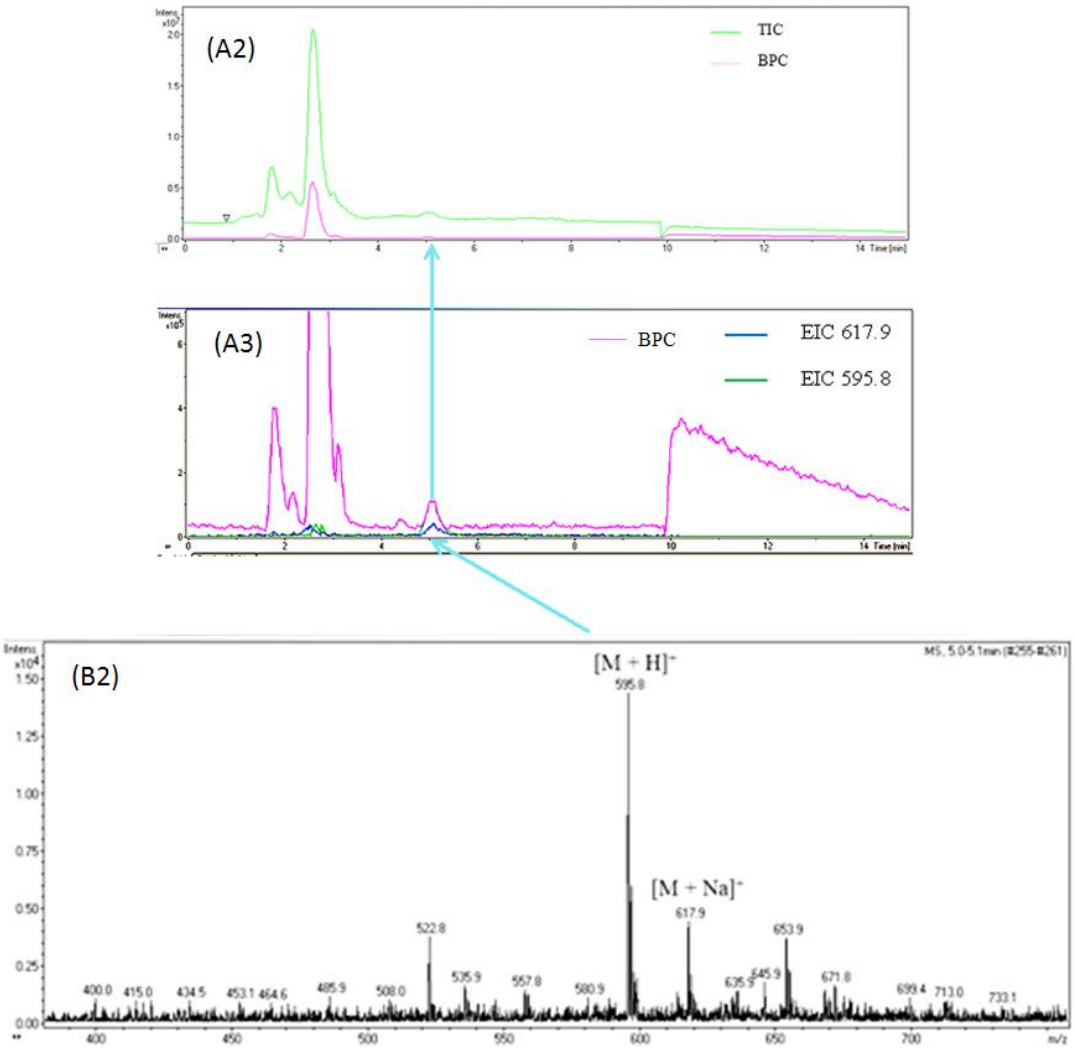

Figure 4.6: LCMS of *S. sahachiroi* chloroform crude extract showing production of azinomycin A. HPLC chromatograms (A2) and (A3) of *S. sahachiroi* chloroform extract and positive ion electrospray mass spectrum (B2) showing peaks respectively at $[M+H]^+$ = 595.8 and $[M+Na]^+$ = 617.9 consistent with azinomycin A production.

Azinomycin B (**Figure 4.5**) was seen in the intact form $[M+H]^+$ = 623.8, as a sodiated addut $[M+Na]^+$ = 645.7 and as a sodiated adduct in the hydrolysed form $M+Na]^+$ = 663.8. Similarly, azinomycin A was produced as an intact metabolite, sodiated adduct and sodiated adduct in the hydrolysed form. **Figure 4.6** shows only the intact form $[M+H]^+$ = 595.8 and the sodiated adduct $[M+Na]^+$ = 617.9.

It is noteworthy to mention that the production of azinomycin B was not seen in any of the fermentation broths after optimising the culture growth. Azinomycin A was the only secondary metabolite analogue reliably produced with or without exogenously supplemented naphthoic acid analogues as seen in **Figures 4.7** and **4.10-4.20 (section 4.2.3)**

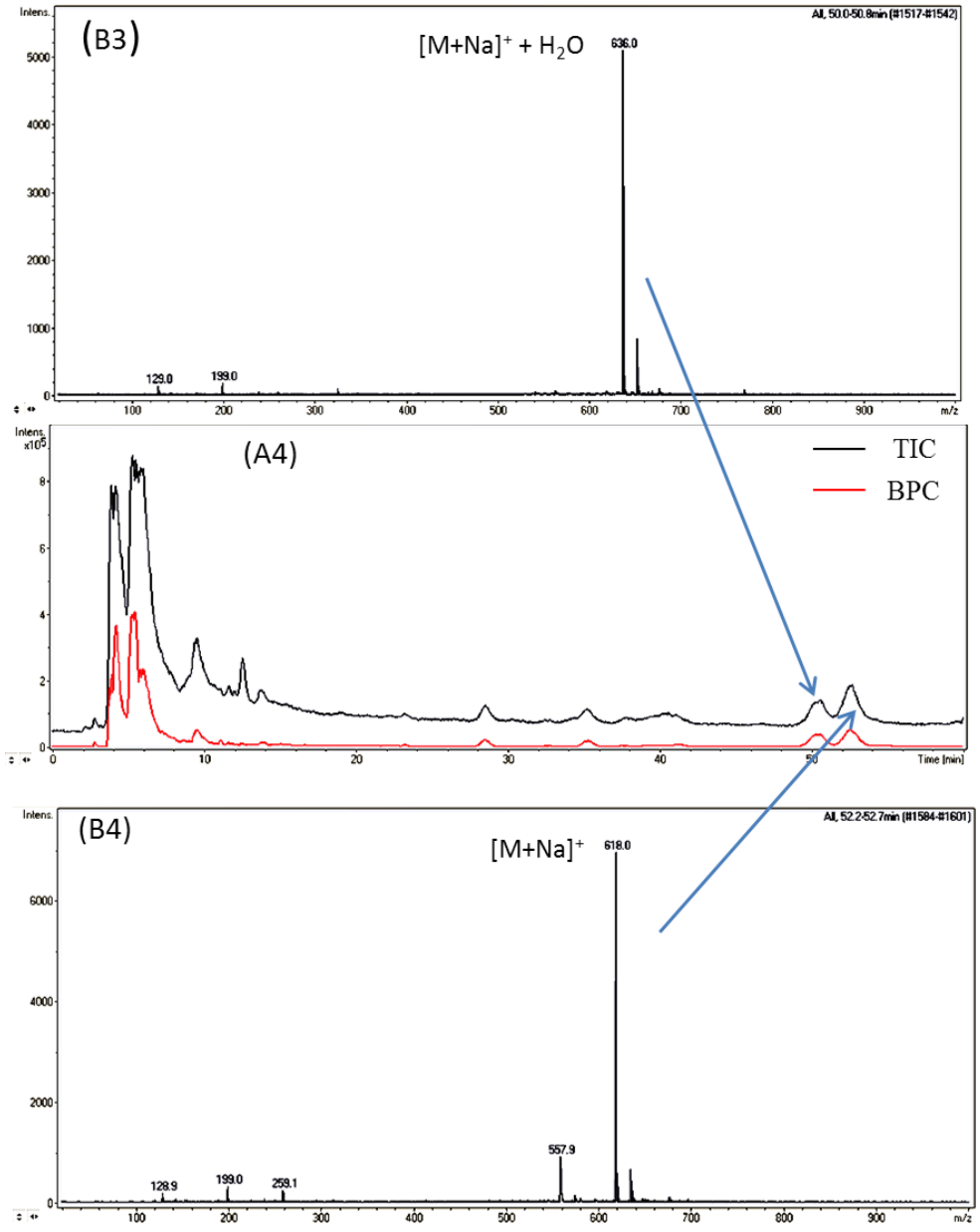

Figure 4.7: LCMS of *S. sahachiroi* showing the production of azinomyicin A and the hydrolysed form. HPLC chromatograms (A4) and positive ion electrospray mass spectra (B3) and (B4) showing the production of azinomycin A as sodium adduct $[M+Na]^+$ at m/z = 618 and in the hydrolysed form $[M+Na]^+ + H_2O$ at m/z = 636 from *S. sahachiroi* crude extract.

A consistent production of azinomycin A was seen in the fermentation extracts **(Figure 4.7)** without feeding any exogenous precursor to the culture broth during this experiment.

4.2.2 Time course study of the production of azinomycin A

To characterize the behaviour of the azinomycin producer *S. sahachiroi*, a time course study was conducted to analyse bacterial growth. The growth was assessed by total viable-colony counts **(Chap. 2, section 2.2.2 Microbiology)** and a detailed growth curve was prepared **(Figure 4.8)**.

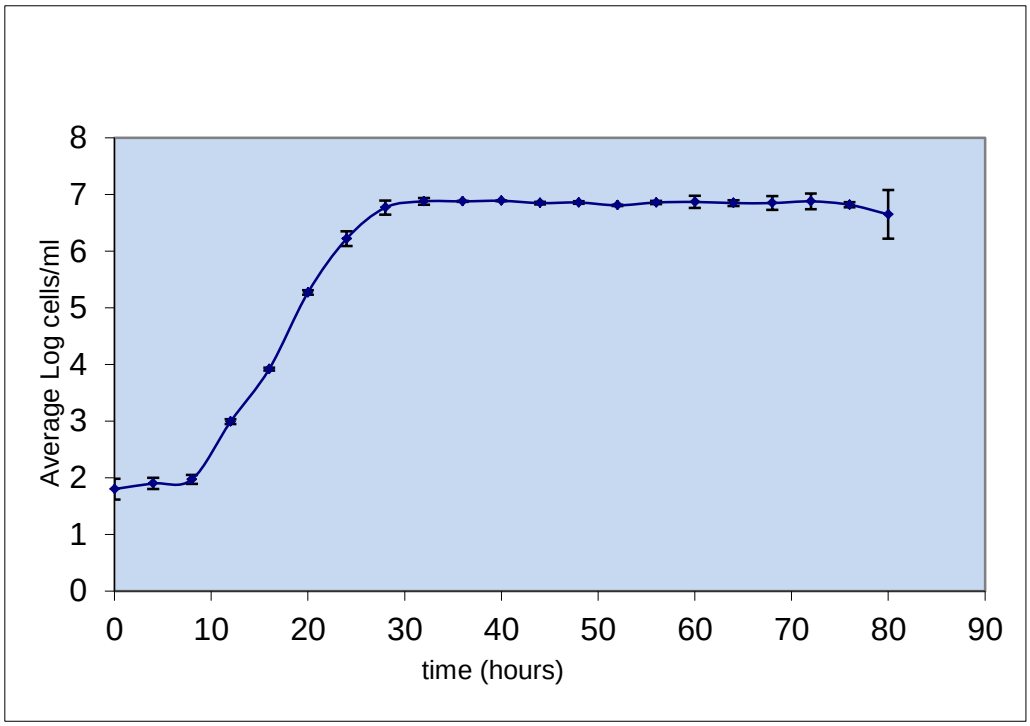

Figure 4.8: Growth curve of *Streptomyces sahachiroi*. Microbial growth was measured every 4 h for a period of 80 h. Developmental phases: lag phase from 0 to 8 h, log phase from 8 to 24 h, Transition phase from 24 to 28 h and stationary phase from 28 to 80 h. Error bars indicate ± AVEDEV.

Figure 4.8 demonstrates the growth curve of *S. sahachiroi* by using bacterial cell viable counts. The cultures grew exponentially with a doubling time of about 1.11 h in PS5 medium at 30 ^{o}C. The cultures enter stationary phase about 28 hours after inoculation.

In order to establish the time-course production of azinomycin A, the culture fermentation broth was harvested after different time periods (each 4 h time interval),

extracted with chloroform and concentrated. Quantitative LCMS analysis was conducted using reversed-phase silica (C18 column, ACE5, 250 × 4.6mm) with water and methanol solution (45:55) as the solvent. Azinomycin detection was done with UV detection (350 nm) and mass-based identification **(Section 2.2.2 Microbiology)**. The time course of azinomycin A production was estimated by integrating the areas under the peaks for each HPLC chromatogram consistent with azinomycin A production and then plotted as a graph of peak area in arbitrary units (A.U) against time (in hours) **Figure 4.9**.

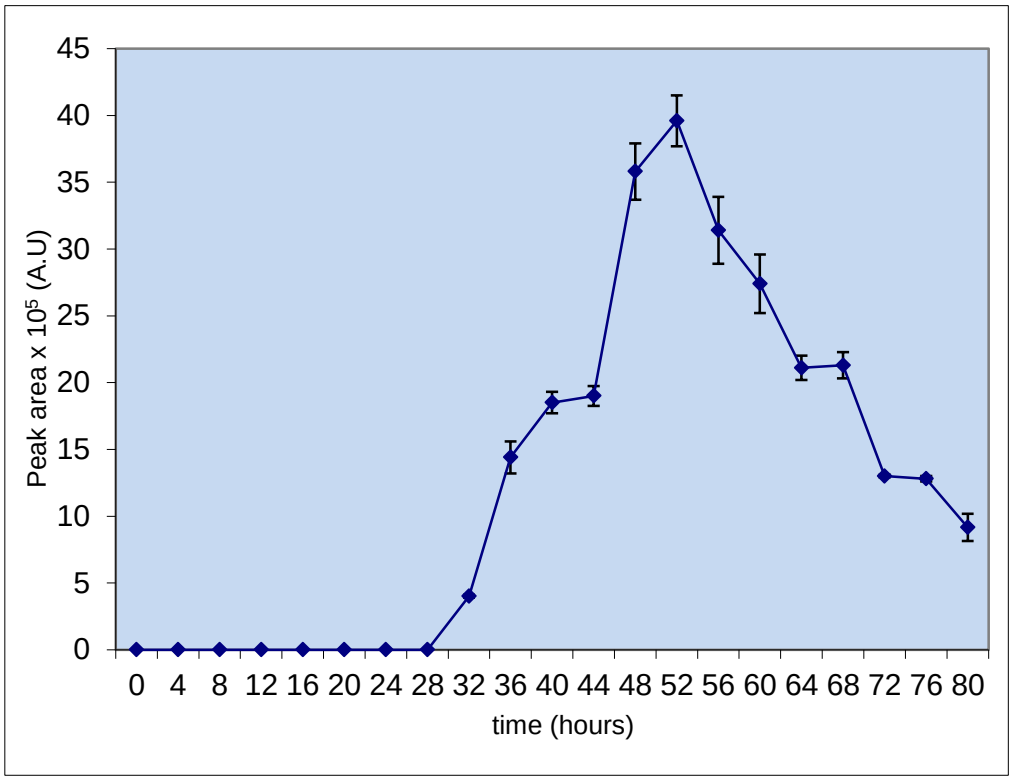

Figure 4.9: Time course of the production of azinomycin A. Microbial production of azinomycin A started just after 28 h and reached it maximum at 52 h. Error bars indicate ± AVEDEV.

As shown in **Figure 4.9**, maximum production of azinomycin A occurred at 52 h and started shortly after 28 of incubation. In comparison with **Figure 4.8**, the production of the secondary metabolite, azinomycin A, occurred during the late transition phase and continued throughout parts of the stationary phase. These conditions enabled us to proceed to the feeding studies by PDB.

4.2.3 Novel azinomycin A analogues by PDB

Precursor-directed biosynthesis method is a potentially powerful way to generate novel metabolites by introducing exogenous materials into biosynthetic pathways of *S. sahachiroi*. Thus, commercially available and synthetic naphthoic acids were fed to *S. sahachiroi* cultures as shown in **scheme 4.1**.

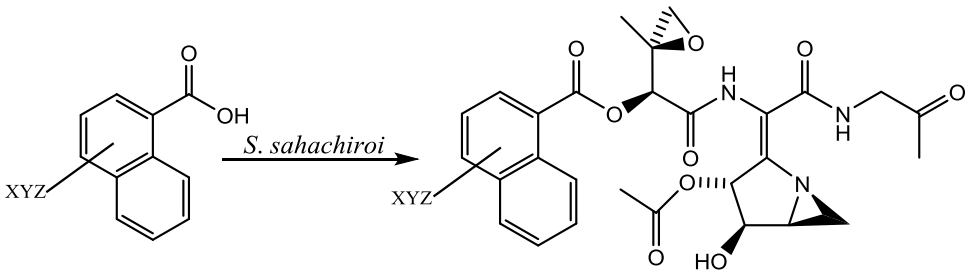

Naphthoic acid analogues Azinomycin A analogues

Scheme 4.1: General strategy adopted for feeding naphthoic acid analogues to *S. sahachiroi* culture broth.

1 mM of Naphthoic acid analogues were fed to the *S. sahachiroi* cultures 24 h after incubation at a concentration of 1 mM. Successful results were achieved subsequent to feeding naphthoic acids **97** and **99-101** as shown in **Table 4.2** and **Figures 4.10-4.20**.

Compound	Expected Azinomycin A Analogue	Result
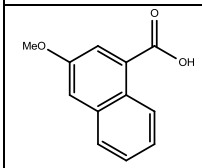 **97** 3-methoxy-1-naphthoic acid	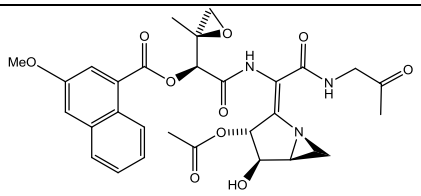	Production of azinomycin A analogue.
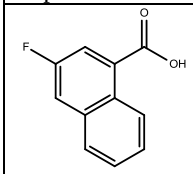 **98** 3-fluoro-1-naphthoic acid	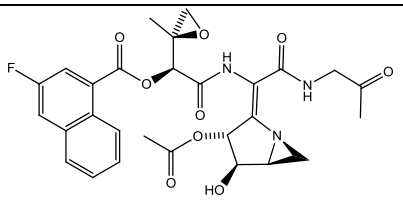	No production.
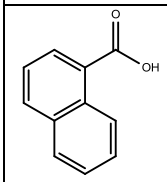 **99** 1- naphthoic acid	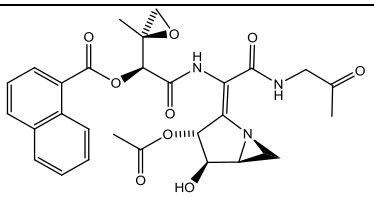	Production of azinomycin A analogues (+ 3′-methoxy one).
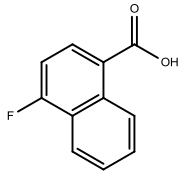 **100** 4-fluoro-1-naphthoic acid	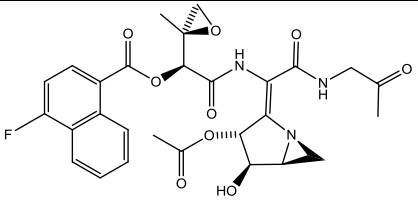	Production of azinomycin A analogue.
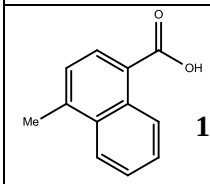 **101** 4-methyl-1-naphthoic acid	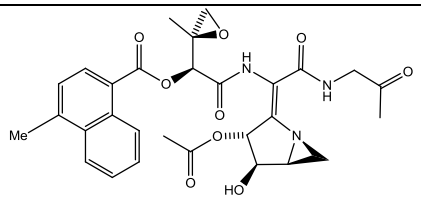	Production of azinomycin A analogue.
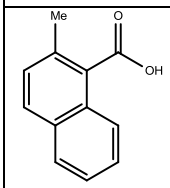 **102** 2-methyl-1-naphthoic acid	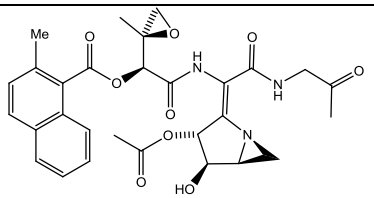	No production.
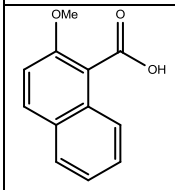 **103** 2-methoxy-1-naphthoic acid	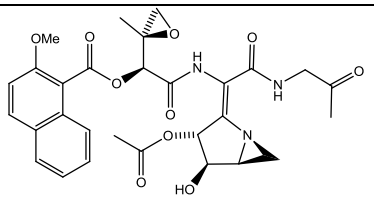	No production.

Table 4.2: Evaluation of naphthoic acid analogues for incorporation into azinomycin A biosynthesis pathway.

Compound	Expected amide	Result
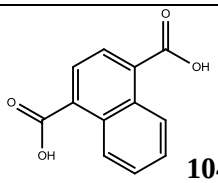 **104** 1,4-naphthalene dicarboxylic acid	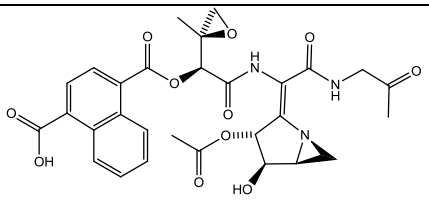	No production.
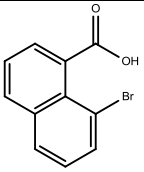 **105** 8-bromo-1-naphthoic acid	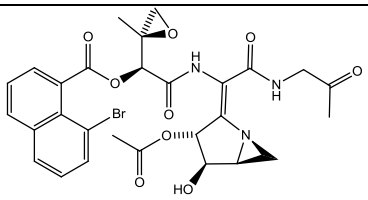	No production.
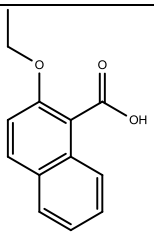 **106** 2-ethoxynaphthoic acid	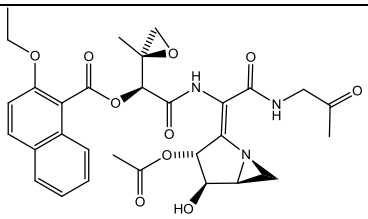	No production.
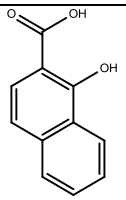 **107** 1-hydroxy-2-naphthoic acid	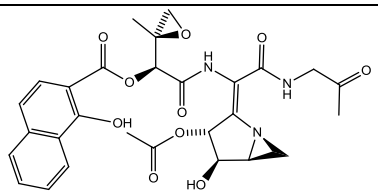	No production.
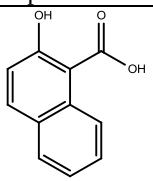 **108** 2-hydroxy-1-naphthoic acid	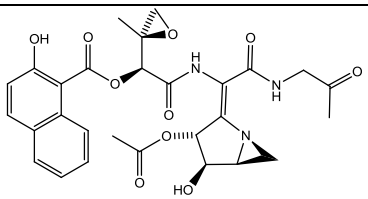	No production.
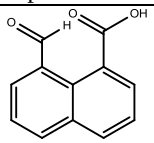 **109** 1,8-naphthalaldehydic acid	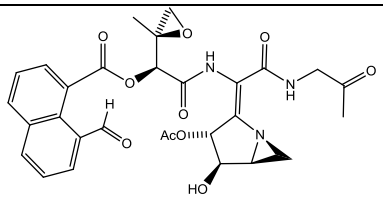	No production.

Table 4.2: Evaluation of naphthoic acid analogues for incorporation into azinomycin A biosynthesis pathway.

4.2.4 Azinomycin A and analogues from prep HPLC extracts from feeding of 1-naphthoic acid

Three novel azinomycin A analogues incorporating 1-naphthoic acid were discovered in the fermentation culture of *S. sahachiroi*. The novel metabolites were detected by LCMS as sodium and potassium salts and hydrolysed salt adducts m/z (mass-to-charge ratio) = 574/592/608, 590/606 and 604/622/638 (**Figures 4.10-4.14**).

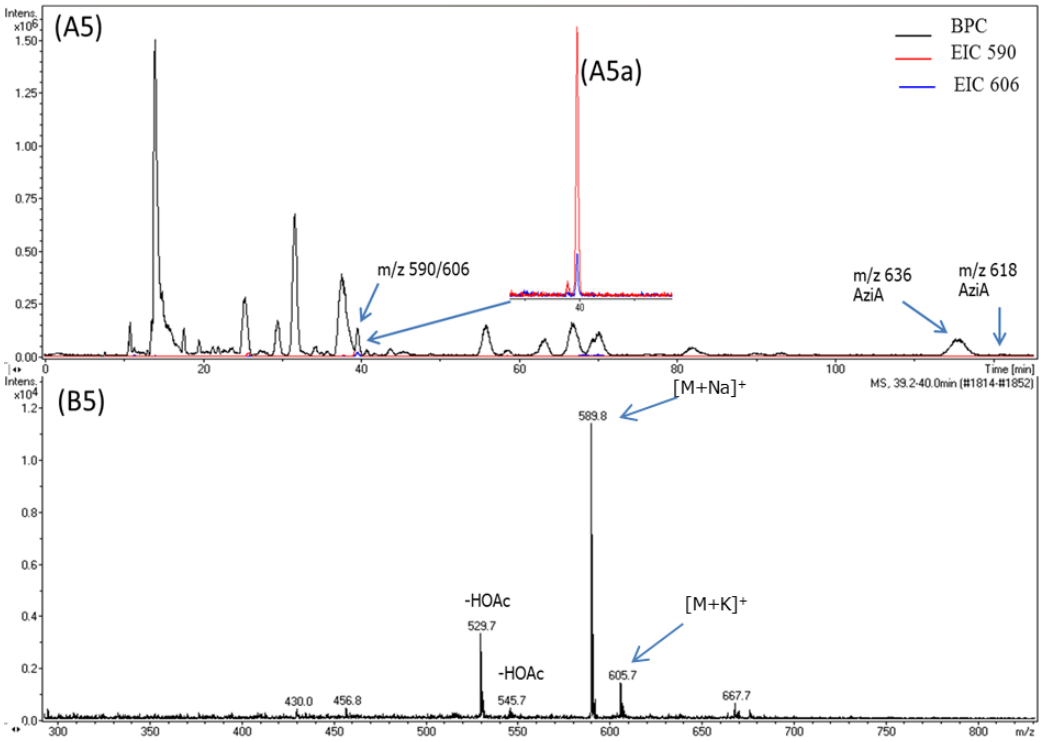

Figure 4.10: LCMS analysis of the extract from feeding of 1-naphthoic acid to *S. sahachiroi*. (A5): Chromatograms from prep HPLC. (A5a): magnification of EICs for m/z 590/606. (B5): Positive ion electrospray mass spectrum. A new peak at R_t = 39.2-40.0 min has MS data, $[M+H]^+$ m/z = 589.8, consistent with incorporation of the naphthoic acid into azinomycin A analogue after hydroxylation.

Fig. 4.10 shows a new HPLC peak at 39.2-40.0 mins (A5) that has MS data for m/z = 590 ($M+Na^+$) and 606 ($M+K^+$) consistent with incorporation of the naphthoic acid into azinomycin A (**Scheme 4.2**) after hydroxylation, most likely by the cytochrome P450 involved in generating the natural naphthoic acid intermediate.

The MS peak at m/z = 530 corresponds to fragment of the main ions at m/z 589.8 formed by loss of HOAc (**Scheme 4.2**). Fragments m/z = 530 and 546 represent the same ion as sodium and potassium adducts respectively.

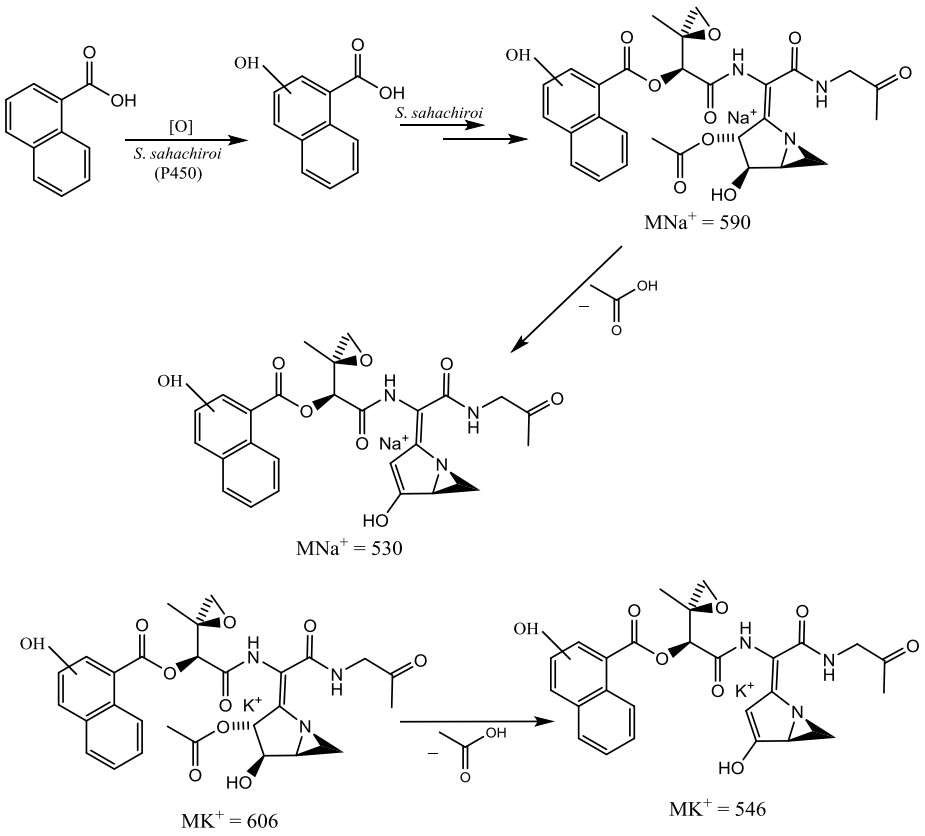

Scheme 4.2: Proposed biosynthesis and fragmentation of the new metabolite.

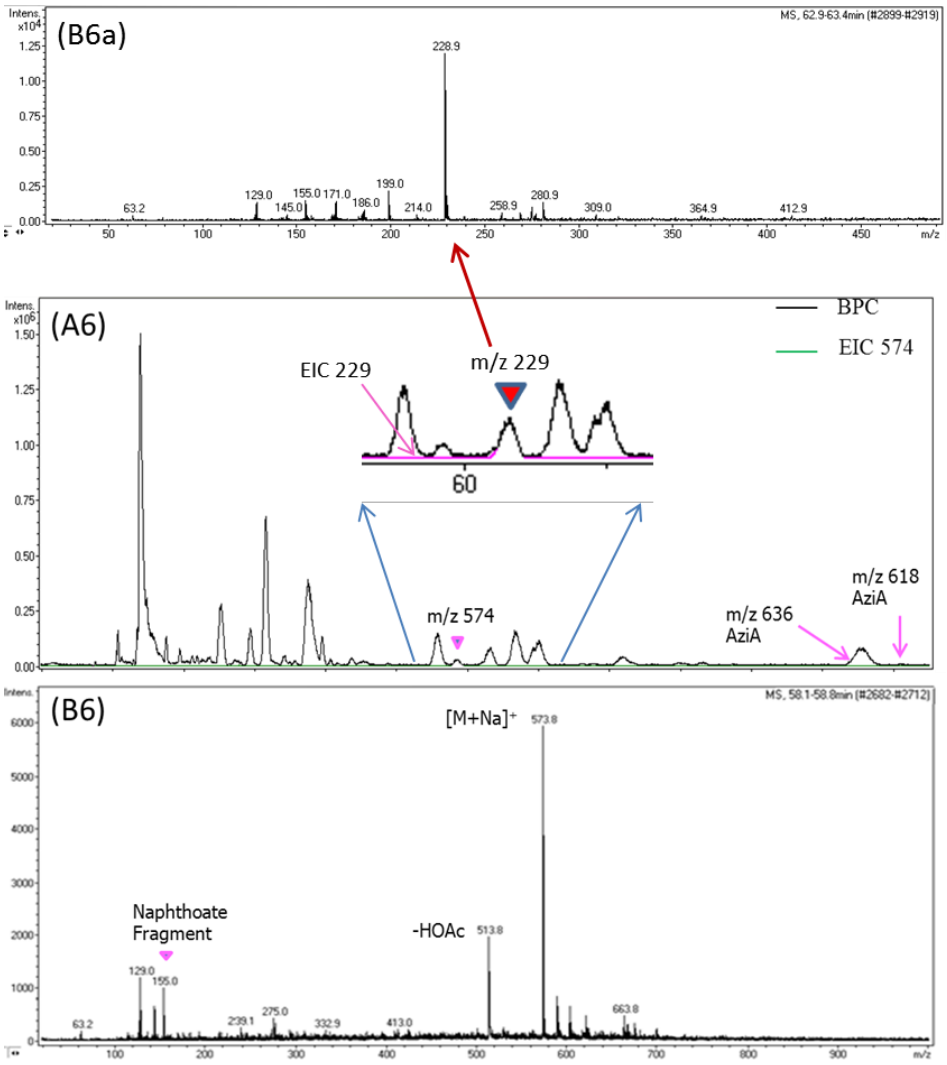

Figure 4.11: LCMS analysis of the extract from feeding of 1-naphthoic acid to *S. sahachiroi* (A6): Chromatograms from prep HPLC. (B6) and (B6a): Positive ion electrospray mass spectra. A new peak at R_t = 58.1-58.8 min (B6) has MS data, $[M+Na]^+$ = 573.8, consistent with incorporation of the unmodified naphthoic acid into azinomycin A analogue. The peak at R_t = 62.9-63.4 min (B6a) has MS data, $[M+H]^+$ = 228.9 and might be a metabolite from *S. sahachiroi*'s extract or simply an artefact signal detected by the mass spectrometer.

A peak at R_t = 58.1-58.8 min (A6) and m/z = 574 ($M+Na^+$) (B6) is consistent with the incorporation of 1-napthoic acid into the azinomycin biosynthetic pathway without additional modification (**Scheme 4.3**). The MS fragment with m/z = 514 is consistent with loss of HOAc from the precursor ion at m/z 573.8 (**Scheme 4.3**). The MS fragment with m/z = 155 is the naphthoate fragment consistent of the loss of m/z = 419 from ion at m/z 573.8 (**Scheme 4.3**).

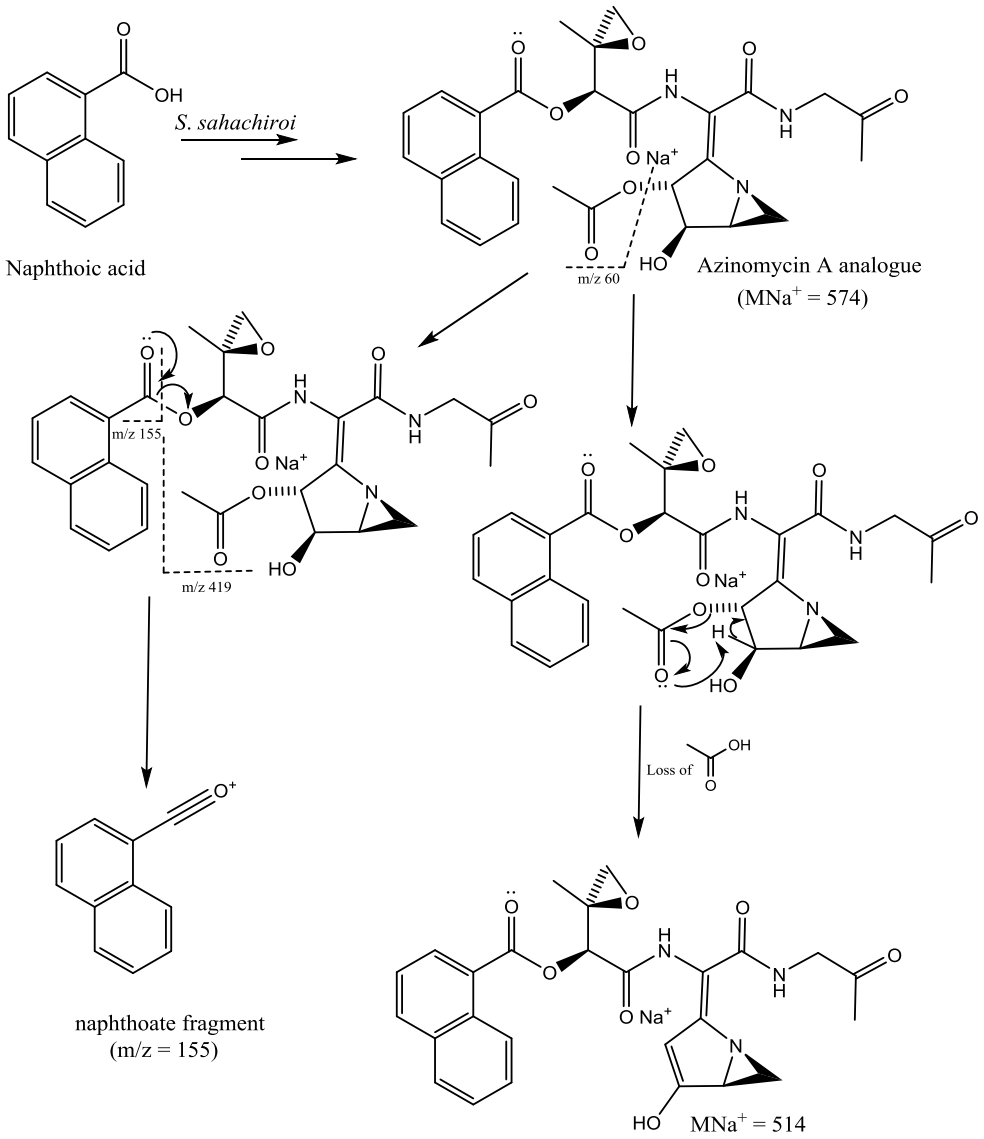

Scheme 4.3 Incorporation of 1-naphthoic acid into the azinomycin A biosynthesis pathway. Spontaneous fragmentation results in the production of two fragments at m/z = 155 and 514.

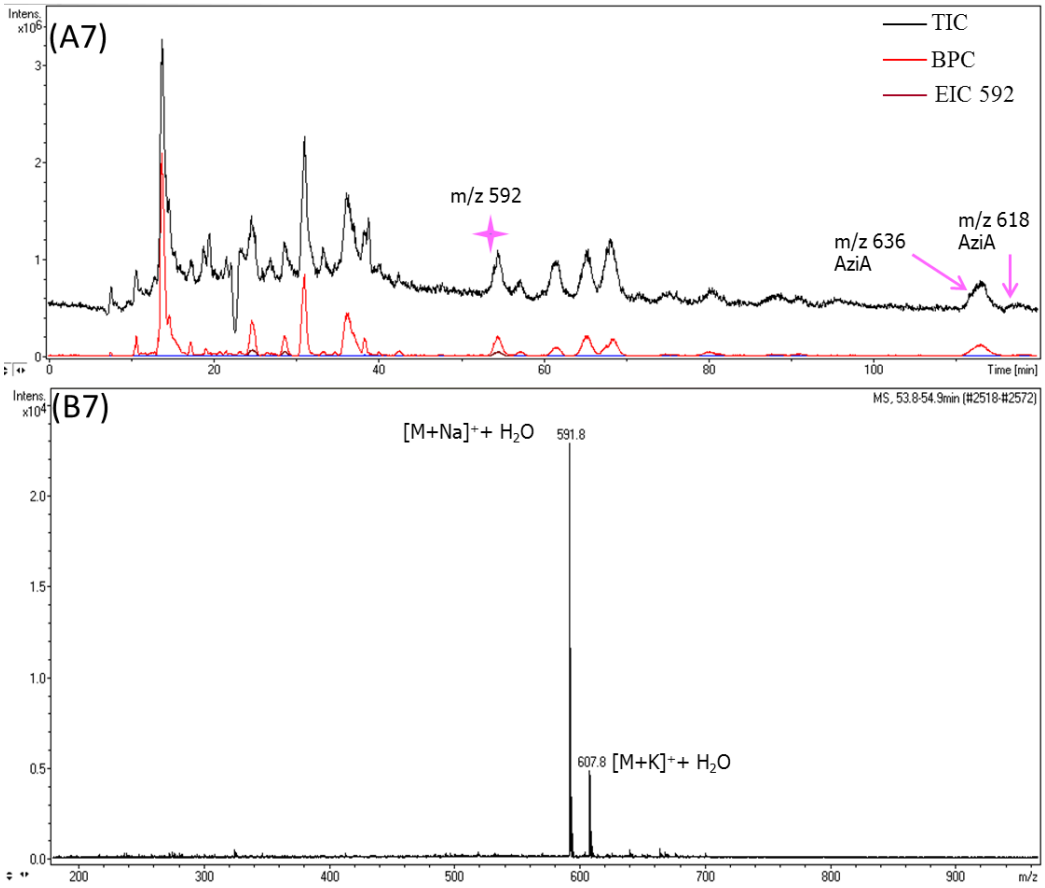

Figure 4.12: LCMS analysis of the extract from feeding of 1-naphthoic acid to *S. sahachiroi* (A7): Chromatograms from prep HPLC. (B7): Positive ion electrospray mass spectrum. A new peak at R_t = 53.8-54.9 min has MS data, $[M+Na]^+$ = 592 and corresponds to the hydrolysed form of ion metabolite of m/z = 574. The additional peak for MS data, $[M+K]^+$ = 608 corresponds to the potassium adduct of the same new metabolite.

Data from **Figure 4.12** indicate that a substantial amount of hydrolysis of the azinomycin A analogue (m/z = 574, **Figure 4.11**) has occurred leading to the formation of the metabolite with m/z 592 and 608 (A7), as outlined in **scheme 4.4**.

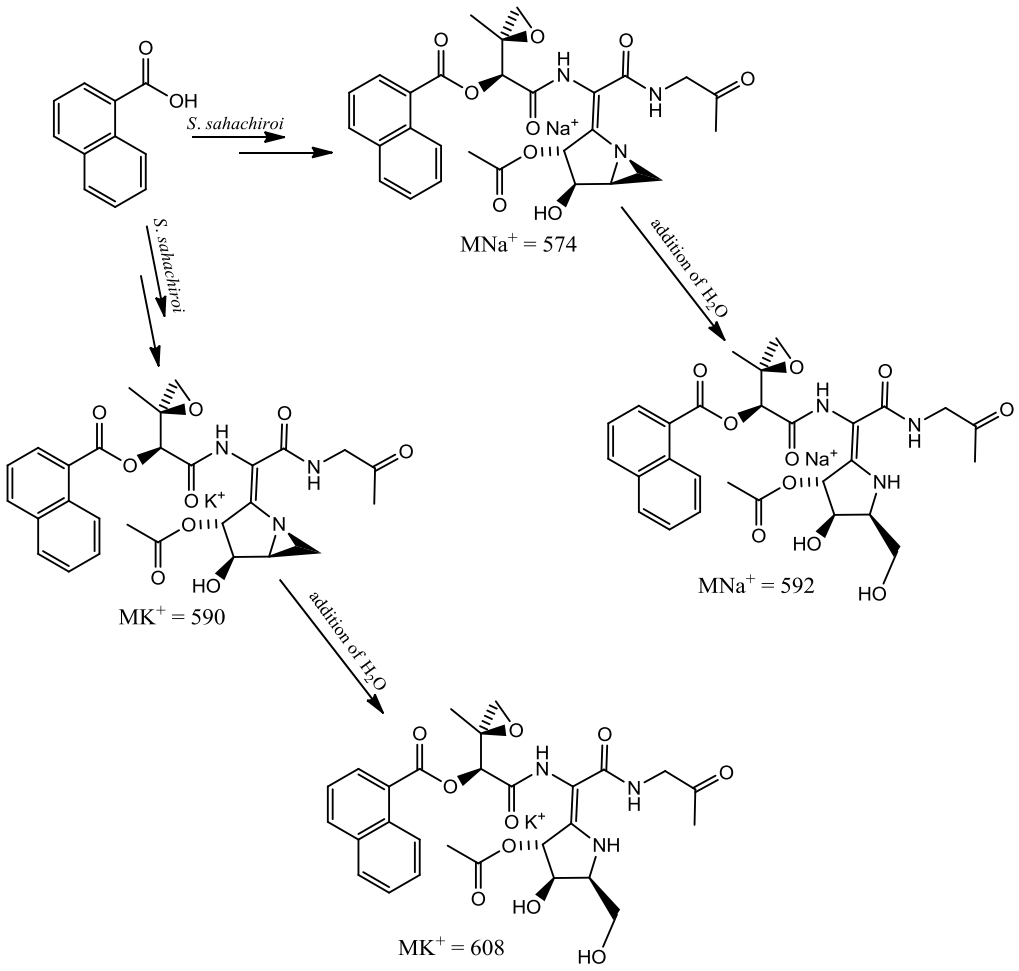

Scheme 4.4: A possible biosynthesis pathway for the production of the metabolites with m/z = 592 and 608.

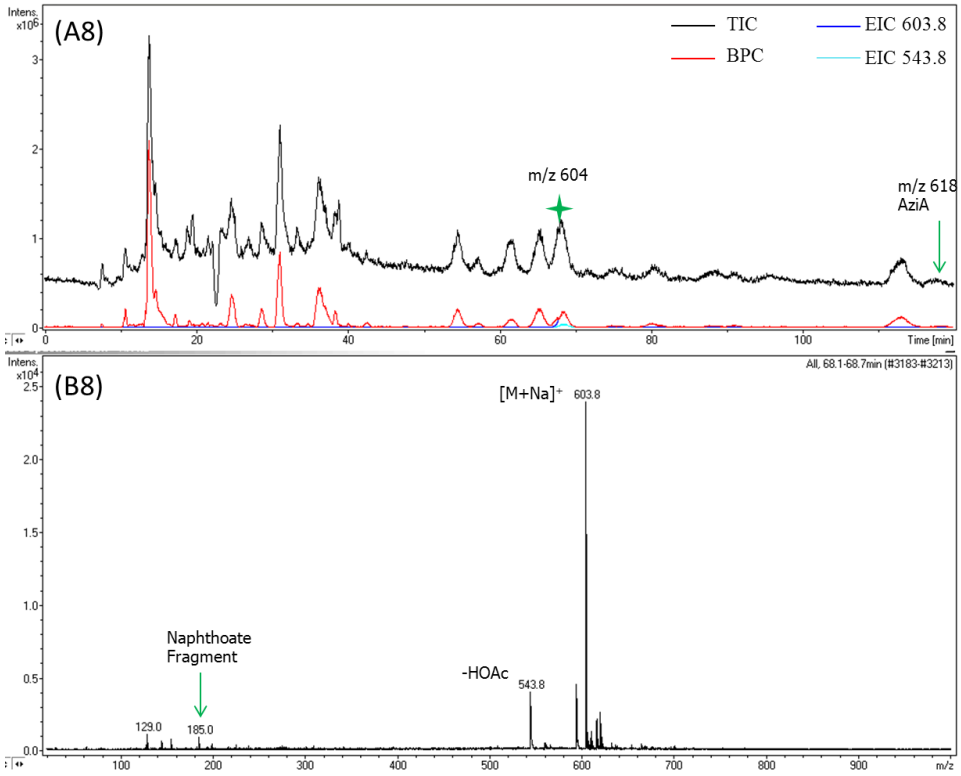

Figure 4.13: LCMS analysis of the extract from feeding of 1-naphthoic acid to *S. sahachiroi* (A8): Chromatograms from prep HPLC. (B8): Positive ion electrospray mass spectrum. A new peak at R_t = 60.1-60.7 min has MS data, $[M+Na]^+$ = 603.8, consistent with incorporation of the naphthoic acid into azinomycin A analogue after hydroxylation and methylation.

The peak at 60.1-60.7 minutes has m/z 604 (**Figure 4.13**), consistent with the sodium adduct of the metabolite formed by incorporation of 1-naphthoic acid after hydroxylation and methylation (**Scheme 4.5**).

The ion at m/z 185 is consistent with the naphthoate fragment formed from this metabolite (**Scheme 4.6**).

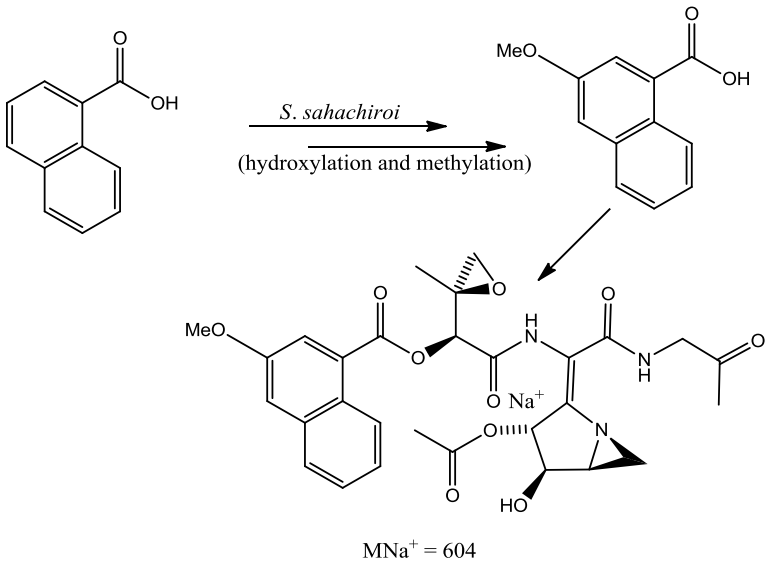

Scheme 4.5: Incorporation of 1-naphthoic acid into the azinomycin A pathway leading to the metabolite with m/z = 604.

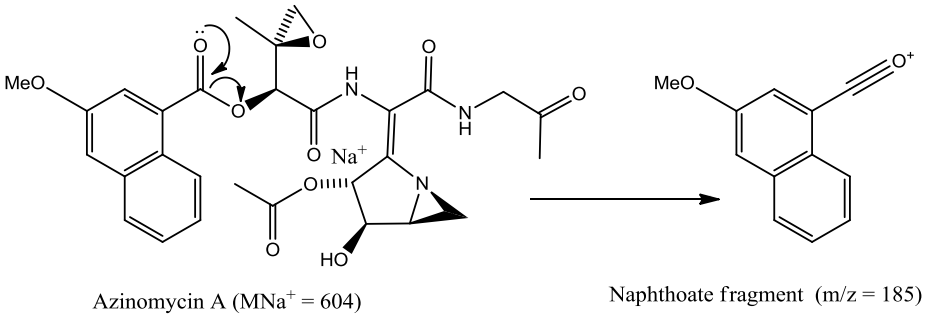

Scheme 4.6: Mechanism of formation of fragment m/z = 185 from the azinomycin A analogue (m/z = 604).

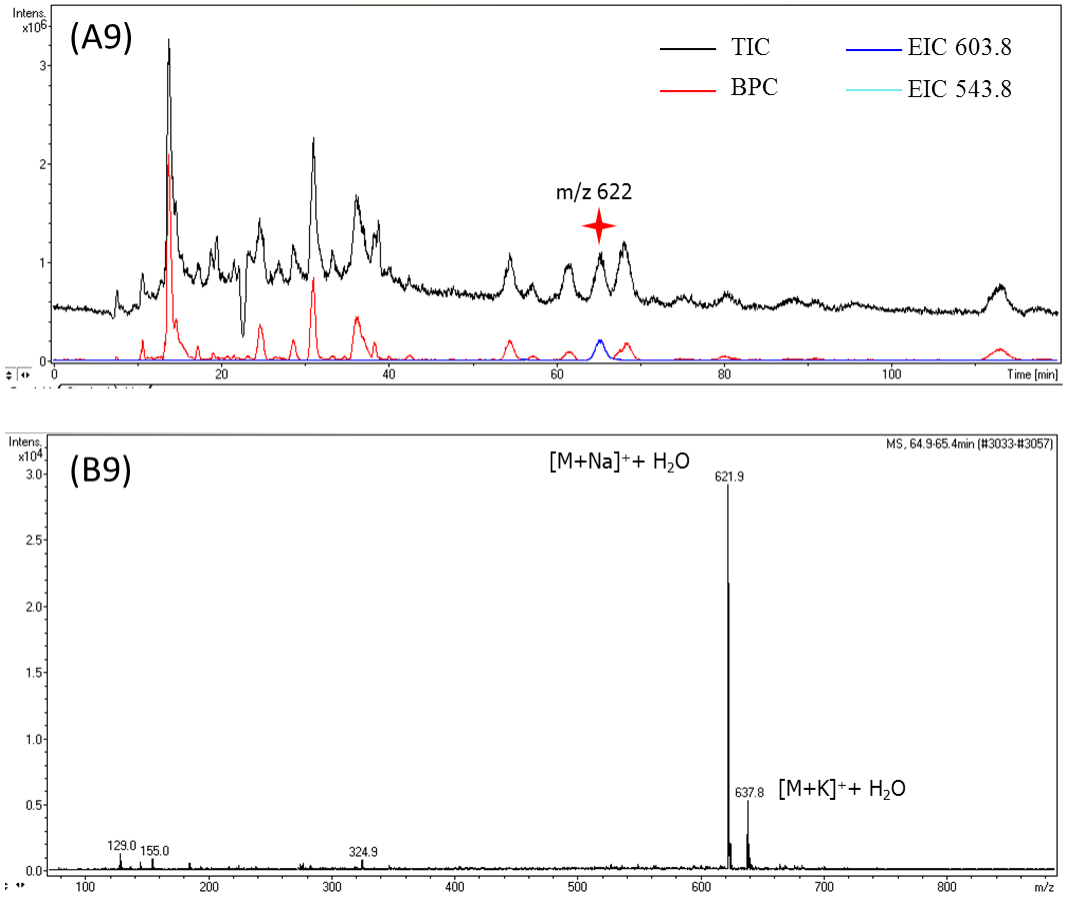

Figure 4.14: LCMS analysis of the extract from feeding of 1-naphthoic acid to *S. sahachiroi* (A9): Chromatograms from prep HPLC. (B9): Positive ion electrospray mass spectrum. A new peak at R_t = 64.9-65.4 min has MS data, $[M+Na]^+$ = 621.9, consistent with the hydrolysed ion for m/z = 604 (**Figure 4.13)**.
The additional peak for MS data, $[M+K]^+$ = 608 corresponds to the potassium adduct of the same metabolite.

A significant amount of hydrolysis of this metabolite (m/z = 604) is apparent, leading to the formation of the metabolite with m/z = 622 and 638 (A9), seen in **Figure 4.14**, and illustrated in **scheme 4.7**.

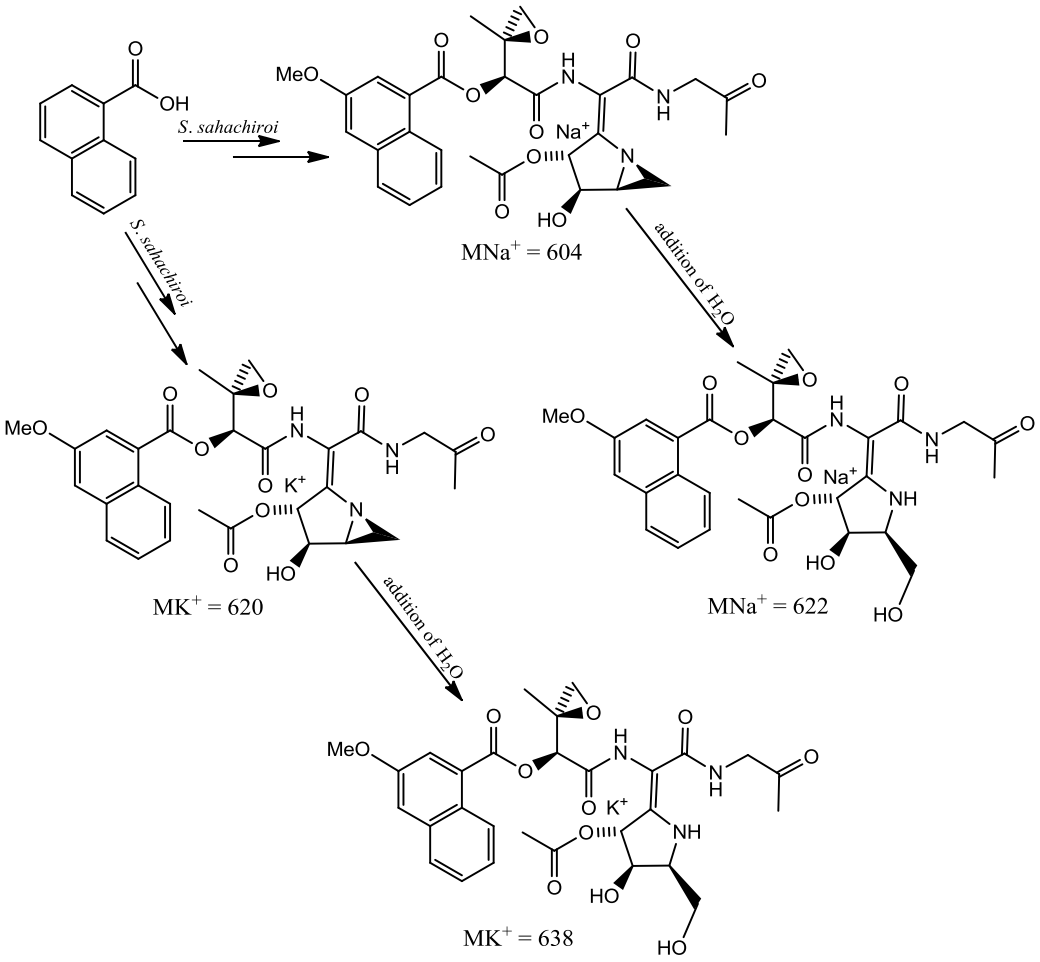

Scheme 4.7: A possible biosynthesis pathway for the production of the metabolites for m/z = 622 and m/z = 638.

In our fragmentation mechanisms, we assume that it is the aziridine ring that is hydrolysed. In fact Salvati *et al*. managed to isolate and identify the hydrolysis product of azinomycin B showing that the hydrolysis took place in the aziridine ring (Salvati *et al*., 1992).

4.2.5 Azinomycin A and analogues from prep HPLC extracts from feeding of 4-methyl-1-naphthoic acid

Two novel azinomycin A analogues incorporating 4-methyl-1-naphthoic acid were discovered in the fermentation culture of *S. sahachiroi*. The novel metabolites were detected by LCMS as sodium adducts (m/z 588 and 604) or hydrolysed sodium adducts (m/z 606 and 622) (**Figures 4.15-4.16**).

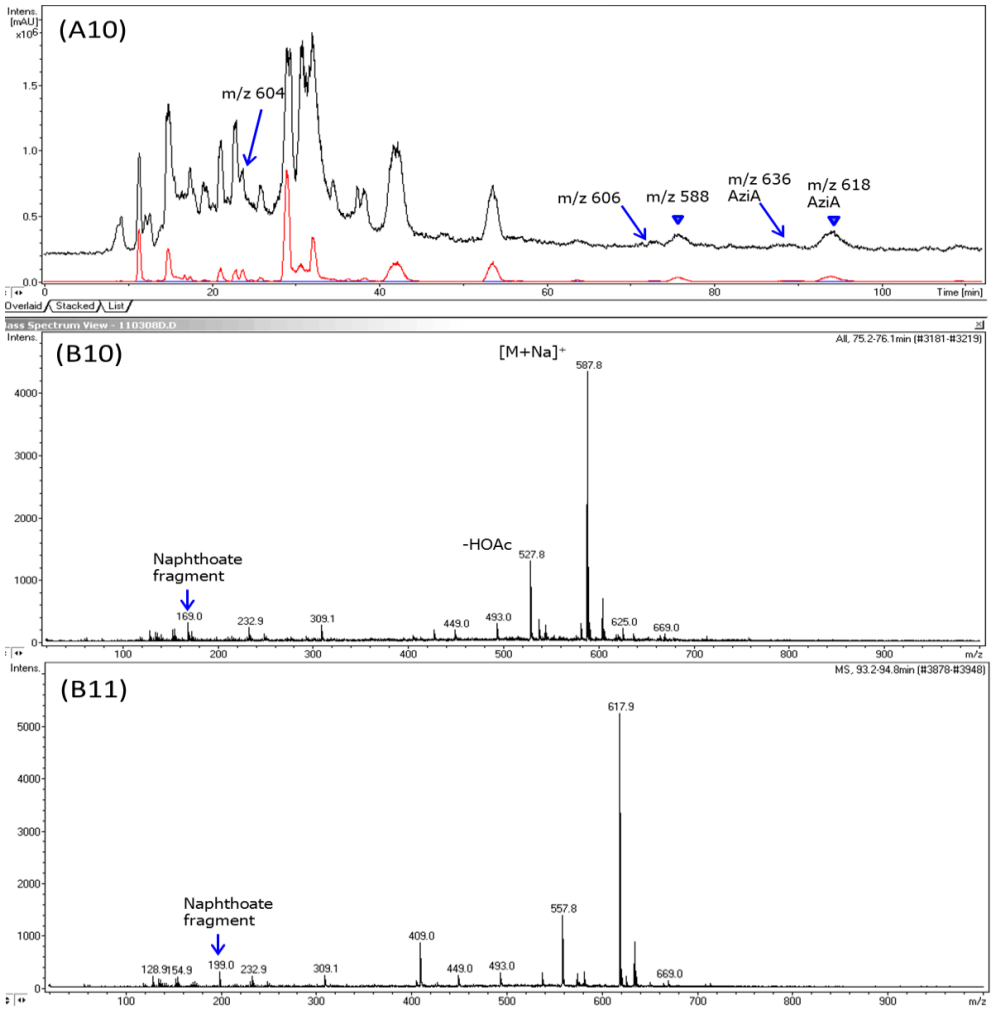

Figure 4.15: LCMS analysis of the extract from feeding of 4-methyl-1-naphthoic acid to *S. sahachiroi* (A10): Chromatograms from prep HPLC. (B10) and (B11): Positive ion electrospray mass spectra. A new peak at R_t = 75.2-76.1 min has MS data, $[M+Na]^+$ = 587.8 (B10), consistent with incorporation of 4-methyl-1-naphthoic acid into the azinomycin A analogue. The peak at R_t = 93.2-94.8 min has MS data, $[M+Na]^+$ = 617.9 (B11) consistent with azinomycin A.

We observed new HPLC peaks that are consistent with 4-methyl-1-naphthoic acid being accepted and incorporated into *S. sahachiroi's* enzymatic machinery, resulting in the production of new azinomycin A analogues. The new metabolite shown as (B10) in **Figure 4.15** with sodium adduct m/z = 588 is consistent with incorporation of 4-methyl-1-naphthoic acid. The MS peak for m/z = 528 is the fragment of the main ion (m/z = 588) after the spontaneous loss of the acetyl functional group in the MS.

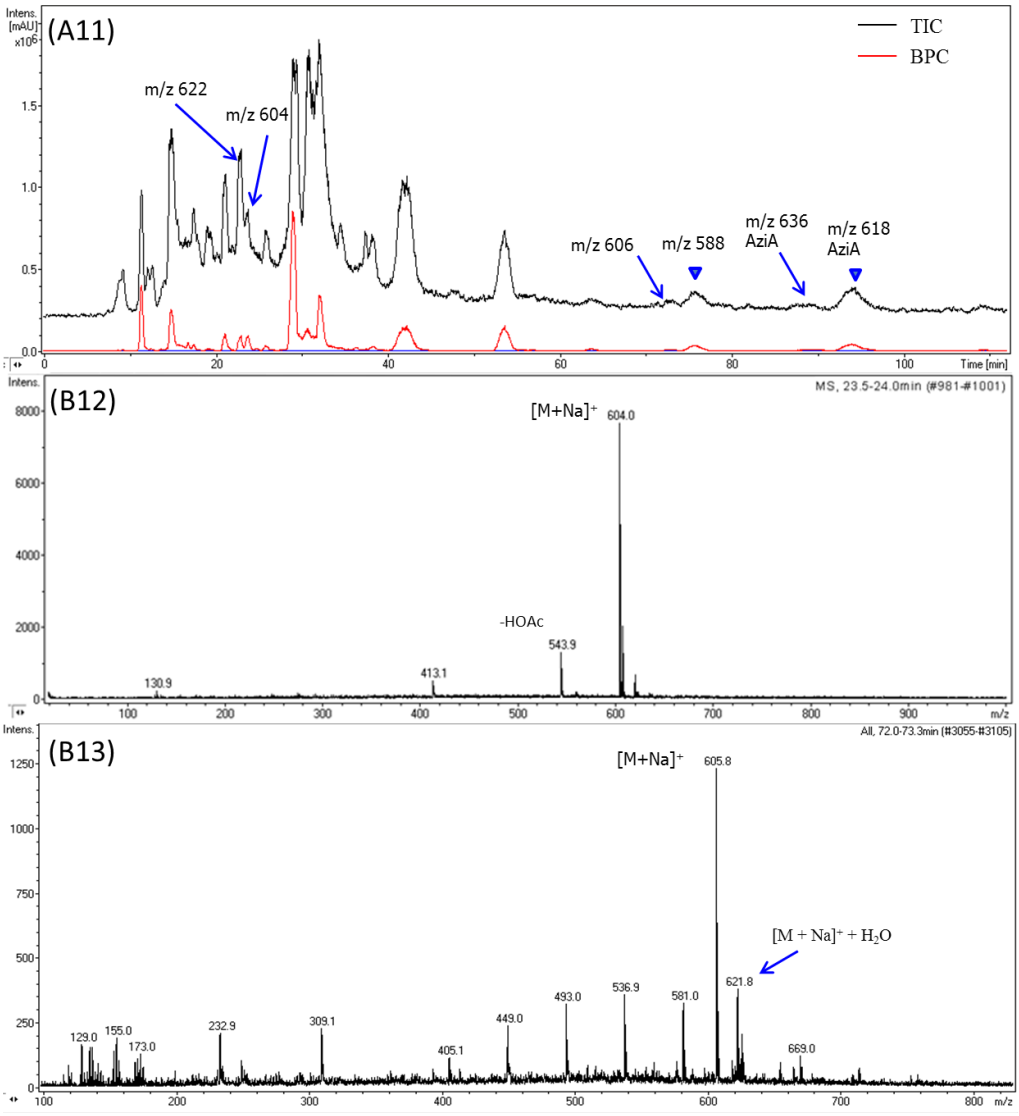

Figure 4.16: LCMS analysis of the extract from feeding of 4-methyl-1-naphthoic acid to *S. sahachiroi* (A11): Chromatograms from prep HPLC. (B12) and (B13): Positive ion electrospray mass spectra. New peak at R_t = 23.5-24.0 min has MS data, $[M+Na]^+$ = 604.0 (B12), consistent with incorporation of 4-methyl-1-naphthoic acid into azinomycin A analogue after hydroxylation. Peak at R_t = 72.0-73.3 min has MS data, $[M+Na]^+$ = 605.8 (B13), consistent with metabolite for m/z = 588 (**Figure 4.15**, (B10)) being hydrolysed.

Figure 4.16 shows that the peak at 23.5-24 min (B12) has MS data consistent with incorporation of 4-methyl-1-naphthoic acid with extra hydroxylation. Also the peak for m/z = 544 (same figure) represents the fragment of the main ion (m/z = 604) after the spontaneous loss of the acetyl functional group in the MS.

In (B13), MS peaks for m/z =606 and m/z = 622 are respectively consistent with the hydrolysed form of the new metabolites for m/z = 588 (B10) and m/z = 604 (B12).

The possible biosynthesis of the new metabolites incorporating the precursor 4-methyl-1-naphthoic acid is described in **scheme 4.8**.

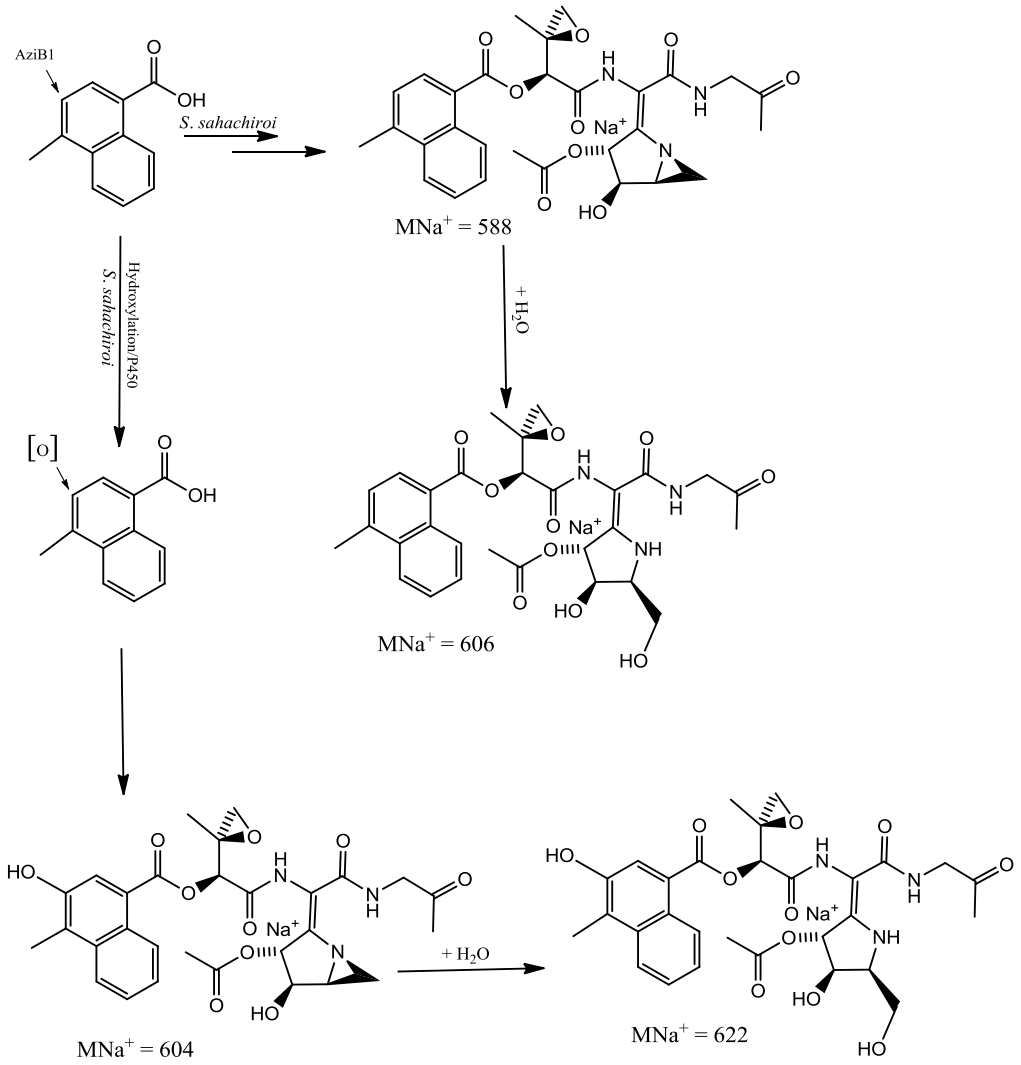

Scheme 4.8: A possible biosynthetic pathway for the production of the new metabolites shown in **Figures 4.15-4.16**.

Previous feeding of 4-methyl-1-naphthoic acid resulted in the biotransformation of naphthoic acid to amide (**Chapter 3**) and an additional major product that has MS data consistent with additional hydroxylation, perhaps before amide formation by the same cytochrome P450 involved in azinomycin biosynthesis **(scheme 4.8)**.

The production, by *S. sahachiroi* fermentation culture, of the new metabolites incorporating the feeding analogue with and without hydroxylation suggests a competition role between the enzymes involved in the azinomycin A biosynthesis pathway (details in **section 4.3**).

4.2.6 Azinomycin A and analogues from extracts from feeding of 4-fluoro-1-naphthoic Acid

Two novel azinomycin A analogues incorporating 4-fluoro-1-naphthoic acid were discovered in the fermentation culture of *S. sahachiroi*. The novel metabolites were detected by LCMS as sodium or hydrolysed sodium adducts (m/z = 592 and 610) and with HCl added (m/z = 628 and 630) (**Figures 4.17-4.18**).

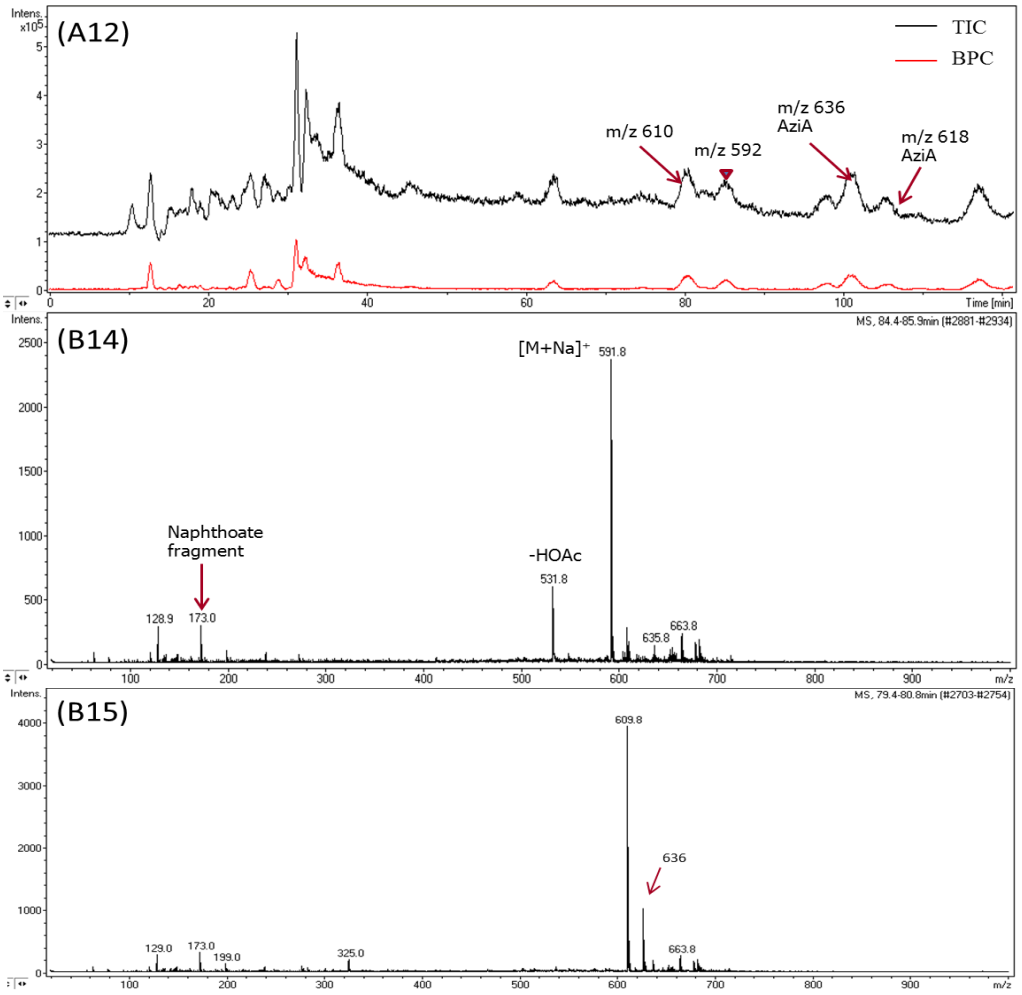

Figure 4.17: LCMS analysis of the extract from feeding of 4-fluoro-1-naphthoic acid to *S. sahachiroi* (A12): Chromatograms from prep HPLC. (B14) and (B15): Positive ion electrospray mass spectra. New peak at R_t = 84.4-85.9 min has MS data, $[M+Na]^+$ = 591.8 (B14), consistent with incorporation of 4-fluoro-1-naphthoic acid into azinomycin A analogue. Peak at R_t = 79.4-80.8 min has MS data, $[M+Na]^+$ = 609.8 (B15), consistent with metabolite for m/z = 592 (B14) being hydrolysed.

4-fluoro-1-naphthoic acid has also been accepted and incorporated by the azinomycin A producer. A new metabolite (m/z = 592) was detected by LCMS analysis ((B14), **Figure 4.17**), corresponding to a fluorinated azinomycin A analogue. The produced metabolite was subject to a spontaneous fragmentation in the MS and a new daughter ion has been formed at m/z 532, consistent with the loss of the acetyl functional group ((B14), **Figure 4.17**). A significant amount of the new metabolite has been hydrolysed resulting in the formation of an HPLC peak with m/z = 610 ((B15), **Figure 4.17**).

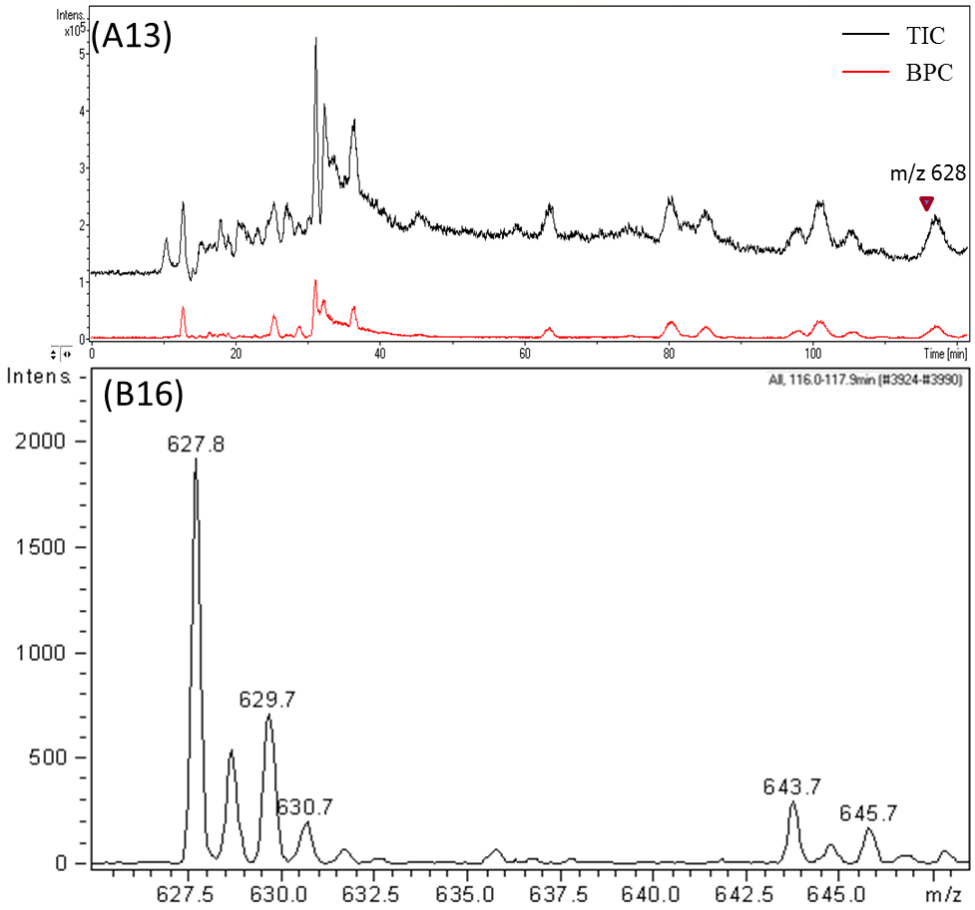

Figure 4.18: LCMS analysis of the extract from feeding of 4-fluoro-1-naphthoic acid to *S. sahachiroi* (A13): Chromatograms from prep HPLC. (B16): Positive ion electrospray mass spectrum. New peak at R_t = 116.0-117.9 min has MS data, $[M+Na]^+$ = 627.8 and 629.7 (B14), consistent with incorporation of 4-fluoro-1-naphthoic acid into azinomycin A analogue with HCl added.

Figure 4.18 shows the presence of a metabolite that may be a chlorinated analogue of azinomycin A from the same fermentation culture. The ions at m/z 628 and 630 are present in a 3:1 ratio, corresponding to the relative abundances of ^{35}Cl and ^{37}Cl. When extracted ion chromatograms (EICs) of ions at m/z 628 and 630 were plotted, they coincide together.

4.2.7 Azinomycin A and analogues from prep HPLC extracts from feeding of 3-methoxy-1-naphthoic acid

A novel azinomycin A analogue incorporating 3-methoxy-1-naphthoic acid was discovered in the fermentation culture of *S. sahachiroi*. The novel metabolite was detected by LCMS in the intact form (m/z = 582), as sodium and hydrolysed sodium adducts (m/z = 604 and 622 (**Figure 4.20**), respectively) and as hydrolysed potassium adduct (m/z = 638, **Figure 4.20**).

Initial results using analytical method are shown in **Figure 4.19.**

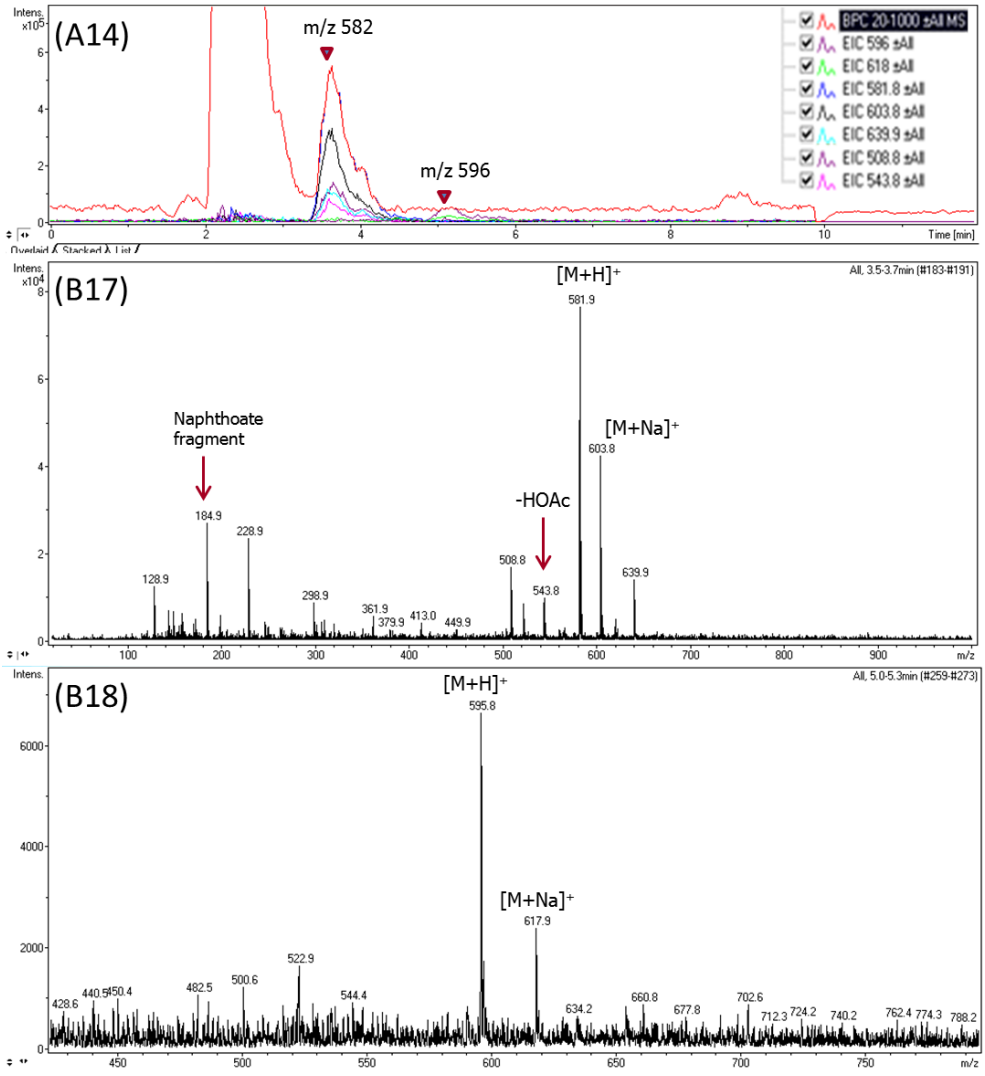

Figure 4.19: LCMS of extract from feeding of 3-methoxy-1-naphthoic acid to *S. sahachiroi*. (A14): HPLC chromatograms. (B17) and (B18): Positive ion electrospray mass spectra. A new peak at 3.5-3.7 min has MS data for m/z = 582 consistent with an azinomycin A analogue incorporating the fed precursor. The mass spectrum (B18) displays azinomycin A.

The LCMS data shown in **Figure 4.19** are the results of the initial analysis of 3-methoxy-1-naphthoic acid extract after using a C18 microbore column (ACE3, 100 × 2.1 mm). A significant amount of a new metabolite was produced and was still in the native/intact form (m/z = 582). A less amount was shown as sodium adduct (m/z = 604). No hydrolysis has occurred yet. Similarly azinomycin A was shown only as an intact form (m/z = 596) or as sodium adduct (m/z = 618). MS peaks for m/z = 544 and m/z = 185 are fragments of the main ions $[M+H]^+$ = 581.9. The first fragment (for m/z = 544) has resulted after the loss of the acetyl functional group (-HOAc) from the parent ion (for m/z = 582) and the second corresponds to the naphthoate fragment. The fragmentation mechanism for the naphthoate fragment is identical to the one shown in **scheme 4.6**.

The results from prep HPLC from feeding of 3-methoxy-1-naphthoic acid are shown in **Figure 4.20.**

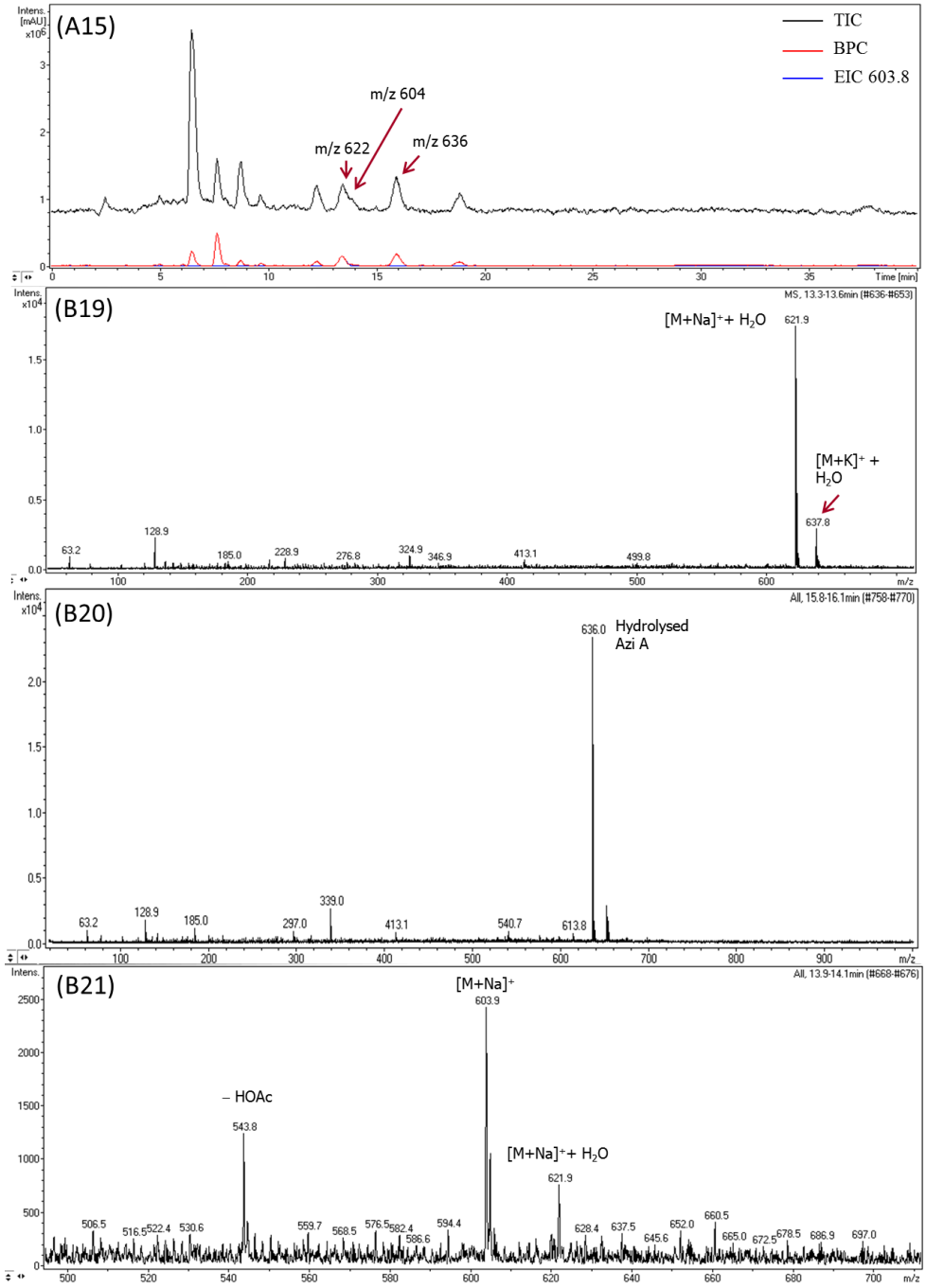

Figure 4.20: LCMS of extract from feeding of 3-methoxy-1-naphthoic acid to *S. sahachiroi*. (A15): HPLC chromatograms. (B19): Positive ion electrospray mass spectrum showing hydrolysed new metabolite for m/z = 622. (B20): Positive ion electrospray mass spectrum showing hydrolysed azinomycin A for m/z = 636. (B21): Positive ion electrospray mass spectrum showing new metabolite for m/z = 604.

A brief comparison between the results from the initial analytical analysis (**Figure 4.19)** and the data from prep HPLC analysis of 3-methoxy-1-naphthoic acid extract **(Figure 4.20)** shows that a substantial amount of azinomycin A (for m/z = 636) and its analogue (for m/z = 622) has been hydrolysed in solution.

The analysis of the MS data in (B19) shows another peak for m/z = 638 which is consistent with the same new metabolite but as potassium adduct. The possible biosynthesis pathway for the production of the new metabolite with m/z = 582 and its salt adducts is described in **scheme 4.9**.

In relation to the new metabolite for m/z = 604, there is a strong correlation between the MS data from feeding 1-naphthoic acid ((B8), **Figure 4.13**) and feeding 3-methoxy-1-naphthoic acid **(**(B21), **Figure 4.20).** In both cases the produced metabolites are identical. The assumption was made based on retention time comparison. In fact, both metabolites had the same retention time when their corresponding crude extracts were run under the same LCMS conditions.

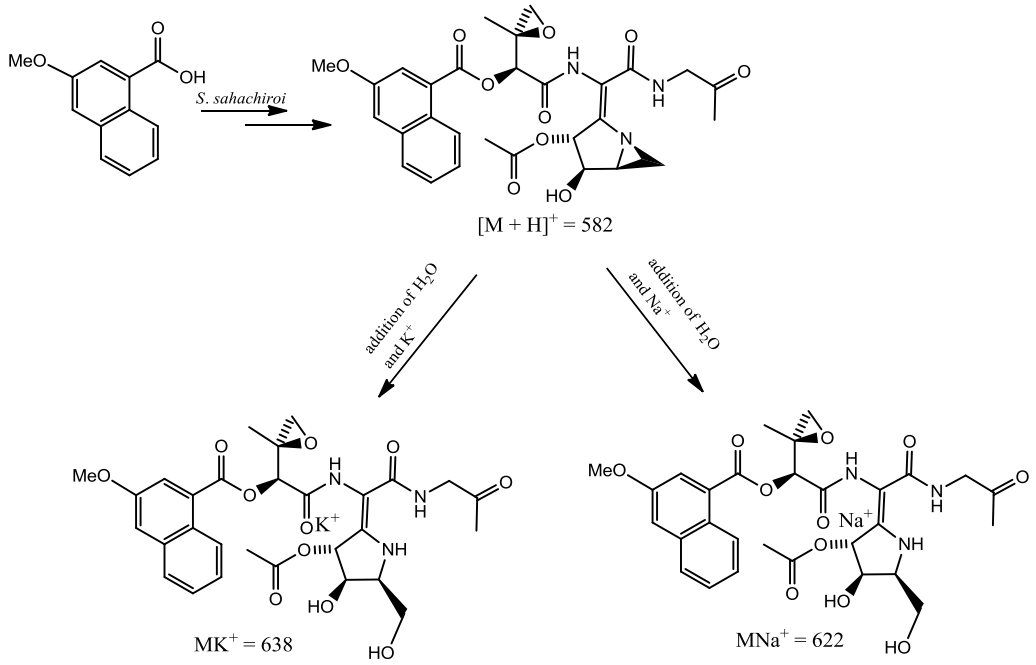

Scheme 4.9: Incorporation of 3-methoxy-1-naphthoic acid in the azinomycin A biosynthesis pathway and the possible biosynthesis pathway for the production of the metabolites for m/z = 622 and m/z = 638.

4.2.8 Towards purification of azinomycin A and related analogues by prep HPLC

The purification and isolation of azinomycin A and its subsequent analogues was performed as described in **section 2.2.1 (Chapter 2).** The separation was first started on C18 microbore column (ACE3, 100 × 2.1 mm) since it requires less time and less solvent and sample and then optimised on an analytical column (C18, ACE5, 250 × 4.6 mm). The developed method was then transferred to the prep. HPLC column (C18 column (ACE5 250 × 21.2 mm) with some modifications to the sample preparation. During analytical HPLC, sample from *S. sahachiroi's* crude extract (30 mg) from feeding 3-methoxy-1-naphthoic acid **97** was dissolved in the minimum amount of chloroform (2 mL), centrifuged for 5 min at 6000 rpm in an MSE MicroCentaur machine and then an aliquot (50 µL) was transferred to an LCMS vial containing 950 µL of a pre-degassed mobile phase consisting of a mixture of water and methanol (25:75). Using the microbore column, Azinomycin A and its analogues were seen after LCMS analysis but the HPLC peaks were unresolved as shown in **Figure 4.21**.

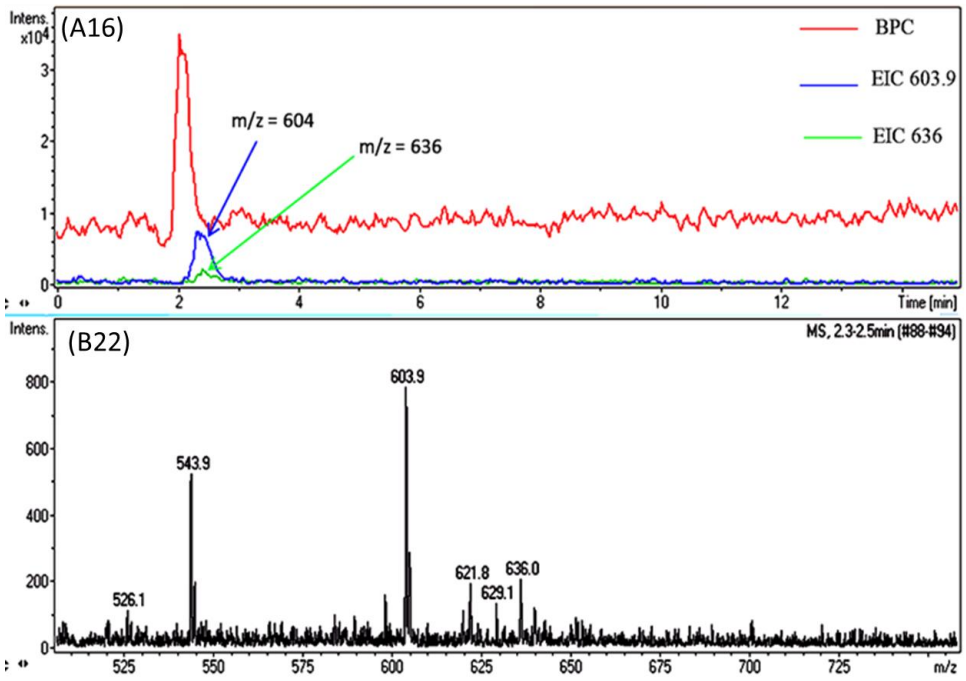

Figure 4.21: Microbore HPLC of extract from feeding of 3-methoxy-1-naphthoic acid to *S. sahachiroi's* culture broth. (A16): HPLC chromatograms. (B22): Positive ion electrospray mass spectrum. Peaks at R_t = 2.3-2.5 min for m/z = 604 and 636 are not fully separated when using water and methanol at a ratio of 25:75.

A more polar mobile phase consisting of water and methanol (35:65) was attempted in order to achieve better resolution. Yet, the HPLC peaks of hydrolysed azinomycin A (m/z = 636) and its analogues (m/z = 604 and 622) were still not fully separated **(Figure 4.22)**. However, azinomycin A (for m/z = 618) was well separated from its analogues.

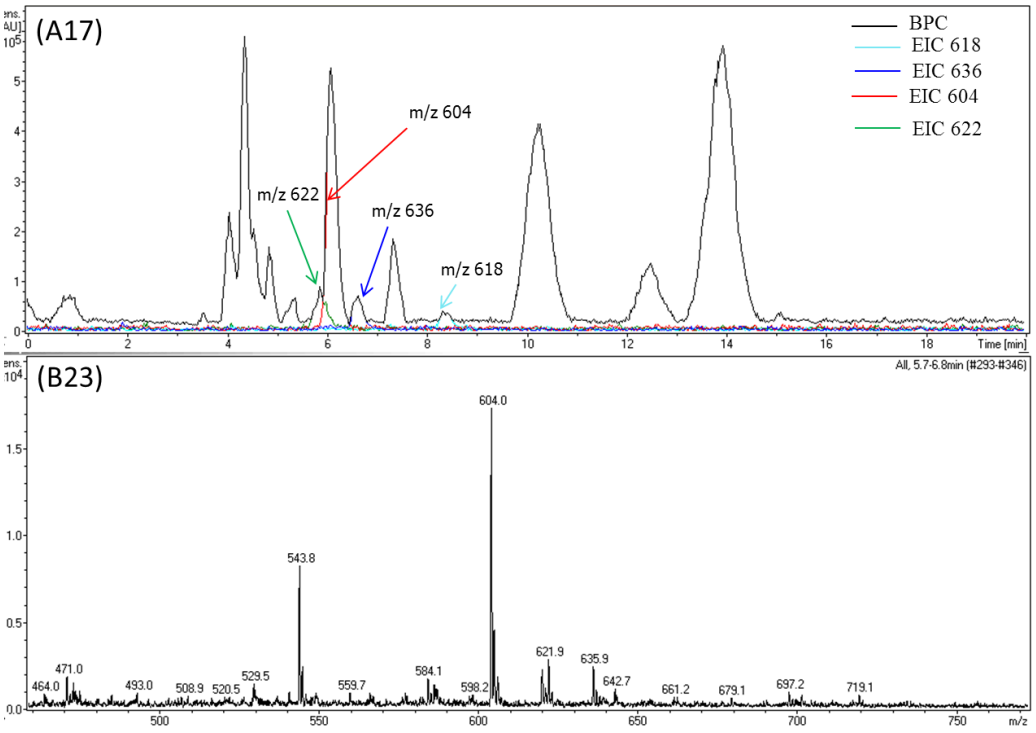

Figure 4.22: Analytical HPLC of extract from feeding of 3-methoxy-1-naphthoic acid to *S. sahachiroi*. (A17): HPLC chromatograms. (B23): Positive ion electrospray mass spectrum. EIC peaks for hydrolysed azinomycin A and its analogues (m/z = 604 and 622) are still partially overlapping. Water and methanol at a ratio of 35:65 were used as the mobile phase.

Keeping the same solvent system, the solvent ratio mixture (50:50) was introduced to further slowdown the mobile phase by increasing the polarity of the solvent system. However EIC peaks for hydrolysed azinomycin A (m/z = 636) and it analogue (for m/z = 622) were still partially overlapping as shown in **Figure 4.23.**

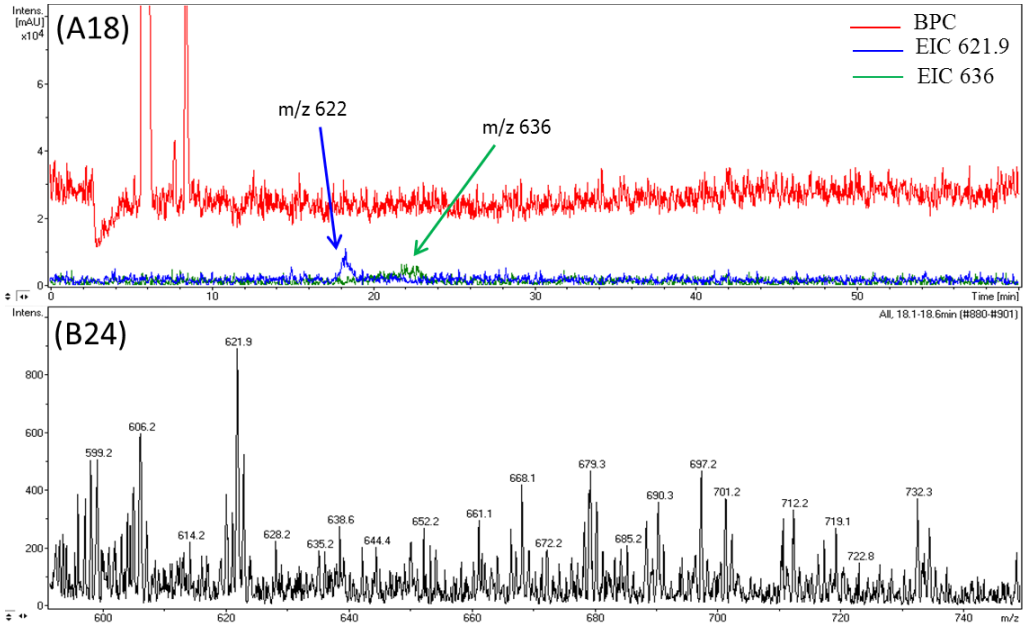

Figure 4.23: Analytical HPLC of extract from feeding of 3-methoxy-1-naphthoic acid to *S. sahachiroi*. (A18): HPLC chromatograms. (B24): Positive ion electrospray mass spectrum. EIC peaks for hydrolysed azinomycin A (m/z = 636) and its analogue (m/z = 622) were still partially overlapping. Water and methanol at a ratio of 50:50 were used as the mobile phase.

A further change of the solvent ratio mixture (60:40) was tried towards a good separation between the target peaks. A fairly good separation between azinomycin A and its analogues was achieved but with longer elution time as shown in **Figure 4.24**.

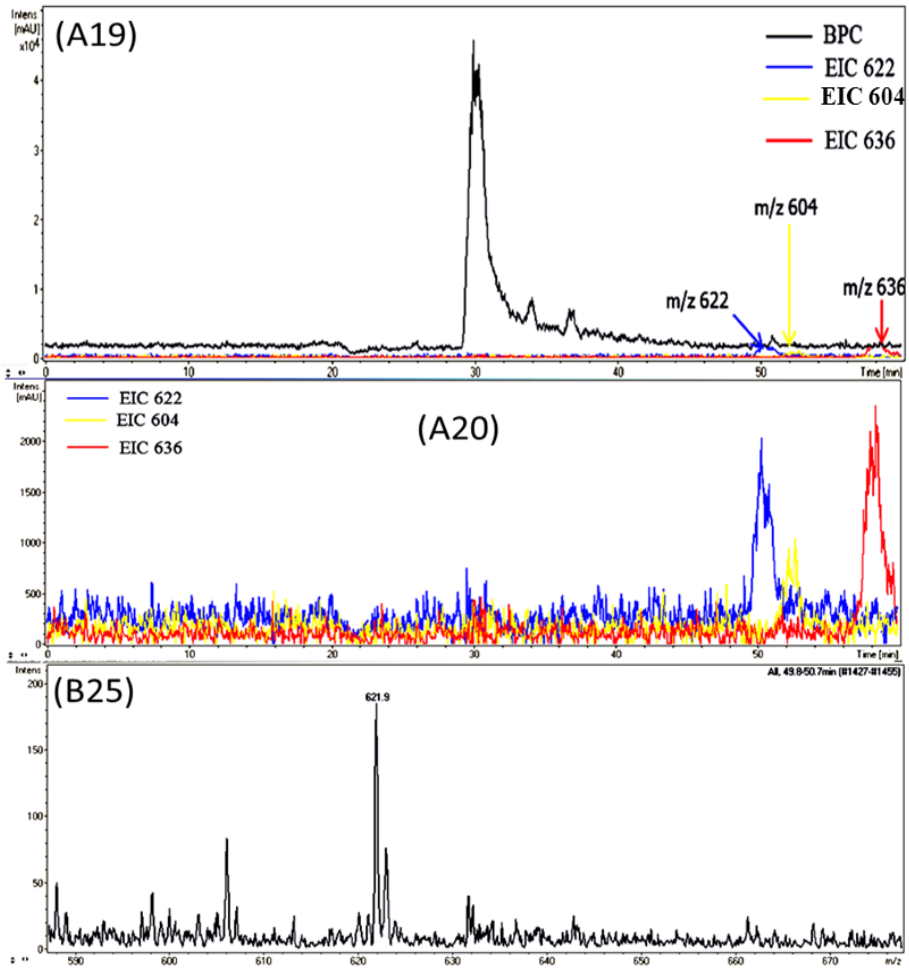

Figure 4.24: Analytical HPLC of extract from feeding of 3-methoxy-1-naphthoic acid to *S. sahachiroi*. (A19) and (A20): HPLC chromatograms. (B25): Positive ion electrospray mass spectrum. A fairly good EIC peaks separation between hydrolysed azinomycin A (for m/z = 636) and its analogues (for m/z = 622 and for m/z = 604). Water and methanol at a ratio of 60:40 were used as the mobile phase.

Then a clear separation between the target peaks at reasonable eluting time was achieved with the same mobile phase at the ratio of 45:55 as shown in **Figure 4.25**.

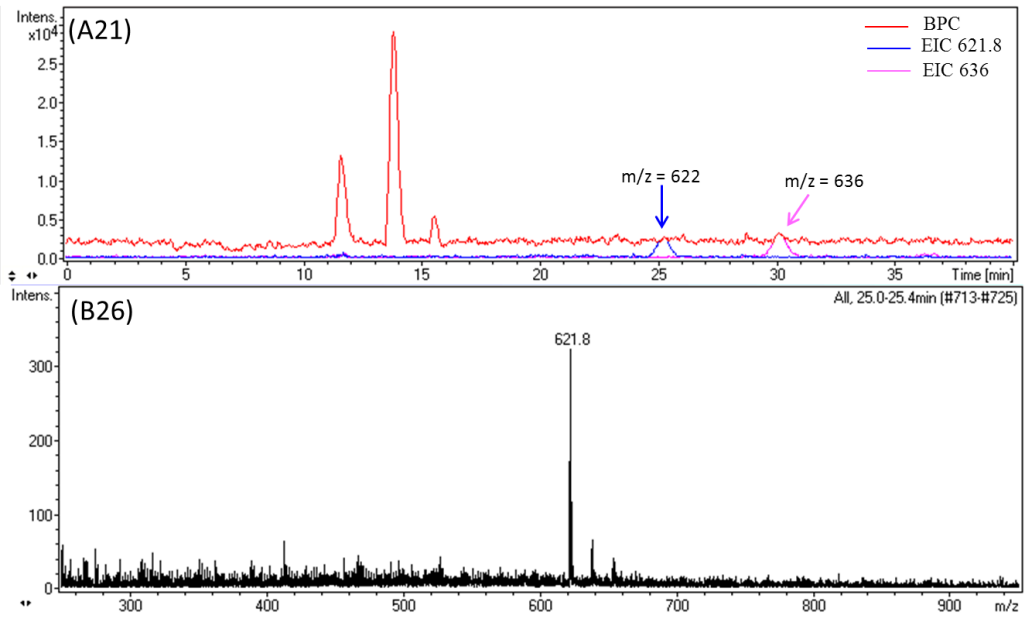

Figure 4.25 Analytical HPLC of extract from feeding of 3-methoxy-1-naphthoic acid to *S. sahachiroi*. (A21): HPLC chromatograms. (B26): Positive ion electrospray mass spectrum. A clear separation between EIC peaks for hydrolysed azinomycin A (for m/z = 636) and its analogue (for m/z = 622). Water and methanol at a ratio of 45:55 were used as the mobile phase.

The method was also used to confirm the full separation between the target peaks from crude extracts after feeding 1-naphthoic acid, 4-methyl-1-naphthoic acid and 4-fluoro-1-naphthoic acid compounds.

After optimisation of the analytical HPLC and before proceeding to prep HPLC separation and sample collection, a few changes to sample preparation were required. Since a highly concentrated sample was needed, all attempts to dissolve bacterial crude extract in the minimum amount of HPLC solvent system had failed. Therefore a mixture of 20% chloroform and 80% HPLC mobile phase was needed for complete solubility of the extract. Then the sample was centrifuged for 5 min at 6000 rpm in an MSE MicroCentaur machine. Aliquots of 200 µL of analyte solution were transferred to LCMS vials containing a 200 µL glass insert. A few crucial technical steps were taken in consideration before starting the separation and collection of sample fractions:

1) As MS method is a destructive identification technique where the sample cannot be recovered, only a very small sample amount was needed to reach the MS instrument. Hence a T shaped splitter with a long tube (60 cm) was set up to connect to the MS electrode **(Figure 4.26)**.
2) DAD is a non-destructive detection technique therefore most of the volume of the identified target peak should be collected in the Falcon tube. Hence a short tubing (2 cm long) was placed at the opposite site of the splitter for that purpose **(Figure 4.26)**.
3) There was a time lag (2 sec) between sample arrival at the DAD and MS detectors. That was taken into account during the identification and collection of the target peaks. In fact, initial prep HPLC runs using only 5 µl as the injection volume of extract were carried out to correlate DAD peaks with MS ones. All other prep HPLC parameters were kept the same as described in **section 2.2.1 (Prep HPLC)**.

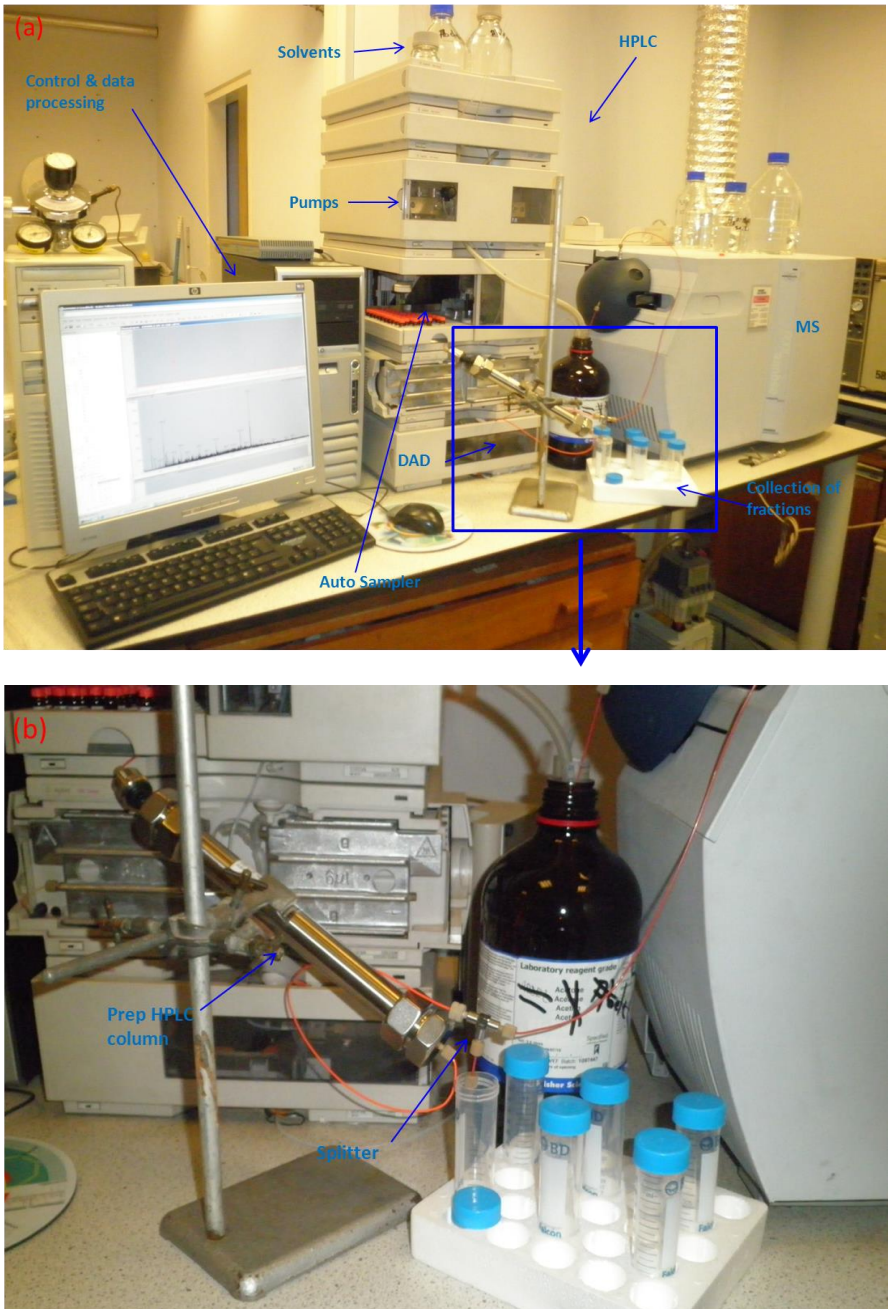

Figure 4.26: Pictures of the LCMS instruments. (a): annotated picture of the LCMS instruments used during the course of this study. (b): magnified region shown with blue square in (a).

The separation and sample collection proceeded as described in **section 2.2.1**. **(Prep HPLC).** Analytical scale HPLC analyses of the isolated azinomycin A and its analogues are shown in **Figures 4.27-4.32.**

During the course of prep HPLC work, azinomycin A (as sodium and hydrolysed adducts) and four novel azinomycin A analogues were separated and isolated. The isolated novel analogues are as follow: m/z = 592 from feeding 1-naphthoic acid, m/z = 622 from feeding 1-naphthoic acid and 3-methoxy-1-naphthoic acid, m/z = 610 and 628/630 from feeding 4-fluoro-1-naphthoic acid to *S. sahachiroi*.

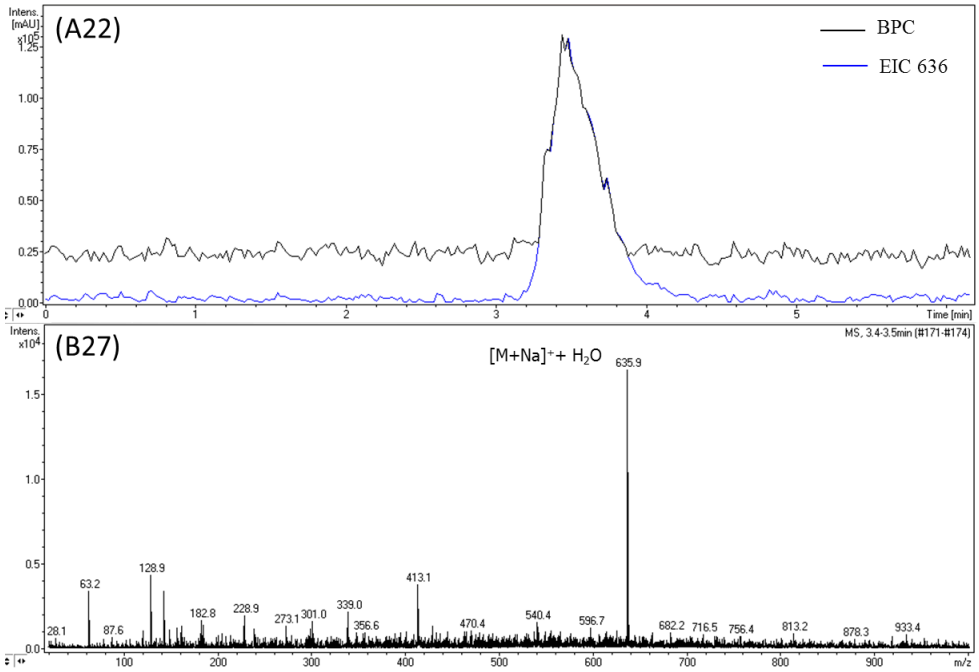

Figure 4.27: Analytical HPLC of hydrolysed azinomycin A (m/z = 636) after prep HPLC purification. (A22): HPLC chromatograms. (B27): Positive ion electrospray mass spectrum.

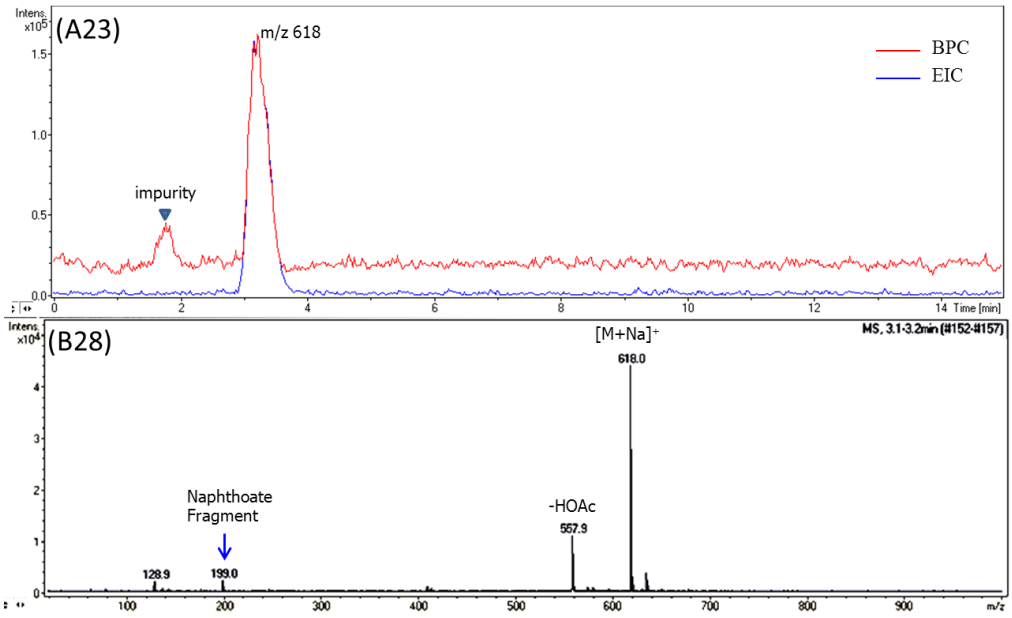

Figure 4.28: Analytical HPLC of purified azinomycin A (m/z = 618). (A23): HPLC chromatograms. (B28): Positive ion electrospray mass spectrum. An impurity peak (for m/z = 409) is shown in (A23) in addition to the azinomycin peak at 3.1-3.2 min. The MS peaks for m/z = 558 and m/z = 199 are the characteristic of the spontaneous fragmentation of the azinomycin parent ion.

The impurity peak shown in **Figure 4.28** (A23) could have originated from plastic pipette tips (http://www.bmss.org.uk/Docs/MSTG_web_version.pdf).

The results presented in **Figures 4.27** and **4.28** represent the LCMS analysis after combining all similar azinomycin prep HPLC purified fractions. Azinomycin A was isolated from all the four scaled up fermentation crude extracts from feeding 1-naphthoic acid, 4-methyl-1-naphthoic acid, 4-fluoro-1-naphthoic acid and 3-methoxy-1-naphthoic acid. However, the final yields (~ 1 mg azinomycin A and ~ 200 µg of the hydrolysed form) were only enough for MS/MS, TLC analysis and melting point calculation.

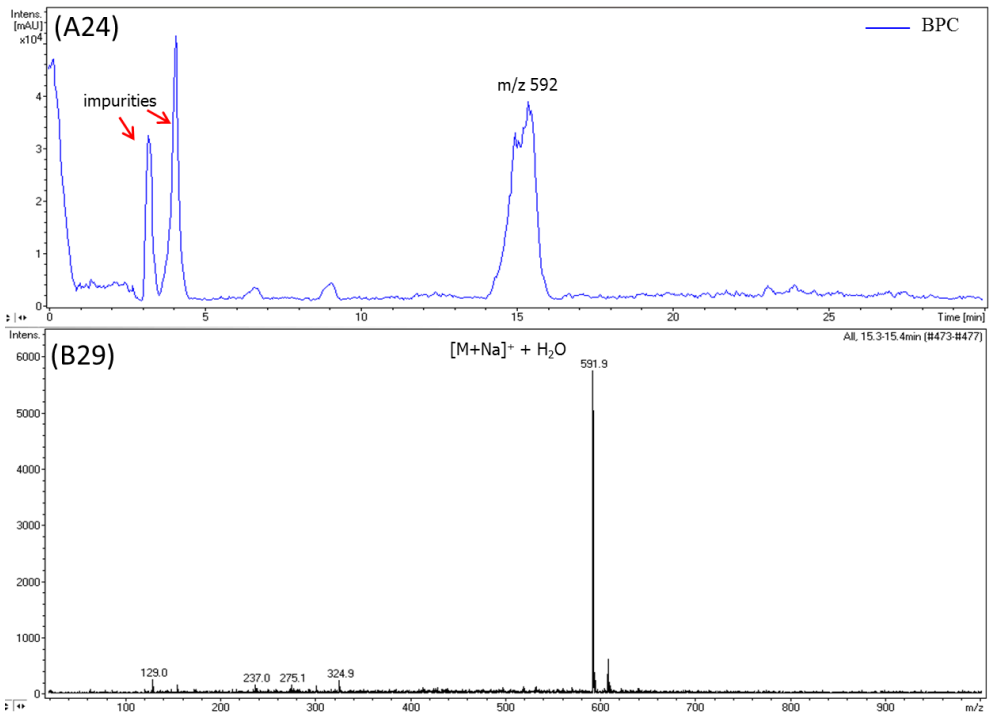

Figure 4.29: Purified azinomycin A analogue (m/z = 592, hydrolysed form) from prep HPLC after feeding 1-naphthoic acid. (A24): HPLC chromatograms. (B29): Positive ion electrospray mass spectrum. A substantial amount of impurities (m/z = 676 and 365) is found in (A24). The amount of isolated product (~ 200 µg) could only allow LCMS analysis.

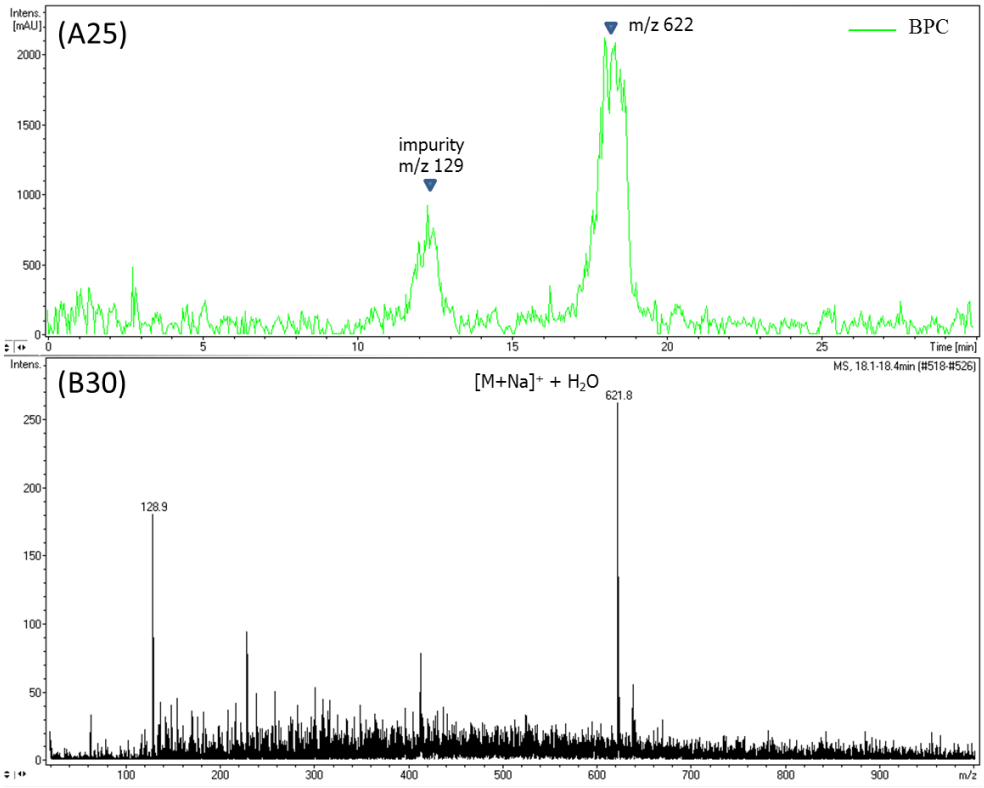

Figure 4.30: Purified azinomycin A analogue (m/z = 622, hydrolysed form). (A25): HPLC chromatogram. (B30): Positive ion electrospray mass spectrum. The purified prep HPLC fractions from feeding 1-naphthoic acid and 3-methoxy-1-naphthoic acid crude extracts were added together hoping to increase the yield. But, only traces were collected allowing only LCMS analysis. For the peak with m/z = 129 corresponds to a common contaminant.

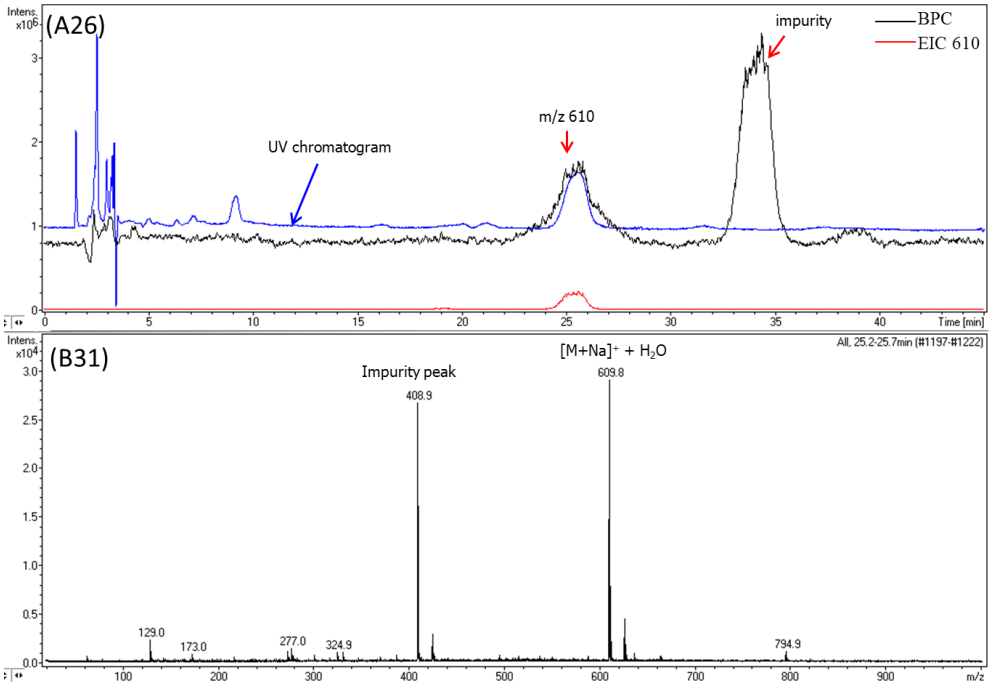

Figure 4.31: Towards purified azinomycin A analogue (m/z = 610, hydrolysed form) from prep HPLC of feeding 4-fluoro-1-naphthoic acid crude extract. (A26): HPLC chromatograms. (B31): Positive ion electrospray mass spectrum. The amount of isolated product (~ 500 µg) could only allow LCMS analysis.

Figure 4.31 shows a perfect alignment between UV chromatogram peak and HPLC peak for the new azinomycin analogue (m/z = 610, hydrolysed form) at 25.2-25.7 min. On the other hand, the impurity peak (m/z = 409) does not absorb UV light at 350 nm as shown in (A26). The EIC for m/z = 409 is seen at two different retention times (R_t ~ 26 min and ~ 35 min). A considerable amount of impurities was detected after prep HPLC purification. The impurities might have originated from plastic pipette tips.

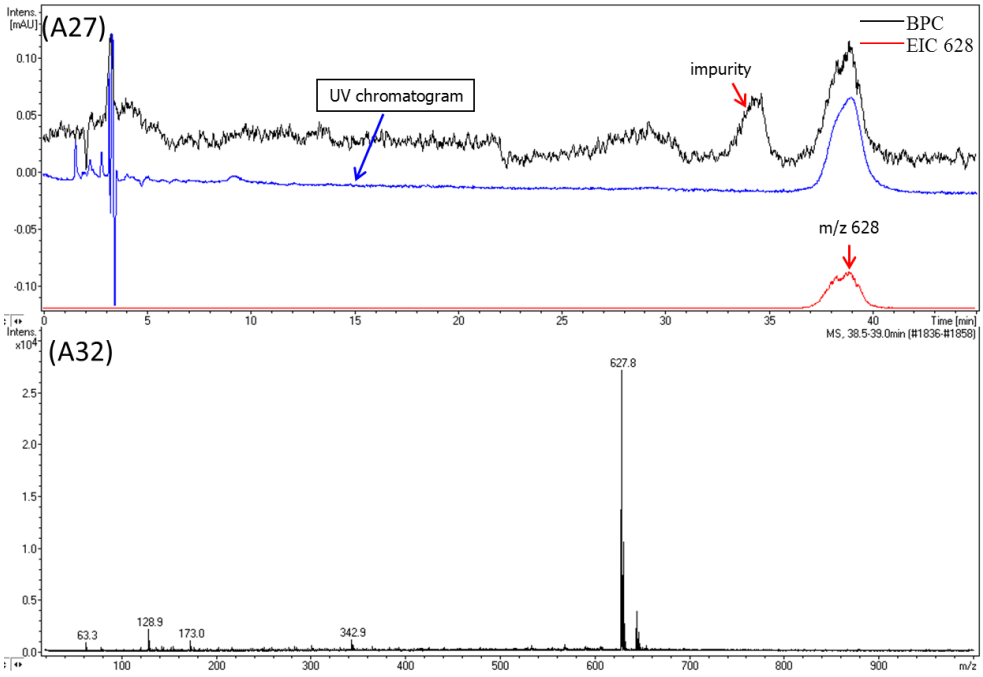

Figure 4.32: Towards purified azinomycin A analogue (m/z = 628, metabolite with added HCl) from prep HPLC of feeding 4-fluoro-1-naphthoic acid crude extract. (A27): HPLC chromatograms. (B32): Positive ion electrospray mass spectrum. The final yield of the isolated new compound (~ 300 µg) was only enough for LCMS analysis.

Figure 4.32, (A27) shows a total overlap between UV chromatogram peak and HPLC peak for the new azinomycin analogue (m/z = 628) at 38.5-39.0 min. The impurity related peak shown here (A27) is identical to the one shown in **Figure 4.31** and also does not absorb UV light at 350 nm.

4.2.9 Tandem mass spectrometry (MS/MS) assignment of azinomycin A and related analogues

The yields of the purified azinomycins and related analogues were not enough for full NMR analysis. Therefore, MS/MS was used as an alternative method for structural characterisation. Our analysis looked for correlations between the fragmentation patterns of azinomycin A and its analogues (using both purified fractions and crude extracts), to provide support for the assumption that the new metabolites are new analogues of azinomycin A. For that purpose, MS/MS was performed in the ion trap of the mass spectrometer with helium as collision gas. In MS/MS, precursor ions are accumulated in the ion trap then the precursor ion of interest (azinomycin A for example) is mass-selected while other ions are ejected from the ion trap. An increase in the activation energy inside the spectrometer results in collisions between helium gas and the selected ion. This allows the fragmentation of the precursor ion and therefore the generation of daughter ions that are then analysed to generate a fragment mass spectrum.

For each successful MS/MS experiment, similar patterns between the purified compound and the related feeding crude extract were obtained. The results are summarised in **Figures 4.33-4.39**.

LCMS/MS of azinomycin A (m/z = 636)

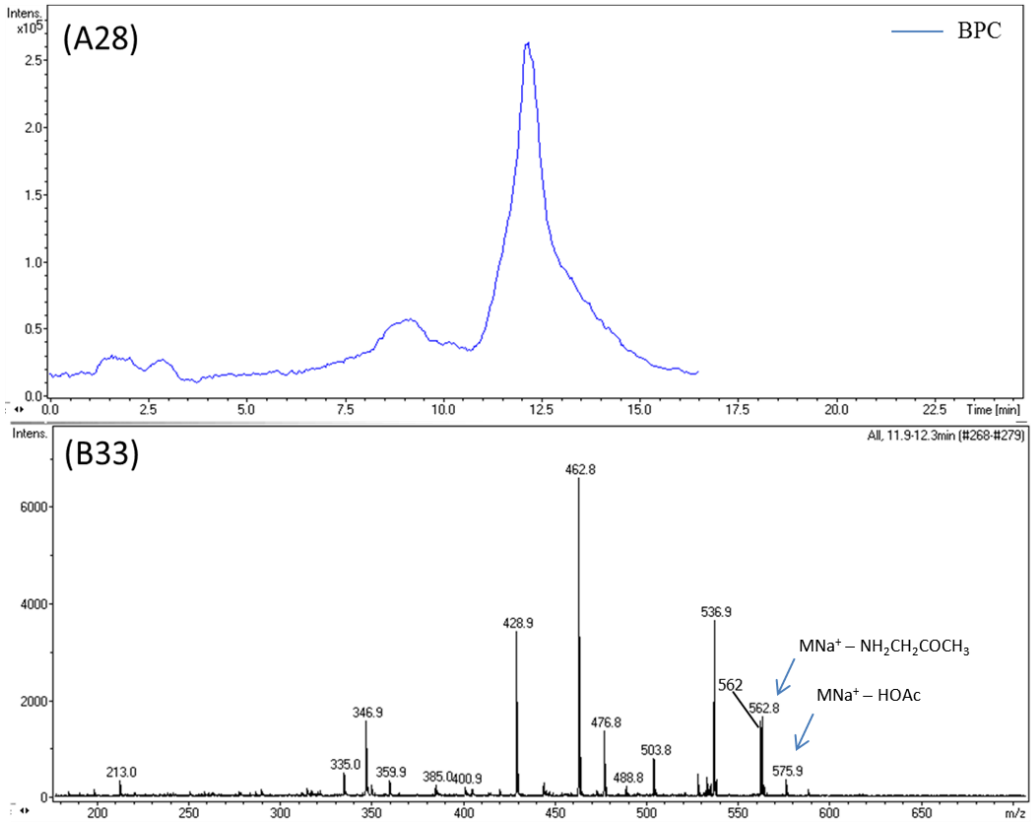

Figure 4.33: LCMS/MS of purified azinomycin A in the hydrolysed form (m/z = 636). (A28): HPLC chromatogram. (B33): Product ion MS/MS spectrum from fragmentation of the $[M+Na]^+$ parent ion.

The fragmentation pattern shown in **Figure 4.33** and summarised in **Table 4.3** may be explained by the following reactions. The ion at m/z 576 corresponds to the loss of HOAc from the parent ion (path (a), **Scheme 4.10**). The ion at m/z 563 corresponds to the loss of $NH_2CH_2COCH_3$ from the parent ion. The ion at m/z 562 corresponds to the loss of a radical proton from ion with m/z = 563. The first fragment (m/z 563) results from the intramolecular rearrangement that precedes fragmentation. The fragmentation mechanism for both fragments is described in **scheme 4.10**, path (b). The ion at m/z 537 corresponds to the loss of $CONCH_2COCH_3$ from the parent ion after an intramolecular rearrangement (path (c), **Scheme 4.10**). The ion with m/z = 429 corresponds to the loss of AcO, OH, H_2COH and H from ion with m/z = 537 by radical fragmentations (path (c), **Scheme 4.10**). The ion at m/z 504 corresponds to the loss of radical $NHCH_2COCH_3$ from the ion of m/z 576 following homolytic fission of the amide bond (path (d), **Scheme 4.10**). The ion of m/z 477 corresponds to

the loss of HOAc from the ion of m/z 537 (path (e), **Scheme 4.10**). The major ion of m/z 463 corresponds to the loss of the sodiated fragment $NHCH_2CONa^+CH_3$ from the parent ion with m/z = 636 followed by hydrolysis and then the loss of HOAc group as described in path (f), **scheme 4.10**. The ion of m/z 347 corresponds to the loss of the naphtthoate fragment from the parent ion followed by the loss of radical $NHCH_2COCH_3$ in a similar mechanism as in path (d) and finally the loss of water.

m/z	**Ion**	**Groups associated with the mass lost**
636	MNa^+	-
576	$MNa^+ - 60$	HOAc
563	$MNa^+ - 73$	$NH_2CH_2COCH_3$
562	$MNa^+ - 74$	$NH_2CH_2COCH_3$ and H (as radical proton)
537	$MNa^+ - 99$	$CONCH_2COCH_3$
504	$MNa^+ - 132$	HOAc and $NHCH_2COCH_3$ (as radical)
477	$MNa^+ - 159$	$CONCH_2COCH_3$ and HOAc
463	$MNa^+ - 173$	$NHCH_2CONa^+CH_3$, H_2O and HOAc
429	$MNa^+ - 207$	$CONCH_2COCH_3$, and (AcO, OH, H_2COH and H) as radicals
347	$MNa^+ - 289$	Naphthoate, $NHCH_2COCH_3$ (as radical) and H_2O

Table 4.3: Summary of ions and groups associated with the mass lost during MS/MS of purified hydrolysed azinomycin A.

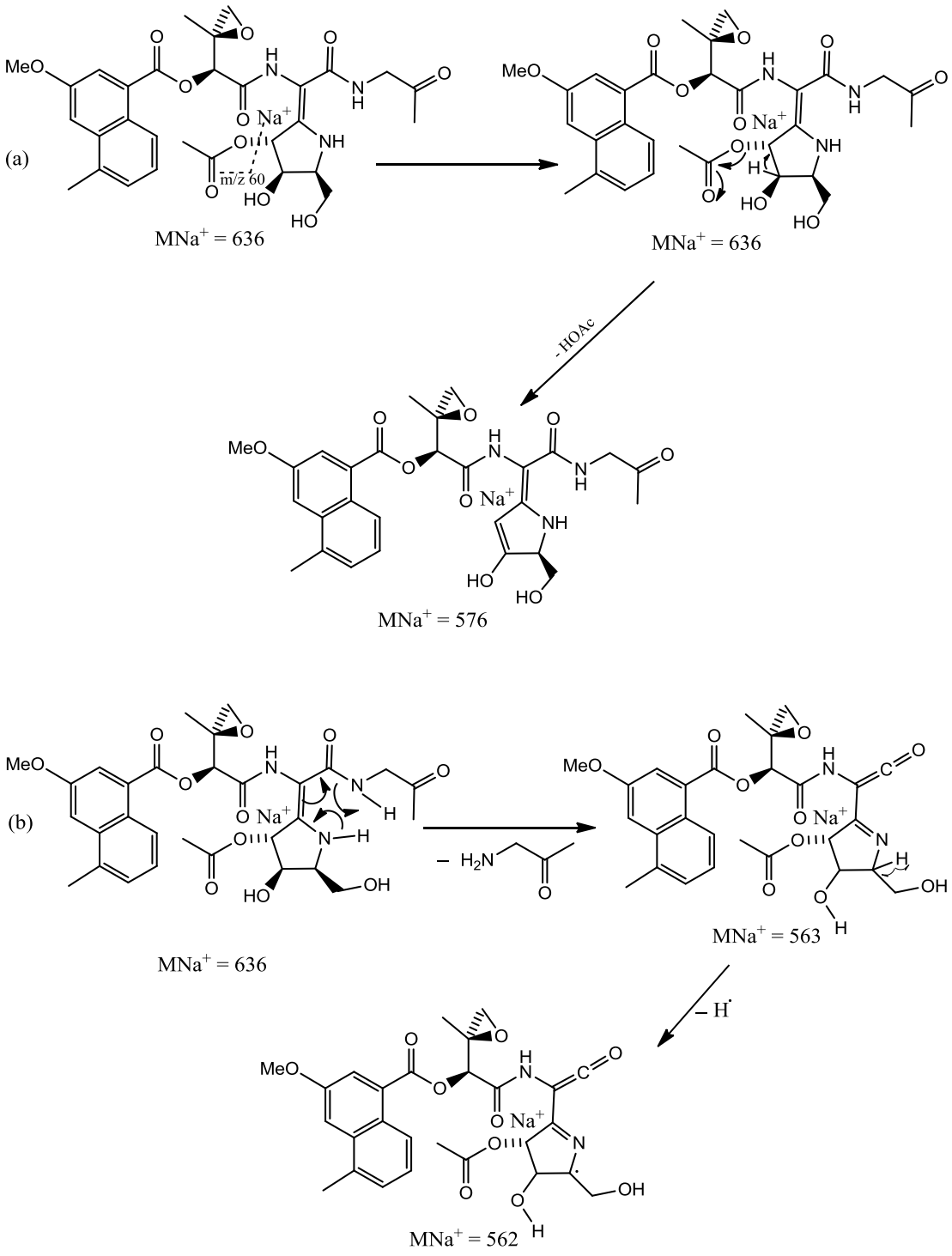

Scheme 4.10: Paths (a) and (b).

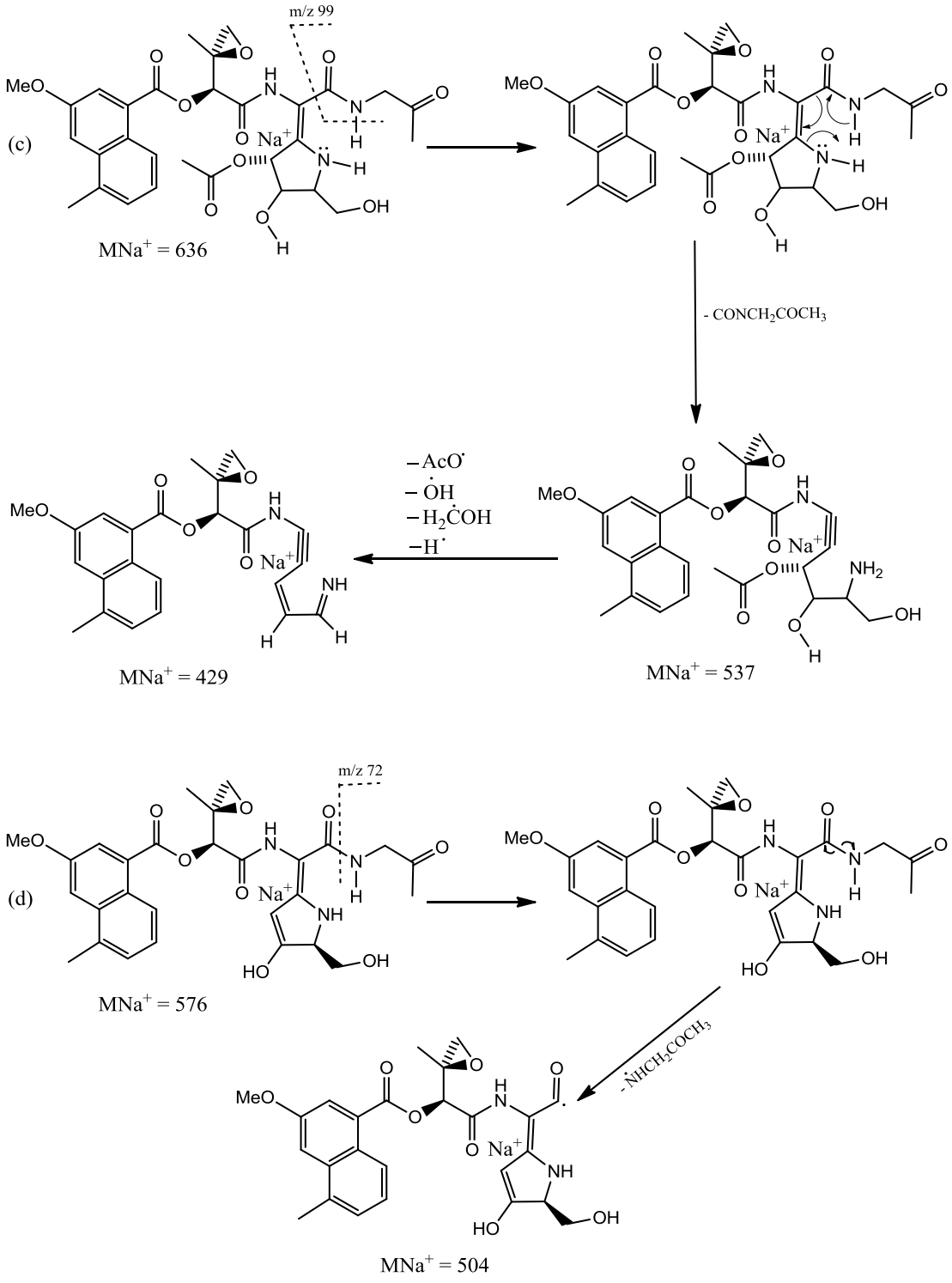

Scheme 4.10: Paths (c) and (d).

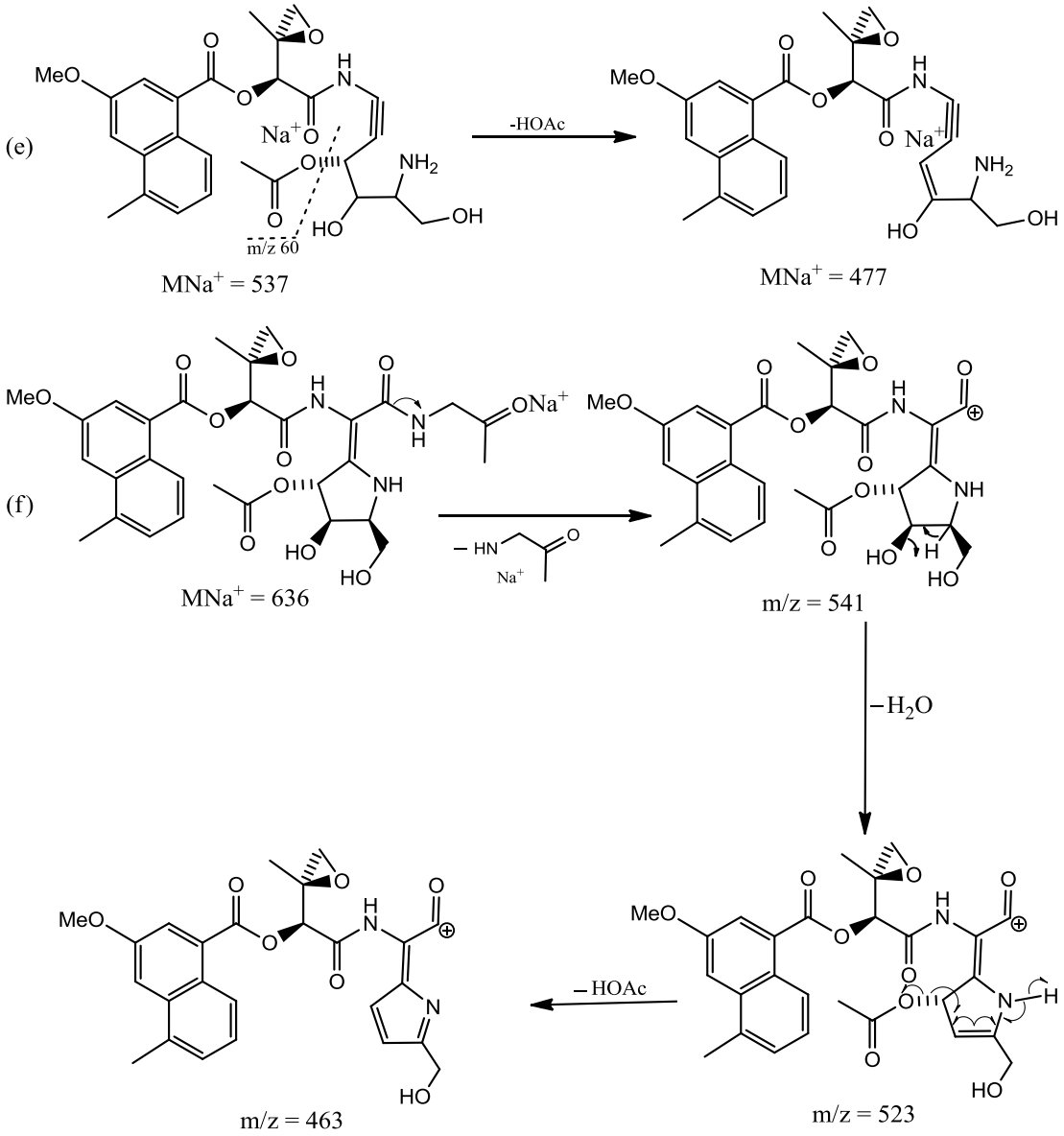

Scheme 4.10: Paths (e) and (f).

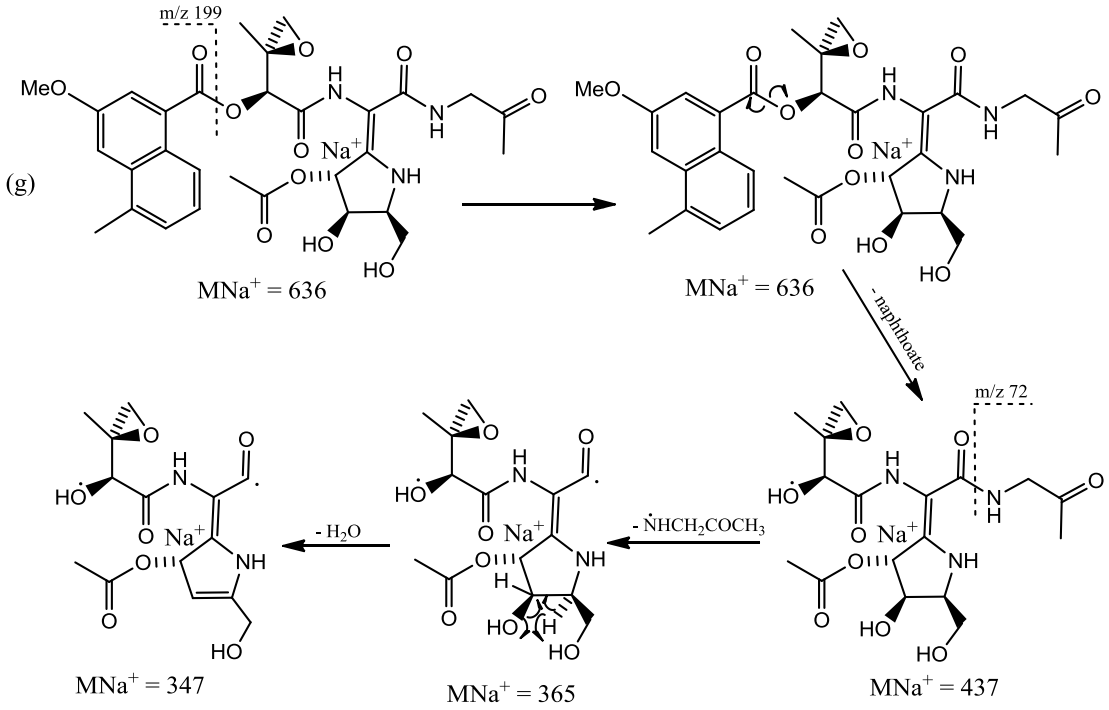

Scheme 4.10: Path (g).

LCMS/MS of azinomycin A (m/z = 618)

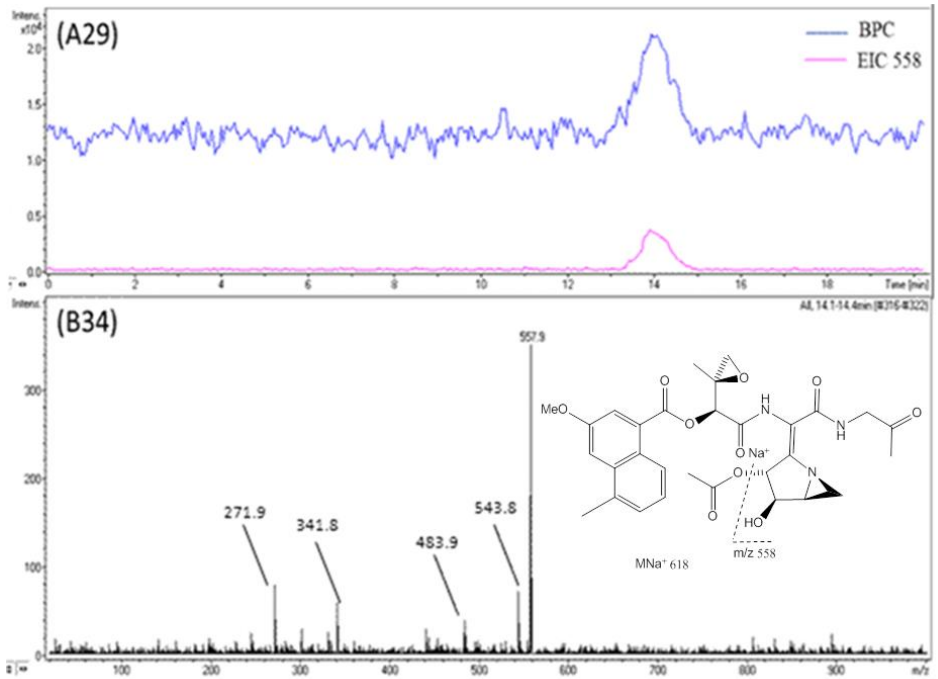

Figure 4.34: LCMS/MS of purified azinomycin A (m/z = 618). (A29): HPLC chromatograms. (B34): Product ion MS/MS spectrum of azinomycin A ion showing different fragmentation patterns compared to the hydrolysed form.

LCMS/MS of purified azinomycin analogues with m/z = 622

Azinomycin A analogue with m/z = 622 was produced after feeding 1-naphthoic acid, and 3-methoxy-1-naphthoic acid and has a retention time, R_t = 64.9-65.4 min (**Figure 4.14)**. Another azinomycin A analogue with the same mass (m/z = 622), but different retention time [R_t = 22.2-23.3 min; ((B11), **Figure 4.16**)] was produced after feeding 4-methyl-1-naphthoic acid. MS/MS of the purified fractions and crude prep HPLC extracts from feeding 1-naphthoic acid and 3-methoxy-1-naphthoic acid compared to MS/MS of the crude prep HPLC extract from feeding 4-methyl-1-naphthoic acid revealed the same fragmentation patterns as shown in (B35), **Figure 4.35**. However, their chromatograms appeared at different retention times ((A30) at R_t = 7.1-7.3 min for the first two feeding compounds and (M) at R_t = 11.1-13.7 min for the third one).

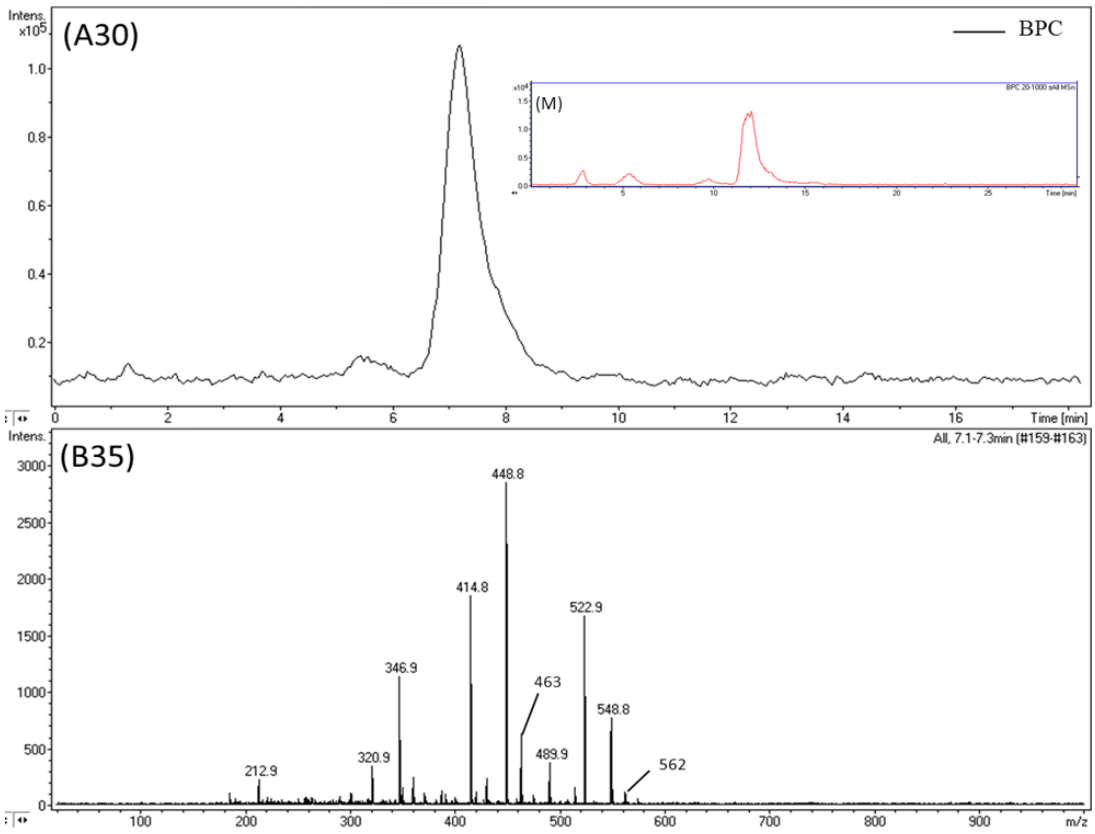

Figure 4.35: LCMS/MS of purified azinomycin A analogues (m/z = 622). (A30) and (M): HPLC chromatograms. (B35): Product ions MS/MS spectrum of azinomycin A analogue ions.

The fragment ions from m/z = 622 form a similar pattern (**Figure 4.35**) to that for hydrolysed azinomycin A (**Figure 4.33**), with mass shifts of 14 for certain fragment ions. This implies that these fragments contain the naphthoate group, which lacks CH_2 compared to the natural naphthoate, and that the fragments are formed by the same mechanisms (**Scheme 4.10**) as for the hydrolysed azinomycin A.

Scheme 4.11 (paths (h)-(n)), describe the fragmentation pathways for fragment ions from m/z = 622.

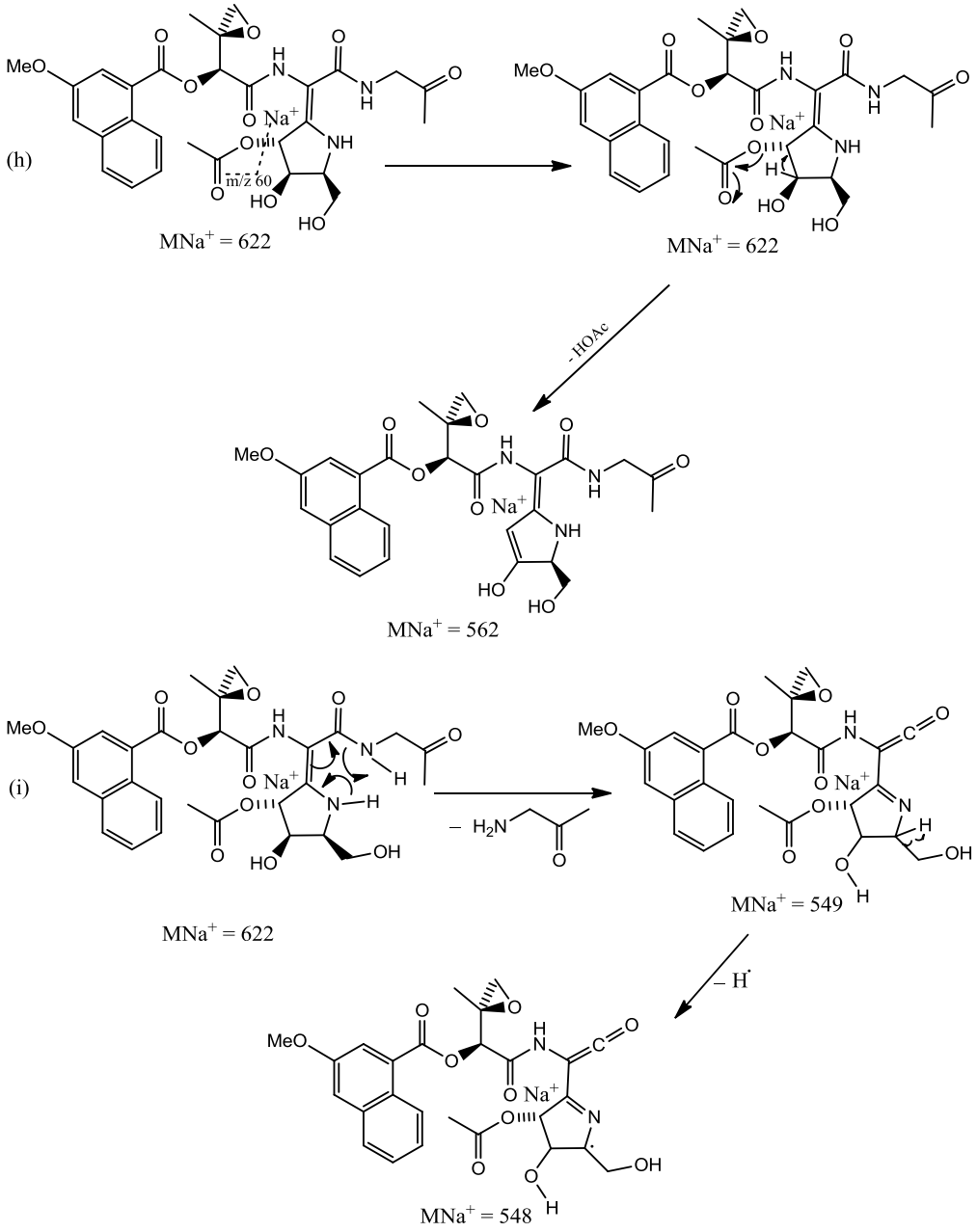

Scheme 4.11: Paths (h) and (i).

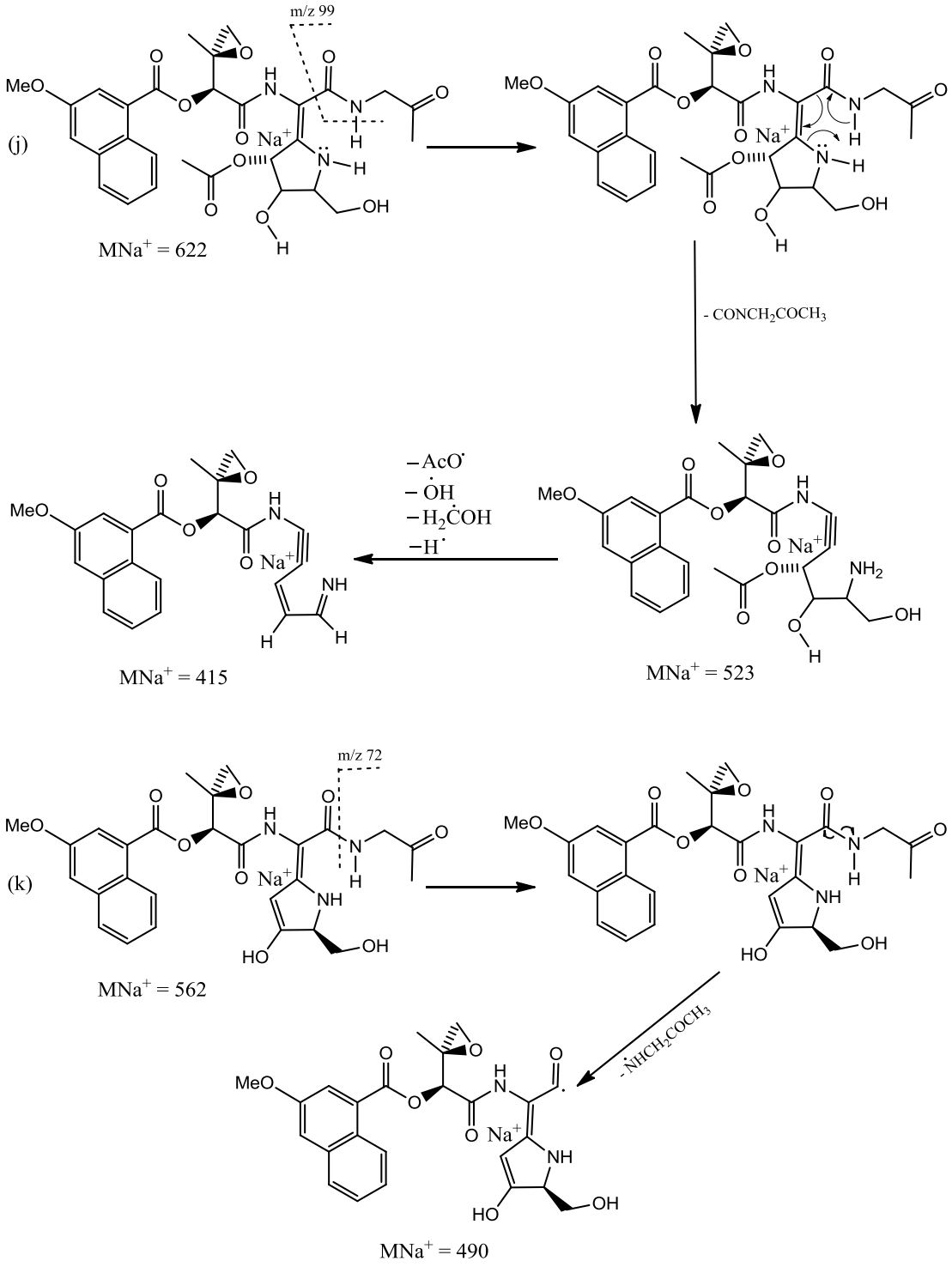

Scheme 4.11: Paths (j) and (k).

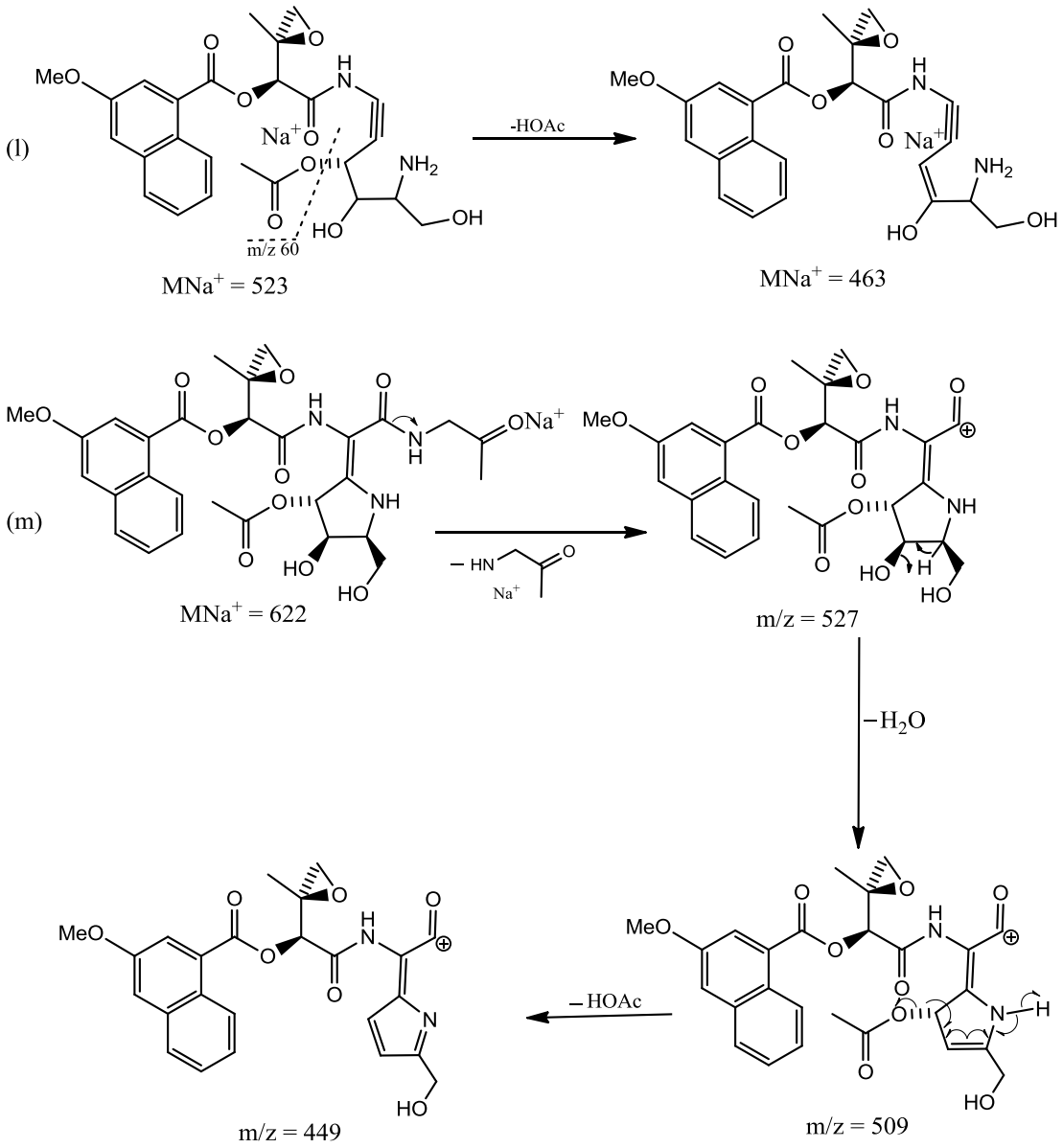

Scheme 4.11: Paths (l) and (m).

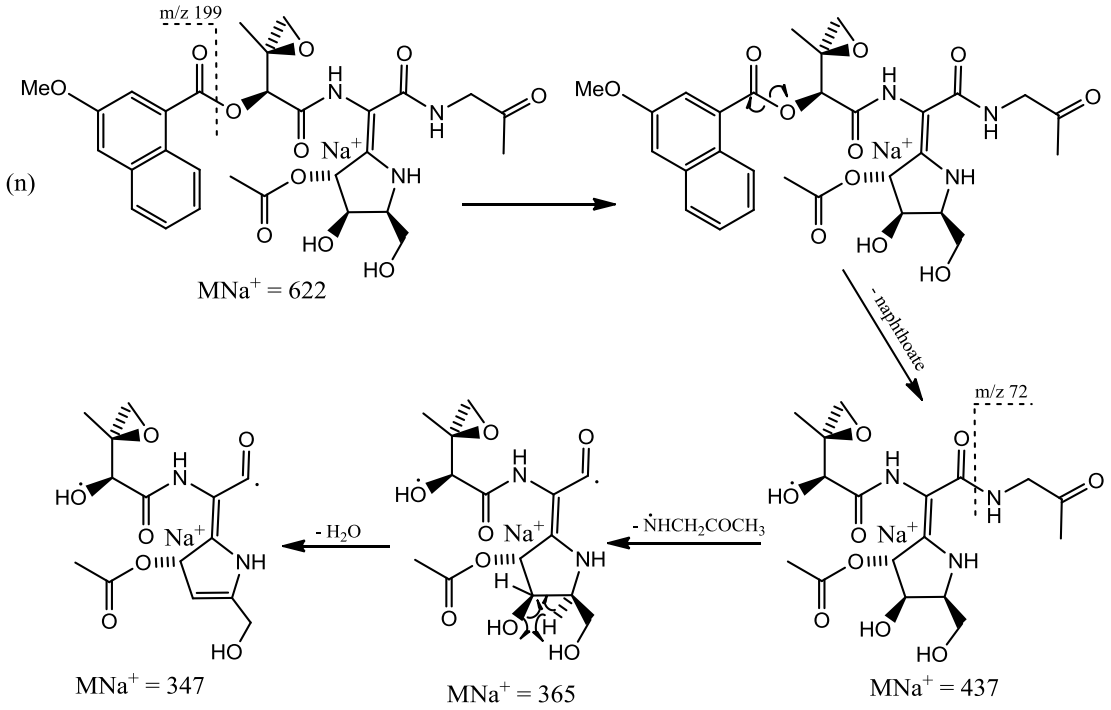

Scheme 4.11: Path (n).

Identical fragmentation mechanisms can explain the same fragment ions that result from the metabolite with m/z 622, from feeding 4-methyl-1-naphthoic acid. The only difference resides in the isomeric substitution on the naphthalene ring.

The LCMS/MS data for the azinomycin A analogue with m/z = 592 (hydrolysed form) formed from feeding 1-napthoic acid are presented in **Figure 4.36**.

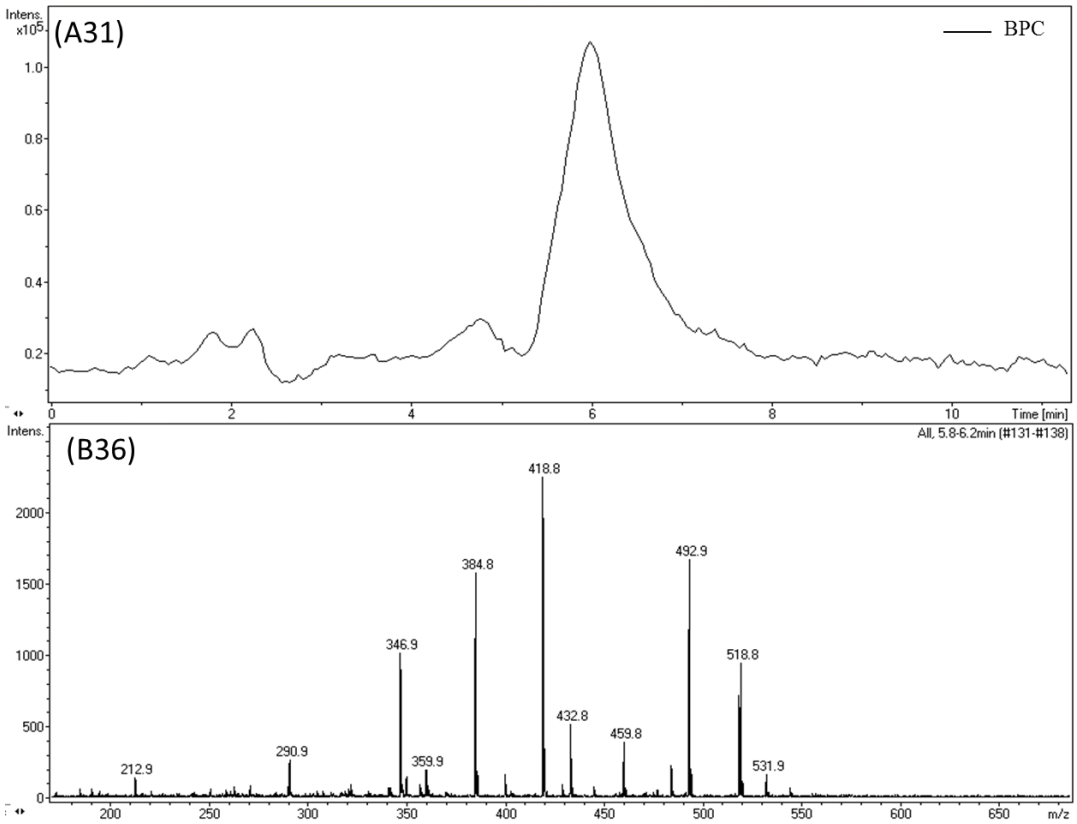

Figure 4.36: LCMS/MS of purified azinomycin A analogue from feeding 1-naphthoic acid (m/z = 592, hydrolysed form). (A31): HPLC chromatogram. (B36): Product ions MS/MS spectrum from m/z 592 parent ion.

There is a strong correlation between the fragmentation pattern seen in **Figure 4.36** and those in **Figure 4.35** and **Figure 4.33.** Comparison between fragments in **Figure 4.33** and **Figure 4.36** shows a difference of mass of 44 indicating the incorporation of 1-naphthoic acid into the azinomycin A biosynthesis pathway lacking the methoxy group at C3' and the methyl group at C5' of the naphthyl group. Therefore the fragmentation pattern in **Figure 4.36** can be explained by the same mechanisms as in **scheme 4.10**, only diverging in the substituents on the naphthoate.

In **Figure 4.36** and **Table 4.4**, the ion at m/z 532 corresponds to the loss of HOAc from the parent ion (m/z = 592, sodiated and hydrolysed forms). The ion at m/z 519 corresponds to the loss of $NH_2CH_2COCH_3$ from the parent ion by the intramolecular rearrangement that precedes fragmentation. The ion at m/z 493 corresponds to the

loss of $CONCH_2COCH_3$ from the parent ion after an intramolecular rearrangement. The ion with m/z = 385 corresponds to the loss of AcO, OH, H_2COH and H from ion with m/z = 493 by radical fragmentations. The ion at m/z 460 corresponds to the loss of radical $NHCH_2COCH_3$ from the ion of m/z 532 following homolytic fission of the amide bond. The ion of m/z 433 corresponds to the loss of HOAc from the ion of m/z 493. The major ion of m/z 419 corresponds to the loss of the sodiated fragment $NHCH_2CONa^+CH_3$ from the parent ion with m/z = 592 followed by hydrolysis and then the loss of HOAc. The ion of m/z 347 corresponds to the loss of the naphtthoate fragment from the parent ion followed by the loss of radical $NHCH_2COCH_3$ and water.

m/z	**Ion**	**Groups associated with the mass lost**
592	MNa^+	-
532	$MNa^+ - 60$	HOAc
519	$MNa^+ - 73$	$NH_2CH_2COCH_3$
493	$MNa^+ - 99$	$CONCH_2COCH_3$
460	$MNa^+ - 132$	HOAc and $NHCH_2COCH_3$ (as radical)
433	$MNa^+ - 159$	$CONCH_2COCH_3$ and HOAc
419	$MNa^+ - 173$	$NHCH_2CONa^+CH_3$, H_2O and HOAc
385	$MNa^+ - 207$	$CONCH_2COCH_3$, and (AcO, OH, H_2COH and H) as radicals
347	$MNa^+ - 289$	Naphthoate, $NHCH_2COCH_3$ (as radical) and H_2O

Table 4.4: Summary of ions and groups associated with the mass lost during MS/MS of purified hydrolysed azinomycin A analogue with m/z = 592.

Figure 4.37 shows the LCMS/MS data for the unhydrolysed azinomycin A analogue (m/z 604, $M+Na^+$) formed after feeding 3-methoxy-1-naphthoic acid or 1-naphthoic acid. The fragment m/z 544 corresponds to loss of the acetyl group from the parent ion.

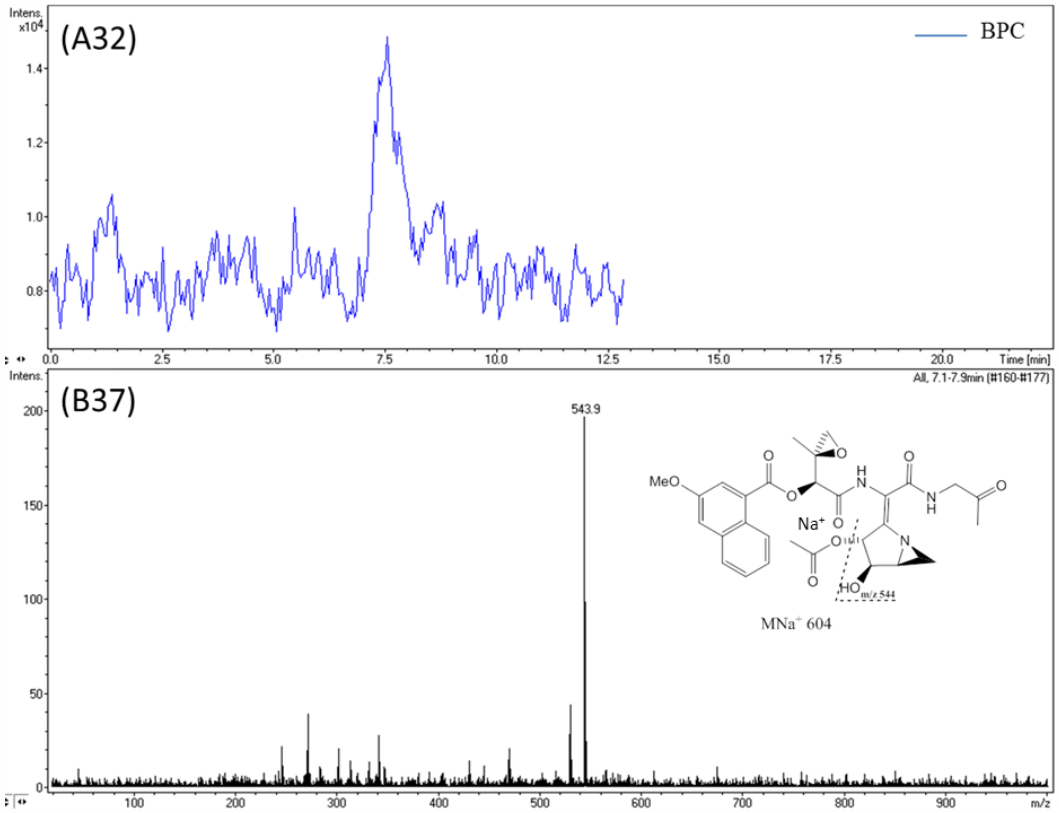

Figure 4.37: LCMS/MS of azinomycin A analogue (m/z = 604) from feeding 3-methoxy-1-napthoic acid. (A32): HPLC chromatogram. (B37): Product ions MS/MS spectrum from m/z 604.

The LCMS/MS data for the hydrolysed azinomycin A analogue (m/z = 610, $M+Na^+$) from feeding purified 4-fluoro-1-napthoic acid is shown in **Figure 4.38**. The fragmentation pattern is in good correlation with the previous ones (**Figures 4.33**, **4.35-4.36**). Hence, the fragmentation mechanisms are likely the same and are shown in **scheme 4.12**, paths (o)-(u).

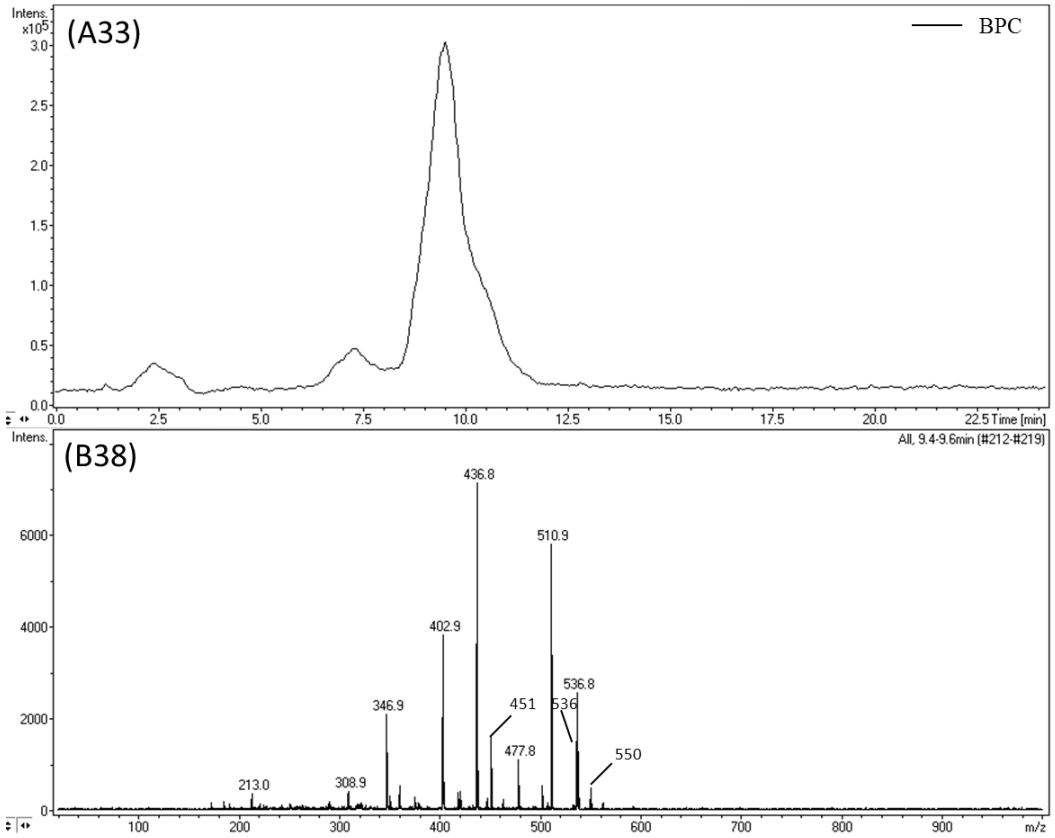

Figure 4.38: LCMS/MS of the hydrolysed azinomycin A analogue (m/z = 610) from feeding 4-fluoro-1-napthoic acid. (A33): HPLC chromatogram. (B38): Product ion MS/MS spectrum for m/z 610.

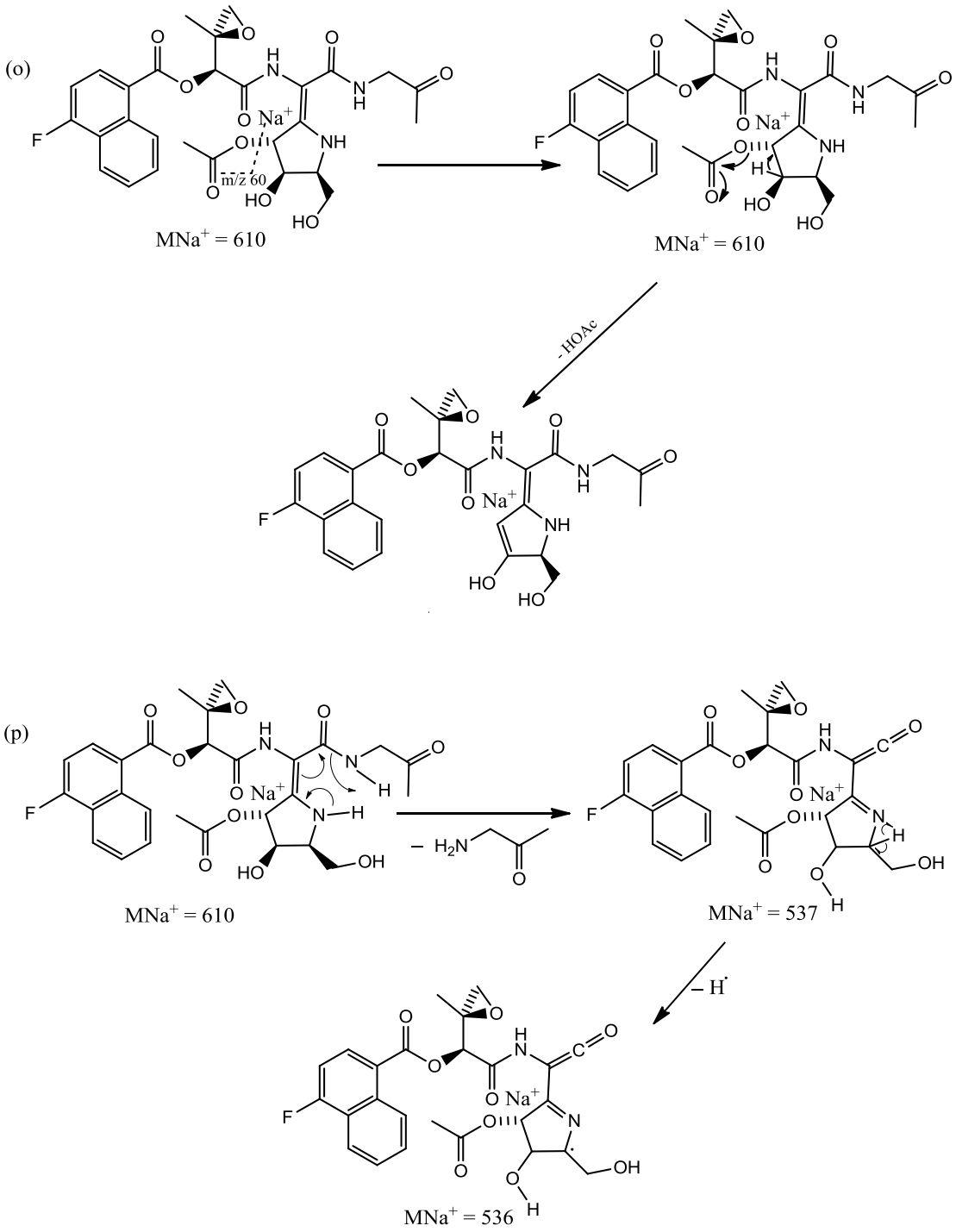

Scheme 4.12: Paths (o) and (p).

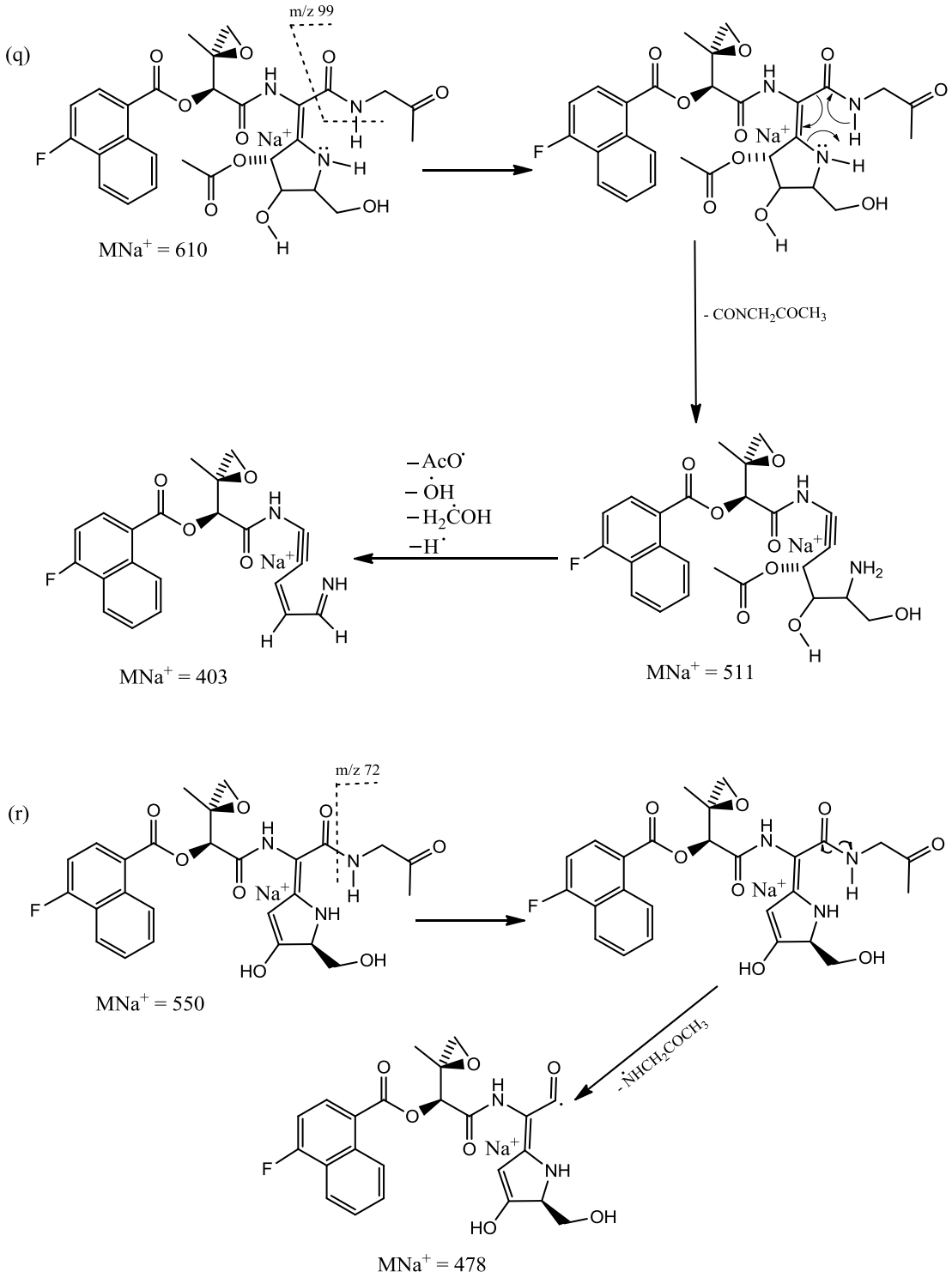

Scheme 4.12: Paths (q) and (r).

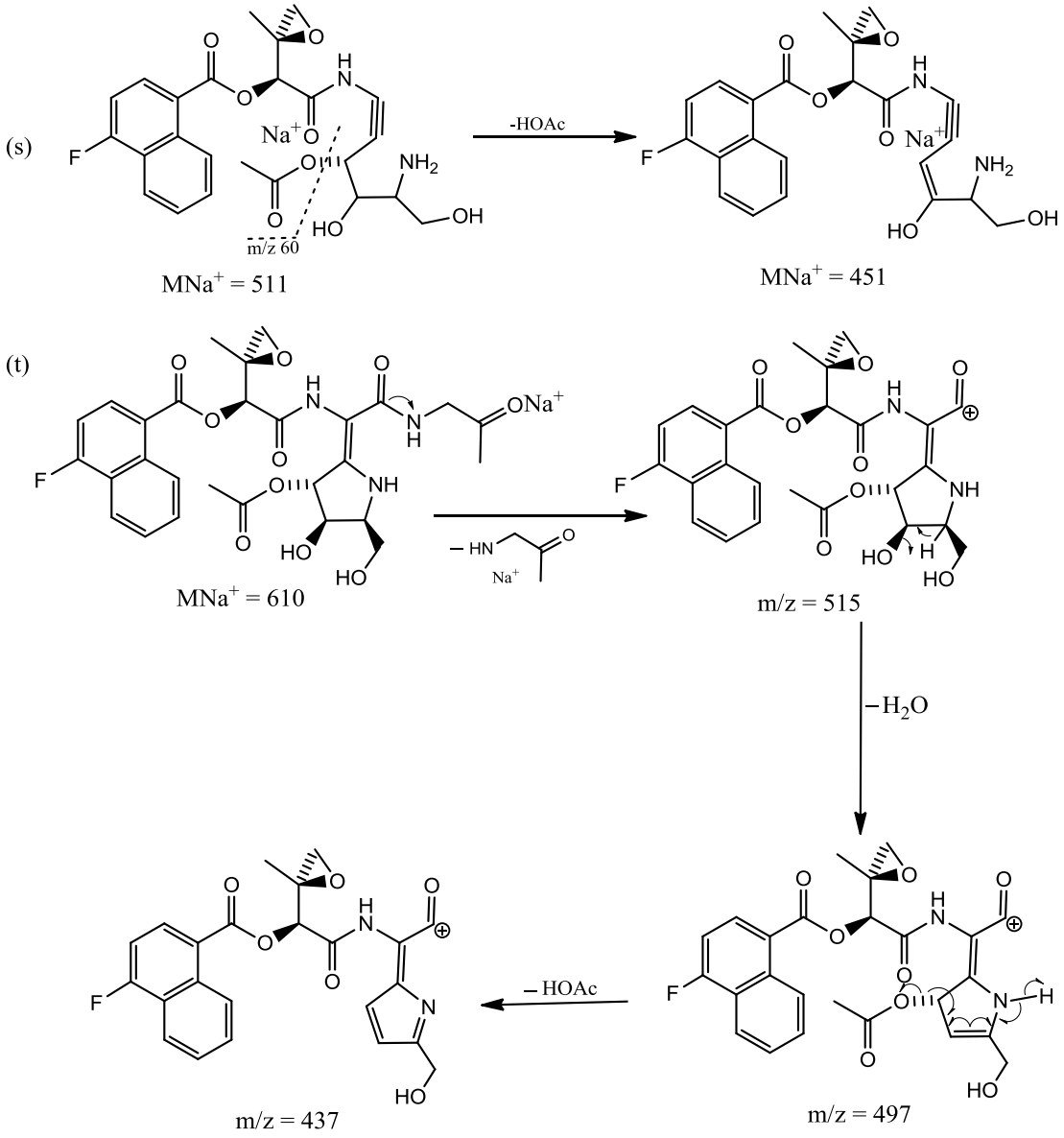

Scheme 4.12: Paths (s) and (t).

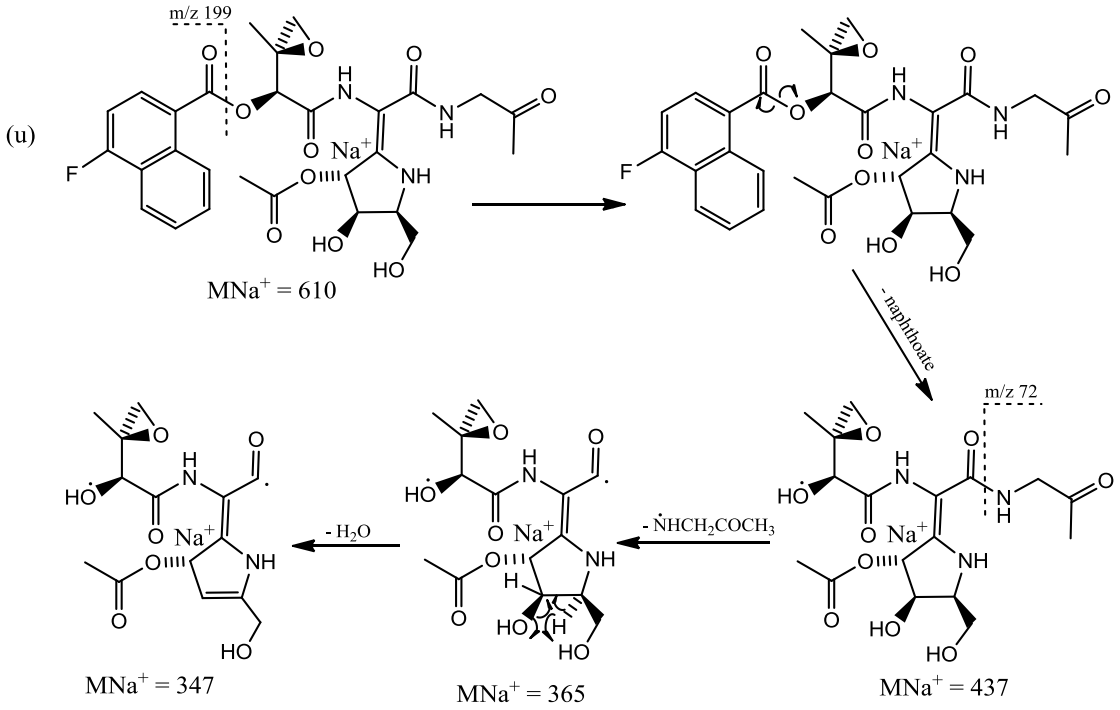

Scheme 4.12: Path (u).

The LCMS/MS data for the presumed chlorinated azinomycin A analogues (m/z = 628) from feeding 4-fluoro-1-napthoic acid is shown in **Figure 4.39**.

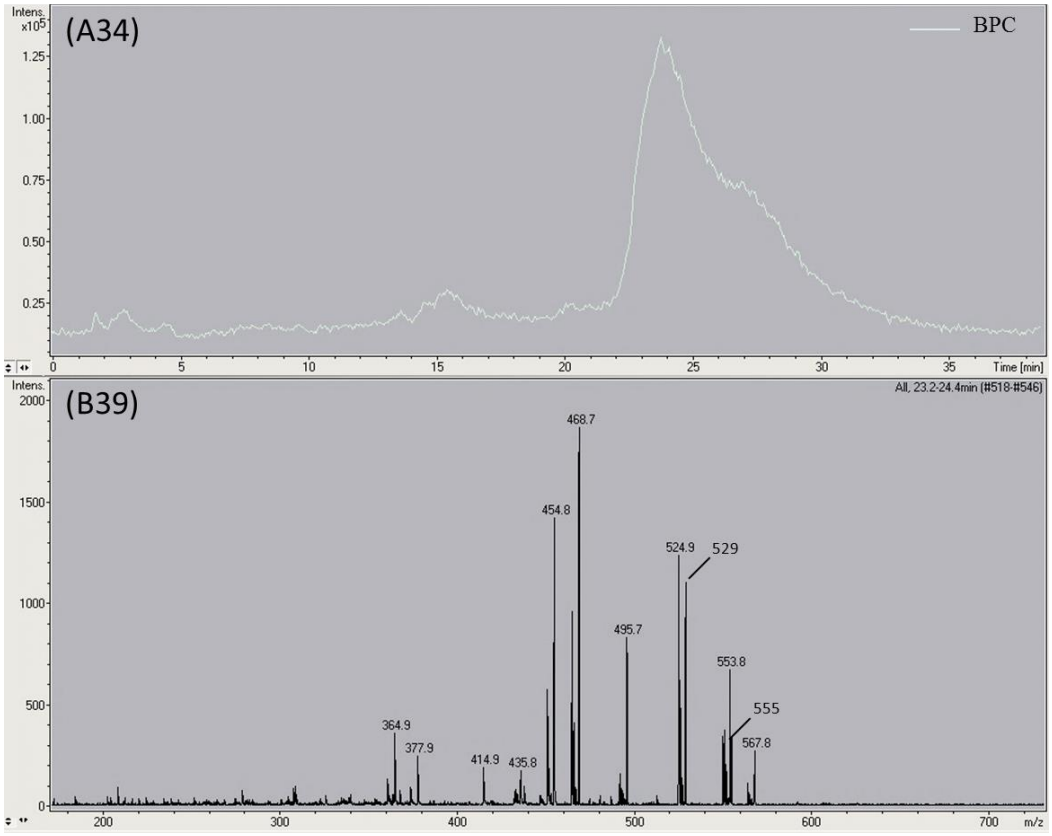

Figure 4.39: LCMS/MS of the chlorinated azinomycin A analogue (m/z = 628) from feeding 4-fluoro-1-napthoic acid. (A34): HPLC chromatogram. (B39): Product ion MS/MS spectrum of m/z 628.

There is an association between most of the fragment ions seen in **Figure 4.39** and those in **Figure 4.38**, with a difference of 18 mass units between each correlated pair of ions **(Table 4.5).** This implies replacement of OH by ^{35}Cl in each of these fragment ions, most likely at the end of the carbon chain of the aziridine component as shown in **scheme 4.13**, paths (v_1)-(v_6). The additional ions 4 mass units lower in mass may arise from intermolecular reaction of the chlorinated fragment ions with MeOH solvent molecules, resulting in substitution of CH_3O for Cl.

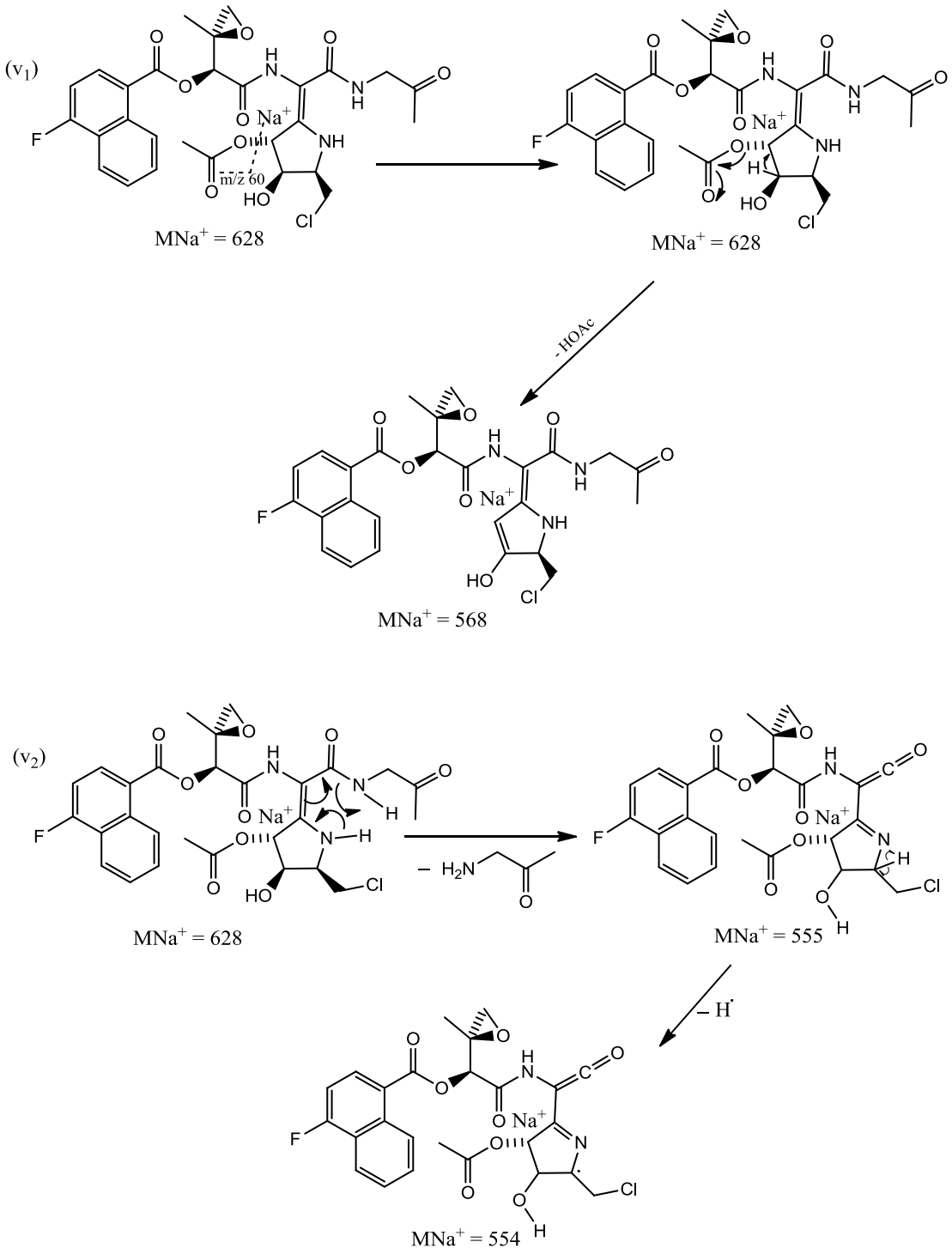

Scheme 4.13: Paths (v_1) and (v_2).

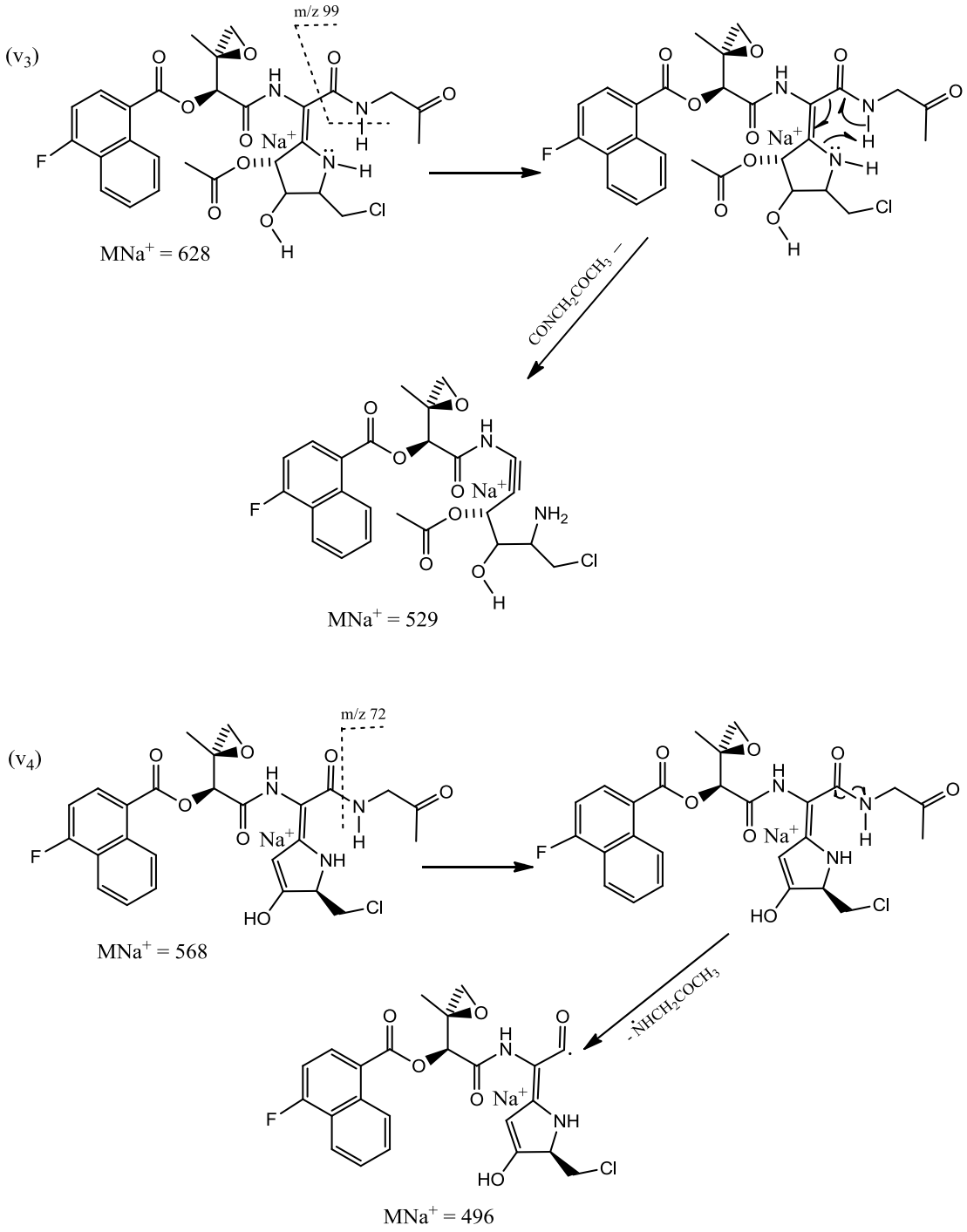

Scheme 4.13: Paths (v_3) and (v_4).

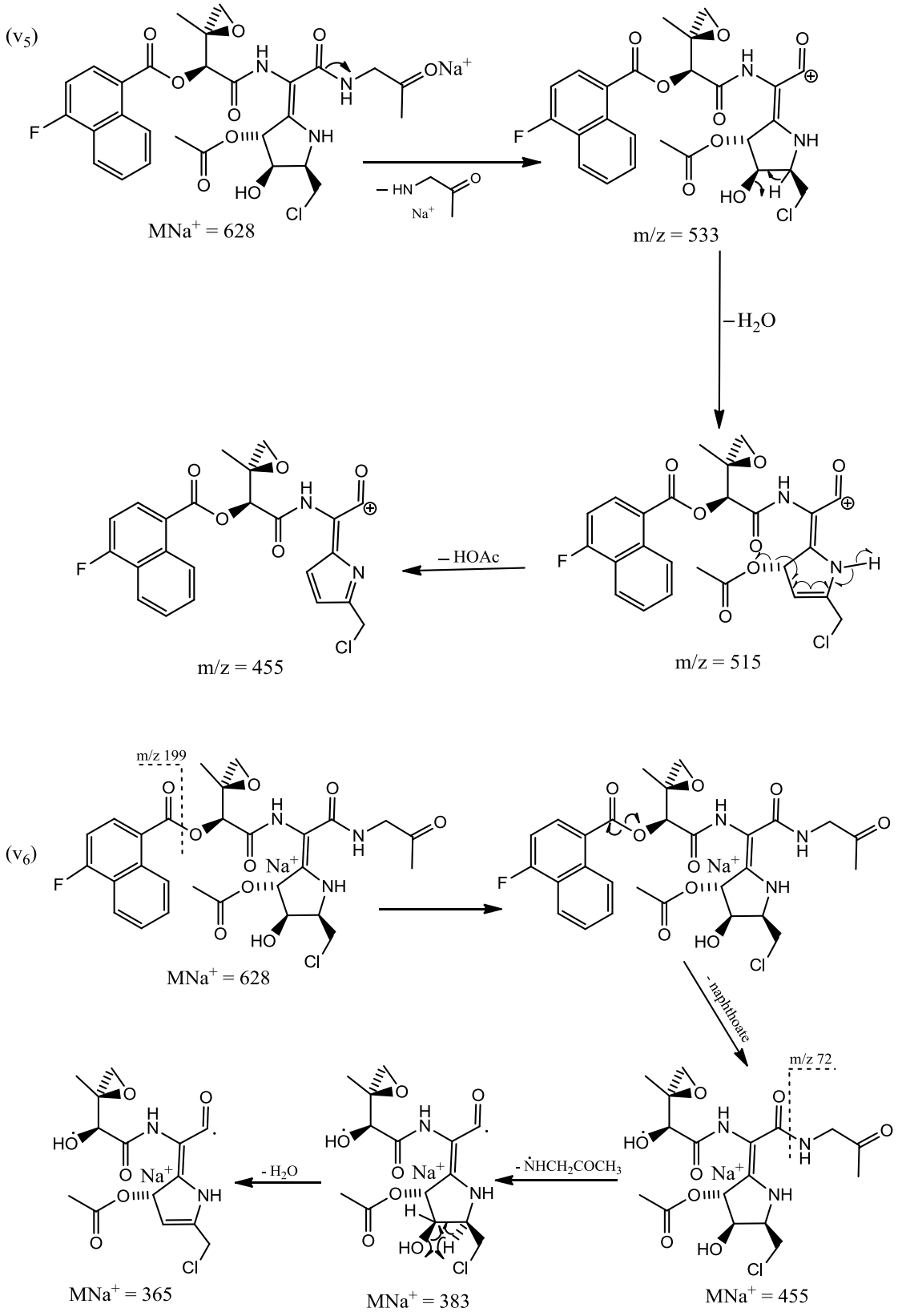

Scheme 4.13: Paths (v_5) and (v_6).

Fragments of chlorinated azinomycin A analogue (m/z 628/630)	Fragments of azinomycin A analogue (m/z 610)
MNa^+ (m/z)	MNa^+ (m/z)
365	347
455	437
469	451
496	478
529	511
554	536
555	537
568	550

Table 4.5: Comparison between the major MS/MS product ions of hydrochlorinated and hydrolysed azinomycin A analogues (m/z 628/630 and 610 respectively). There is a correlation between each pair of ions within the same row (difference of 18 mass units).

The LCMS/MS for the unhydrolysed azinomycin A analogue (m/z = 592) after feeding 4-fluoro-1-napthoic acid is shown in **Figure 4.40**. The new azinomycin A analogue could not be purified as the corresponding UV absorption peak was too small, so these data come from the crude extract.

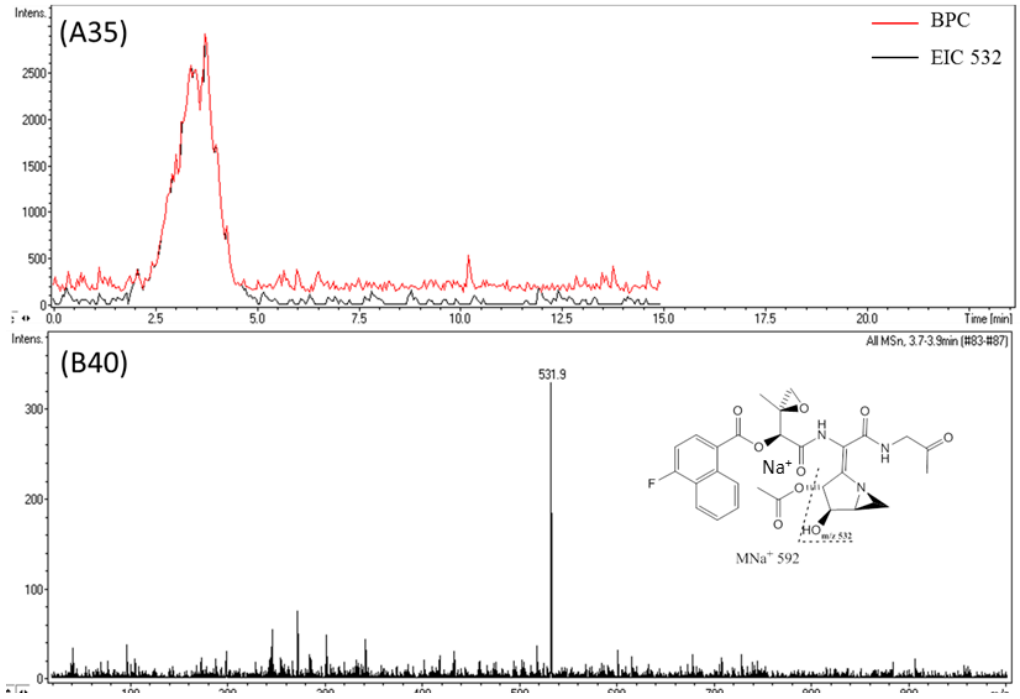

Figure 4.40: LCMS/MS of azinomycin A analogue (m/z = 592) from 4-fluoro-1-napthoic acid feeding. (A35): HPLC chromatogram of MS/MS data only. (B40): Product ions MS/MS spectrum of m/z 592. The fragment m/z 532 corresponds to the loss of the acetyl group from the parent ion.

The LCMS/MS for the azinomycin A analogue (m/z = 588) after feeding 4-methyl-1-napthoic acid is shown in **Figure 4.41**. The new azinomycin A analogue was not purified as the UV absorption peak was too small to collect fractions during prep HPLC purification, so this data is from the crude extract.

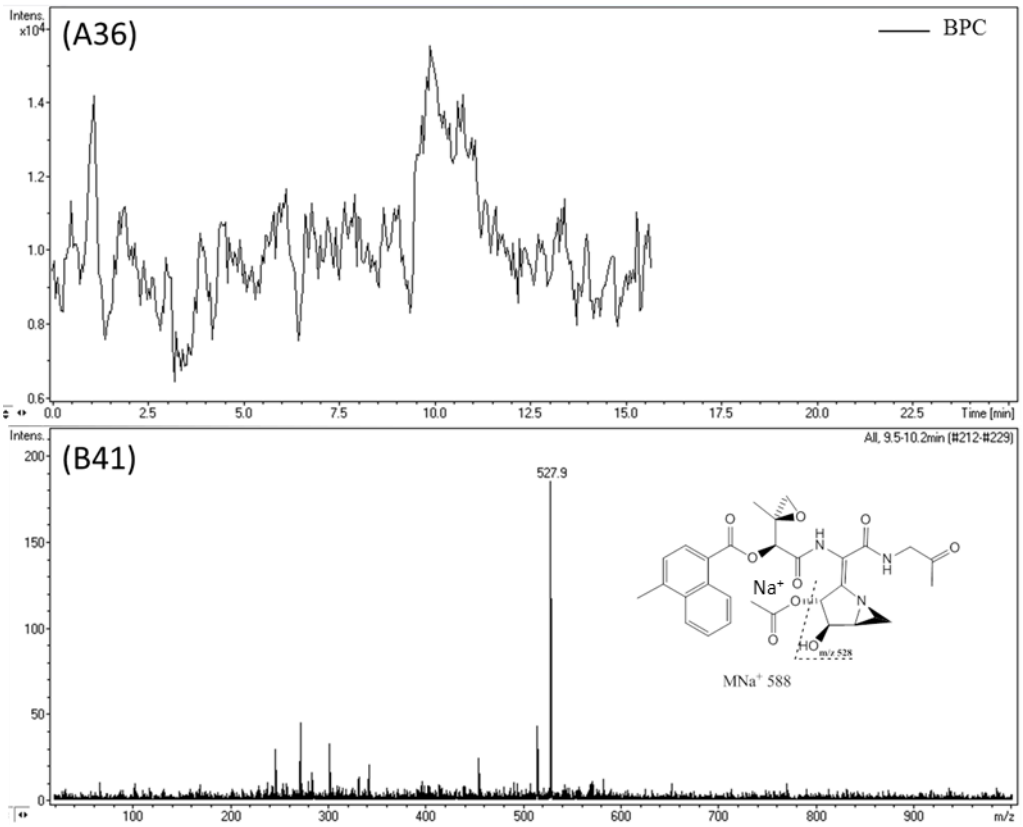

Figure 4.41: LCMS/MS of azinomycin A analogue (m/z = 588) from 4-methyl-1-napthoic acid feeding. (A36): HPLC chromatogram of MS/MS data only. (B41): Product ions MS/MS spectrum of m/z 588. The fragment m/z 528 corresponds to the loss of the acetyl group from the parent ion.

The LCMS/MS data for the purified hydrolysed azinomycin A analogue (m/z = 606) from feeding 4-methyl-1-napthoic acid.

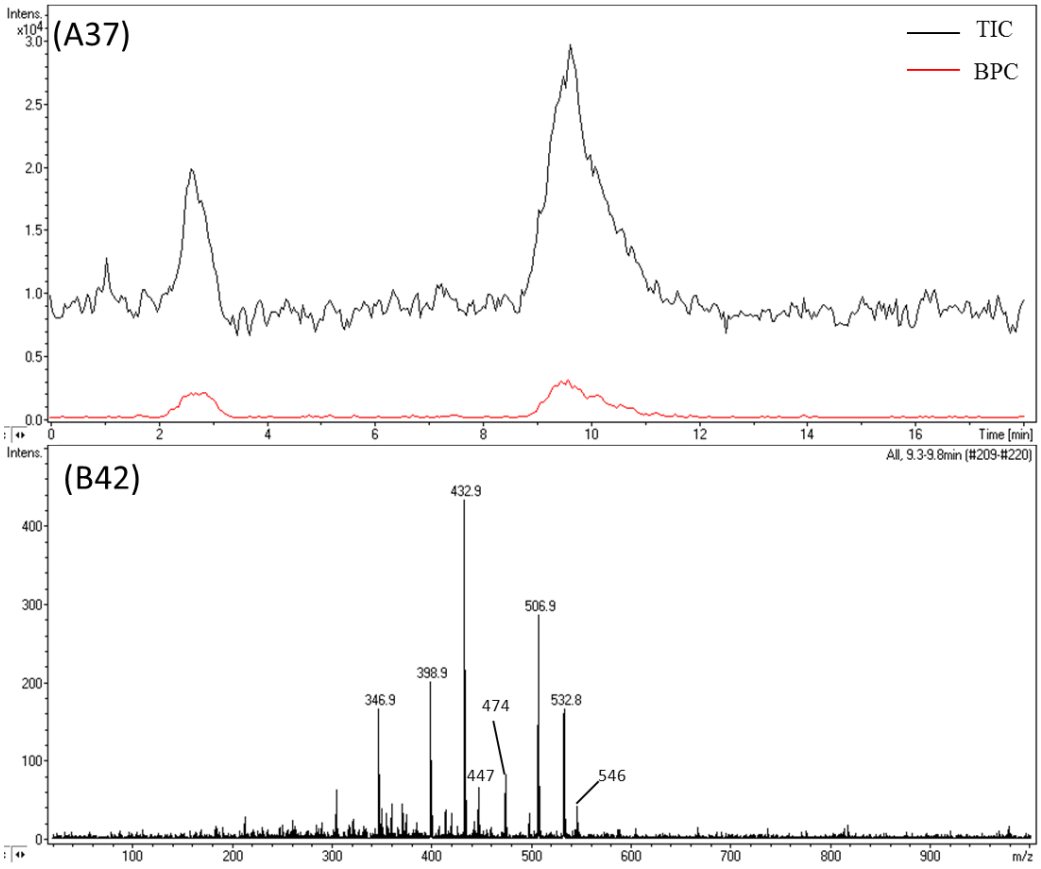

Figure 4.42: LCMS/MS of azinomycin A analogue (m/z = 606) from feeding 4-methyl-1-napthoic acid. (A37): HPLC chromatogram of purified extract. (B42): Product ion MS/MS spectrum of m/z 606.

The fragmentation pattern shown in **Figure 4.42** correlates well with that for the native azinomycin A derivative**.** Hence, the fragmentation mechanisms are similar to **scheme 4.10** as described in **scheme 4.14**.

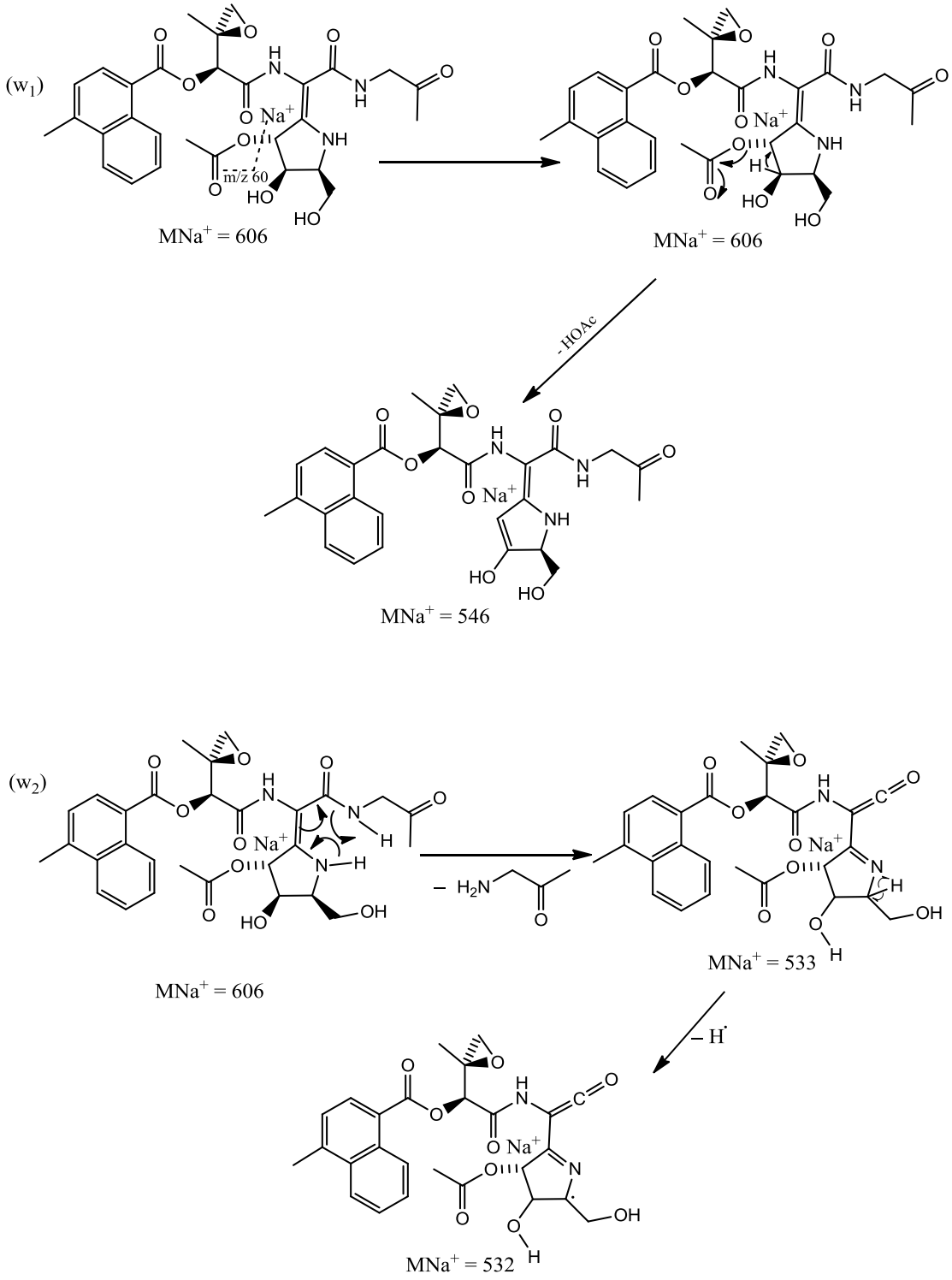

Scheme 4.14: Paths (w_1) and (w_2).

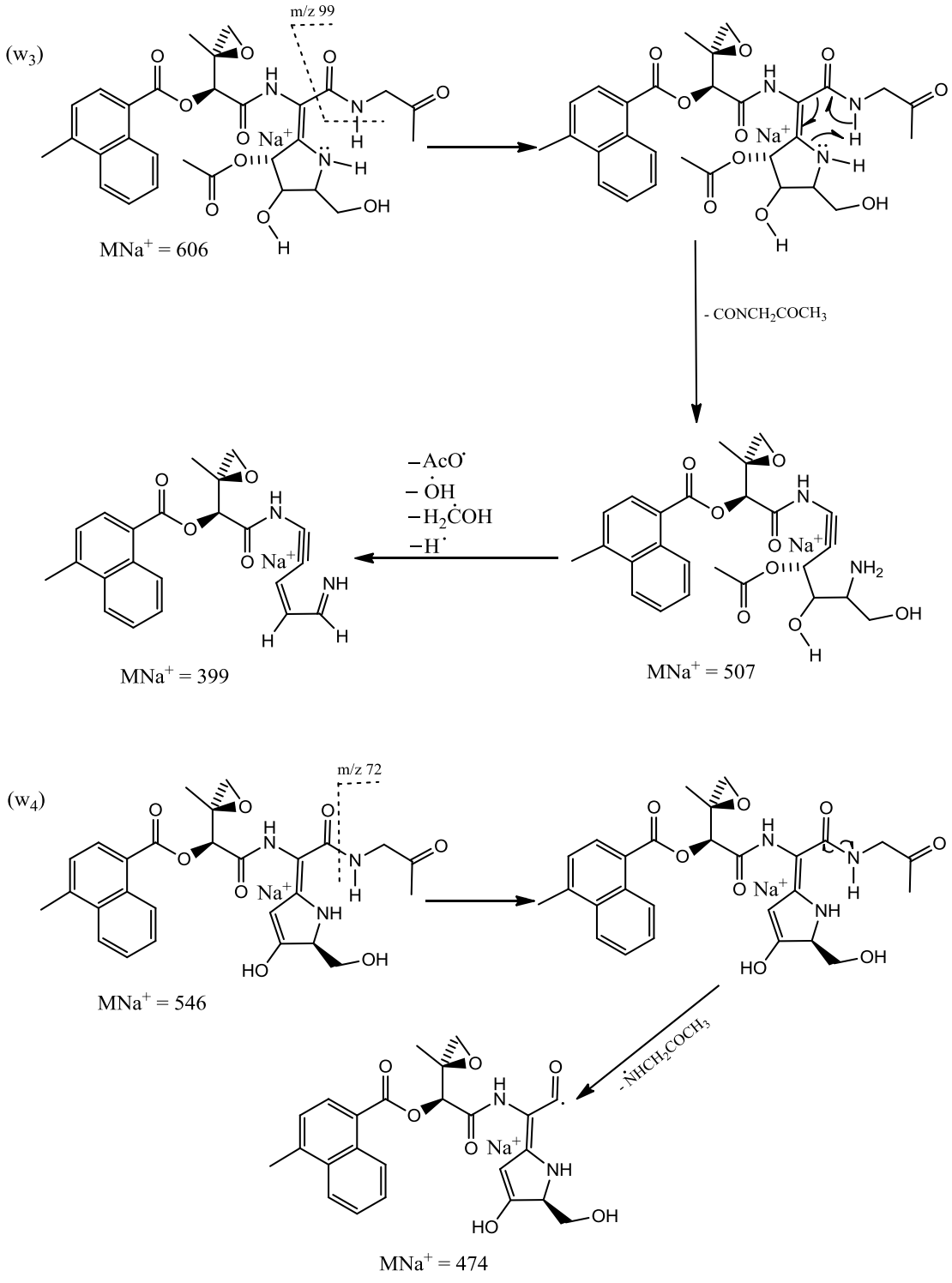

Scheme 4.14: Paths (w_3) and (w_4).

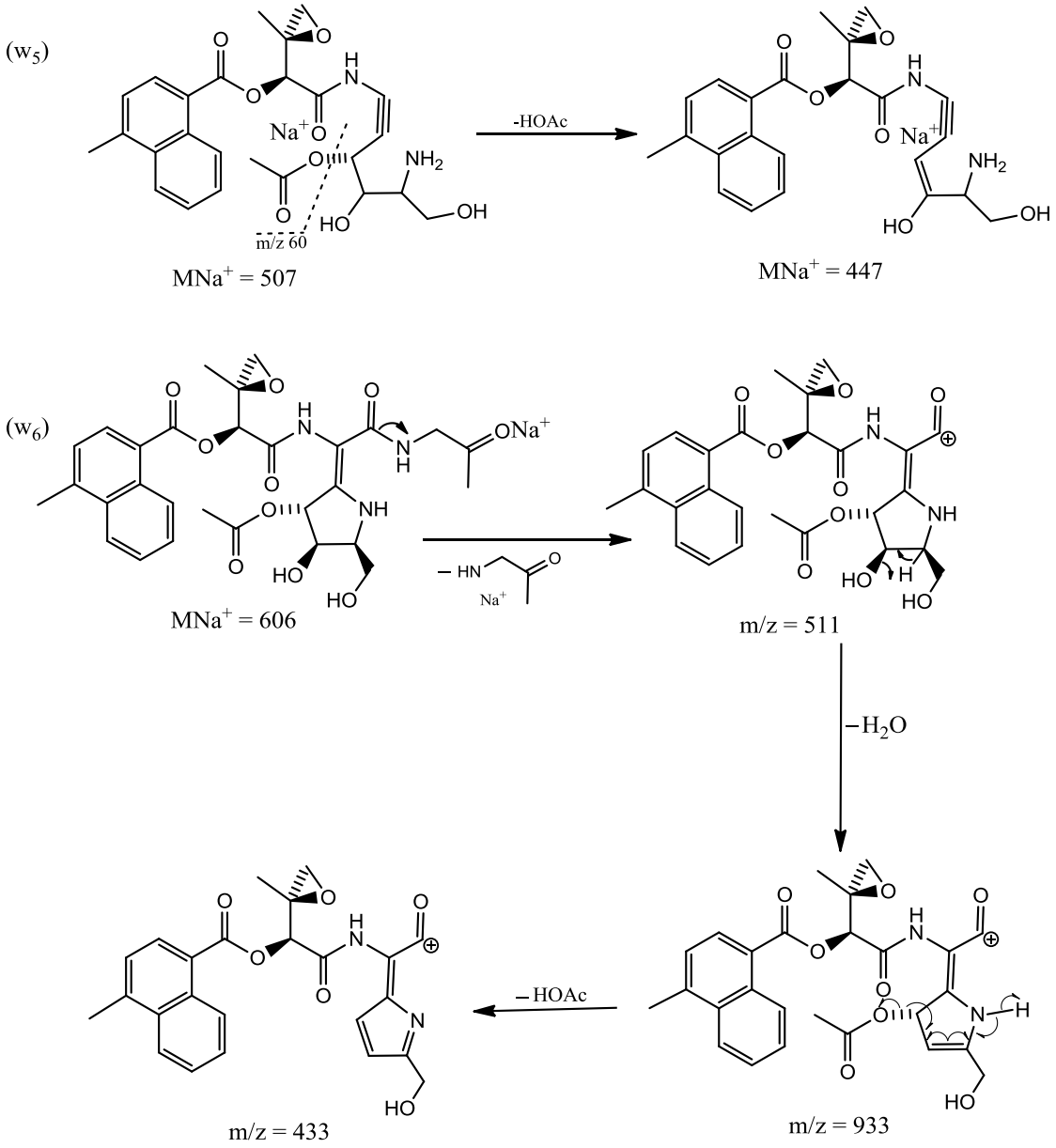

Scheme 4.14: Paths (w_5) and (w_6).

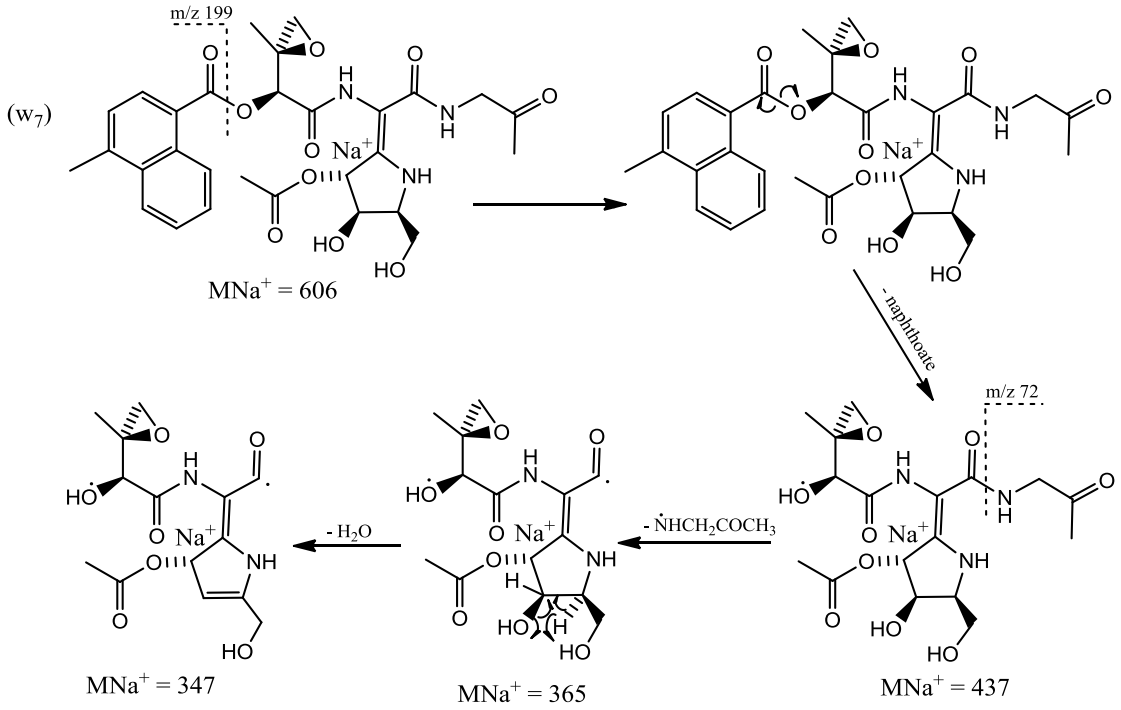

Scheme 4.14: Path (w_7).

Scheme 4.14 describes the fragmentation patterns of hydrolysed azinomycin A analogue (m/z = 606) feeding from 4-methyl-1-napthoic acid.

4.3 Discussion

4.3.1 Novel azinomycin A analogues from precursor-directed biosynthesis

Our data are in agreement with the conclusion that azinomycin A and its analogues were produced after feeding compounds 1-naphthoic acid, 4-methyl-1-naphthoic acid, 4-fluoro-1-naphthoic acid and 3-methoxy-1-naphthoic acid (**section 4.2.3**, **Table 4.2**) to *S. sahachiroi* fermentation cultures. Prep HPLC isolation of azinomycin A and its analogues afforded very low yields that were not enough for NMR characterisation (**section 4.2.8**, **Figures 4.27-4.32**). The low yields of native azinomycin A and its analogues could be explained by the necessity of further optimisation of the incubation temperature and the medium pH, by the requirement of testing *S. sahachiroi*'s growth and azinomycins production in wider range of carbon and nitrogen sources and by the need of optimisation of inoculum's age and size.

Some contaminants were found within the purified fractions and could be of exogenous origin. These contaminants might have been extracted from plastic pipette tips during sample preparation using chloroform following prep HPLC isolation (**Figures 4.28-4.30**). Also they could have come up from the same prep HPLC crude extracts.

In the absence of NMR data, we used tandem mass spectrometry to characterise and confirm the identities of the purified compounds with m/z 636 and 618 (**Figures 4.27** and **4.28** respectively) as azinomycin A and its hydrolysed derivative. The results shown in **Figure 4.33, scheme 4.10** and **Figure 4.34** conform to literature data (Yokoi *et al*., 1986 and Zhao *et al*., 2008) with respect to the loss of acetyl group ($C_2H_4O_2$), naphthoate fragment (m/z 199) and the aminoacetone ($NHCH_2COCH_3$). Therefore the purified compounds are azinomycin A (m/z 618, $M+Na^+$) and the hydrolysed form of azinomycin A (m/z 636, $M+Na^+$). The fragmentation mechanisms of all the fragments in **Figure 4.33** are fully described in **scheme 4.10**. A comparison between the fragmentation patterns of azinomycin A and its hydrolysed derivative (**Figure 4.33**) and the fragmentation patterns of all the novel analogues (**Figures 4.35-4.42**) reveals a strong correlation with consistent mass shifts that match the structural

changes in the naphthoic acids. The fragmentation mechanisms of the known natural products and these new analogues must be similar and are described in **schemes 4.11-4.14**. Therefore the novel metabolites are most likely analogues of azinomycin A differing only in the substituents within the naphthoate region.

Results (**Figure 4.11)** of prep HPLC from feeding 1-naphthoic acid show a new peak at 58.1-58.8 min with m/z 574 for the sodium adduct. This mass is consistent with incorporation of the naphthoic acid analogue into azinomycin A biosynthesis pathway. Previous biosynthetic studies (Ding *et al*., 2010) showed the incorporation and adenylation of a range of commercially available naphthoic acid analogues by NRPS enzyme AziA1. By analogy, our results indicate the incorporation and activation of 1-naphthoic acid by the same adenylation domain of AziA1 and then being transferred to peptidyl carrier protein (PCP) domain of AziA1 for starting the assembly of azinomycin A analogue fragments. Additionally, the azinomycin analogue with m/z 574 has been produced after incorporation of 1-naphthoic acid directly into the azinomycin A biosynthesis pathway without hydroxylation and methylation. This implies that the cytochrome P450 processes the unnatural 1-naphthoic acid substrate less efficiently than its native substrate.
Prep HPLC chromatogram (**Figure 4.11**, **(**A6)) also reveals the presence of an exciting peak at 62.9-63.4 min with m/z 229 (**Figure 4.11**, B6a) and might be an interesting metabolite from *S. sahachiroi*'s extract or simply a cross contaminant encountered during the experimental work.

Results (**Figure 4.10)** of prep HPLC from feeding 1-naphthoic acid show a new peak at 39.2-40.0 min with m/z 590 for the sodium adduct. This mass is consistent with incorporation of the naphthoic acid analogue into azinomycin A biosynthesis pathway with an extra oxygen atom. This must be due to hydroxylation of 1-naphthoic acid by a cytochrome P450 hydroxylase prior to its incorporation into the azinomycin A analogue. This explanation is in analogy with previous experimental facts established by many authors. In fact, previous biosynthesis studies (Corre and Lowden, 2004a; Zhao *et al*., 2008; Ding *et al*., 2010) have confirmed similar results. The authors have established and confirmed that the naphthoate fragment (5-methyl-1-naphthoic acid) of azinomycins A and B is being hydroxylated and methylated before being incorporated into the complete azinomycin skeleton.

The precise position of the hydroxylation could be predicted (but not confirmed) to have occurred in position C3' of the naphthalene ring (similar to Azinomycin A biosynthesis) (Zhao *et al*., 2008). Support for this hypothesis comes from the presence in the same fermentation of an analogue with sodium adduct m/z 604 (**Figure 4.13**) consistent with the incorporation of 1-naphthoic acid into azinomycin A biosynthesis pathway after hydroxylation and then methylation. Feeding of 3-methoxy-1-napthoic acid (**Figure 4.19,** (B17)) forms a new metabolite with m/z 604 consistent with the incorporation of the fed precursor into the azinomycin A biosynthesis pathway. Both of these metabolites with m/z 604 have the same LCMS retention time when run using the same conditions. It is very likely that the incorporation of hydroxyl and methyl groups into 1-naphthoic acid has been done by the same tailoring enzymes (cytochrome P450 hydroxylase AziB1 and *O*-methyl transferase AziB2 respectively) as that involved in the modifications to 5-methyl-naphthoic acid prior to incorporation into the native azinomycin skeleton (Zhao *et al*, 2008; Ding *et al*., 2010).

Results (**Figures 4.15)** of prep HPLC from feeding 4-methyl-1-napthoic acid show a new peak at 75.2-76.1.0 min with m/z 588 for the sodium adduct. This mass is consistent with incorporation of the 4-methyl-1-naphthoic acid analogue into azinomycin A biosynthesis pathway. Additional new peak at R_t = 23.5-24.0 min with m/z 604 (**Figure 4.16**) has MS data consistent with incorporation of the 4-methyl-1-naphthoic acid analogue into azinomycin A biosynthesis pathway after hydroxylation, most probably at C3′ position and by the same cytochrome P450 involved in azinomycin biosynthesis. Data (**Figure 4.17)** from feeding 4-fluoro-1-napthoic acid show a new peak at R_t = 84.4-85.9 min with m/z 592 consistent with incorporation of the 4-fluoro -1-naphthoic acid analogue into azinomycin A biosynthesis pathway. Two extra analogues (4-methyl-1-naphthoic acid and 4-Fluoro-1-naphthoic acid) of the natural starter unit, 3-methoxy-5-methyl-naphthoic acid were activated and incorporated by AziA1 to produce azinomycin analogues suggesting a potential for production by precursor-directed biosynthesis of more new azinomycin analogues differing in their naphthoic acid moieties.

Together, these results begin to reveal the extent of substrate flexibility of the enzymes in the azinomycin biosynthetic gene cluster. The NRPS-related enzyme AziA1 is expected to activate the naphthoic acid intermediate by initial reaction with ATP to form an acyl adenylate, which then reacts with the SH group of a phosphopantetheinyl cofactor on the peptidyl carrier protein domain of AziA1. The enzyme-bound naphthoate is then combined with the other building blocks by the action of the other NRPS enzymes.

The results presented in this chapter demonstrate that AziA1 is able to activate alternative naphthoic acid substrates. Our results are complementary to those of Ding (Ding *et al*., 2010) who found that AziA1 could activate a variety of substituted naphthoic acids *in vitro*. Our results also show that the subsequent enzyme reactions in azinomycin biosynthesis can also tolerate structural changes in the naphthoate group.

4.3.2 Chlorinated metabolites

In previous work conducted by Dr. Jason Taylor, a postdoctoral fellow, it was shown that fermentation extracts without adding any naphthoic acids, contained apparently chlorinated azinomycins with $M+Na^+$ ions at m/z 654/656 consistent with azinomycin A analogue and 672/674 consistent with azinomycin B analogue.

The origin of the chlorine atoms in the azinomycin A analogue for m/z 628/630 **(Figure 4.18)** is not known. It may be just an artefact of sample preparation *via* decomposition of chloroform, or it may arise from a side reaction of the azinomycin A analogue with chloride in the fermentation medium. However, a biosynthetic origin of chlorine is possible. In this case, if the latter was the case, could the new chlorinated metabolite act as a biosynthetic precursor to the aziridine or epoxide ring? There is a number of well-known examples of chlorinated natural products such as vancomycin, chlortetracycline (Vaillancourt *et al*., 2006) and 593A (Gribble GW, 2010). The structure of 593A is shown in **Figure 4.43.**

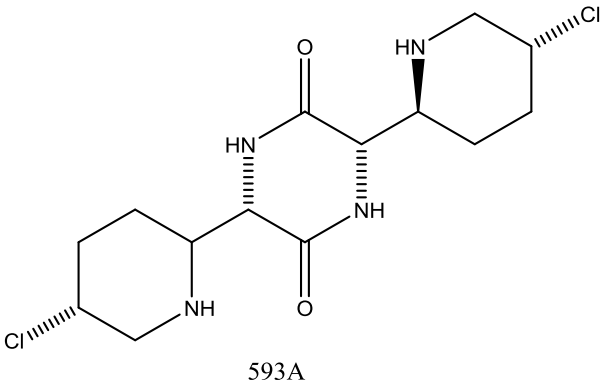

593A

Figure 4.43: Chemical **s**tructure of 593A.

The fragmentation patterns shown in **Figure 4.39** correlate closely with those in **Figure 4.38** with an 18 mass unit difference between each correlated pair of daughter ions (**Table 4.5)** and could be explained by the addition of HCl. Three chlorinated isomers were suggested (**F_1-F_3**, **Figure 4.44**). Isomer **F_2** is assumed to be the chlorinated metabolite with m/z 628/630 as the presumed structure explains well most of the fragmentation patterns shown in **Figure 4.39**.

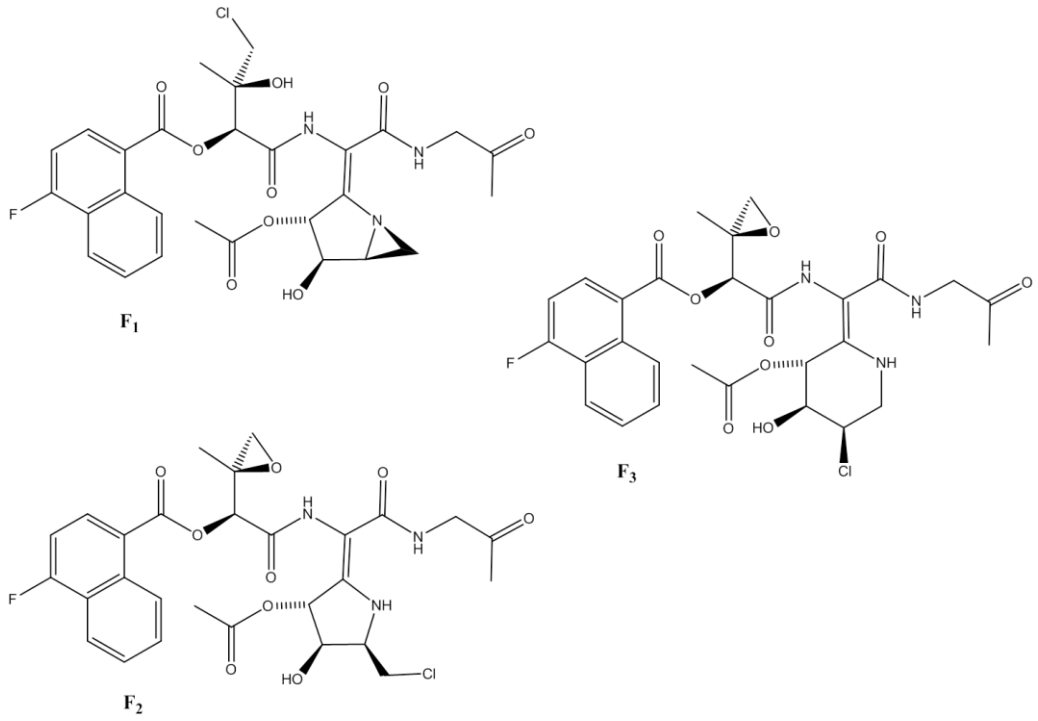

Figure 4.44: Suggestion of possible chlorinated analogues of azinomycin A subsequent to feeding 4-fluoro-1-naphthoic acid to *S. sahachiroi*.

Chapter 5: Overall Conclusions and Future Work

The results presented in this project provide evidence that precursor-directed biosynthesis is a useful way to prepare azinomycin A analogues not encountered in nature. The successful incorporation of synthetic and commercially available unnatural naphthoic acid (NPA) substrates demonstrates convincingly that there is a degree of substrate flexibility in azinomycin A biosynthesis (**Chapter 4**). The non-ribosomal peptide synthetase (NRPS) AziA1 that incorporates and activates 3-methoxy-5-methyl-NPA (the natural start unit for the azinomycin biosynthesis) must have flexibility.

We also observed biotransformation of a number of naphthoic acid analogues into their corresponding amides by *S. sahachiroi* (**Chapter 3**). This provides more evidence on the broad substrate specificity of the enzymes in *S. sahachiroi*.

Several of the observed azinomycin A analogues were isolated and purified (**Chapter 4**) using prep HPLC and then were characterised by diode array detection and electrospray tandem mass spectrometry. The low yields and persistence of impurities in the isolated fractions hampered further characterisation by 1D and 2D NMR. Biological studies could not yet be conducted for the same reasons.

The substrate flexibility of AziA1 and its tolerance to a range of NPA analogues could be extrapolated to other monocyclic substrates. For example, a variety of commercially available benzoic acid analogues (**Table 5.1**) could be fed to *S. sahachiroi* fermentation culture (in a similar fashion to NPA analogues) and the possible recognition, activation (by AziB, a type I iterative PKS) and tolerance (by AziA1) could be investigated by LCMS analysis.

Compound to be fed to *S. sahachiroi*	General strategy for feeding experiments
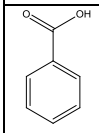 Benzoic acid	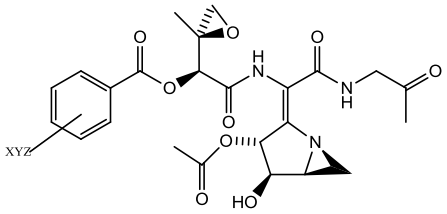 Azinomycin A analogues 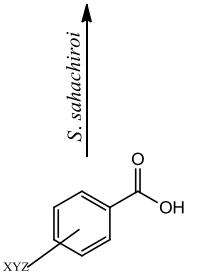 Benzoic acid analogues
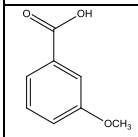 3-methoxybenzoic acid	
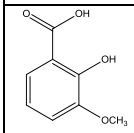 2-hydroxy-3-methoxybenzoic acid	
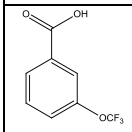 3-(trifluoromethoxy)benzoic acid	
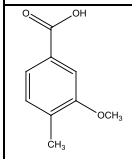 3-methoxy-4-methylbenzoic acid	
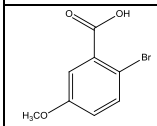 2-bromo-5-methoxybenzoic acid	

Table 5.1: Proposed benzoic acid analogues for future feeding to *S. sahachiroi* culture broth.

All attempts to characterise azinomycin A and its analogues by NMR were unsuccessful due to the low yield products isolated by Prep HPLC (**Chapter 4**). Therefore, it is essential to improve *S. sahachiroi* growth conditions (and may be the separation techniques as well) to enable, not only a consistent and reliable production of azinomycin A, but production of azinomycin B as well and their respective analogues in reasonable yields. For that purpose and in order to determine the best carbon and nitrogen source to provide the maximum yield of azinomycins by *S. sahachiroi*, it is possible to substitute the original glucose and yeast extract in GYM medium with other carbon and nitrogen sources. For example, glucose could be substituted with fructose, galactose, ribose, sucrose, maltose or lactose and yeast extract with ammonium sulphate, ammonium chloride, sodium nitrate, urea, peptone, beef extract or soybean. Furthermore, bacterial growth conditions may be further optimised by increasing the agitation speed to 300 rpm as it will provide higher

oxygen concentrations in *S. sahachiroi* fermentation flasks which, is essential for achieving a better production performance (Loptanev *et al*., 1973; Chen and Wilde, 1990).

Precursor-directed biosynthesis (PDB) proved to be a promising approach to generate novel analogues of azinomycin A (**Chapter 4**). This technique may be extended to a mutant strain of *S. Streptomyces* by inactivating *aziB*, the gene encoding for the enzyme AziB, a type I iterative PKS responsible for the production of 5-methyl-NPA. Therefore, it would be possible to biosynthesise only the required azinomycin A analogues by supplementing the resultant mutant with analogues of 5-methyl-NPA as illustrated in **Figure 5.1**.

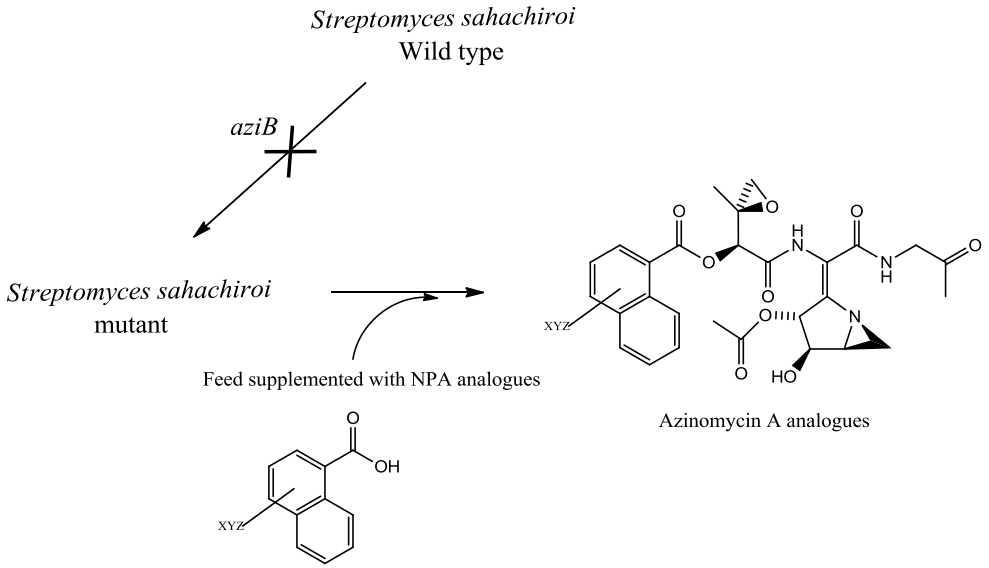

Figure 5.1: Mutasynthesis of azinomycin A analogues using NPA analogues supplement.

Mutasynthesis utilises a mutant strain of *S. sahachiroi* Wild type in conjunction with feeding of chemically modified 5-methyl-NPA intermediates. The implementation of this technique will enable the production of azinomycin analogues exclusively with a possible improvement in the final yield production.

Chapter 6: References

Ahlert, J., Shepard, E., Lomovskaya, N., Zazopoulos, E., Staffa, A., Bachmann, B.O., Huang, k., Fonstein, L., Czisnyl, A., Whitwam, R.E., Farnet, C.M. and Thorson, J.S.: The calicheamicin gene cluster and its iterative type I enediyne PKS. *Science*, **2002**, *297*(*5584*), 1173-1176.

Anderson, M.G., Kibby, J.J., Rickards, R.W. and Rothschild, J.M.: Biosynthesis of the mitomycin antibiotics from 3-amino-5-hydroxybenzoic acid. *J. Chem. Soc. Chem. Commun*., **1980**, (*24*), 1277-1278.

Ando, T., Ishii, M., Kajiura, T., Kameyama, T., Miwa, K. and Sugiura, Y.: A new non-protein enediyne antibiotic N1999A2: Unique enediyne chromophore similar to neocarzinostatin and DNA cleavage feature. *Tetrahedron Lett*., **1998**, *39*(*36*), 6495-6498.

Argoudelis, A.D., Reusser, F., Whaley, H.A., Baczynskyj, L., Mizsak, S.A. and Wnuk, R.J.: Antibiotics produced by *Streptomyces ficellus*. I. Ficellomycin. *J. Antibiot*., **1976**, *29*(*10*), 1001-1006.

Armstrong, R.W., Salvati, M.E. and Nguyen, M.: Novel interstrand cross-links induced by the antitumor antibiotic carzinophilin/azinomycin B. *J. Am. Chem. Soc.*, **1992**, *114(8)*, 3144-3145.

Barrios-Gonzales, J., Fernandez, F.J., Tomasini, A. and Mejia, A.: Secondary Metabolites Production by Solid-State Fermentation. *MJM*., **2005**, *1(1)*, 1-6. Review article.

Begleiter A.: Clinical applications of quinone-containing alkylating agents. *Front. Biosci*., **2000**, *5*, e153-171.

Bentley, R. and Bennett, J.W.: Constructing polyketides: from collie to combinatorial biosynthesis. *Annu. Rev. Microbiol*., **1999**, *53*, 411-446.

Bérdy, J.: Bioactive microbial metabolites. *J. Antibiot*., **2005**, *58(1)*, 1-26. Review Article.

Bezanson, G.S. and Vining, L.C.: Studies on the biosynthesis of mitomycin C by *Streptomyces verticillatus*. *Can. J. Biochem*., **1971**, *49*(*8*), 911-918.

Birch, A.J., Massy-Westropp, R.A. and Moye, C.J.: Studies in relation to biosynthesis. VII. 2-Hydroxy-6-methylbenzoic acid in *Penicillium griseofulvum* Diercks. *Aus. J. Chem*., **1955**, *8*(*4*), 539-544.

Birkinshaw, J.H., Bracken, A. Morgan, E.N. and Raistrick, H.: Studies in the biochemistry of micro-organisms. 78. The molecular constitution of mycophenolic acid, a metabolic product of *Penicillium brevi-compactum* Dierckx. Part 2. Possible structural formulae for mycophenolic acid. *Biochem. J*., **1948**, *43(2)*, 216-223.

Böhm, H.J., David, B., Bendels, S., Kansy, M., Kuhn, B., Müller, K., Obst-Sander, U. and Stahl, M.: Fluorine in medicinal chemistry. *ChemBioChem*., **2004**, *5*(*5*), 637-643.

Borissow, C.N., Graham, C.L., Syvitski, R.T., Reid, T.R., Blay, J. and Jakeman, D.L.: Stereochemical integrity of oxazolone ring-containing jadomycins. *ChemBioChem*., **2007**, *8*(*10*), 1198-1203.

Bormann, C., Lauer, B. Kálmánczhelyi, A., Süssmuth, R. and Jung, G.: Novel nikkomycins Lx and Lz produced by genetically engineered *Streptomyces tendae* Tü901. *J. Antibiot*., **1999**, *52(2)*, 102-108.

Brenno, A.D.N. and Alexandre, A.M.L.: Recent developments in the chemistry of deoxyribonucleic acid (DNA) intercalators: Principles, design, synthesis, applications and trends. *Molecules*, **2009**, *14(5)*, 1725-1746.

Brouwer, N., Liu, Q., Harrington, D., Kohen, J., Vemulpad, S., Jamie, J., Randall, M. and Randall, D.: An ethnopharmacological study of medicinal plants in new south Wales. *Molecules*, **2005**, *10(10)*, 1252-1262.

Brunati, M., Marinelli, F., Bertolini, C., Gandolfi, R., Daffonchio, D. and Molinari, F.: Biotransformations of cinnamic and ferulic acid with actinomycetes. *Enzyme Microbial. Technol*., **2004,** *34(1)*, 3-9.

Bushley, K.E. and Turgeon, B.G.: Phylogenomics reveals subfamilies of fungal nonribosomal peptide synthetases and their evolutionary relationships. *BMC. Evol. Biol*., **2010**, *10(26)*.

Cane, D.E. and Walsh, C.T.: The parallel and convergent universes of polyketide synthases and nonribosomal peptide synthetases. *Chem. Biol*., **1999,** *6*(*12*), 319-325.

Cane, D.E., Walsh, C.T. and Khosla, C.: Harnessing the biosynthetic code: combinations, permutations, and mutations. *Science*, **1998,** *282* (*5386*), 63-68.

Carmichael, W.W.: Cyanobacteria secondary metabolites--the cyanotoxins. *J. Appl. Bacteriol*., **1992**, *72(6)*, 445-459.

Chan, Y.A., Podevels, A.M., kevany, B.M. and Thomas, M.G.: Biosynthesis of polyketide synthase extender units. *Nat. Prod. Rep*., **2009**, *26*(*1*), 90-114. Review Article.

Chen, H.C. and Wilde, F.: The effect of dissolved oxygen and aeration rate on antibiotic production of Streptomyces fradiae. *Biotechnol. Bioeng*., **1990**, *37*(*6*), 591-595.

Coleman, R.S., Christopher, H.B., Antonio, N., Robert, W.B. and Edgar, S.D.: Role of the azinomycin naphthoate and central amide in sequence-dependent DNA alkylation and cytotoxicity of epoxide-bearing substructures. *Org. Lett*., **2002b**, *4(20)*, 3545-3548.

Coleman, R.S., Li, J. and Navarro, A.: Total synthesis of azinomycin A. *Angew. Chem. Int. Ed. Engl.*, **2001**, *40(9)*, 1736-1739.

Coleman, R.S., Ronelito, J. P., Christopher, H. B. and Antonio, N.: Studies on the mechanism of action of azinomycin B: Definition of regioselectivity and sequence selectivity of DNA cross-link formation and clarification of the role of the naphthoate. *J. Am. Chem. Soc*., **2002a**, *124*(*44*), 13008-13017.

Collie, J. N. and Myers, W. S.: VII-The formation of orcinol and other condensation products from dehydracetic acid. *J. Chem. Soc*., **1893**, *63*, 122-128.

Collie, J.N.: CLXXI.-Derivatives of the multiple keten group. *J. Am. Chem. Soc.*, **1907**, *91*, 1806-1813.

Cooke, H.A., Zhang, J., Griffin, M.A., Nonaka, K., Van, L.S.G., Shen, B. and Bruner, S.D.: Characterisation of NcsB2 as a promiscuous naphthoic acid/coenzyme A ligase integral to the biosynthesis of the enediyne antitumor antibiotic neocarzinostatin. *J. Chem. Soc*., **2007**, *129*(*25*), 7728-7729.

Corre, C. and Lowden, P.A.S.: The first biosynthetic studies of the azinomycins: acetate incorporation into azinomycin B. *Chem. Commun*., **2004a**, *44(8)*, 990-991.

Corre, C., Landreau, C.A.S., Shipman, M. and Lowden, P.A.S.: Biosynthetic studies on the azinomycins: The pathway to the naphthoate fragment. *Chem. Commun.*, **2004b**, (*22*), 2600-2601.

Cottreau, K.M., Spencer, C., Wentzell, J.R., Graham, C.L., Borissow, C.N., Jakeman, D.L. and McFarland, S.A.: Diverse DNA-cleaving capacities of the jadomycins through precursor-directed biosynthesis. *Org. Lett*., **2010**, *12*(*6*), 1172-1175.

Das, S. and Rosazza, J.P.N.: Microbial and enzymatic transformations of flavonoids. *J. Nat. Prod*., **2006**, *69*(*3*), 499-508.

Den Hollander, J.A., Behar, K.L. and Shulam, R.G.: ^{13}C NMR study of transamination during acetate utilization by *Saccharomyces cerevisiae*. *Proc. Natl. Acad. Sci. USA.*, **1981**, *78*(*5*), 2693-2697.

Ding, W., Deng, W., Tang, M., Zhang, Q., Tang, G., Bi, Y. and Liu, W.: Biosynthesis of 3-methoxy-5-methyl naphthoic acid and its incorporation into the antitumor antibiotic azinomycin B. *Mol. Biosyst*., **2010**, *6(6)*, 1071-1081.

Donadio, S. and Katz, L.: Organisation of the Enzymatic Domains in the Multifunctional Polyketide Synthase Involved in Erythromycin Formation in Saccharopolyspora Erythraea. *Gene*, **1992**, *111*(*1*), 51-60.

Dozen, Y. and Fujishima, S.: "Syntheses of naphthalenepolycarboxylic acids by the aqueous sodium bichromate oxidation of methylnaphthonitriles". *J. Synth. Org. Chem. Jpn*., **1972**, *30*(*2*), 150-153.

Edo, K., Mizugaki, M., Koide, Y., Seto, H., Furihata, K., Otake, N. and Ishida, N.: The structure of neocarzinostatin chromphore possessing a novel bicycle [7,3,0]dodecadiyne system. *Tetrahedron Lett.*, **1985**, *26*(*3*), 331-334.

Evangelopoulos, D. and S. Bhakta.: Rapid methods for testing inhibitors of mycobacterial growth. *Methods Mol. Biol*., **2010,** *642*, 193-201.

Fickers, P.: Antibiotic compounds from *Bacillus*: Why are they so amazing? *Am. J. Biochem. Biotech*., **2012**, *8*(*1*), 40-46.

Fischbach, M.A. and Walsh, C.T.: Assembly-Line Enzymology for Polyketide and Nonribosomal Peptide Antibiotics: Logic, Machinery, and Mechanisms. *Chem. Rev*., **2006**, *106*(*8*), 3468-3496. Review Article.

Flores-Sanchez, I.J. and Verpoorte, R.: Plant polyketide synthases: a fascinating group of enzymes. *Plant. Physiol. Biochem*., **2009**, *47*(*3*), 167-174. Review Article.

Foulke-Abel, J., Agbo, H., Zhang, H., Mori, S. and Watanabe, C.M.H: Mode of action and biosynthesis of the azabicycle-containing natural products azinomycin and ficellomycin. *Nat. Prod. Rep*., **2011a**, *28(4)*, 693-704.

Foulke-Abel, J., Kelly, G.T., Zhang, H. and Watanabe, C.M.H.: Characterization of AziR, a resistance protein of the DNA cross-linking agent azinomycin B. *Mol. Biosyst*., **2011b**, *7(9)*, 2563-2570.

Frenzel, R., Domschke, G., Roessler, L. and Mayer, R.: "Carbamidation of aromatic compounds with isocyanatotrimethylsilane". *Journal für Praktische Chemie*/*Chemiker-Zeitung*., **1993**, *335*(*6*), 558-560.

Fujiwara, T. and Saito, I.: Highly efficient DNA interstrand crossling induced by an antitumor antibiotic, carzinophilin. *Tetrahedron Lett*., **1999**, *40(2)*, 315-318.

Gaisser, S., Trefzer, A., Stockert, S., Kirschning, A. and Bechthold, A.: Cloning of an avilamycin biosynthetic gene cluster from Streptomyces viridochromogenes Tü57. *J. Bacteriol*., **1997**, *179*(*20*), 6271-6278.

Galm, U., Hager, M.H., Van Lanen, S.G., Ju, J., Thorson, J.S. and Shen, B.: Antitumor antibiotics: bleomycin, enediynes, and mitomycin. *Chem. Rev*., **2005**, *105*(*2*), 739-758. Review Article.

Gaudreau, C., Girouard, Y., Ringuette, L. and Tsimiklis, C.: Comparison of disk diffusion and agar dilution methods for erythromycin and ciprofloxacin susceptibility testing of *Campylobacter jejuni* subsp. *jejuni*. *Antimicrob. Agents Chemother*., **2007**, *51(4)*, 1524-1526.

George, G., Yarbrough, D.P., Taylor, R.T., Rowlands, M.S., Crawford, M.S. and Linda, L.L.: Screening microbial metabolites for new drugs theoretical and practical issues. *J. Antibiot*., **1993,** *46(4)*, 535- 44. Review Article.

Glawischnig, E., Gierl, A., Tomas, A., Bacher, A. and Eisenreich, W.: Retrobiosynthetic nuclear magnetic resonance analysis of amino acid biosynthesis and intermediary metabolism: metabolic flux in developing maize kernels. *Plant Physiol*., **2001**, *125*(*3*), 1178-1186.

Goss, R.J., Shankar, S. and Fayad, A.A.: The generation of "unnatural" products: synthetic biology meets synthetic chemistry. *Nat. Prod. Rep*., **2012**, *29*(*8*), 870-889. Review Article.

Gribble, G.W.: Naturally occurring organohalogen compounds - A comprehensive update (Progress in the chemistry of organic natural products vol. 91). **2010**, pp: 220-230. Springer-Verlag/Wien. Germany.

Grünewald, J. and Mohmed, A.M.: Chemoenzymatic and template-directed synthesis of bioactive macrocyclic peptides. *Microbiol. Mol. Biol. Rev*., **2006**, *70*(*1*), 121-146.

Gummert, J.F., Tuija, I. And Randall, E.M.: Newer immunosuppressive drugs: A Review. *J. Am. Soc. Nephrol*., **1999**, *10*(*6*), 1366-1380. Review Article.

Gurram, S.P., Rama, P., Sivadevuni, G. and Solipuram, M.R.: Oxidation of meloxicam by Streptomyces griseus. *I.J.B*., 2**009**, *7*(*3*), 209-214.

Hartley, J.A., Hazrati, A., Kelland, L.R., Khanim, R., Shipman, M., Suzenet, F. and Walker, L.F.: A synthetic azinomycin analogue with demonstrated DNA cross-linking activity: Insights into the mechanism of action of this class of antitumor agent. *Angew. Chem. Int. Ed. Engl*., **2000**, *39*(*19*), 3467-3470.

Hashimoto, M., Matsumoto, M., Yamada, K. and Terashima, S.: Synthetic studies of carzinophilin. Part 4: Chemical and biological properties of carzinophilin analogues. *Tetrahedron*, **2003**, *59(17)*, 3089-3097.

Hata, T. and Sugawara, R.: Mitomycin, a new antibiotic from Streptomyces. II. Description of the strain. *J. Antibiot*. (Tokyo), **1956b**, *9*(*4*), 147-151.

Hata, T., Hoshi, T., Kanamori, K., Matsumae, A., Sanno, Y., Shima, T. and Sugawara, R.: Mitomycin, a new antibiotic from Streptomyces. I. *J. Antibiot*. (Tokyo), **1956a**, *9*(*4*), 141-146.

Hata, T., Koga, F., Sano, Y., Kanamori, K., Matsumae, A., Sugawara, R., Hoshi, T. and Shima, T.: 'Carzinophilin, a new tumor inhibitory substance produced by Streptomyces'". *J. Antibiot*., **1954**, *SER***.** *A*, 107-112.

Hejblum, G., Jarlier, V., Grosset, J. and Aurengo, A.: Automated interpretation of disk diffusion antibiotic susceptibility tests with the radial profile analysis algorithm. *J. Clin. Microbiol*., **1993**, *31(9)*, 2396-2401.

Hertweck, C.: The biosynthetic logic of polyketide diversity. *Angew. Chem. Int. Ed*., **2009**, *48*(*26*), 4688-4716.

Hill, A.M. and Thompson, B.L.: Novel soraphens from precursor directed biosynthesis. *Chem. Commun.*, **2003**, (*12*), 1360-1361.

Hiroshi, Y. and Ryoichi, K.: Antibiotic resistance in bacteria and its future for novel antibiotic development. *Biosci. Biotechnol. Biochem.*, **2006**, *70(5)*, 1060-1075.

Hodginson,T.J. and Shipman, M.: Chemical synthesis and mode of action of the azinomycins. *Tetrahedron*, **2001**, *57(21)*, 4467-4488.

Hopwood, D.A. and Sherman, D.H.: Molecular genetics of polyketides and its comparison to fatty acid biosynthesis. *Annu. Rev. Genet.*, **1990**, *24*, 37-66. Review Article.

Hopwood, D.A.: Forty years of genetics with Streptomyces : from *in vivo* through *in vitro* to *in silico*. *Microbiology*, **1999**, *145(9)*, 2183-2202. Review Article.

Hopwood, D.A.: Genetic contributions to understanding polyketide synthases. *Chem. Rev.*, **1997**, *97*(*7*), 2465-2497. Review Article.

Hornemann, U. and Aikman, M.J.: Mitomycin biosynthesis by *Streptomyces verticillatus*. Incorporation of the amino-group of D-[15N]glucosamine into the aziridine ring of mitomycin B. *J. Chem. Soc. Chem. Commun.*, **1973**, (*3*), 88-89.

Hornemann, U. and Cloyd, J.D.: Studies on the biosynthesis of the mitomycin antibiotics by *Streptomyces verticillatus*. *J. Chem. Soc. Chem. Commun.*, **1971**, (*7*), 301-302.

Hornemann, U. and Heins, M.J.: Stereochemical relationship between mitomycins A, B, and C. *J. Org. Chem.*, **1983**, *50*(*8*), 1301-1302.

Hornemann, U., Eggert, J.H. and Honor, D.P.: Role of D-[4-14C]erythrose and [3-14C]pyruvate in the biosynthesis of the meta-C-C6-N unit of the mitomycin antibiotics in *Streptomyces verticillatus*. *J. Chem. Soc. Chem. Commun.*, **1980**, (*1*), 11-13.

Hornemann, U., Kehrer, J.P. and Eggert, J.H.: Pyruvic acid and D-glucose as precursors in mitomycin biosynthesis by *Streptomyces verticillatus*. *J. Chem. Soc. Chem. Commun.*, **1974b**, (*24*), 1045-1046.

Hornemann, U., Kehrer, J.P., Nunez, C.S. and Ranieri, R.L.: D-glucosamine and L-citrulline, precursors in mitomycin biosynthesis by *Streptomyces verticillatus*. *J. Am. Chem. Soc.*, **1974a**, *96*(*1*), 320-322.

IG Farben Industrie AG.: "An improved process for converting cyannaphthalene-sulphonic acids, and products of conversion derived therefrom". Patent GB296010 (**1927**).

Ishida, N., Miyazaki, K., Kumagai, K. and Rikimaru, M.: Neocarzinostatin, an antitumor antibiotic of high molecular weight. Isolation, physiochemical properties and biological activities. *J. Antibiot*. (Tokyo), **1965**, *18*, 68-76.

Ishizeki, S., Ohtsuka, M., Irinoda, K., Kukita, K., Nagaoka, K. and Nakashima, T.: Azionomycins A and B, new antitumor antibiotics. III. Antitumor activity. *J. Antibiot*. (Tokyo), **1987**, *40*(*1*), 60-65.

Ismail, F.M., Levitsky, D.O. and Dembitsky, V.M.: Aziridine alkaloids as potential therapeutic agents. *Eur. J. Med. Chem.*, **2009**, *44*(*9*), 3373-3387. Review Article.

Iwao, O.: Use of fluorine in the medicinal chemistry and chemical biology of bioactive compounds – A case study on fluorinated Taxane anticancer agents. *ChemBioChem*., **2004,** *5(5)*, 628-635.

Iyer, V.N. and Szybalski, W.: A molecular mechanism of mitomycin action: Linking of complementary DNA strands. *Proc. Natl. Acad. Sci. USA*., **1963**, *50*(*2*), 355-362.

Iyer, V.N. and Szybalski, W.: Mitomycins and porfiromycin: Chemical mechanism of activation and cross-linking of DNA. *Science*, **1964**, *145*(*3627*), 55-58.

Jekkel, A.; Barta, I.; Boros, S.; Süt"o, J.; Horváth, Gy.; Szabó, Zs.; and Ambrus, G.: Microbial transformation of mycophenolic acid Part II. *J. Mol. Catal. B*: *Enzym.* **2002**, *19(20)*, 209-214.

Jorgensen, J.H. and Ferraro, M.J.: Antimicrobial Susceptibility Testing: General Principles and Contemporary Practices. *Clin. Infect. Dis*., **1998**, *26(4)*, 973-988.

Kawashima, A. H., Seto, M.K., Uchida, K. and Otake, N.: Preparation of fluorinated antibiotics followed by ^{19}F NMR spectroscopyI. Fluorinated vulgamycins. *J. Antibiot*., **1985,** *38(11)*, 1499-1505.

Kawata, S., Ashizawa, S. and Hirama, M.: Synthetic study of kedarcidin chromophore: revised structure. *J. Am. Chem. Soc*., **1997**, *119*(*49*), 12012-12013.

Kelly, G.T, Liu, C., Smith III, R., Coleman, R.S. and Watanabe, C.M.H.: Cellular effects induced by the antitumor agent azinomycin B. *Chem. Biol*., **2006**, *13(5)*, 485-492.

Kelly, G.T., Sharma, V. and Watanabe, C.M.H.: An improved method for culturing Streptomyces sahachiroi: biosynthetic origin of the enol fragment of azinomycin B. *Bioorg. Chem*., **2008**, *36(1)*, 4-15.

Kennard, O.: DNA-drug interactions. *Pure App. Chem*., **1993**, *65(6)*, 1213-1222.

Kennedy, J.: Mutasynthesis, chemobiosynthesis, and back to semi-synthesis: combining synthetic chemistry and biosynthetic engineering for diversifying natural products. *Nat. Prod. Rep.*, **2008**, *25(1)*, 25-34.

Khaw, L.E., Böhm, G.A., Metcalfe, S., Staunton, J. and Leadlay, P.F.: Mutational biosynthesis of novel rapamycins by a strain of *Streptomyces hygroscopicus* NRRL 5491 disrupted in rapL, encoding a putative lysine cyclodeaminase. *J. Bacteriol.*, **1998**, *180*(*4*), 809-814.

Khosla, C., Tang, Y., Chen, A.Y., Schnarr, N.A. and Cane, D.E.: Structure and mechanism of the 6-deoxyerythronolide B synthase. *Annu. Rev. Biochem.*, **2007**, *76*, 195-221. Review Article.

Kibby, J.J., McDonald, I.A. and Rickards, R.W.: 3-amino-5-hydroxybenzoic acid as a key intermediate in ansamycin and maytansinoid biosynthesis. *J. Chem. Soc. Chem. Commun.*, **1980**, (*16*), 768-769.

Kim, C.G., Kirschning, A., Bergon, P., Zhou, P., Su, E., Sauerbrei, B., Ning, S., Ahn, Y., Breuer, M., Leistner, E. and Floss, H. G.: Biosynthesis of 3-Amino-5-hydroxybenzoic acid, the precursor of mC7N units in ansamycin antibiotics. *J. Am. Chem. Soc.* **1996**, *118*(*32*), 7486-7491.

Kim, C.G., Yu, T.W., Fryhle, C.B., Handa, S. and Floss, H.G.: 3-Amino-5-hydroxybenzoic acid synthase, the terminal enzyme in the formation of the precursor of mC7N Units in rifamycin and related antibiotics. *J. Biol. Chem.*, **1998**, *273*(*11*), 6030-6040.

Kirsch, E.J. and Korshalla, J.D.: Influence of biological methylation on the biosynthesis of mitomycin A. *J. Bacteriol.*, **1964**, *87*(*2*), 247-255.

Kleinkauf, H. and Von Dohren, H.: A nonribosomal system of peptide biosynthesis. *Eur. J. Biochem.*, **1996**, *236(2)***,** 335-351. Review Article.

Komoda, T., Sugiyama, Y. and Hirota, A.: Biosynthesis of tetrapetalones. *Org. Biomol. Chem.*, **2007**, *5*(*10*), 1615-1620.

Kuo, M.S., Yurek, D.A. and Mizsak, S.A.: Structure elucidation of ficellomycin. *J. Antibiot.* (*Tokyo*), **1989**, *42*(*3*), 357-360.

Lam, K.S.: New aspects on natural products in drug discovery. *Trends Microbiol.*, **2007**, *15(6)*, 279-289. Review Article.

Landreau, C.A.S., LePla, R.C., Shipman, M., Slawin, A.M.Z. and Hartley, J.A.: Delineating noncovalent interactions between the azinomycins and double-stranded DNA: Importance of the naphthalene substitution pattern on interstrand cross-linking efficiency. *Org. Lett.*, **2004**, *6(20)*, 3505-3507.

Lee, J.P., Tsao, S.W., He, X.G., Chang, C.J. and Floss, H.G.: Biosynthesis of naphthomycin A in *Streptomyces collinus*. *Can. J. Chem.*, **1994**, *72*(*1*), 182-187.

Leet, J.E., Schroeder, D.R., Hofstead, S.J., Golik, J., Colson, K.L., Huang, S., Klohr, S.E., Doyle, T.W. and Matson, J.A.: Kedarcidin, a new chromoprotein antitumor antibiotic: Structrue elucidation of kedarcidin chromophore. *J. Am. Chem. Soc*., **1992**, *114*(*20*), 7946-7948.

Ligon, J., Hill, S., Beck, J., Zirkle, R., Molnár, I., Zawodny, J., Money, S. and Schupp, T.: Characterization of the biosynthetic gene cluster for the antifungal polyketide soraphen A from *Sorangium cellulosum* So ce26. *Gene,* **2002**, *285*(*1-2*), 257-267.

Liu, C., Kelly, G.T. and Watanabe, C.M.H.: *In vitro* biosynthesis of the antitumor agent azinomycin B. *Org. Lett*., **2006**, *8(6)*, 1065-1068.

Liu, W., Christenson, S.D., Standage, S. and Shen, B.: Biosynthesis of the enediyne antitumor antibiotic C-1027. *Science,* **2002**, *297*(*5584*), 1170-1173.

Liu, W., Nonaka, K., Nie, L., Zhang, J., Christenson, S.D., Bae, J., Van, L.S.G., Zazopoulos, E., Farnet, C.M., Yang, C.F. and Shen, B.: The neocarzinostatin biosynthetic gene cluster from Streptomyces carzinostaticus ATCC 15944 involving two iterative type I polyketide synthases. *Chem. Biol*., **2005**, *12*(*3*), 293-302.

Lohman, J.R., Huang, S.X., Horsman, G.P., Dilfer, P.E., Huang, T., Chen, Y., Wendt-Pienkowski, K. and Shen, B.: Cloning and sequencing of the kedarcidin biosynthetic gene cluster from Streptoalloteichus sp. ATTCC53650 revealing new insights into biosynthesis of the enediyne family of antitumor antibitics. *Mol. Biosyst*., **2013**, *9*(*3*), 478-491.

Lopatnev, S.V., Kleiner, G.I. and Bylinkina, E.S.: Effect of aeration and agitation on the biosynthesis of nystatin. *Antibiotiki*, **1973**, *18*(*7*), 608-613.

Lown, J.W. and Majumdar, K.C.: Studies related to antitumor antibiotics. Part IX. Reactions of carzinophilin with DNA assayed by ethidium fluorescence. *Can. J. Biochem*., **1977**, *55(6)*, 630-635.

Luo, Y., Lin, S., Zhang, J., Cooke, H.A., Bruner, S.D. and Shen, B.: Regiospecific *O*-methylation of naphthoic acids catalysed by NcsB1, an O-methyltransferase involved in the biosynthesis of the enediyne antitumor antibiotic neocarzinostatin. *J. Biol. Chem*., **2008,** *283*(*21*), 14694-14702.

Malpartida, F. and Hopwood, D.A.: Molecular cloning of the whole biosynthetic pathway of a Streptomyces antibiotic and its expression in a heterologous hot. *Nature,* **1984**, *309*(*5967*), 462-464.

Manteca, A., Fernandez, M. and Sanchez, J.: Mycelium development in *Streptomyces antibioticus* ATCC11891 occurs in an orderly pattern which determines multiphase growth curves. *BMC. Microbiol*., **2005**, *5(51)*.

Mao, Y., Varoglu, M. and Sherman, D.H.: Molecular characterization and analysis of the biosynthetic gene cluster for the antitumor antibiotic mitomycin C from *Streptomyces lavendulae* NRRL 2564. *Chem*. *Biol*., **1999**, *6*(*4*), 251-263.

Mara, B., Flavia, M., Christina, B., Raffaella, G., Daniella, D. and Francesco, M.: Biotrasformation of cinnamic and ferulic acid with actinomycetes. *E.M.T*., **2004**, *34*(*1*), 3-9.

Mervyn, J.B.: Regulation of secondary metabolism in streptomycetes. *Curr*. *Opinion Microbiol*., **2005**, *8(2)*, 208-215.

Minow, Y., Araki, M. and Kanehisa, M.: Comprehensive analysis of distinctive polyketide and nonribosomal peptide structural motifs encoded in microbial genomes. *J*. *Mol*. *Biol*., **2007,** *368*(*5*), 1500-1517.

Molnár, I., Aparicio, J.F., Haydock, S.F., Khaw, L.E., Schwecke, T., König, A., Staunton, J. and Leadlay, P.F.: Organisation of the biosynthetic gene cluster for rapamycin in *Streptomyces hygroscopicus*: analysis of genes flanking the polyketide synthase. *Gene*, **1996**, *169*(*1*), 1-7.

Moran, M.A., Laura, T.R. and Roberte, H.: Evidence for Indigenous *Streptomyces* Populations in a Marine Environment Determined with a 16S rRNA Probe *Appl*. *Environ*. *Microbiol*., **1995**, *61(10)*, 3695-3700.

Murray, K.K.: Glossary of terms for separations coupled to mass spectrometry. *J*. *Chromat*. *A*, **2010**, *1217(25)*, 3922-3928.

Muth, W.L. and Nash, C.H.: Biosynthesis of Mycophenolic Acid: Purification and Characterization of *S*-Adenosyl-l-Methionine:Demethylmycophenolic Acid *O*-Methyltransferase. *Antimicrob*. *Agents*. *Chemother*., **1975**, *8(3)*, 321-327.

Nagaoka, K., Matsumoto, M., Oono, J., Yokoi, K., Ishizeki, S. and Nakashima, T.: Azinomycins A and B, new antitumor antibiotics I. Producing organism, fermentation, isolation and characterization. *J*. *Antibiot*., **1986**, *39(11)*, 1527-1532.

Nancy L.P., Arnold, L.D. and Mary, F.R.: The immediate precursor of the nitrogen-containing ring of rapamycin is free pipecolic acid. *Enzyme Microb*. *Technol*., **1993**, 15(*7*), 581-585.

Nicolaou, K.C., Vourloumis, D., Winssinger, N. and Baran, P.S.: The Art and Science of Total Synthesis at the Dawn of the Twenty-First Century. *Angew*. *Chem*. *Int*. *Ed*., **2000**, *39(1)*, 44-122. Review Article.

Ogasawara, Y. and Liu, H.: Biosynthetic studies of aziridine formation in azicemicins. *J*. *Am*. *Chem*. *Soc*., **2009**, *131*(*50*), 18066-18068.

Olano, C., Méndez, C. and Salas. J.A.: Antitumor Compounds from Marine Actinomycetes. *Mar*. *Drugs*., **2009**, *7(2)*, 210-248.

Osmialowska, R.B., Dagmara, J., Aleksandra, S.K., Keith, F.C. and Jolanta, Z.C.: Replisome Localization in Vegetative and Aerial Hyphae of *Streptomyces coelicolor*. *J. Bacteriol*., **2006**, *188(20)*, 7311-7316.

Ozcengiz, G. and Demain, A.L.: Rencent advances in the biosynthesis of penicillins, cephalosporins and clavams and its regulation. *Biotechnol. Adv*., **2013**, *31*(*2*), 287-311. Review Article.

Paz, M.M.: Reductive activation of mitomycin C by thiols: kinetics, mechanism, and biological implications. *Chem. Res. Toxicol*., **2009**, *22*(*10*), 1663-1668.

Reddy, B.S.P., Sharma, S.K. and Lown, J.W.: Recent Developments In Sequence Selective Minor Groove DNA Effectors. *Curr. Med. Chem*., **2001**, *8(5)*, 475-508.

Ren, F., Hogan, P.C., Anderson, A.J. and Myers, A.G.: Kedarcin chromophore–synthesis of its proposed structure and evidence for a stereochemical revision. *J. Am. Chem. Soc*., **2007**, *129*(*17*), 5381-5383.

Reusser, F.: Ficellomyicin and feldamycin inhibitors of bacterial semi conservative DNA replication. *Biochemistry*, **1977**, *16*(*15*), 3406-3411.

Ritacco, F.V., Graziani, E.I., Summers, M.Y., Zabriskie, T.M., Yu, K., Bernan,V.S., Carter, G.T. and Greenstein, M.: Production of novel rapamycin analogues by precursor-directed biosynthesis. *Appl. Environ. Microbiol*., **2005**, *71*(*4*), 1971-1976.

Rix, U., Zheng, J., Rix, R., Lily. L., Greenwell, L., Yang, K. and Rohr, J.: The dynamic structure of jadomycin B and the amino acid incorporation step of its biosynthesis. *J. Am. Chem. Soc*., **2004**, *126*(*14*), 4496-4497.

Roze, L.V., Chanda, A. and Linz, J.E.: Compartmentalization and molecular traffic in secondary metabolism: A new understanding of established cellular processes. *Fungal. Genet. Biol*., **2011**, *48(1)*, 35-48. Review article.

Russel, P.J.: iGenetics. *Int. Ed*., **2002**, 40-43.

Schiltz, P. and Kohn, H.: Studies on the reactivity of reductively activated mitomycin C. *J. Am. Chem. Soc*., **1993**, *115*(*23*), 10510-10518.

Salvati, M.E., Moran, E.D. and Armstrong, R.W.: Simplified method for the isolation of thermally labile drug-DNA adducts: Characterization of chlorambucil and carzinophilin/azinomycin B alkylation products. *Tetrahedron Lett*., **1992**, *33(26)*, 3711-3714.

Sharma, V., Kelly, G.T. and Watanabe, C.M.H.: Exploration of the molecular origin of the azinomycin epoxide: Timing of the biosynthesis revealed. *Org. Lett*., **2008**, *10*(*21*), 4815-4818.

Sharma, V., Kelly, G.T., Foulke-Abel, J. and Watanabe, C.M.H.: Aminoacetone as the penultimate precursor to the antitumor agent azinomycin A. *Org. lett.*, **2009**, *11*(*17*), 4006-4009.

Shen, B., Liu, W., and Nonaka, K.: Enediyne natural products: biosynthesis and prospects towards engineering novel antitumor agents. *Curr. Med. Chem.*, **2003**, *10*(*21*), 2317–2325.

Shirahata, k. and Hirayama, N.: Revised absolute configuration of mitomycin C. X-ray analysis of 1-N-(p-bromobenzoyl)mitomycin C. *J. Am. Chem. Soc.*, **1983**, *105*(*24*), 7199-7200.

Shu, Y.Z.: Recent natural products based drug development: A pharmaceutical industry perspective. *J. Nat. Prod.*, **1998**, *61*(*8*), 1053-1071.

Sieber, S.A. and Marahiel, M.A.: Molecular mechanisms underlying nonribosomal peptide synthesis: approaches to new antibiotics. *Chem. Rev.*, **2005**, *105*(*2*), 715-738.

Smith, S. and Tsai, S.C.: The type I fatty acid and polyketide synthases: A tale of two megasynthases. *Nat. Prod. Rep.*, **2007**, *24*(*5*), 1041-1072. Review Article.

Suresh, K., Lipman, G., Cummings, R. and Tomasz, M.: Mitomycin C-DNA adducts generated by DT-diaphorase. Revised mechanism of the enzymatic reductive activation of mitomycin C. *Biochemistry*, **1997**, *36*(*46*), 14128-14136.

Staunton, J. and Weissman, K.J.: Polyketide biosynthesis: a millennium review. *Nat. Prod. Rep.*, **2001**, *18*(*4*), 380-416. Review Article.

Strieker, M., Tanovic, A. and Marahiel, M.A.: Nonribosomal peptide synthetases: structures and dynamics. *Curr. Opin. Struct. Biol.*, **2010**, *20*(*2*), 234-240.

Suresh, K., Lipman, G., Cummings, R. and Tomasz, M.: Mitomycin C-DNA adducts generated by DT-diaphorase. Revised mechanism of the enzymatic reductive activation of mitomycin C. *Biochemistry*, **1997**, *36*(*46*), 14128-14136.

Sutherland, J.B.: Demethylation of veratrole by cytochrome P-450 in *Streptomyces setonii*. *Appl. Environ. Microbiol.*, **1986**, *52(1)*, 98-100.

Syvitski, R.T., Borissow, C.N., Graham, C.L. and Jakeman, D.L.: Ring-opening dynamics of jadomycin A and B and dalomycin T. *Org. Lett.*, **2006**, *8*(*4*), 697-700.

Terawaki, A. and Greenberg, J.: Effect of carzinophilin on bacterial deoxyribonucleic acid: Formation of inter-strand cross-links in deoxyribonucleic acid and their disappearance during post-treatment incubation. *Nature*, **1966a**, *209(5022)*, 481-484.

Terawaki, A. and Greenberg, J.: Inactivation of transforming deoxyribonucleic acid by carzinophilin and mitomycin C. *Biochim. Biophys. Acta*., **1966b**, *119(1)*, 59-64.

Thiericke, R. and Rohr, J.: Biological variation of microbial metabolites by precursor-directed biosynthesis. *Nat. Prod. Rep*., **1993**, *10(3)*, 265-289.

Timothy, L., Lawrence, C., Christopher, C., Rika, R., Sally, O., Elaine, W., Gary, A. and Peter, L.: Precursor-Directed Biosynthesis of 6-Deoxyerythronolide B Analogs in *Streptomyces coelicolor*. Understanding Precursor Effects. *Biotechnol. Prog*., **2000,** *16(4)*, 553-556.

Tomasz, M. and Palom, Y.: The mitomycin bioreductive antitumor agents: cross-linking and alkylation of DNA as the molecular basis of their activity. *Phamacol. Ther*., **1997**, *76*(*l-3*), 73-87. Review Article.

Tong, W.Y., Darah, I. and Latiffah, Z.: Antimicrobial activities of endophytic fungal isolates from medicinal herb *Orthosiphon stamineus* Benth. *J. Med. Plants Research*, **2011**, *5(5)*, 831-836.

Tsuchida, T., linuma, H. and kinoshita, N., Ikeda, T., Sawa, T., Hamada, M. and Takeuchi, T: Azicemicn-A and azicemicin-B, a new antimicrobial agent produced by amycolatopsis .1. Taxonomy, fermentation, isolation, characterisation and biological-activities. *J. Antibiot*., **1995a**, *48*(*3*), 217-221.

Tsuchida, T., linuma, H., kinoshita, N., Ikeda, T., Sawa, R., Takahashi, Y., Naganawa, H., Sawa, T., Hamada, M. and Takeuchi, T.: Azicemicin A, a new antimicrobial antibiotic from Amycolatopsis. *J. Antibiot*., **1993**, *46*(*11*), 1772-1774.

Tsuchida, T., Sawa, R., Takahashi, Y., linuma, H., Sawa, T., Naganawa, H. and Takeuchi, T.: Azicemicn-A and azicemicin-B, new antimicrobial agents produced by amycolatopsis .2. Structure determination. *J. Antibiot*., **1995b**, *48*(*10*), 1148-1152.

Vahlensieck, H.F., Pridzun, L., Reichenbach, H. and Hinnen, A.: Identification of the yeast ACC1 gene product (acetyl-CoA carboxylase) as the target of the polyketide fungicide soraphen A. *Curr. Genet*., **1994**, *25*(*2*), 95-100.

Vaillancourt, F.H., Yeh, E., Vosburg, D.A., Garneau-Tsodikova, S. and Walsh, C.T.: Nature's inventory of halogenation catalysts: oxidative strategies predominate. *Chem. Rev*., **2006**, *106(8)*, 3364-78.

Van Lanen, S.G., Oh, T.J., Liu, W., Wendt-Pienkowski, E. and Shen, B.: Characterization of the maduropeptin biosynthetic gene cluster from actinomadura madurae ATCC 39144 supporting a unifying paradigm for enediyne biosynthesis. *J. Am. Chem. Soc*., **2007**, *129*(*43*), 13082-13094.

Wakaki, S., Marumo, H., Tomioka, K., Shimizu, G., Kato, E., Kamada, H., Kudo, S. and Fujimoto, Y.: Isolation of new fractions of antitumor mitomycins. *Antibiot*. *Chemother*., 1958, *8*(*5*), 228-240.

Walsh, C.T. and Fischbach, M.A.: Natural products version 2.0: connecting genes to molecules. *J*. *Am*. *Chem*. *Soc*., **2010**, *132*(*8*), 2469-2493.

Webb, J.S., Cosulich, D.B., Mowat, J.H., Patrick, J.B., Broschard, R.W., Meyer, W.E., Williams, R.P., Wolf, C.F., Fulmor, W., Pidacks, C., Lancaster, J.E.: The structure of mitomycins A, B and C and profiromycin--Part I. *J*. *Am*. *Chem*. *Soc*., **1962a**, *84*(*16*), 3185-3187.

Webb, J.S., Cosulich, D.B., Mowat, J.H., Patrick, J.B., Broschard, R.W., Meyer, W.E., Williams, R.P., Wolf, C.F., Fulmor, W., Pidacks, C., Lancaster, J.E.: The structure of mitomycins A, B and C and profiromycin--Part II. *J*. *Am*. *Chem*. *Soc*., **1962b**, *84*(*16*), 3187-3188.

Weissman, K.J.: Introduction to polyketide biosynthesis. *Method Enzymol*., **2009**, *459*, 3-16.

Williams, D.H., Stone, M.J., Hauck, P.R. and Rahman, S.K.: Why are secondary metabolites (natural products) biosynthesized? *J*. *Nat*. *Prod*., **1989**, *52(6)*, 1189-208.

Wojciechowski, F. and Leumann, C.J.: Alternative DNA base-pairs: from efforts to expand the genetic code to potential material applications. *Chem*. *Soc*. *Rev*., **2011**, *40*(*12*), 5669-5679. Tutorial Review.

Wu, T.S., Duncan, J., Tsao, S.W., Chang, C.J., Keller, P.J. and Floss, H.G.: Biosynthesis of the ansamycin antibiotic ansatrienin (mycotrienin) by *Streptomyces collinus*. *J*. *Nat*. *Prod*., **1987**, *50*(*1*), 108-118.

Yokoi, k., Nagaoka, K. and Nakashima, T.: Azinomycins A and B, new antitumor antibiotics. II. Chemical structures. *Chem*. *Pharm*. *Bull*., **1986**, *34(11)*, 4554-4561.

Zang, H. and Gates, K. S.: DNA Binding and Alkylation by the "Left Half" of Azinomycin B. *Biochemistry*, **2000**, *39*, 14968-14975.

Zhang, Q., Pang, B., Ding, W. and Liu, W.: Aromatic polyketides produced by bacterial iterative type I polyketide snythases. *ACS*. *Catal*., **2013**, *3*(*7*), 1439-1447. Review Article.

Zhao, Q., He, Q., Ding, W., Tang, M., Kang, Q., Yu, Y., Deng, W., Zhang, Q., Fang, J., Tang, G. and Liu, W.: Characterization of the azinomycin B biosynthetic gene cluster revealing a different iterative type I polyketide synthase for naphthoate biosynthesis. *Chem*. *Biol*., **2008**, *15(7)*, 693-705.

Zourari, A., Accolas, J.P. and Desmazeaud, M.J.: Metabolism and biochemical characteristics of yogurt bacteria. *Lait*, **1992,** *72(1)*, 1-34. Review Article.

Appendices:

Appendix one: 1D NMR and FTIR Figures

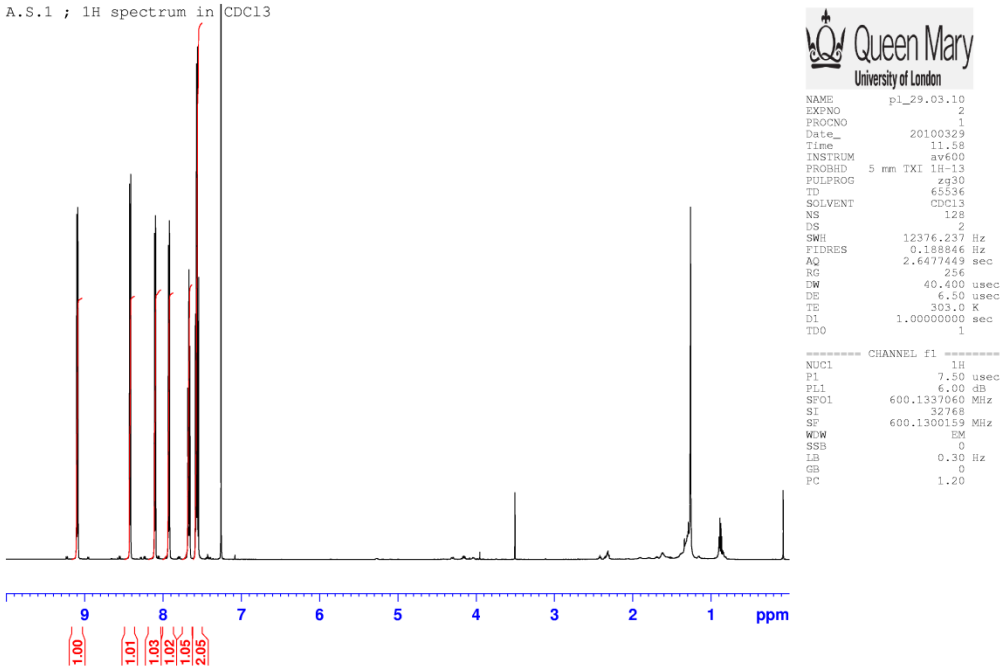

Figure 2.2: Attempt ^{1}H-NMR in $CDCl_3$ of azinmycin A **3**. A brief comparison with the literature data (Sharma *et al*., 2009) shows that the assignment of azinomycin's protons could not be deduced from this spectrum. Peaks are due to the presence of contaminants in the NMR sample.

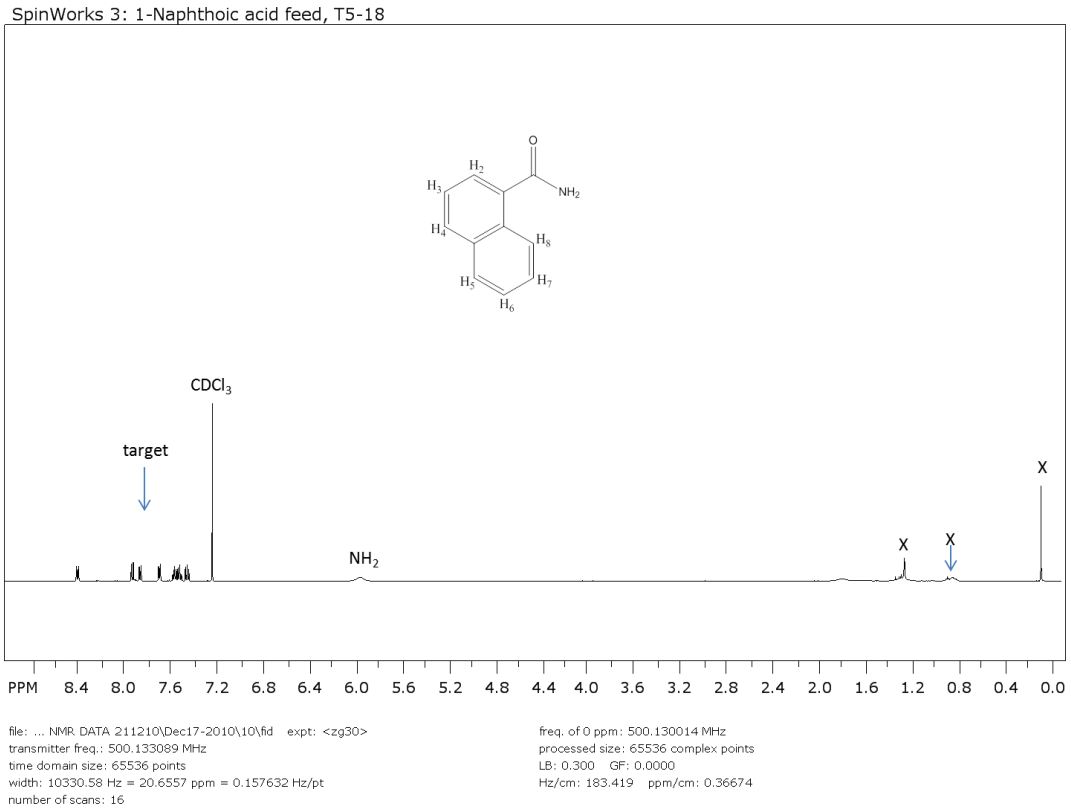

Figure 3.2: ^{1}H-NMR in $CDCl_3$ of 1-naphthoic amide **99a**. The expected ^{1}H signals are seen in the aromatic region at 7.4-8.5 ppm. The amine NH_2 signal is at 5.98 ppm. Some impurities labelled with **X** are detected up field (between 0.8-2.0 ppm) and could be due to solvents from the purification procedure.

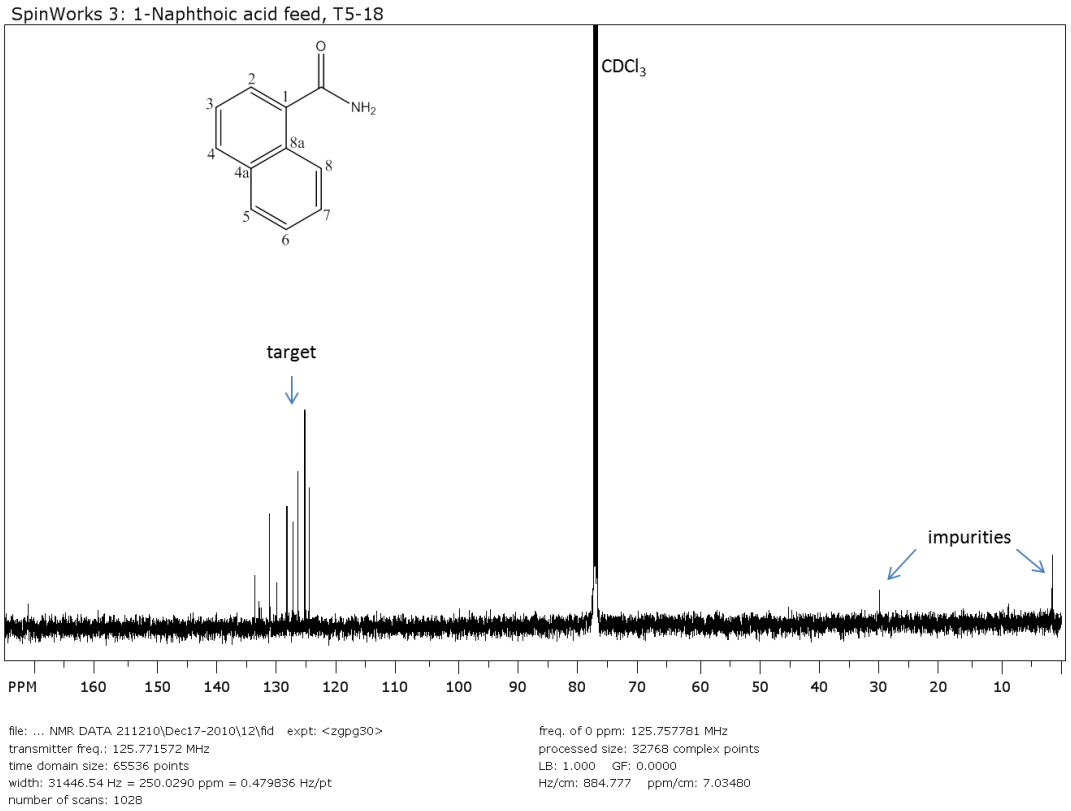

Figure 3.6: ^{13}C-NMR in $CDCl_3$ of 1-naphthoic amide **99a**. The spectrum shows persistence of impurities in the purified target compound **99a**.

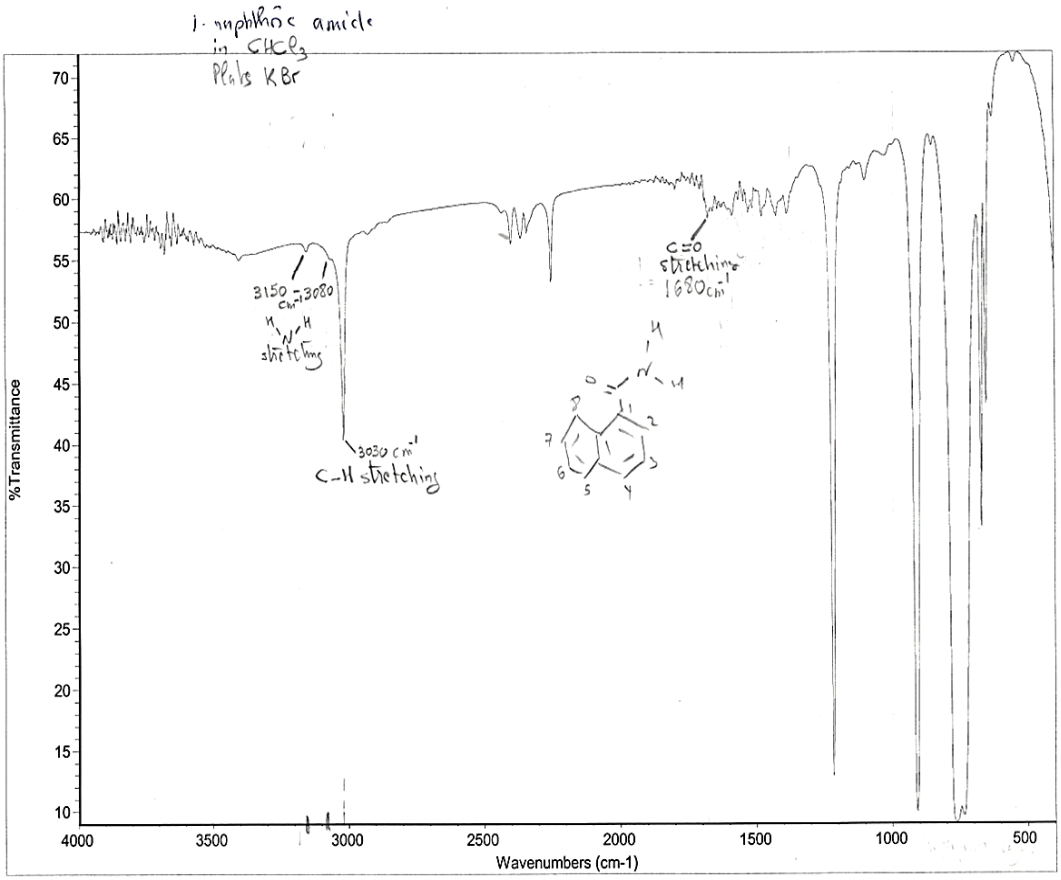

Figures 3.11: The **Figure** shows the acquire FTIR spectrum of 1-naphthoic amide **99a** dissolved in chloroform along with the assignment of the main absorption frequencies. The sample was contained in KBr plates.

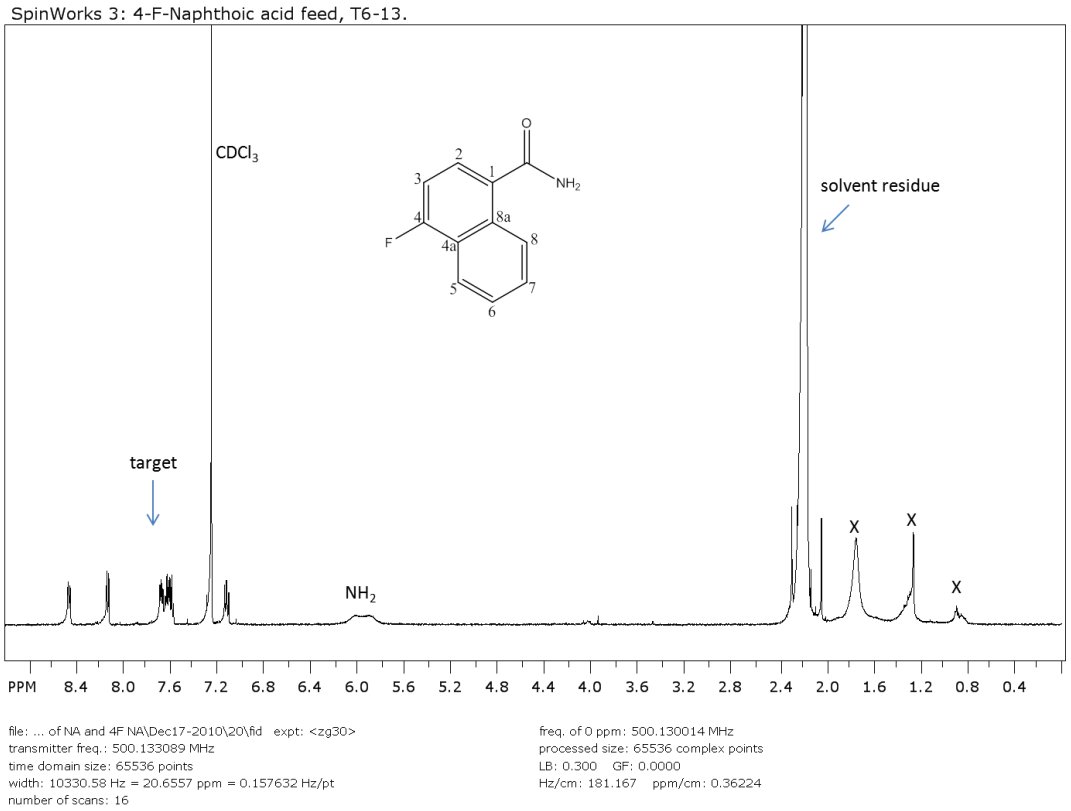

Figure 3.13: ^{1}H-NMR in $CDCl_3$ of 4-fluoro-1-naphthoic amide **100a**. The expected ^{1}H signals are seen in the region at 7-8.5 ppm. The amine NH_2 signal is at 5.96 ppm. Some impurities labelled with **X** and solvent residue are detected up field (0.6-2.4 ppm).

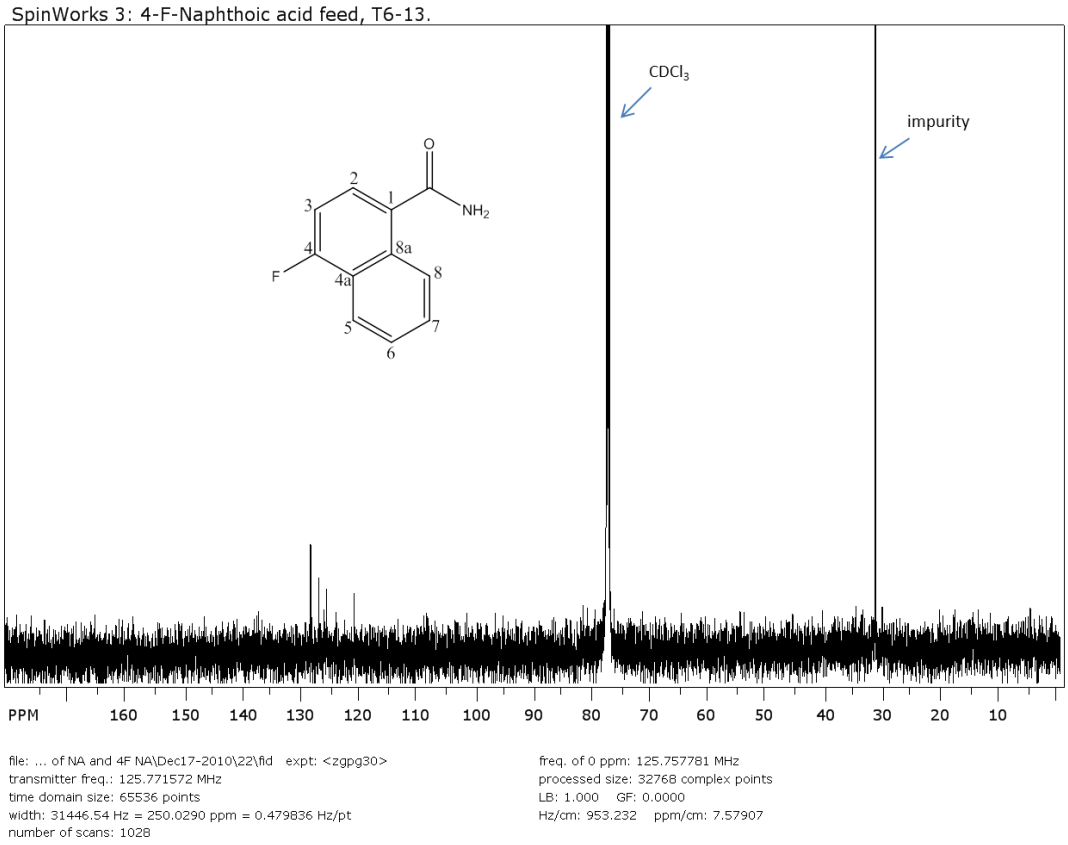

Figure 3.17: ^{13}C-NMR in $CDCl_3$ of 4-fluoro-1-naphthoic amide **100a**. An impurity peak appears at 31 ppm.

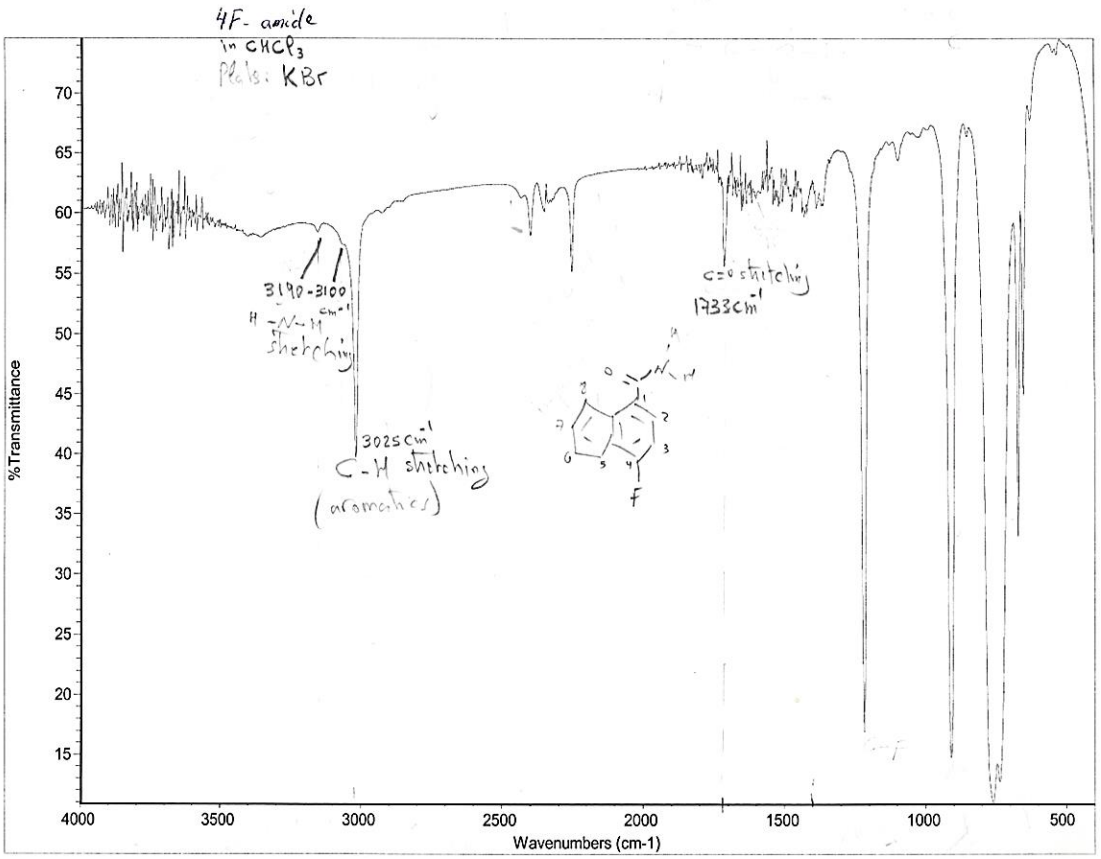

Figure 3.22: FTIR spectrum of 4-fluoro-1-naphthoic amide **100a** in chloroform. The sample was contained in KBr plates. The annotated peaks illustrate the assignment of main absorption frequencies.

Appendix two: Antifungal disk diffusion assay results

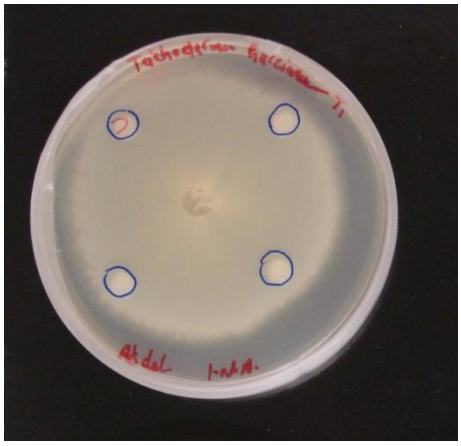

Figure 3.36: DDA for 1-naphthoic amide **99a** at a concentration of 2 mg mL^{-1} against *T. harzarium* T1. The compound has no inhibition growth effect at the tested concentration. MeOH was used for control disk (c).

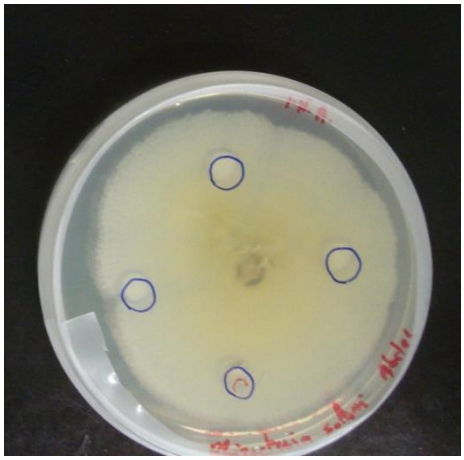

Figure 3.37: DDA for 1-naphthoic amide **99a** at a concentration of 2 mg mL^{-1} against *R. solani.* The compound has no inhibition growth effect at the tested concentration. MeOH was used for control disk (c).

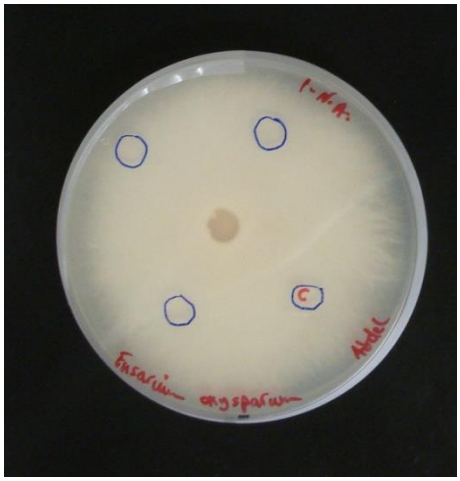

Figure 3.38: DDA for 1-naphthoic amide **99a** at a concentration of 2 mg mL^{-1} against *F. oxysporum.* The compound has no inhibition growth effect at the tested concentration. MeOH was used for control disk (c).

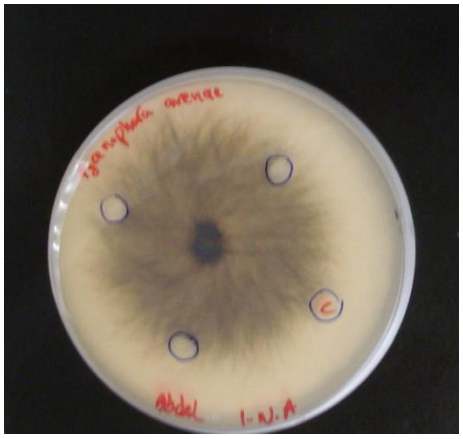

Figure 3.39: DDA for 1-naphthoic amide **99a** at a concentration of 2 mg mL^{-1} against *P. avenea.* The compound has no inhibition growth effect at the tested concentration. MeOH was used for control disk (c).

Appendix three: Antibacterial disk diffusion assay results

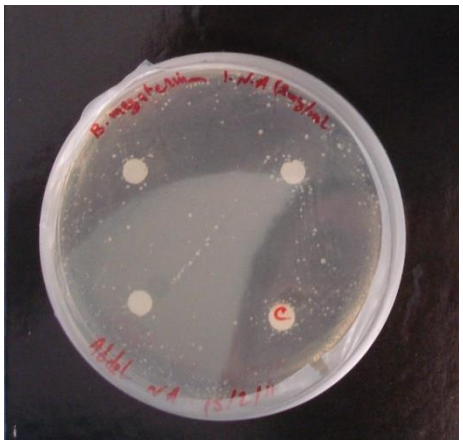

Figure 3.40: DDA for 1-naphthoic amide **99a** at a concentration of 2 mg mL^{-1} against *B. megaterium.* The compound has no inhibition growth effect at the tested concentration. MeOH was used for control disk (c).

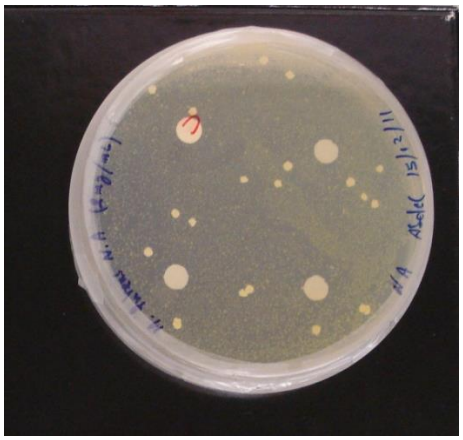

Figure 3.41: DDA for 1-naphthoic amide **99a** at a concentration of 2 mg mL^{-1} against *M. luteus.* The compound has no inhibition growth effect at the tested concentration. MeOH was used for control disk (c).

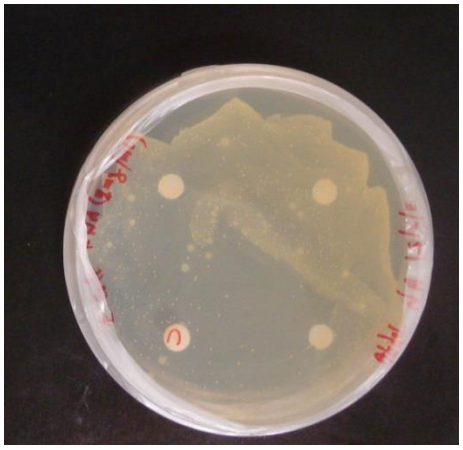

Figure 3.42: DDA for 1-naphthoic amide **99a** at a concentration of 2 mg mL^{-1} against *E. coli*. The compound has no inhibition growth effect at the tested concentration. MeOH was used for control disk (c).

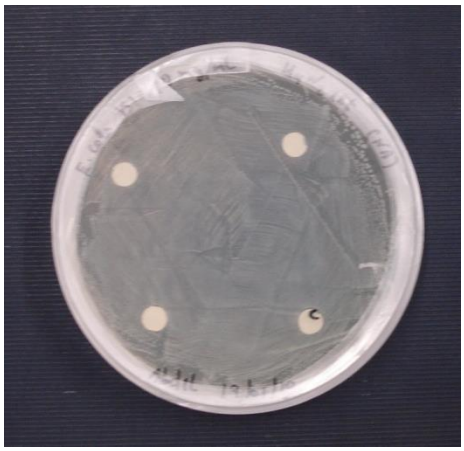

Figure 3.43: DDA for 1-naphthoic amide **99a** at a concentration of 2 mg mL^{-1} against *E. coli* K1. The compound has no inhibition growth effect at the tested concentration. MeOH was used for control disk (c).

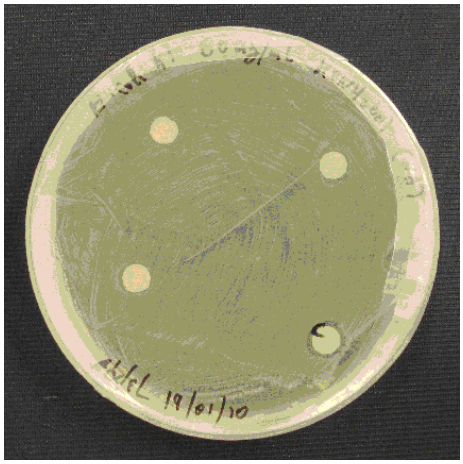

Figure 3.44: DDA for 1-naphthoic amide **99a** at a concentration of 2 mg mL^{-1} against *E. coli* K12. The compound has no inhibition growth effect at the tested concentration. MeOH was used for control disk (c).

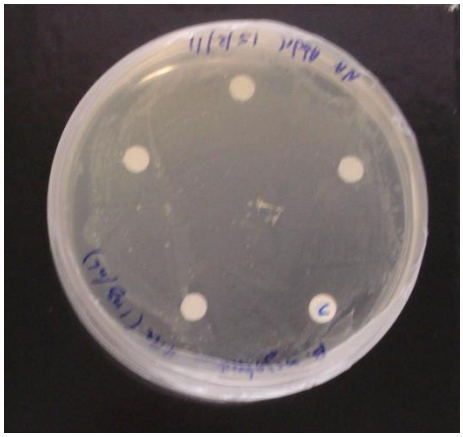

Figure 3.45: DDA for 1-naphthoic amide **99a** at a concentration of 1 mg mL^{-1} against *S. epidermis.* The compound has no inhibition growth effect at the tested concentration. MeOH was used for control disk (c).

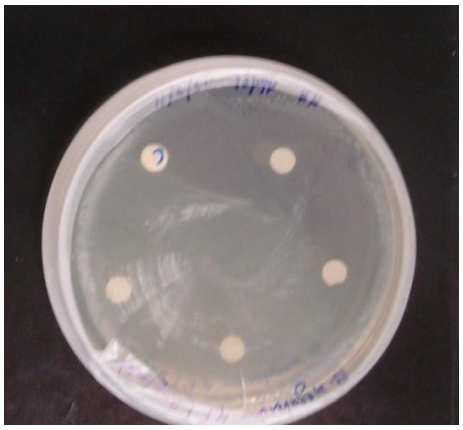

Figure 3.46: DDA for 1-naphthoic amide **99a** at a concentration of 2 mg mL^{-1} against *B. subtilis.* The compound has no inhibition growth effect at the tested concentration. MeOH was used for control disk (c).

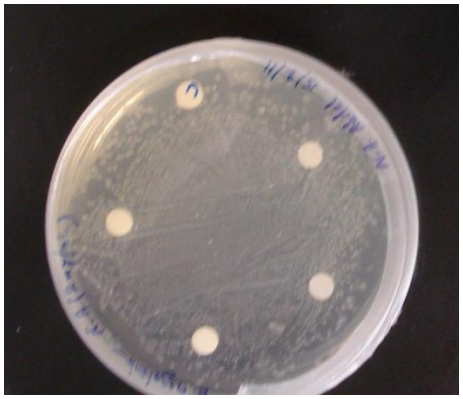

Figure 3.47: DDA for 1-naphthoic amide **99a** at a concentration of 2 mg mL^{-1} against *P. diminitus.* The compound has no inhibition growth effect at the tested concentration. MeOH was used for control disk (c).

Appendix four: Spot culture growth inhibition assay results

The labelling followed for Figures 3.48-3.55:

Top wells from right to left: MeOH control, 0.4 and 4 µg mL^{-1} of 1-naphthoic acid respectively. Bottom wells from right to left: MeOH control, 0.4 and 4 µg mL^{-1} of 4-fluoro-1-naphthoic acid respectively.

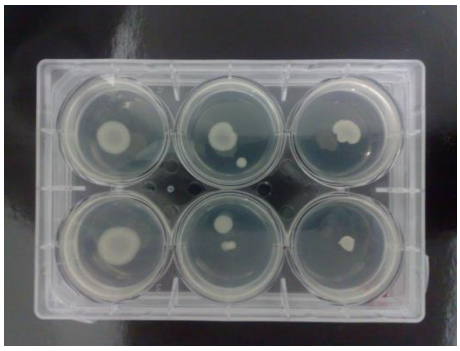

Figure 3.48: SCGIA for 1-naphthoic amide **99a** and 4-fluoro-1-naphthoic amide **100a** against *P. diminitus.*

Figure 3.49: SCGIA for 1-naphthoic amide **99a** and 4-fluoro-1-naphthoic amide **100a** against *S. epidermis.*

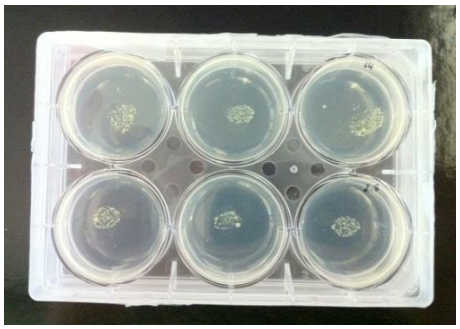

Figure 3.50: SCGIA for 1-naphthoic amide **99a** and 4-fluoro-1-naphthoic amide **100a** against *M. luteus.*

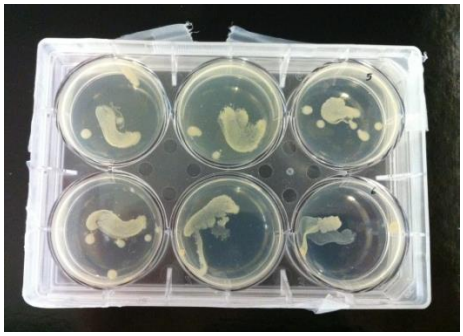

Figure 3.51: SCGIA for 1-naphthoic amide **99a** and 4-fluoro-1-naphthoic amide **100a** against *B. megaterium.*

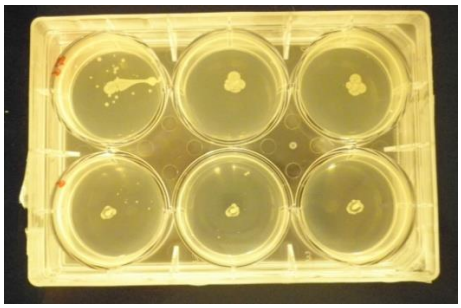

Figure 3.52: SCGIA for 1-naphthoic amide **99a** and 4-fluoro-1-naphthoic amide **100a** against *E. coli.*

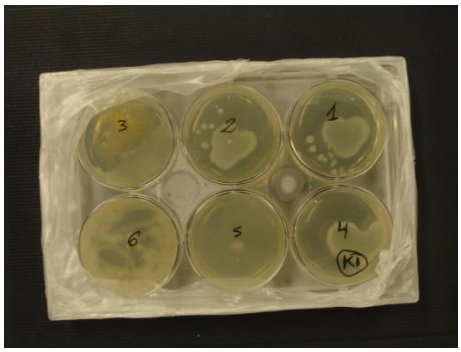

Figure 3.53: SCGIA for 1-naphthoic amide **99a** and 4-fluoro-1-naphthoic amide **100a** against *E. coli* K1.

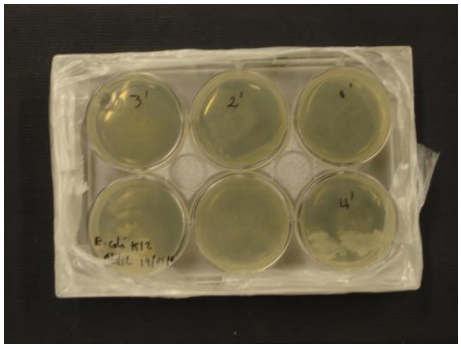

Figure 3.54: SCGIA for 1-naphthoic amide **99a** and 4-fluoro-1-naphthoic amide **100a** against *E. coli* K12.

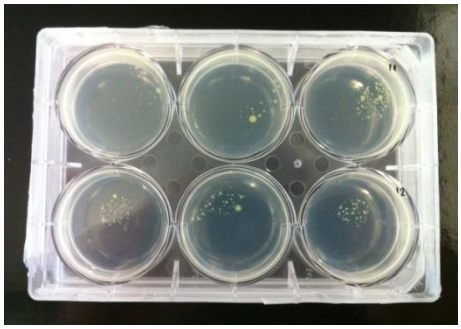

Figure 3.55: SCGIA for 1-naphthoic amide **99a** and 4-fluoro-1-naphthoic amide **100a** against *B. subtilis.*